Contributions by Participants on the Coordinated Research Project on Chemical Durability and Performance Assessment Under Simulated Repository Conditions

PART I: CONTRIBUTIONS BY PARTICIPANTS IN THE CO-ORDINATED RESEARCH PROJECT ON CHEMICAL DURABILITY AND PERFORMANCE ASSESSMENT UNDER SIMULATED REPOSITORY CONDITIONS

1. Summary of the work performed during the CRP on chemical durability and performance assessment under simulated repository conditions
D.O. Russo

2. Chemical durability studies of synthetic brannerite for immobilization of actinide-rich radioiactive waste
Y. Zhang

3. Chemical durability of vitrified high-level waste and spent fuel under simulated repository conditions of a Boom Clay formation
P. Van Iseghem, K. Lemmens, M. Aertsens, C. Cachoir, D. Jacques, V. Pirlet, S. Salah, E. Valcke

4. Chemical durability and performance assessment of HLW forms unter repository conditions
S. Luo

5. Chemically durable iron phosphate glases for vitrifying simulated nuclear waste
A. Moguš-Milanković

6. Effect of microstructure changes on the mobility of radionuclides in simulated HLW ceramics
V. Balek

7. Nuclear glass waste forms physical and chemical properties
J. L. Dussossoy

8. Vitrification of sulphate bearing high level waste (HLW)
P.K. Wattal

9. Studies on applicability of thermodynamic database of radioactive elements and glass alteration behavior for performance analysis of HLW disposal in Japan
M. Yui

10. Long-term dissolution behavior of spent fuel in compacted bentonite and synthetic granitic groundwater
K.S. Chun

11. Studies of mineral-like materials belonging to pyroxene and garnet groups for high level waste immobilization
P.P. Poluektov

12. Immobilization of high-level liquid wastes: general approaches and methodology of choosing matrix materials and technological procedures of their production
P. P. Poluektov, Y. I. Matyunin

13. Influence of radiation, environment and temperature on the interaction of the spent fuel RMBK-1000 and borosilicate glasses under simulated repository conditions
A.S. Aloy, T.V. Sapzhnikova

14. Experimental studies related to chemical durability of spent fuel Ander repository conditions
A. Martínez-Esparza

15. Chemical durability and performance assessment of spent fuel and high level waste under simulated repository conditions
S. King

SUMMARY OF THE WORK PERFORMED DURING THE CRP ON CHEMICAL DURABILITY AND PERFORMANCE ASSESSMENT UNDER SIMULATED REPOSITORY CONDITIONS

D.O. RUSSO

Comisión Nacional de Energía Atómica, Centro Atómico Bariloche, Argentina

Authors and Contributors: M. A. Audero, A. M. Bevilacqua, N. Messi de Bernasconi, M. O. Prado, P. Mateos, D. S. Rodríguez, Mario E. Sterba, Arturo D. Heredia

Abstract

The safe disposal of the high-level wastes arising from reprocessing of the spent fuel comprises, as a first step, immobilizing them in waste forms with high leaching resistance to an aqueous medium. Currently, the most developed process on an industrial scale is the incorporation of the high level wastes into a glass matrix. This is done by melting technology at temperatures from 1400º to 1500º K. One of the main reasons for selecting the glass form material is because of its durability and stability to aqueous corrosion, thermal loading and radiation damage.

With the intention of evaluating other alternatives, more advantageous processes or materials, a research and development program studying the sintering process applied to materials from several sources and with different compositions has been carried out since 1984 at the Nuclear Materials Group, Centro Atómico Bariloche. One of the advantages of the glass sintering process, relative to glass melting, is the lower temperature required (approximately 1050ºK). This implies less demanding conditions for the equipment and a diminution of the evaporation of volatile compounds of some radionuclides (i.e., Ru, Cs, Mo and Te). Furthermore, problems originating from crucible erosion that would lead to uncontrollable variations in the product composition are avoided. Finally, the macrosegregation phenomena occurring in molten glass are minimized.

At our laboratories we studied the cold pressing and sintering method and the hot pressing method, to obtain glass samples containing simulated high-level wastes. The later method was also developed up to semi-industrial scale.

In the field of behavior of the waste forms under simulated repository conditions, our group performed work in the frame of the IAEA/CNEA-CAB Research Contract No. 6745. The corresponding results were presented at various IAEA Coordination Meetings and in the Progress and final Reports of each year [1] – [9]. Those works covered aspects related to the effects of different groundwater conditions, together with gamma and beta radiation on the durability of sintered glass.

Since 1997, although independent of IAEA support, our main work was centered in the studies of the influence of the alpha radiation on the glass forms. The first part of this report summarizes the results obtained in the two last years of study of the behavior of an aluminoborosilicate glass, produced by sintering, in relationship with mechanical and microstructural properties under alpha irradiation.

In 2000, our laboratory joined the CRP again through the present Research Agreement, continuing in the field of high level waste forms but with a change in the type of such wastes. The focus of this new period was shifted to the Research and Test Reactors spent fuels. The different nature and composition of such spent fuels lead us to the study of a different glass matrix: iron-phosphate glasses. The second part of this report shows the work performed up to the end of the CRP.

PART I: "EFFECTS OF ALPHA RADIATION ON SINTERED GLASSES"

1. INTRODUCTION

One important consideration in selecting a solid form for immobilizing HLW is its stability to the radiation damage generated by the decay of radioactive nuclides over long isolation periods (10^4 to 10^6 years). Radiation could produce changes on physical properties and leachability, and thus affect the performance of the waste form in the repository.

High-Level waste glass forms will receive high doses of self-irradiation as the result of a variety of nuclear decay processes that take place in the radioactive nuclei of the waste (fission products and actinides). That means that the material is exposed to the α, β and γ radiation as well as to the recoils of fission fragments.

From all of these, alpha radiation and recoils are, by far, the most effective in producing atom cascades, influencing directly on the mechanical properties of glasses.

To investigate the effects of these interactions on the microstructure of glasses, we have analyzed two ways for producing alpha damage in the glass:

— By doping the glass forms with an alpha source, and
— By promoting internal alpha radiation through neutron bombardment of the glass samples, using the nuclear reaction $^{10}B(n,\alpha)^{7}Li$, where the ^{10}B isotope is one of the natural glass components. With this reaction we also generate ^{7}Li recoils throughout the glass volume.

2. DESCRIPTION OF THE WORK PERFORMED

2.1. Doping with an alpha source

We studied the possibility of using ^{210}Po, a γ-free nuclide that decays to ^{206}Pb (stable). The first part of the work was mainly the calculations needed to determine what concentration of the source should be necessary to simulate long-term effects.

The second activity was related with the purchasing of the source. In former years, we had identified a company that produces several radioactive sources and we tried to contact them again; unfortunately, it was impossible to locate them and a new supplier wasn't found.

In the meanwhile, we did several experiments related with the incorporation of Po analogues into the glass. The later was done in order to evaluate the retention of Po during the sintering process and to optimize the mixing procedures to assure a good homogeneity of the sintered samples.

These works are described in reference [10].

2.2. Inducing alpha radiation in the glass

Regarding this second way, we were planning to irradiate the samples with a neutron flux. To avoid having radioactive samples that we could not analyze in our facilities, we decided that the studies would be carried out using the base glass without adding the simulated wastes.

The work consisted in the preparation of several samples of sintered SG7 glass [1], that were irradiated at different thermal fluences in a research nuclear reactor (RA-6) located in the Bariloche Atomic Center.

After the irradiation, we measured density changes, leaching behavior, mechanical properties (toughness) and microstructural features. References [11] – [14].

PART II: "IRON BASED GLASSES FOR IMMOBILISATION OF URANIUM CONTAINING NUCLEAR WASTES"

1. INTRODUCTION.

Although the majority of glasses studied to date for the immobilization of high-level wastes (HLW) have been based on borosilicate compositions, iron phosphate glasses could be considered candidates for immobilizing wastes with high uranium content. In recent years, much scientific work was done in this field [15 – 19] and the evidence indicates that heavy metal oxides such as UO_2 have a better solubility in iron-phosphate glasses than in borosilicate ones.

When the spent fuel from research reactors (RRSF) is considered, there are some peculiarities that must be taken into account. The main difference is that if reprocessing of this type of fuel is not considered – as is the tendency now - then an "isotopic dilution" step should be performed previously to any immobilization or solidification of the "waste" in a solid form. This dilution is made with natural or depleted uranium. As the end of its operative life, the RRSF is around of 11% enrichment; in order to reach the enrichment consensus on the final waste (no more than 4% enrichment in U^{235}), a great amount of uranium must be added as a diluent. As a consequence, the major constituent of the waste stream will be the uranium compound (as oxide). This is why we started some research activities in the field of iron-phosphate glasses.

In this work, we have studied and analyzed the thermal transformations that occur in iron-phosphate glass forms, typically 26 to 38 wt% Fe_2O_3, 62 to 74 wt% P_2O_5, 0 to 25 wt% UO_2; with Al_2O_3 and Na_2O added as glass modifiers (4 to 17 wt%).

As we have a vast experience in glass sintering applied to borosilicate and aluminoborosilicate glasses [20 – 23], we have also started testing using this technique. We used one of the compositions of iron phosphate glasses prepared by melting and we added different amounts of uranium oxide. In this work we applied the cold pressing and sintering method (also known as pressureless sintering).

We have performed DTA/TG analysis so as to find the glass transition temperature, crystallization temperature and melting point. We also did dilatometric experiences to confirm the data obtained in the DTA/TG experiments and to get the softening point and thermal expansion coefficients. Additional data were obtained from X-Ray diffraction and chemical durability of the glass was evaluated by water corrosion experiments.

2. EXPERIMENTAL

2.1. Samples preparation

At the beginning of the work, three glass compositions were prepared so as to get some preliminary information about the melting behavior of this type of material. The compositions are listed in Table I. We used phosphoric acid (HPO_4) to obtain P_2O_5 and ferric oxide (Fe_2O_3 - technical grade); UO_2 content was obtained by U_3O_8 additions. All batches (~ 50g each) were prepared in a Pyrex™ vessel trying to obtain a mechanically well mixed material prior to the transfer to the smelting pot (silicoaluminate crucibles). These mixtures were air-melted at temperatures between 1473º K and 1573º C for 30 minutes to 1 h. No major corrosion of the crucibles was observed in the first fusion. Part of each melt was cast onto a cold steel plate and the rest was poured into graphite molds. The later were annealed at 923 K during 30 minutes and cooled up to room temperature at 0.3 /min. With this procedure we were able to obtain both quenched and free of tension samples.

TABLE I. COMPOSITION OF THE PRELIMINARY GLASS SAMPLES

Batch ID	**P_2O_5** [wt. %]	**Fe_2O_3** [wt. %]	**UO_2** [wt. %]
FH 1	70.0	30.0	-
FH 2	59.5	25.5	15.0
FH 3	60.0	40.0	-

In the second stage of the work eight glasses were prepared (Table II). In all cases ferric oxide was used as the source of iron, but for phosphorous we also used ammonium dihydrogen phosphate ($NH_4H_2PO_4$), for Al_2O_3 we employed aluminum phosphate ($AlPO_4$) and for Na_2O, we used sodium hydroxide (OHNa) sodium hexametaphosphate ($Na_6(PO_3)_6$)and sodium carbonate (Na_2CO_3). All chemicals were reagent grade. Samples B4, BU1, BS1 and BS2, were all prepared with s HPO_3. In the case of sample BS1, Na was added as OHNa, and in the case of sample BS2, $Na_6(PO_3)_6$ was used. The samples RA1, RAU1, RAU2 and RAU3 were all prepared using $NH_4H_2PO_4$, $AlPO_4$ and Na_2CO_3. These samples were melted at 1523ºK for two hours, in alumina crucibles fabricated in our laboratory with Alcoa A-16™ alumina powder. After melting the glass was poured and annealed as described above.

TABLE II. COMPOSITION SECOND SET OF GLASSES

Batch ID	P_2O_5 [wt. %]	Fe_2O_3 [wt. %]	Na_2O [wt. %]	Al_2O_3 [wt. %]	UO_2 [wt. %]
B4	70.0	30.0	-	-	-
BU1	59.5	25.5	15.0	-	-
BS1	64.5	25.8	9.6	-	-
BS2	59.1	23.7	17.3	-	-
RA1	64.9	22.7	4.3	8.1	-
RAU1	60.0	21.0	4.0	7.5	7.5
RAU2	55.2	19.3	3.7	6.9	15.0
RAU3	48.7	17.0	3.2	6.1	25.0

Finally, based in the test of the two series above mentioned, eleven glass compositions were studied (Table III). In these series the reagents were the same as above with the only difference that for Na_2O, we only used sodium carbonate. All batches were prepared in an agate mortar trying to obtain a mechanically well mixed material prior to the transfer to the smelting pot. These samples were melted at 1523-1623 K for two hours in alumina crucible and annealed as described above.

TABLE III. COMPOSITION OF THE THIRD SERIES OF GLASS SAMPLES

Batch ID	P_2O_5		Fe_2O_3		Na_2O		Al_2O_3		U_3O_8	
	[wt.%]	[mol %]	[wt.%]	[mol %]	[wt.%]	[mol %]	[wt.%]	[mol %]	[wt.%]	[mol %]
M400	65.18	61.40	22.51	18.85	4.27	9.22	8.03			
M40b	60.94	59.54	20.21	17.55	4.13	9.23	7.23	9.83	7.50	3.85
M402	55.59	56.43	19.37	17.48	3.75	8.71	6.84	9.66	14.45	7.71
M401	49.19	52.60	17.11	16.26	3.46	8.48	6.11	9.10	24.13	13.56
CAB1	57.51	60.36	42.49	39.64						
CAB2	61.51	60.36	34.08	29.73	4.41	9.91				
CAB3	60.33	61.22	33.79	30.48			5.88	8.30		
CAB4	67.74	61.11	23.96	20.10	4.65	10.05	6.65	8.74		
DR1	55.66	60.48	35.98	34.75					8.36	4.78
DR2	53.93	60.59	29.88	29.84					16.20	9.57
DR3	50.76	60.82	18.75	19.97					30.50	19.21

The glass M400 was used as the "base glass" for the sintering experiments. We produce around 100 grams of this glass in three batches: once the first was made, we let it cool down in the crucible to room temperature; we added the second batch of the mixed powdered precursors and repeat the temperature cycle. After the third run, the melt was poured in a metal mold as described earlier. After that, we milled the glass to produce a powder having a mean diameter of 20 microns.

Afterwards we prepared three mixtures of the glass powder with 7, 10 y 15 wt. % of U_3O_8.

Pellets were pressed, with this mixture, at 0.15 MPa and sintered at temperatures between 853ºK and 943ºK. The geometric and immersion density of the pellets were determined, and sinterability curves for each load were drawn in order to determine best conditions for the process.

2.2. Characterization

Netzsch STA 409 equipment was used for the differential thermal analysis and thermogravimetric experiences (DAT/TG). Determination of glass transition temperature (Tg) was performed with a Netzsch 402 ES dilatometer.

The aqueous corrosion resistance of monolithic glass samples was determined using the normalized test recommended by the Material Characterization Center, the MCC-1P [24].

The gravimetric or global dissolution rates were calculated according to:

$$R_{grav}(t) = \frac{\Delta m}{S_o \cdot t}$$

where Δm is the sample mass loss expressed in grams after drying at 383 K until constant weight and S_o and t are defined as above.

3. RESULTS AND DISCUSSION

3.1. Melted glass

A typical dilatometric experiment result is shown in Figure 1. From these measurements, the glass transition temperature and the softening point were determined trough out the intersection of the two tangents (as shown in the figure

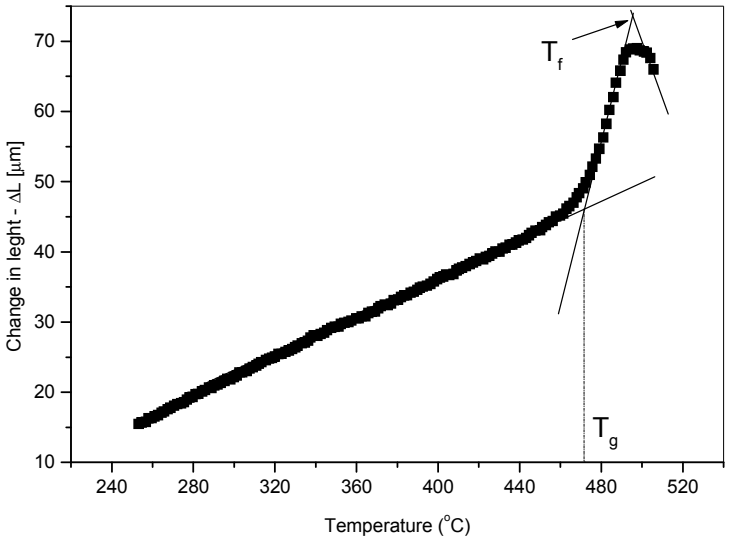

FIG. 1. Typical thermal expansion experiment.
The glass transition temperature and dilatometric softening point..

In Figure 2 we can observe the general thermal behaviour of these glasses, as determined by DTA measurements.

We plot a two-cycle experiment when the sample is heated above its melting temperature (stars in Fig. 2), cooled down to room temperature and remelted (solid line).

We can observe the crystallization peak (Tc) and the melting peak (Tm); there is an always-present peak (AP-Peak) that it is not identified up to now.

It is interesting to note that the crystallization peak that is evident in the first cycle almost disappears when the sample is reheated. In general all the glass samples showed a small weight gain (not plotted) that could be attributed to the change in the redox state of the glass (Fe^{+2}/Fe^{3+}).

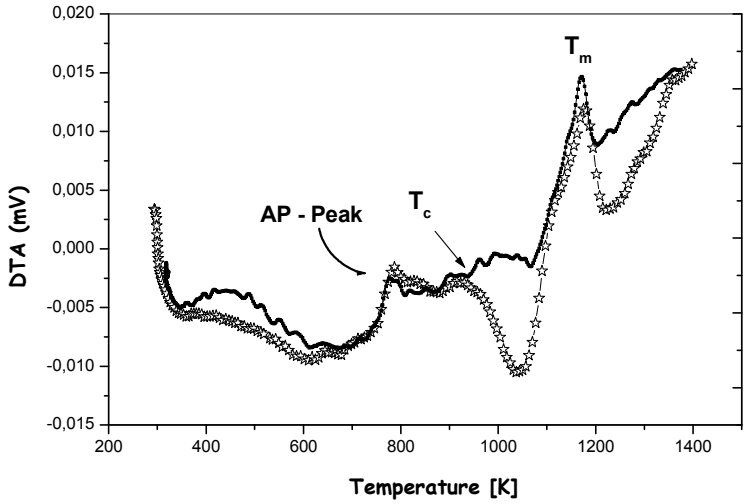

FIG. 2. Typical DTA plot of the glass samples.
Two-cycle experiment.

Using the onset crystallization temperature (Tc), the melting temperature (Tm), and the glass transition temperature (Tg), we have calculated the Hrubý parameter, K_H, which can indicate the glass stability. The Hrubý parameter is defined as:

$$K_H = \frac{T_c - T_g}{T_m - T_c}$$

According to Hrubý, the higher is the value of the parameter for a certain glass, the higher is its stability against crystallization on heating and, presumably, the higher is its vitrifiability on cooling [25]. In Table IV we summarize the values calculated for some glasses.

TABLE IV. CHARACTERISTIC TEMPERATURES AND K_H PARAMETER OF SOME OF THE GLASSES PRODUCED IN THIS WORK AND OTHERS [26]

	Tg [K]	**Tc [K]**	**Tm [K]**	**K_H**
M400	779	1098	1193	3.36
M40b	779	1113	1194	4.12
CAB1	745	1021	1166	1.90
CAB2	705	973	1193	1.22
CAB3	723	1113	1213	3.90
CAB4	713	973	1181	1.25
$0.44Na_2O•0.56SiO_2$	694	903	1208	0.68
$Li_2O•2SiO_2$	733	937	1303	0.56
$Na_2O•2CaO•3SiO_2$	854	1016	1557	0.30

In spite of the preliminary character of this data, we can see that the obtained values are much higher that the ones calculated for glasses that crystallize more easily [12], that are less than 0.7, whereas our glasses exceed 1.2.

In Figure 3 we show what happens with a powdered sample. Again, when heating the crystallization and melting peaks are evident but when cooling down (at rates as low as 1º/min), the sample does not show crystallization. This behaviour leads us to suppose that during the cooling step of the glass production, some still unidentified crystalline phase could be nucleated. This phase would crystallise during the first cycle in the DTA run and on remelting disappears completely.

Of course, this assumption should be proved with more experimental data.

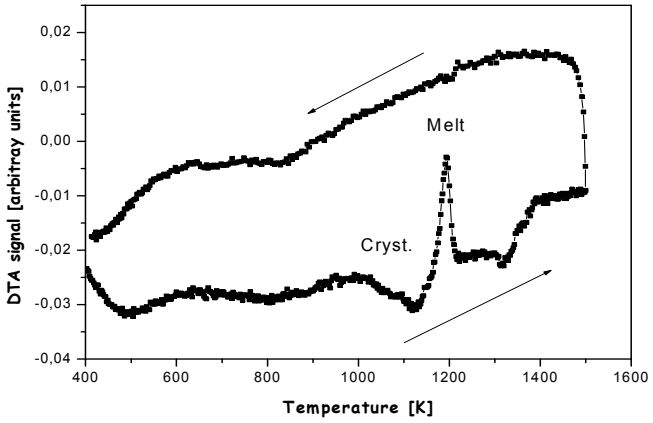

FIG. 3. Behavior of powdered glass samples as determined by DTA runs

Regarding the chemical durability, in Figures 4 to 5 we show the results of MCC-1P tests.

In Figure 4 we can observe that whereas glasses containing Al_2O_3 are more durable than those with Na_2O, when both network modifiers are present in the glass composition, they reduce drastically the durability, almost in one order of magnitude.

The effect of the addition of U_3O_8 is shown in Figure 5. It can be seen that glasses containing up to 16 wt% U_3O_8, show rather low dissolution rates, with higher additions the durability decreases very much.

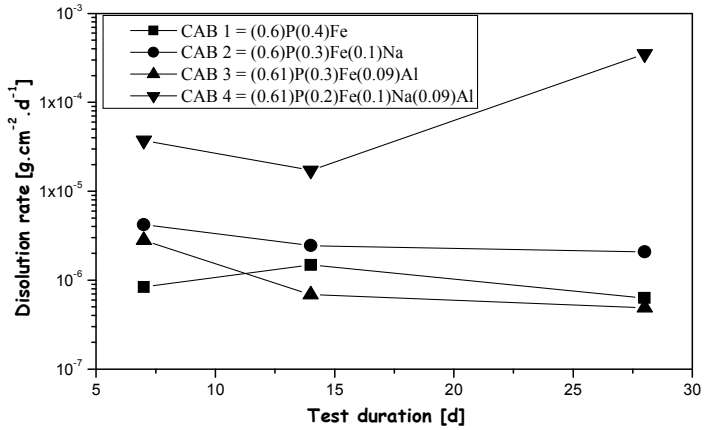

FIG. 4. Effect of Na_2O and Al_2O_3 on the durability of a $0.6P_2O_5 \bullet 0.4\ [(1\text{-}x\text{-}y)Fe_2O_3 \bullet xNa_2O \bullet yAl_2O_3]$ glass

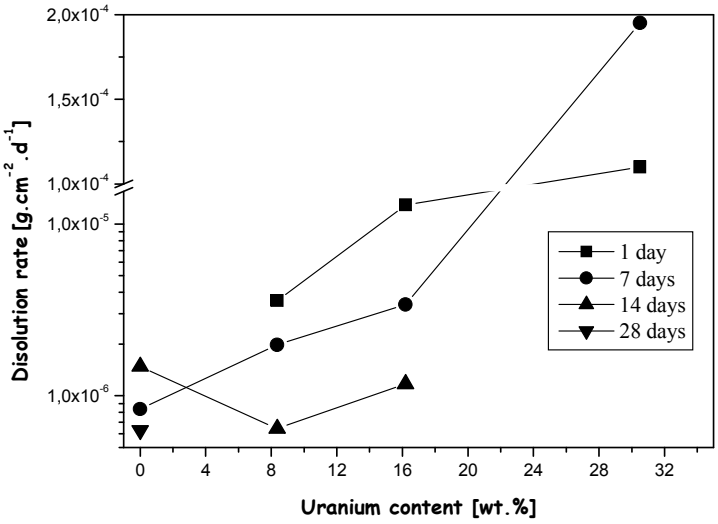

FIG. 5. Effect of U_3O_8 on the durability of a $0.6P_2O_5 \bullet 0.4\ [(1\text{-}x)Fe_2O_3 \bullet xU_3O_8]$ glass

3.2. Sintered glass

The sinterability curves for iron phosphate glass loaded with 7, 10 and 15 % U_3O_8 are shown in Figure 6. We can see that the best densities are in the range 873º–913ºK.

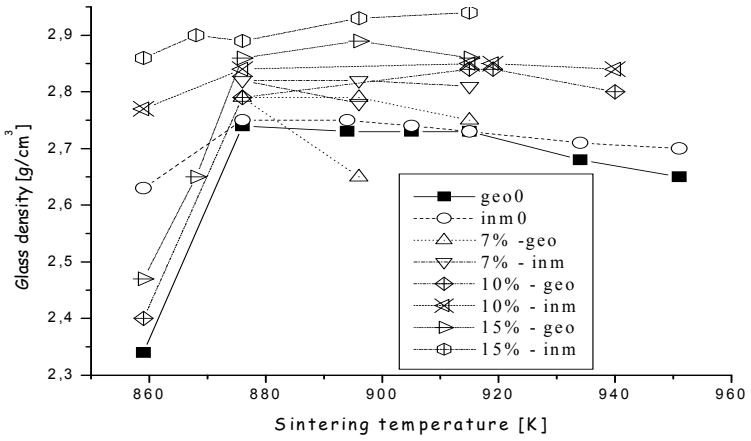

FIG. 6. Sinterability curves for the M400 glass loaded with 0, 7, 10 and 15 % U_3O_8

Pellets with the best density were cut in pieces 1mm width, geometrically measured and put in Teflon containers with deionized water to perform the above mentioned leaching test. As it can be seen in Figure 7, the gravimetric leaching rate for 7 and 10% loading shows values less than $4.5x10^{-5}$ $g.cm^{-2}.day^{-1}$.

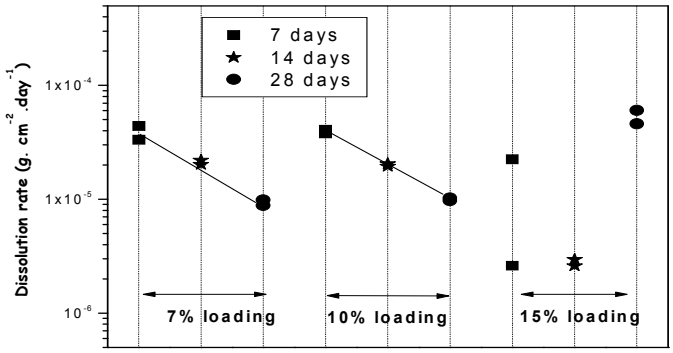

FIG. 7. Dissolution rate of M400 sintered glass with different uranium loads.

As in the sintering process the uranium particles are bonded to the glass matrix by a solid state diffusion process, we wanted to see how "sticked" these particles were. As it can be seen on the following SEM photographs (Figs. 8 and 9), uranium particles were well bonded to the matrix.

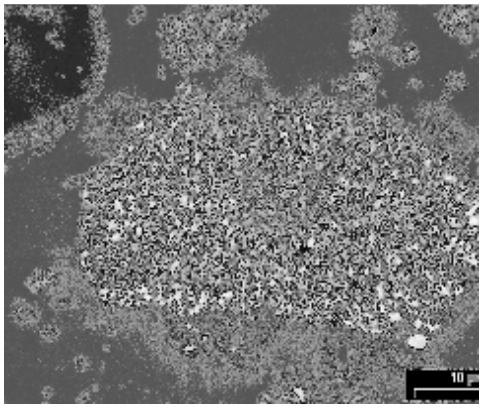

FIG. 8. An uranium particle in a polished sample of iron phosphate glass

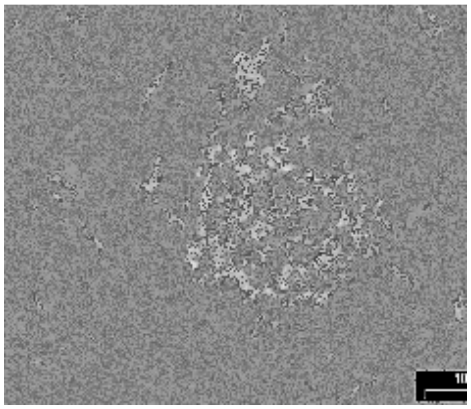

FIG. 9. An uranium particle in an unpolished sample of iron phosphate glass, leached for 28 days.

We can conclude that, at least in these preliminary tests, the best results have been found with 7 and 10% loading in the iron phosphate glass M400 developed in our laboratory, while with higher loads the results are not so good. The first mentioned samples show low dissolution rates and SEM examination proved the uranium is tightly bonded in the glass. Furthermore samples after leaching tests have shown the particles still firmly bonded in the glass.

4. CONCLUSIONS

We think that these results show that the studied glasses are very promising as potential matrices for hosting the wastes arising form the conditioning of spent fuels from research reactor as well as other uranium bearing wastes.

The sintering technique appears to be very suitable to be applied with these glasses taking into account the lower processing temperatures.

Having in mind the technological objective of developing a good waste form, as durable as possible and with the simplest technique, much more work is necessary so as to understand the complex interaction between the constituents of the glass,.

REFERENCES

[1] M. AUDERO, A. BEVILACQUA, N. MESSI DE BERNASCONI, D. RUSSO AND M. STERBA. Progress Report IAEA/CNEA-CAB Research Contract No. 6745/RB. July 1993.

[2] M. AUDERO, A. BEVILACQUA, N. MESSI DE BERNASCONI, D. RUSSO AND M. STERBA. Final Report of the Research Contract IAEA N°6745/RB**.** October 1993.

[3] D. RUSSO, N. MESSI DE BERNASCONI, M. STERBA, A. HEREDIA, J. SBRILLER AND M. SANFILIPPO. Progress Report IAEA/CNEA-CAB Research Contract No. 6745/R1/RB. October 1994.

[4] D. RUSSO, N. MESSI DE BERNASCONI, M. STERBA, A. HEREDIA, J. SBRILLER AND M. SANFILIPPO. Final Report of the Research Contract IAEA N° 6745/R1/RB. December 1994.

[5] D. RUSSO, N. MESSI DE BERNASCONI, M. STERBA, A. HEREDIA, J. SBRILLER AND M. SANFILIPPO. Final Report IAEA/CNEA-CAB Research Contract No. 6745/R1/RB. January 1995.
[6] D. RUSSO, N. M. DE BERNASCONI, M. STERBA, A. HEREDIA, J. SBRILLER, S. PRASTALO AND M. SANFILIPPO. Progress Report IAEA/CNEA-CAB Research Contract No. 6745/R2/RB. October 1995.
[7] D. RUSSO, N. MESSI DE BERNASCONI, M. STERBA, A. HEREDIA, M. SANFILIPPO, S. PRASTALO AND J. SBRILLER. Final Report IAEA/CNEA-CAB Research Contract No. 6745/R2/RB. January 1996.
[8] N. MESSI DE BERNASCONI, A. BEVILACQUA AND D. RUSSO. Progress Report IAEA/CNEA-CAB Research Contract No. 6745/R3/RB. February 1997.
[9] N. M. DE BERNASCONI, M. PRADO, A. BEVILACQUA, M. ARRIBERE, D. RUSSO, A. HEREDIA, S. PRASTALO, J. SBRILLER, Final Report IAEA/CNEA-CAB Research Contract No. 6745/R4/RB. July 1997.
[10] A. BEVILACQUA, M. STERBA AND A. HEREDIA. "Actinide alpha decay of reprocessed CANDU spent fuel and proposed ^{210}Po doped sintered glass accelerated test". International Conference Actinides '97". Baden-Baden, Alemania. Poster session II T8, September 1997.
[11] N. M. DE BERNASCONI, M. PRADO, A. BEVILACQUA AND M. ARRIBÉRE. “Daño por radiación alfa en bloques vítreos sinterizados”, VII Congresso Geral de Energía Nuclear, Brasil (1998).
[12] M. PRADO, N. M. DE BERNASCONI, A. BEVILACQUA, M. ARRIBERE. “Efectos de la radiación alfa en la dureza y la tenacidad a la fractura de un vidrio aluminoborosilicato utilizado para inmovilizar residuos”. VII Congresso Geral de Energía Nuclear, Belo Horizonte, Brasil. (1998).
[13] M. PRADO, N. MESSI, I. TORRIANI, T. PLIVELIC, A. BEVILACQUA, M. ARRIBERE. “Effect of alpha radiation on the microstructure of a borosilicate glass”. Report of Project No. 488/99, Laboratório Nacional de Luz Síncroton (LNLS), Brasil. November 1999.
[14] M. PRADO, I. TORRIANI, T. PLIVELIC, N. MESSI, A. BEVILACQUA, M. ARRIBERE. “SAXS study of microheterogeneities of an alumino-borosilicate glass”, X Reunião Anual de Usuarios, LNLS, Campinas, Brasil. February 2000.
[15] C.S. RAY, X. FANG, M. KARABULUT, G. MARASINGHE, D. DAY. J. NON-CRYST. Solids, 249 (1999) 1-16.
[16] B.C. SALES, L.A. BOATNER. J. NON-CRYST. Solids, 79 (1986) 83-116.
[17] D.E. DAY, Z. WU, C.S. RAY, P. HRMA. J. NON-CRYST. Solids, 241 (1998) 1.
[18] M.G. MESKO, D.E. DAY. J. NUCL. Mater, 273 (1999) 27-36.
[19] B. SAMUNEVA, P TZVETKOVA, I GUGOV, V DIMITROV. J. MATER. Sci. 15 (1996) 2180.
[20] M. AUDERO, A. BEVILACQUA, N. M. DE BERNASCONI, D. RUSSO, M. STERBA. "Immobilization of Simulated High-Level Waste in Sintered Glasses". Journal Nuclear Mater. 223 (1995) 151-156.
[21] A. BEVILACQUA, N. MESSI, D. RUSSO, M. AUDERO, M. STERBA, A. HEREDIA. "Argentine Experience on Immobilization of Simulated High-Level Liquid Wastes in Sintered Borosilicate, Aluminosilicate and Aluminoborosilicate Glasses". SPECTRUM’96, Vol 3 (1996) 2019 - 2026.
[22] A. BEVILACQUA, N. M. DE BERNASCONI, D. RUSSO, M. AUDERO, M. STERBA, A. HEREDIA. "Immobilization of Simulated High-Level Liquid

Wastes in Sintered Borosilicate, Aluminosilicate and Alumino-Borosilicate Glasses". J. Nuclear Mater. 229 (1996) 187-193.
[23] D. RUSSO, N. DE BERNASCONI, M. STERBA, A. HEREDIA, M. SANFILIPPO, S. PRASTALO, J. SBRILLER. “Sintered Glasses for High-Level Wastes”. Sci. Basis for Nuclear Waste Manag. 465 (1997) 205.
[24] Materials Characterization Center Test Methods, PNL-3990, Battelle Pacific Northwest Laboratories (1981).
[25] A. HRUBÝ. Czech J. Phys. B 22 (1972) 1187.
[26] A. CABRAL, A. CARDOSO AND E. D. ZANOTTO. J. NON-CRYST. Solids 320 (2003) 1.

CHEMICAL DURABILITY STUDIES OF SYNTHETIC BRANNERITE FOR IMMOBILIZATION OF ACTINIDE-RICH RADIOACTIVE WASTES

Y. ZHANG

Australian Nuclear Science & Technology Organisation, Menai, Australia

Authors and Contributors: B. S. Thomas, M. Blackford, H. Li, Z. Zhang, E. Loi, T. McLeod, M. Carter, M. Colella, E. Drabarek, B. D. Begg, and E. R. Vance

Abstract

This report summarises the work being carried out at ANSTO since 2000 under research agreement No. AUL-10644. It covers the dissolution of synthetic brannerite in acidic and alkaline fluids [1], the effects of solution pH and U valence state on the dissolution of U-substituted thorutite [2], and kinetic modelling of the oxidative dissolution of brannerite [3].

The dissolution of synthetic brannerite in aqueous media at 40^{o}C and 90^{o}C under atmospheric redox conditions has been studied. At 40^{o}C, the presence of phthalate as a buffer component in the pH range of 2 to 6 has little effect on uranium release from brannerite. Bicarbonate increases uranium release and enhances the dissolution of brannerite. Compared to UO_2, brannerite is more resistant to dissolution in bicarbonate solutions. In under-saturated conditions at 90^{o}C, the dissolution of brannerite is incongruent (preferential release of uranium) at pH 2 and nearly congruent at pH 11. TEM examinations reveal a polymorph of TiO_2 (pH 2 specimen) and a fibrous Ti-rich material (pH 11 specimen) as secondary phases. XPS analyses indicate the existence of U(V) and U(VI) species on the surfaces of specimens both before and after leaching, and U(VI) was the dominant component on the specimen leached in the pH 11 solution.

The dissolution of the thorium analogue of brannerite ($ThTi_2O_6$-I) and U(IV)/U(V) doped Th-brannerite ($Th_{0.97}U_{0.03}Ti_2O_6$-II and $Th_{0.955}U_{0.03}Ca_{0.015}Ti_2O_6$-III) in aqueous media under atmospheric condition has been studied to elucidate the effects of pH and uranium valence state on the dissolution rate. The dissolution of I is nearly stoichiometric but slightly preferential release of U occurs for II and preferential release of Ca and U occurs for III. The V-shape pH dependence previously observed for U-brannerite only occurs for U (not other matrix elements) for II, indicating that the pH dependence is related to the U oxidation state upon dissolution. The normalised U dissolution rates of III are nearly an order of magnitude higher than those of II for pH values over 3, suggesting brannerite is less durable with U(V) doping. TEM examination of specimens after leaching revealed few surface alteration products, which is consistent with the nearly stoichiometric dissolution of thorium brannerite.

Previous data in the literature have been combined with new experimental results, dealing with the release of uranium from brannerite as a function of solution pH and aqueous carbonate species, in oxygenated solutions. From these data we have developed a conceptual model for uranium release from brannerite consisting of two reaction steps: oxidation of surface uranium(IV) atoms, and subsequent detachment of

U(VI) atoms into solution, which is catalysed by surface coordination with protons (acidic media) or carbonate species (alkaline media in equilibrium with the atmosphere). A kinetic rate law is derived for this simple reaction mechanism and fitted to experimental data. The resulting predictive equation for uranium release qualitatively describes the pH-dependent behaviour observed in experiment, and quantitatively gives an upper limit for uranium release from brannerite over a range of conditions and experiment types.

1. INTRODUCTION

Brannerite (UTi_2O_6, monoclinic crystal system with space group C2/m, and both U and Ti occupying distorted octahedral coordination polyhedra), which exists naturally in many uranium ore bodies, has attracted recent attention as a minor phase in the pyrochlore-rich ceramic formulations designed to immobilise surplus plutonium [4]. In these ceramic formulations, brannerite is formed as a minor phase constituting around 15% of the ceramic by volume [5]. One such brannerite phase with composition $Ca_{0.08}Gd_{0.14}Hf_{0.11}U_{0.53}Pu_{0.21}Ti_2O_6$ was calculated to contain 20% of the total uranium content of the waste form and more than 15% of the total plutonium content, as well as around 10% of the neutron absorbers, Gd and Hf [5]. Further, the brannerite phase is often formed around residual actinide oxide phases, which are potentially less durable than the titanate phases. Therefore, the dissolution behaviour of brannerite phases is important in evaluating possible mobilization of actinides in the environment. More extensive dissolution studies of synthetic brannerite have been performed [6-7], showing brannerite to be less durable than zirconolite and pyrochlore but more durable than perovskite.

In our early work, KHphthalate was used in the buffer solutions for pH 2-6. However, it has been reported that phthalate slightly enhances the dissolution of natural minerals [8]. In addition, the effect of bicarbonate in alkaline solutions on the dissolution of brannerite should be considered. The purpose of the current work is to provide data to quantify the effects of phthalate and bicarbonate on the dissolution of synthetic brannerite under atmospheric redox conditions and further elucidate the nature of the surface alteration products by TEM and XPS examination of ion-beam-thinned specimens leached in under-saturated conditions.

Our earlier work [9] has also shown the ability to stabilise U(V) in brannerite via the addition of Ca for charge compensation. It is of interest to examine the effect of different U valence states on dissolution kinetics, including the effect of pH, and compare with the thorium analogue of brannerite, thorutite, and to elucidate further the nature of the surface alteration products at atmospheric redox conditions.

We also aim to develop an understanding of the chemical processes controlling the dissolution of brannerite, and to construct mathematical models to describe these processes. Such models will be invaluable in predicting the long-term behaviour of brannerite-bearing waste forms over a wide range of repository conditions.

2. EXPERIMENTAL

2.1. Sample preparation

Synthetic U-brannerite (UTi_2O_6) and Th analogue of brannerite ($ThTi_2O_6$-I) and U(IV)/U(V) doped Th-brannerite ($Th_{0.97}U_{0.03}Ti_2O_6$-II and $Th_{0.955}U_{0.03}Ca_{0.015}Ti_2O_6$-III) were made by the alkoxide/nitrate route [10]. The U-brannerite sample contains mainly brannerite with minor rutile inclusions (~5% TiO_2 and trace amounts of reduced Ti oxide) and only a trace amount of UO_2 (< 0.1%). The Th-brannerite samples contain mainly brannerite with minor rutile inclusions (~5% TiO_2) and trace amounts of ThO_2 (< 0.1%). Powdered samples (75-150 μm) for the dissolution tests were washed with acetone to remove fines from the surfaces. The surface areas were measured by the BET method. The ion-beam-thinned (IBT) TEM specimens were prepared in the conventional manner [1]

2.2. Electron microscopy and x-ray photoelectron spectroscopy

Scanning electron microscopy (SEM) was carried out with a JEOL 6400 instrument operated at 15 kV, and fitted with a NORAN Voyager IV X-ray Microanalysis System (EDX).

Transmission electron microscopy (TEM) was carried out with a JEOL 2010F equipped with a Link-ISIS EDX system, operated at 200 kV and calibrated for quantitative thin-film analyses using an extensive set of natural and synthetic reference materials [11].

X-ray Photoelectron Spectroscopy (XPS) measurements were performed in ultra-high vacuum with a VG ESCALAB 220i-XL system employing a monochromatic Al K□ (1486.7 eV) X-ray source [1].

2.3. Test methods

Batch equilibrium tests for U-brannerite were carried out in polystyrene containers on a shaking bench (once per second) within an oven at 40°C. A series of phthalate or bicarbonate solutions with concentrations ranging from 10^{-4} to 10^{-2} M, with constant pH (pH 4 for phthalate and pH 8 for bicarbonate) and constant ionic strength (0.01 M) were used. The solution pH was adjusted using 1 M HCl and the ionic strength was adjusted using KCl. The initial solid concentration was 0.02 g in 30 mL solution. Aliquots (2 mL) were regularly taken, run through 0.25 μm filters, and acidified with 3% by volume of analytical grade HNO_3. An inductively coupled plasma mass spectrometer (ICP-MS) was used to determine the concentrations of U and Ti.

Dynamic dissolution tests, described elsewhere [12], for IBT specimens of U-brannerite and Th-brannerite, were conducted at 30-90°C using pH 2 and pH 11 solutions (0.001M KCl solutions with HCl or KOH) and flow rates of 15-50 mL d^{-1} in an open atmosphere. The leachates were collected daily in the first week and then twice per week, and were acidified with 3% by volume of analytical grade HNO_3. ICP-MS was used to determine the concentrations of U, Th, Ca and Ti in the leachates. The IBT specimens, after 4 weeks, were gently rinsed with deionised water and dried at 90°C for TEM and XPS examinations.

3. RESULTS AND DISCUSSION

3.1. Dissolution of synthetic brannerite in acidic and alkaline fluids [1]

Effect of phthalate

The initial uranium release rate (at 10 min.) is weakly dependent on phthalate concentration with the reaction order of 0.19 ± 0.08. After 1 hr, the uranium release rate appears to approach a constant value. The weak rate dependence of phthalate in the first 10 minutes might be related to the initial dissolution of U(VI) and U(V) species present on the brannerite surface [13], which could be controlled by phthalate. In the case of titanium there is no obvious rate dependence on phthalate concentration. Generally the uranium release rate is about two or three orders of magnitude higher than that of titanium, indicating incongruent dissolution of brannerite.

Over the experimental time period (20 days), uranium concentrations in solutions do not seem to reach saturation. However, titanium reaches apparent equilibrium after 7 days with the saturation concentrations dependent on phthalate concentrations. Therefore the phthalate ion increases titanium solubility. However, it is unlikely that slightly increasing titanium solubility would have any significant effect on uranium release since the uranium release rate is overall 100 times higher than titanium release rate with the highest phthalate concentration.

Effect of bicarbonate

Uranium concentrations in solutions do not reach saturation and uranium release rate is found to be dependent strongly on bicarbonate concentration over the testing time period with the reaction order varying from ~0.52 at 10 minutes to ~0.69 after 7 days. This implies that bicarbonate enhances the dissolution of brannerite under alkaline and atmospheric conditions. A direct comparison between brannerite (40^{o}C) and UO_2 (45^{o}C) [14] in bicarbonate solutions at the same atmosphere and essentially the same methodology is shown suggests that brannerite is more resistant to dissolution than UO_2 in bicarbonate solutions.

Titanium releases, however, show no dependence on bicarbonate concentration at pH 8, either in release rate or equilibrium concentration (~3 ppb), indicating that unlike phthalate at pH 4, bicarbonate does not interact strongly with titanium, either on the solid surface or in solution.

Dissolution of IBT specimens

For the pH 2 solution, the cumulative elemental releases show linear relationships versus time, indicating constant (but different) release rates for both uranium and titanium. The dissolution of brannerite in the pH 2 solution is incongruent and preferential release of uranium occurs, as found previously [6].

In the case of the pH 11 solution, the less linear and lower release of uranium than titanium suggests that some dissolved uranium may adsorb back onto the secondary phase and the sample itself or even the Teflon vessel wall. Overall, the dissolution of the IBT specimen in the pH 11 solution appears to be nearly congruent.

TEM examination of IBT specimens

The IBT specimen exposed to the pH 11 solution at 90°C for 4 weeks shows large areas of a fibrous secondary phase associated with the original brannerite. In contrast, primary rutile (TiO_2) appears to be unaffected. Energy dispersive x-ray (EDX) spectroscopy shows that the Ti-rich secondary phase contains varying amounts of uranium and trace amounts of other elements, although the remaining underlying brannerite makes determination of the secondary phase composition difficult. Selected area electron diffraction indicates that the secondary phase is amorphous.

Compared to the pH 11 specimen, the IBT specimen leached in the pH 2 solution at 90°C for 4 weeks shows large areas of apparently unaltered brannerite as well as a relatively small amount of secondary phase. The primary rutile grains appear to have been partially etched. EDX spectroscopy indicates that the secondary phase is mainly TiO_2 with differing amounts of uranium and trace amounts of other elements. Selected area electron diffraction confirms that the secondary phase is polycrystalline, probably anatase and/or brookite.

XPS examination of IBT specimens

The two leached IBT specimens (in the pH 11 and pH 2 solutions respectively), as well as an unleached IBT specimen, were examined by XPS.

The brannerite surface prior to leach testing already contained a large amount of U(V) probably as a result of surface oxidation due to the ion-beam-thinning procedure. The distribution of the U(IV), U(V) and U(VI) components on the surface was quite similar to that leached in the pH 2 solution. The specimen leached in the pH 11 solution, however, was oxidised much more than the pH 2 specimen. This would support the conclusion that U(VI) was incorporated in the long fibrous U-bearing but Ti-rich alteration product covering a high percentage of the pH 11 specimen surface, as observed by TEM. The U/Ti ratio determined from XPS was reduced from 0.59 before leaching to 0.37 after leaching in the pH 2 solution, consistent with the conclusion of preferential release of uranium at pH 2. Since large areas of the pH 11 surface were covered by an alteration product layer thicker than the probing depth of XPS (≤ 5 μm), the U/Ti ratio of the pH 11 surface (0.46) does not reflect the true U/Ti ratio of the leached brannerite surface.

3.2. The effects of pH and U valence state on the dissolution of Th-brannerite [2]

The dissolution of $ThTi_2O_6$-I in the pH 2 solution at 30°C is nearly stoichiometric, but slightly preferential release of U(IV) relative to Th and Ti occurs in $Th_{0.97}U_{0.03}Ti_2O_6$-II. Preferential release of Ca and U occur in $Th_{0.955}U_{0.03}Ca_{0.015}Ti_2O_6$-III.

SEM examination of the samples after dissolution tests showed smooth surfaces of unaltered brannerite particles, which is consistent with low and near stoichiometric dissolution of the testing materials. TEM examination of the IBT-specimen of II after 4 weeks in a pH 2 solution revealed a few secondary phases, mainly TiO_2 which contained small amounts of Th and U. The dissolution of $ThTi_2O_6$ and end-member UTi_2O_6 in the pH 2 solution at 70°C highlights stoichiometric dissolution of $ThTi_2O_6$,

and the preferential release of U with respect to Ti in UTi_2O_6. Th-brannerite is more durable than its U counterpart.

There is no obvious pH dependence of U release rates for III except at pH < 3. For II, there is probably a minimum of U release rate at pH near 8. Note this happens for U, but not for Th and Ti, which was observed previously for U-brannerite [6], indicating that it is probably related to U oxidation state upon dissolution.

The normalised U release rates for U(V) doped Th-brannerite are about an order of magnitude higher than those for U(IV) doped Th-brannerite at pHs over 2, highlighting some sensitivity of brannerite dissolution to U valence state.

3.3. Kinetic modeling of oxidative dissolution of brannerite [3]

The previously described experimental evidence leads to the following postulates regarding the mechanism of uranium release from brannerite in dilute solutions open to the atmosphere:

1. Uranium release rate is independent of time (under fixed conditions);

2. Uranium release rate is controlled by chemical reaction at the surface of the dissolving brannerite at all times;

3. Uranium release is promoted by the activity of hydrogen ions;

4. Uranium release is promoted by the activity of aqueous carbonate species (as derived from the atmosphere in alkaline solutions);

5. Uranium release is dependent on redox conditions (*e.g.* activity of dissolved oxygen).

We assume that the overall mechanism consists of two basic reactions. The first reaction is the oxidation of uranium(IV) to uranium(VI) on the brannerite surface. The second reaction involves surface complexation (specifically protonation or carboxylation) of the uranium(VI) sites, followed by detachment of U(VI) from the lattice. Similar oxidation dissolution models have been proposed for UO_2 [14-15], though with some differences in specific assumptions and chemical equations. These two reactions are described here by the following chemical equations, with their corresponding rate constants displayed on the right hand side. In this description, surface complexation and detachment have been combined into a single equation.

$$S-\mathrm{U(IV)O_2}+\frac{1}{2}\mathrm{O_2}\rightarrow S-\mathrm{U(VI)O_3} \qquad k_X$$

$$S-\mathrm{U(VI)O_3}+n\mathrm{L}\rightarrow \text{“}\mathrm{UL}_n\text{”}(\mathrm{aq})+S-\mathrm{U(IV)O_2} \qquad k_L$$

S represents the surface of the brannerite, in which uranium atoms are bound; these U atoms may also be coordinated to atoms or molecules in solution. L represents a single complexing agent, *e.g.* H^+ or carbonate species. No attempt is made to balance the second chemical equation; the solution species “UL*n*” is representative only since precise surface and solution species of uranium are unknown, and incorporates all solution species of U(VI). The reaction order *n* with respect to the

ligand L is an "average" value, representing ligand promoted detachment *via* a number of intermediates.

4. CONCLUSIONS

Although phthalate can increase the solubility of titanium, it has no significant effect on the dissolution of brannerite in a pH 4 buffer solution under atmospheric condition since the dissolution of uranium is dominant and generally over 100 times higher than that of Ti. Bicarbonate at pH of 8 increases the uranium release rate and therefore enhances the dissolution of brannerite. The dissolution of IBT specimens in under-saturated conditions in pH 2 (HNO_3) and pH 11 (KOH) solutions indicate: 1) higher elemental releases at pH 2 than those at pH 11; 2) preferential release of uranium at pH 2 and close to stoichiometric release at pH 11; 3) a polymorph at pH 2 and fibrous Ti-rich material at pH 11 as secondary phases. Overall, brannerite is more resistant to dissolution than UO_2 in both acidic and alkaline solutions, under atmospheric conditions.

Unlike the end-member U-brannerite, the dissolution of Th-brannerite (thorutite) is nearly stoichiometric in the pH 2 solution at 30-70^{o}C. However slight preferential release of U occurs for dilute U(IV) substituted Th-brannerite relative to Th and Ti. Preferential releases of Ca and U occur in dilute U(V) substituted Th-brannerite relative to Th. Uranium behaves similarly in the dissolution process of end-member U-brannerite and dilute U(IV) doped Th-brannerite in that both have a minimum of uranium release rate at pH near 8. Overall, brannerite is less durable in respect of U dissolution rate with dilute U(V) doping than U(IV)doping (except at pH 2) and Th-brannerite is appreciably more durable than its U-counterpart.

A descriptive and predictive model for the rate of uranium release from brannerite as a function of solution pH and total concentration of aqueous carbonate species, in aerated solutions, has been developed. This model accounts for the observed dependence of uranium release rate on pH in an open atmosphere, including the minimum at near-neutral pH. Further, the model can be used quantitatively to give upper limits for uranium release over a range of pH at 40^{o}C, for a variety of experiment types. This study highlights the importance of redox conditions, solution pH and the presence of aqueous (including atmosphere-derived) carbonate species on the release of uranium from brannerite and other materials. The current twostep model could be refined by a study of surface charge and adsorption of ligands and oxygen, as well as the effects of temperature. We envisage that such a model may apply to other uranium-containing materials, *via* a simple re-fitting of parameters to experimental data.

REFERENCES

[1] Y. Zhang, B.S. Thomas, G.R. Lumpkin, M. Blackford, Z. Zhang, M. Colella and Z. Aly, *J. Nucl. Mater.,* 321, 1(2003), 1-7.

[2] Y. Zhang, E. Loi, M. Blackford, T. Mcleod and B. Begg, in: *Scientific Basis for Nuclear Waste Management XXVII.* (V. M. Oversby, L. O. Werme, eds), Materials Research Society, Warrendale, PA (2004), 279-284.

[3] B. Thomas and Y. Zhang, *Radiochimica Acta*, 91, (2003)463-472.

[4] Jostsons, L Vance, B. Ebbinghaus: Immobilization of Surplus Plutonium in Titanate Ceramics. In: *Global '99: Nuclear Technology – Bridging the Millennia* (CD-ROM). American Nuclear Society, La Grange Park, IL (1999).
[5] M. W. A. Stewart, E. R. Vance, A. Jostsons, K. Finnie, R. A. Day, B. B. Ebbinghaus, In: *Scientific Basis for Nuclear Waste Management XXV*. (B. P. McGrail, G. A. Cragnolino, eds.), Materials Research Society, Pittsburgh, PA (2002), pp. JJ11.22.1–JJ11.22.8.
[6] Y. Zhang, K. P. Hart, W. L. Bourcier, R. A. Day, M. Colella, B. Thomas, Z. Aly, A. Jostsons, *J. Nucl. Mater*. 289, (2001), 254.
[7] S. K. Roberts, W. L. Bourcier, H. F. Shaw, *Radiochim. Acta* 88, (2000), 539.
[8] D.E. Grandstaff, *Water-Rock Interaction 1980*, 72.
[9] E.R. Vance, J.N. Watson, M.L. Carter, R.A. Day, G.R. Lumpkin, K.P. Hart, Y.J. Zhang, P.J. McGlinn, M.W.A. Stewart and D.J. Cassidy, *Ceram. Trans*. 107 (2000), 561.
[10] A.E. Ringwood, S.E. Kesson, K.D. Reeve, D.M. Levins, E.J. Ramm, in: W. Lutze, R.C. Ewing (Eds.), Radioactive Waste Forms for the Future, North-Holland, Amsterdam, 1988, 233.
[11] G.R. Lumpkin, K.L. Smith, M.G. Blackford, R Giere and C.T. Williams, *Micron*, 25 (1994), 6, 581-87.
[12] K.G. Knauss, T.J. Wolery, *Geochim. Cosmochim. Acta*, 50 (1986), 2481-2497.
[13] K.S. Finnie, Z. Zhang, E.R. Vance and M. Carter, *J. Nucl. Mater*., 317 (2003), 46-53.
[14] J. de Pablo, I. Casas, J. Giminez, M. Molera, M. Rovira, L. Duro and J. Bruno, *Geochim. Cosmochim. Acta,* 63 (1999), 3097.
[15] L. H. Johnson, D. W. Shoesmith: Spent Fuel. In: *Radioactive Waste Forms for the Future*. (W. Lutze, R. C. Ewing, eds.) Elsevier/North-Holland, Amsterdam (1988), 635–698.

CHEMICAL DURABILITY OF VITRIFIED HIGH-LEVEL WASTE AND SPENT FUEL UNDER SIMULATED REPOSITORY CONDITIONS OF A BOOM CLAY FORMATION

Pierre Van Iseghem, Karel Lemmens, Marc Aertsens, Christelle Cachoir, Diederik Jacques, Véra Pirlet, Sonia Salah, Elie Valcke, Waste & Disposal, SCK•CEN, B-2400 Mol, Belgium

Abstract

The Belgian programme is considering both the closed and open fuel cycle options. In the closed cycle, HLW glasses from the former Eurochemic reprocessing plant and from the French R7T7 plants are studied. R&D is focused on the interaction with the Boom Clay disposal host and potential near field environments. In surface laboratory testing we developed new set-ups to investigate various coupled processes: (1) combined glass leaching / Si diffusion in clay, (2) diffusion/sorption/precipitation of Si in clay, (3) effect of the presaturation of clay with Si, and (4) the mobile concentrations of e.g. Np, Tc, Se in clay slurries after leaching from glass. In the CORALUS *in situ* test, we installed four tubes in the underground laboratory (SCK•CEN site), and retrieved two of them after an interaction time of ~1 year (90°C) and ~3 years (30°C).

The R&D on the geological disposal of spent fuel in Boom Clay is focused on two major issues: (1) study the effect of α-activity on the dissolution of α-doped UO_2 (simulating spent fuel ages between 150 and 90000 years), and (2) study the influence of Boom Clay and potential backfill materials (apatite, cement, sand) on the α-doped UO_2 dissolution rate. Different experimental set-ups have been elaborated. Flow-through tests in clay water and static tests in clay slurries were carried out in reducing conditions.

We report the main results obtained on both HLW glass and doped UO_2. Both HLW glass and UO_2 show a similar evolution of the dissolution behaviour with time in the clay containing media. After an initial relatively fast dissolution characterized by sorption onto the clay, a much lower dissolution rate is observed. For both waste forms this results in expected lifetimes during geological disposal of 10^5 years or more.

Introduction

In Belgium seven nuclear power plants (NPP) are operated, which together generate a total installed capacity of 5.5 GW(e). About 55% of the total electricity need is actually provided by the NPP's. Besides several nuclear facilities are in operation in Belgium, including fuel fabrication, materials research reactors, *etc*. To cope with the long-living and high-level nuclear waste that is generated from the various nuclear activities, already in the late 70's screening studies were initiated by SCK•CEN on the Boom Clay formation as a potential host for that type of waste. The HADES underground research laboratory (URL) in Boom Clay was built in the early

80's at a depth of ~220m. Today this URL infrastructure has been extended with a second shaft, and the total length of the underground gallery is more than 200m now. This URL has enabled to investigate the possibilities to construct underground galleries in Boom Clay at that depth, and to perform various kinds of experiments (mechanical, corrosion, migration, *etc*) in *in situ* conditions. Research was focused on the reference design for geological disposal that was proposed at that time by NIRAS/ONDRAF, the national agency for fissile materials and radioactive waste. This design basically consists of a central stainless steel disposal tube (in which the HLW canisters are inserted), backfilled with a clay/sand mixture. NIRAS/ONDRAF recently completed SAFIR2 (Safety Assessment and Feasibility Interim Report 2), that summarizes the knowledge accumulated over the past ten years [1]. SAFIR2 will serve as a basis for the Belgian government to evaluate the national research, development and demonstration programme on geological disposal on long-living and high-level radioactive waste.

The present situation is that Belgium has to consider both the closed and open fuel cycle, because of a moratorium decided by the Belgian government on future reprocessing. Part of the spent commercial NPP nuclear fuel has been reprocessed and vitrified by COGEMA, and all of the high-level reprocessing waste generated by the former EUROCHEMIC plant has been vitrified. Some 2200 packages (total volume of 241 m^3) PAMELA glass were produced by BELGOPROCESS, to condition the high-level reprocessing waste generated by the former EUROCHEMIC plant. Presently 420 HLW glass packages of 0.18 m^3 have been produced by COGEMA and returned to Belgium, corresponding with the current partial reprocessing option [1]. In total four glass compositions are to be considered: two borosilicate glasses (the R7T7 SON68 and the PAMELA SM513) and two high Al_20_3 (~20 wt%) borosilicate PAMELA glasses SM527 and SM539. Their composition is listed in Table I.

TABLE I. MAIN CONSTITUENTS OF THE HLW GLASSES CONSIDERED IN BELGIUM. SON68 IS THE COGEMA R7T7 REFERENCE GLASS, THE OTHER GLASSES ARE DWK/PAMELA REFERENCE GLASSES.

(wt%)	SON68	SM513	SM527	SM539
SiO_2	45.48	52.15	38.75	35.28
B_2O_3	14.02	13.08	21.70	25.58
Na_2O	9.86	9.05	8.64	9.21
Li_2O	1.98	4.18	3.1	3.49
Al_2O_3	4.91	3.59	19.96	19.83
Ca0	4.04	4.54	3.87	5.05
TiO_2	/	4.54	1.55	0.003
FP oxides	13.38	4.46	1.58	0.96
Balance	6.33	4.41	0.85	0.6

In addition, we investigate the direct disposal of the remaining, unreprocessed spent fuel. The Belgian NPP's will generate over their 40 years of operation some 4160 tHM spent UOX fuel, with burn-ups ranging from 33 to 55 GWd/tHM, and 67 tHM spent MOX fuel with a burn-up of 45 GWd/tHM.

The experimental approach is linked with the assessment of the performance (PA) of the disposal design [2], by providing input data for PA calculations. PA uses in particular the estimations for the glass matrix dissolution rate observed in experiments in conditions relevant for the geological environment. The radionuclide concentrations that are measured in solution in such experiments are taken into account for the selection of 'solubility' (in fact: maximum solution concentrations) limits for radionuclides in PA calculations. The experimental programme further aims to consolidate the scientific basis for the parameter values provided to PA, by interpreting the experimental results in terms of mechanisms, amongst other by modeling.

1. VITRIFIED HIGH-LEVEL WASTE

1.1. Experimental approach

The experiments performed in the period 1998-2004 were mainly a continuation of the earlier programme [3]. The tests were designed for different aims:

- to quantify specific process parameters
- to study coupled processes (glass dissolution/diffusion through clay). Figure 1 shows the experimental set-up of this test.
- to account for new engineered materials
- to account for the temperature during geological disposal (30°C)
- to improve experimental conditions (compared to the previous programme), in particular keeping reducing conditions (other parameters: (pre)saturation of the clay, pressure, presence of humic acids in liquid fraction)
- to obtain information on the soluble fraction of elements leached and the fraction sorbed on solids (clay and other): in case of radionuclide leaching studies, we centrifuged the clay, and ultrafiltered the solution through 100,000 or 10,000 MWCO filters to obtain the soluble RN concentration (10,000 MWCO corresponds with 2 nm particles, considered as the lower limit for mobility in Boom Clay)

The experiments are summarized in Table II. We currently used glass coupons in the tests 2, 4, 5, 6, achieving S/V ratios of ~100 m^{-1}. In case of test 7 we used powdered glass to achieve a high S/V of 2500 m^{-1}. Experiments 4, 5 and 7 were performed on glasses SON68 and SM539, experiments 2 and 6 on glass SON68 only. We studied the leaching behaviour of the following radionuclides: ^{99}Tc, ^{237}Np, ^{79}Se, ^{126}Sn, ^{93}Zr and ^{107}Pd, by doping the glasses with inactive isotopes. These radionuclides are amongst the most critical radionuclides in the performance assessment studies [1]

The general objectives of this R&D are to investigate the long-durability of the glasses in simulated geological disposal conditions (to conclude about the barrier function of the glass) and to identify the release behaviour of the radionuclides

immobilized in the glass. In general terms, we consider Boom Clay as one of the most aggressive media for glass dissolution. This is why, although we selected various media in our R&D on the inactive glasses, including the addition of glass frit, our conclusions can be considered conservative if one would decide to consider other near field (backfilling) materials. As for the radionuclide leaching study our focus was on the most likely backfill material in the reference design.

TABLE II: TYPE OF EXPERIMENTS ON HLW GLASS DURABILITY PERFORMED DURING THE 1998-2004 PROGRAMME

Test no	Description	Main output
1	Influence of silica release on clay characteristics	Silica sorption on clay at high Si concentrations
2	Combined leaching - diffusion test with ^{32}Si doped glass in Boom Clay (30°C, 90°C)	Coupled leaching/diffusion of Si
3	Si sorption characteristics of Boom Clay and FoCa clay (25°C)	Si sorption characteristics of the clays
4	Dissolution in clay at in situ density (30°C, 90°C)	Glass dissolution in contact with Boom Clay or candidate backfill (FoCa clay mixed with glass frit)
5	Dissolution in clay slurries (40°C)	Same as in test no 4, but with analysis of liquid fraction of slurries; effect of addition of glass frit
6	Dissolution of glass doped with ^{99}Tc and ^{237}Np in clay slurry (40°C)	Radionuclide concentration and speciation in near field conditions
7	Dissolution of glass doped with Sn, Se, Pd, Zr in clay slurry (40°C)	Concentration of these critical nuclides in near field conditions

In addition to the laboratory experimental programme we designed the CORALUS *in situ* test, that provides a demonstration in realistic disposal conditions of the results and conclusions of laboratory work. The CORALUS test is conceived as an integrated test, as it involves various coupled processes (glass dissolution/migration through clay; effects of radiation, radiolysis, thermal gradient). An outline of the test is shown in Figure 2. The test includes highly active α-doped SON68 glass samples, clay-based backfill materials exerting a high swelling pressure, contact with the clay host formation, controlled temperature, and presence of γ-radiation. Each module includes glass samples doped with ~0.85 weight% of one of the radionuclides selected ($^{237}NpO_2$, $^{239}PuO_2$, or $^{241}Am_2O_3$) and inactive glass samples. Three modules per CORALUS tube are loaded with different backfill materials: dried Boom Clay (module A), Ca-bentonite mixed with sand and graphite (60/35/5 wt%; module B – a Belgian candidate backfill), and Ca-bentonite mixed with powdered SON68 glass frit (95/5 wt%; module C – a French candidate backfill). The addition of the powdered glass frit aims at establishing high solution concentrations of the main glass constituents (Si, Al, B, Na, Ca, Zr, Li, and Zn), to reduce the chemical potential difference of these elements between glass and interstitial solution, thus

decreasing the glass dissolution rate

The CORALUS *in situ* tests comprise four modular test tubes, placed in the Boom Clay in the underground research facility (URF) HADES (Mol, Belgium), for durations up to 10 years. Two tubes are operated at 30°C and do not include γ-sources, and are running for 3.3 and 10 years, respectively. They simulate the long-term during geological disposal, after the thermal phase, and advanced corrosion of the overpack and canister. The two other tubes are operated at 90°C and include γ-sources, and run for 1.2 and 6 years, respectively. They simulate an early failure scenario, ~50 years after disposal.

A complete report and discussion of the experimental details and results of these programmes can be found in [4-11]. Results of analytical and geochemical odeling [12-14] are not discussed in this report.

1.2. Laboratory tests on inactive glass

We report some results of tests 2 and 4. Figure 3 presents mass loss data for glass SON68 (both the inactive and the ^{32}Si-doped glass) in Boom Clay at *in situ* density at 30°C. Figure 4 shows the experimental and fitted ^{32}Si-profile in the clay after 887 days at 30°C.

In test 4, the dissolution rate at 30°C based on the mass losses is constant during the first year at ~0.01 $g.m^{-2}.day^{-1}$, and is slightly decreasing afterwards (less than a factor of two) – see Figure 3. By pre-saturating clay with glass frit, we also attempt to obtain glass dissolution data for the very long-term, when the clay will be saturated with respect to silica. These tests were done in clay slurries, by pre-saturating the clay for ~8 months (~5 mg silica immobilized per g clay). Glass dissolution rates in pre-saturated clay were in the order 10^{-4} to 10^{-5} $g.m^{-2}.day^{-1}$ (40°C; solution pH over the entire duration is between 8.5 – 9.0). Such low dissolution rates would result in glass package lifetimes upon contact with the geological environment of more than 10^6 years, so we can conclude that the vitrified waste will probably be a good barrier for radionuclide release (more detailed estimations of the lifetime of glass packages in geological disposal would also require to account for the increased surface area due to cracking of the glass). Our interpretation of these tests compared with the current state-of-the-art (for instance, see [15,16]) is that (a) the diffusion of silica in the clay at low temperature is relatively well understood and can be coupled to glass dissolution for simple cases (constant dissolution rate, no precipitation), but the validity of the coupling with the first order rate remains to be demonstrated, and (b) the dissolution rate measured in the pre-saturated clay slurries might correspond with the long-term ("residual") dissolution rate. Further evidence and understanding is needed.

Dissolution rates of glass SM539 in the tests discussed here are usually about the same as for glass SON68. For both glasses we have not observed any resumption of the dissolution rate in the "final dissolution" stage reported above (tests at low temperature - 30°C or 40°C). Such resumption would have suggested that secondary phases are formed once saturation of the solution is achieved, causing this enhanced dissolution.

In test 2 the results of mass loss are in agreement with those from test 4 (conditions are similar; see Figure 3), but in addition ^{32}Si diffusion profiles through

the clay are obtained. The interest of this test is mainly that we were able to interpret the coupled process of glass dissolution/Si migration through clay with existing models for the "simple" systems. The first order glass dissolution rate law was used for glass dissolution, with the dissolution rate determined by a silica concentration in solution at the glass/clay interface of 15 to 21 mg/l. A diffusion equation was used to calculate the ^{32}Si profile in the clay in contact with the glass.

1.3 Laboratory tests on doped glass

We report some results of tests 6 and 7. The leaching behaviour of Np and Tc in a FoCa clay slurry (simulating a candidate backfill) was particularly sensitive to the redox condition of the medium. When appropriate reducing conditions were achieved (Eh about -200mV, similar as in real Boom Clay) Np and Tc reduced from V, resp VII valence (in the glass) to IV (both Np and Tc) valence state. The Np and Tc concentrations in solution (ultrafiltered through 100,000 MWCO filter) were nearly constant during the two years leach test, and were extremely low. Their average values are given in Table III (see "near field"). One can observe that these values are much lower than the solubilities obtained from percolation migration tests ("far-field" values) [1] and the solubility as calculated from the existing thermodynamic database (fourth column). In the last column it can be seen that performance assessment is very conservative in selecting radionuclide solubilities from the R&D programmes, keeping large safety margins. Some of the questions are whether the RN concentrations measured in our tests correspond to the thermodynamicaly stable values, or whether the solubility limiting phase predicted is really the right one.

TABLE III: COMPARISON OF THE NEAR-FIELD CONCENTRATIONS OBTAINED FROM OUR LEACH TESTS WITH THE FAR-FIELD CONCENTRATIONS

(Mol/l)	[RN] near-field	[RN] far-field	Solubility limiting solid phase	Best estimate PA (values)
^{237}Np	$1.5x10^{-10}$	$6.7x10^{-10}$	$Np(OH)_4$ ($5x10^{-9}$M)	10^{-6}
^{99}Tc	$5.6x10^{-10}$	10^{-8}	$TcO(OH)_2$ (10^{-8}M)	$3x10^{-8}$

The leaching behaviour of ^{79}Se, ^{126}Sn, ^{93}Zr and ^{107}Pd from glass in near-field clay media was investigated by melting inactive isotopes in the glass. Their leaching behaviour was recorded by ICP-MS, after substracting their concentration in the blank. In fact, their concentrations in solution (after ultrafiltration) were hardly above the corresponding background concentrations, and they were nearly constant with time (two years test). We conclude that their soluble concentrations are very low. We compare them with the concentrations obtained from percolation migration tests (far field medium) – see Table IV [16]. The Se leaching behaviour appears to be puzzling, because of its complex chemistry: in our work Se is probably VI-valent (selenate SeO_4^{2-}), corresponding to its oxidation state in the glass. But most studies on Se behaviour in the far field assume Se to be in its reduced form (selenite, SeO_3^{2-} , or

other forms such as $FeSe_2$, FeSe, Se – [17]), where Se has much lower solubility. The reduction kinetics of Se (VI) is not really known, but appears to be slow.

Therefore our work suggests that the geochemistry of Se should be better characterized. For all radionuclides studied here, we recommend that the "long-term" soluble concentrations in the near field should be better characterized (value, speciation).

TABLE IV: COMPARISON OF THE NEAR-FIELD CONCENTRATIONS OBTAINED FROM OUR LEACH TESTS WITH THE FAR-FIELD CONCENTRATIONS

Element	[RN] (near-field)	[RN] (far-field)	Solubility limiting solid phase	[RN] best estimate PA
Se	$2.5x10^{-7}$	$5x10^{-9}$ ($2.4x10^{-8}$ in the Boom Clay water)	Se (cr)	$5.5x10^{-8}$
Zr	$5.5x10^{-9}$		ZrO_2, $ZrSiO_4$	$6x10^{-7}$
Pd	$9.4x10^{-9}$	$2x10^{-8}$	$Pd(OH)_2$, Pd	10^{-7}
Sn	$4.2x10^{-9}$		SnO_2,$Sn(OH)_4$	$3x10^{-5}$

1.4 In situ tests

The four CORALUS tubes have been installed by the latest end of 2003. The interstitial solutions of the three backfill materials have been regularly analyzed chemically (anions, cations, organic constituents, dissolved gas, pH-Eh). The first duration at each temperature condition has been stopped, and the glass and clay (radionuclide migration, mineralogy) samples analyzed. Analysis and interpretation is still in progress. We show some radionuclide migration profiles through the clay in Figure 5.

Many of the glass samples were broken after retrieval and analysis. We believe that this is because of test concept reasons (pressure gradient between outer and inner side of the (thin) glass sample), rather than due to intrinsic glass failure. The main conclusions on the glass dissolution and radionuclide migration so far are:

1. The results compare fairly well with the surface laboratory test results for the same conditions in undisturbed Boom Clay. The SON68 mass losses in module A (with dried Boom Clay backfill) compare well with the mass losses in laboratory test no 4 (see above): 0.01 g/m²/day at 30°C, and 0.3–0.5 g/m²/day at 90°C, but without γ

irradiation. The alteration at 90 °C is considerably higher than at 30 °C. We measure differences in mass loss by a factor of 20.
2. The addition of powdered glass frit to the backfill material has a beneficial effect: it diminishes the glass alteration considerably, probably with about two orders of magnitude, or even more.
3. The α-doped glasses behave rather similarly as the inactive ones. We observe slightly thicker alteration layers for the active samples, the thickness seems to increase with increasing αβγ-activity of the samples. Because of the lack of sufficient mass loss data, we cannot conclude that this goes along with an increased mass loss.
4. The order of radionuclide activity at the interface glass/clay is: Dried Boom Clay > Bentonite with sand and graphite > Bentonite with glass frit, in agreement with the different degree of alteration of the glass in the different backfill materials. The radioactivity migrated in the backfills drops very sharply over the first few mm of clay, demonstrating the strong retardation of the radionuclide migration.
5. The migration distance of Am is longer than for Np (and Pu). We attribute this to colloid migration in case of Am, as Am is forming soluble complexes with the humic acids present in Boom Clay. Further interpretation of the migration profiles based on migration processes in undisturbed clay is impossible, because in CORALUS processes are too complex (different radionuclide source, clay was partially disturbed, *etc*).

2. SPENT FUEL

2.1. Experimental approach

The first project on spent fuel dissolution at SCK•CEN started in 1996, and studied the dissolution kinetics and solubility of UO_2 in clay waters. The results showed the importance of pre-dissolving the oxidized UO_2 surface, and the effect of carbonates and humic acids in the water on the U-solubility [18]. Here, we discuss the second project, that aims to get more insight into Boom Clay/spent fuel interaction processes. Therefore static dissolution tests with α-doped UO_2 were performed, followed by sequential extraction experiments. The main objectives of the static dissolution experiments were to determine the dissolution rate of UO_2 in Boom Clay conditions, and to study the effect of α-activity on the dissolution kinetics of UO_2 , to verify the predicted increase of the UO_2 dissolution rate with increasing α-radiolysis [19]. The aim of the sequential extraction experiments was to gain a mechanistic understanding of the U retention/migration mechanisms and to study U partitioning/ fractionation occurring during UO_2 dissolution.

R&D on spent fuel will be considered only in a later stage, as we first want to identify and understand the basic processes of the unirradiated UO_2 matrix. It may be obvious that the dissolution behaviour of "real" spent fuel may be different from unirradiated (doped) UO_2 , because of the presence of fission products and transuranics, potential heterogeneities, *etc.*

We conceived the experimental programme as to determine the UO_2 dissolution behaviour over very long timescales, in as realistic as possible environments. We therefore used α-doped UO_2 (manufactured via the sol-gel process at the ITU) with varying amounts of ^{238}Pu (to generate the α-dose) and ^{233}U (corrosion indicator). The maximum fuel age simulated was 90,000 years after disposal for a PWR fuel with a

burn-up of 45 or 55 GWd · tHM^{-1}. We selected three reference media simulating different periods during the geological disposal: "STM" (short term medium), "MTM" (medium term medium) and "LTM" (long term medium). Table V shows more details on these media, together with the kinds of α-doped UO_2 samples used. The dissolution tests were performed in a glove box under anoxic conditions (Ar/0.4%CO_2 atmosphere). The conditions within the tests were made reducing by the addition of iron. The experimental concept is shown in Figure 6.

TABLE V. DESCRIPTION OF THE α-DOPED UO_2 AND COMPOSITION OF THE DIFFERENT MEDIA

uel	uel age	l ded (wt%) Ad ^{233}U	ed (wt%) Add ^{238}Pu	α-activity UO_2] [Bq/g	edium M	Medium composition
1	50	1 4.2 $0 \cdot 10^{-1}$	10^{-2} 3.85 ·	10^{8} 2.45 ·	TM S	BC, BCW, SS, Zr, BCW, pyrite, Fe
2	000	2 4.2 $2 \cdot 10^{-1}$	10^{-3} 5.52 ·	10^{7} 3.64 ·	TM M	BC, BCW, SS, FeOOH, Zr, ZrO_2, pyrite, Fe
3	000	7 4.2 $0 \cdot 10^{-1}$	10^{-3} 3.19 ·	10^{7} 2.17 ·	TM M	BC, BCW, SS, FeOOH, Zr, ZrO_2, pyrite, Fe
4	1000	1 4.2 $2 \cdot 10^{-1}$	10^{-3} 2.49 ·	10^{7} 1.72 ·	TM M	BC, BCW, SS, FeOOH, Zr, ZrO_2, pyrite, Fe
6	9000	8 4.3 $3 \cdot 10^{-1}$	10^{-5} 1.34 ·	10^{6} 1.62 ·	TM L	BC, BCW, pyrite, Fe

BC: Boom Clay, BCW: Boom Clay water, SS: stainless steel, Zr,: Zircaloy-4

The sequential extraction experiments consisted of five operationally well-defined extraction steps, in order to successively extract the amount of uranium from Boom Clay samples associated to (1) the exchangeable fraction, (2) the carbonate-bound fraction, (3) amorphous Si-, Al- and Fe-(oxihydr)oxides, (4) organic matter, and (5) well crystallized Fe-(oxihydr)oxides. The experiments were performed on "unreacted" Boom Clay (main component of the different media used in the leach tests) as well as on two Boom Clay samples having been in contact with α-doped UO_2 (F2 and F6) for 720 days ("reacted" BC).

Details of the experimental approach, and full description of the experimental results can be found in [20,21]

2.2. Results

The dissolution behavior of the α-doped uranium oxides is characterized by an average initial dissolution rate of ~263 $\mu g \cdot m^{-2} \cdot d^{-1}$ and an average "longer-term" rate (between 181 and 720 days) of ~7 $\mu g \cdot m^{-2} \cdot d^{-1}$. The latter rate is obtained by linear regression of the data between 181 and 720 days. Figure 7 shows dissolution rates calculated over the entire test duration. Taking into account the experimental/analytical uncertainties, no definite statement concerning the "longer-term" rate can be made, meaning whether dissolution is really still ongoing or the rate being already close to zero. No influence of α-activity on the dissolution rates of the fuels was observed. The rapid initial rate on the one hand is explained by the dissolution of a surface layer of the composition $UO_{2.3333}$ and on the other hand by the high adsorption capacity of the Boom Clay. As suggested by the geochemical calculations, uranyl-ions released from the surface layer into solution will mainly form uranyl-tri-carbonate complexes $[UO_2(CO_3)_3^{4-}]$, which are supposed to be subsequently and preferentially adsorbed onto the octahedral edge sites of smectites in the clay. Saturation of these sites could then be the reason for the rapid decrease of the

dissolution rate after 90 days. Another possible mechanism impeding further oxidative dissolution of the fuel/surface layer could also be an interaction of humic acids with oxidizing radiolysis species. Concerning aqueous uranium, no solid/crystalline U-phase was determined to control the measured U-concentrations in solution over time. This suggests that no steady state of the system has been achieved, and that the "longer-term" rate may be close, but not yet equal to zero.

Results of the sequential extraction experiments have shown that organic matter may play an increasing role for U-retention at longer time periods, which seems to be consistent with the fact that U is preferentially associated to the colloidal fraction. This suggests that flocculation / precipitation of U together with these colloids - after reestablishment of the reducing conditions – seems to occur and is able to explain the U/organic matter association at the end of the experimental period.

3. CONCLUSIONS

We have achieved a considerable progress in identifying the long-term dissolution rate and radionuclide release for both HLW glass and spent fuel (simulated by α-doped UO_2), ànd in identifying the underlying processes, in media simulating a geological disposal in Boom Clay, or in clay based backfill materials. In case of HLW glass we used S/V (surface to volume), thermal activation and pre-saturation of the solution with silica to obtain "long-term" data. In case of UO_2 we used as well S/V (by using UO_2 powder) and α-doping (to obtain different ageing periods up to 90,000 years) to obtain long-term data. We also spent particular attention to the experimental conditions, by taking care amongst other to reproduce the redox conditions and chemical composition of the clay waters.

Our experience with HLW glass and UO_2 is that both exhibit quite similar dissolution behaviours in clay containing media. We therefore present the main conclusions of our past R&D programme jointly for both waste forms.

Both glass and UO_2 exhibit very small "long-term" dissolution rates in clay containing media, orders of magnitude lower than the initial values. Both waste forms will have lifetimes of 10^5 years and more in the expected disposal conditions of a Boom Clay formation, and will probably perform as a good barrier.

During this and previous R&D programmes we made strong progress in identifying the major dissolution processes of HLW glass and UO_2 in clay containing media: forward dissolution, the sorption effect of clay, the importance of saturation of the solution (silica in case of glass, Uranium in case of UO_2). The presence of clay clearly induces an enhanced dissolution of both waste forms, but once the clay (and other solids) become saturated with respect to sorption a "final" or "long-term" dissolution rate is observed, up to several orders of magnitude lower than the initial "forward" dissolution rate. We have unsufficient evidence whether this long-term rate is constant or not with time, and yet the process controlling this rate must be identified.

We spent large attention to the leaching behaviour of the most important radionuclides (U, Np, Tc, Se, Sn, Pd, Zr), and identified RN concentrations in the solutions simulating the near field environment. These concentrations (mobile, corresponding to a few nm size) were quite constant with time. We did not perform a

complete speciation of the RN complexes that control these RN concentrations, and we are neither sure that they are equilibrium concentrations.

Strong attention was given to investigating the dissolution behaviour of both HLW glass and UO_2 in as realistic as possible conditions, both in laboratory test conditions and *in situ* (the CORALUS test). Here, many processes (dissolution, migration, sorption, radiolysis, thermal gradient, *etc*) may occur simultaneously. Our laboratory conducted integrated "coupled" tests were quite comprehensively interpreted, also by modelling. The first results of the CORALUS test were obtained, and interpretation is underway.

Overall, one of the largest challenges appears to be the determination of the "long-term" of the dissolution behaviour of both HLW glass and UO_2. We made progress on how to determine this long-term behaviour, *e.g*. by pre-saturating the clay with silica in case of glass dissolution, or by preparing aged UO_2 samples and using media simulating different "ages". A better "calibration" of these long-term dissolution rates in relation to the geological disposal times is still needed, and the underlying processes should be identified. The establishment of an experimental protocol (that may include complementary approaches and methods) to determine the long-term dissolution rate (HLW glass, UO_2) is of a strong interest, in addition. An international effort on this subject would be very relevant and beneficial.

Acknowledgements

We acknowledge the financial support of NIRAS/ONDRAF (the Belgian Agency for Radioactive Waste and Fissile Materials Management) and of the European Commission for most of the projects reported, and the cooperation of many colleagues within SCK•CEN within the projects reported.

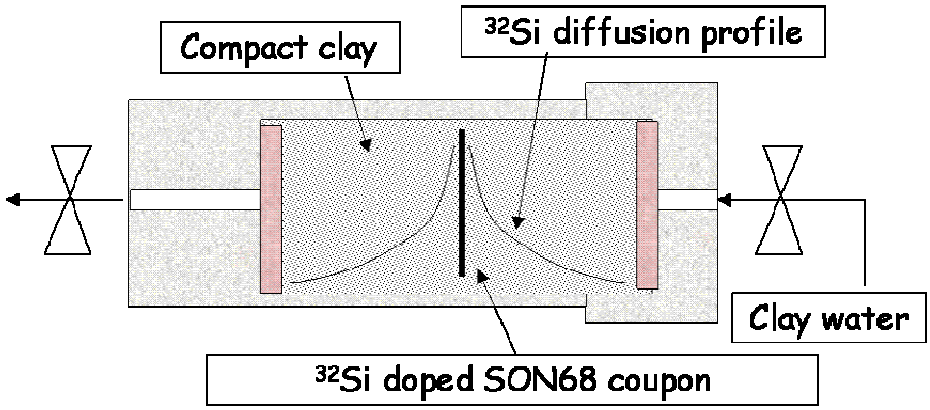

FIG. 1*: Experimental set-up to measure both glass dissolution and silica diffusion in one single experiment*

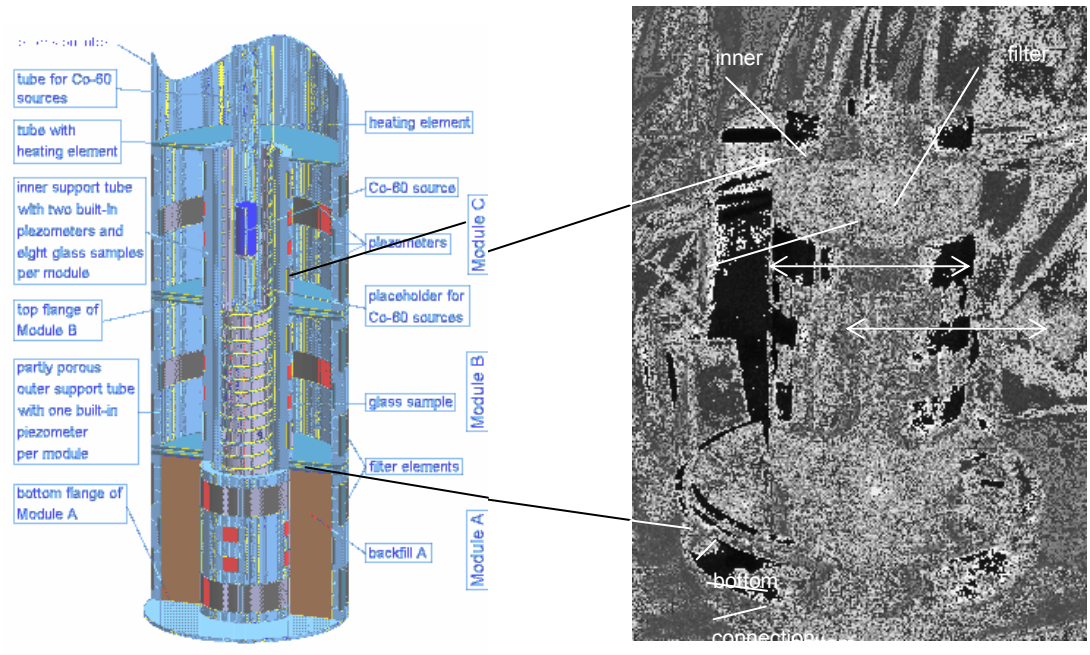

FIG. 2 *(left) Three-dimensional cut-away view of a test tube with ^{60}Co sources. (right) Inner support tube, bottom flange, and connection flange of one module. The photo shows the position of the samples (SON68 and other glass types, and container materials) on the inner support tube and on the flange, and the filter screens and connecting tubes of the inner piezometers (in grey).*

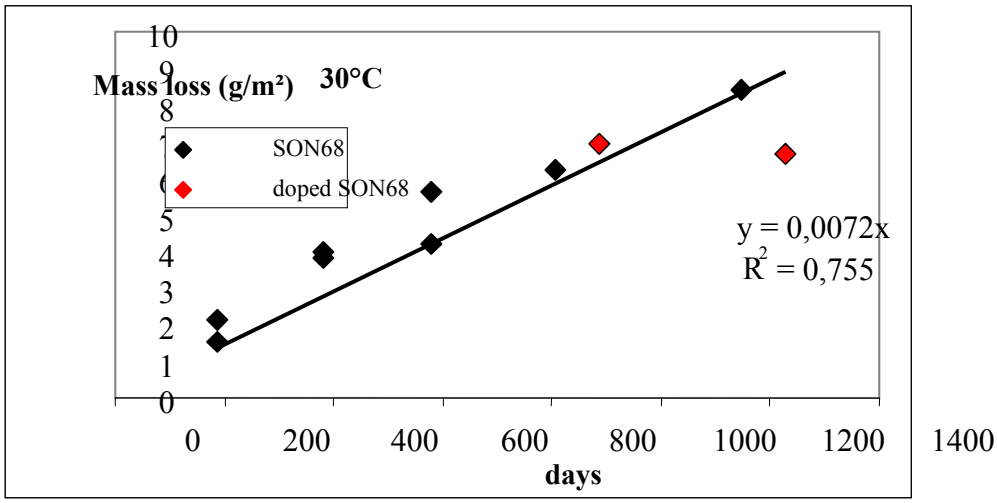

FIG. 3. *Mass losses of the doped and undoped glass in Boom Clay at 30°C*

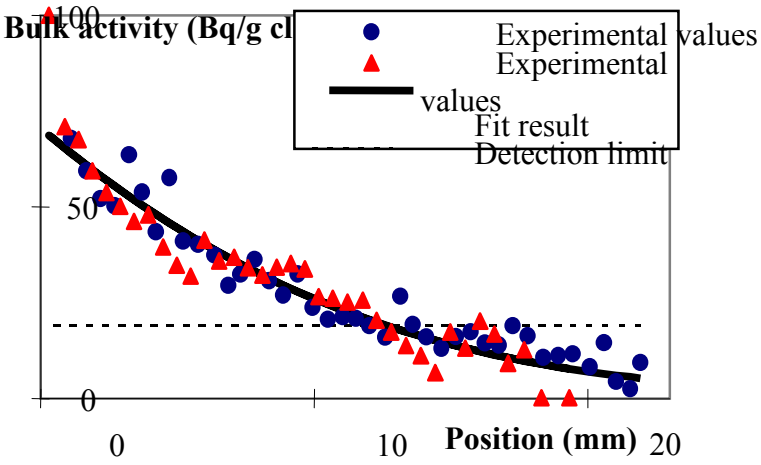

FIG. 4. *Experimental and fitted* ^{32}*Si diffusion profile in the clay after 887 days at 30°C.*

The experimental values of the right and left profile are similar.

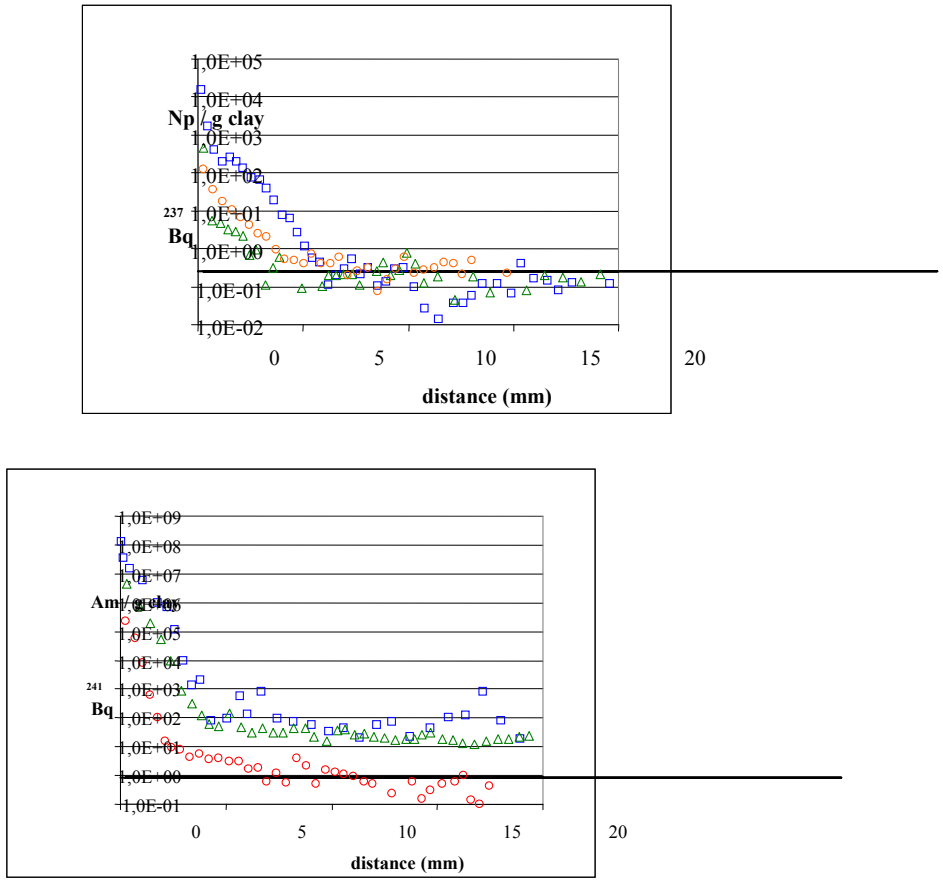

FIG. 5 *Radionuclide migration profiles for Np (left) and Am (right) for the CORALUS test at 90°C, 15 months, including* ^{60}*Co sources. (□) dried Boom Clay, (Δ) Ca-bentonite mixed with sand and graphite, (○) Ca-bentonite mixed with powdered SON68 glass frit*

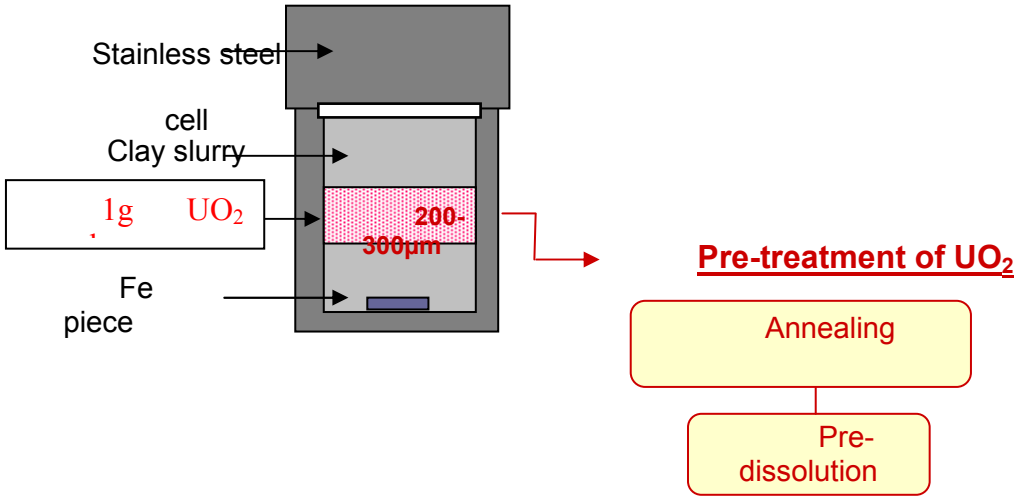

FIG. 6 *Experimental approach of the static dissolution tests on doped UO_2. The tests are done at 25-30°C, in an Ar/0.4% CO2 atmosphere, for test durations between 90-720 days. Pre-dissolution is done in synthetic Boom Clay water (SBCW).*

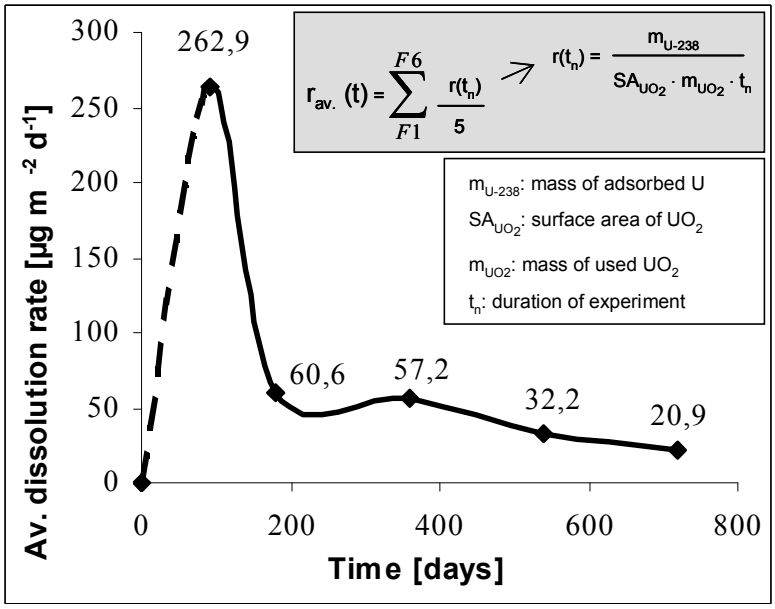

FIG. 7. *Average (of all α-doped UO_2) dissolution rate versus time for ^{238}U*

References

[1]. SAFIR 2. Safety Assessment and Feasibility Interim Report 2. NIROND 2001-06 E (2001). Published by NIRAS/ONDRAF

[2]. J. Marivoet, X. Sillen, D. Mallants, P. De Preter. "Performance assessment of geological disposal of high-level radioactive waste in a plastic clay formation". Mat. Res. Soc. Symp. Proc. Vol 713 (2002). 189-200

[3]. P. Van Iseghem, M. Aertsens, K. Lemmens, P. Lolivier, V. Pirlet, E. Valcke, Wei Jiang "Long-term behaviour of high-level waste forms in clay repository conditions" Final report for IAEA agreement No 6795/CF, 1997

[4]. Lemmens K., Aertsens M., "Validation of glass dissolution and Si diffusion parameters with a combined glass dissolution-diffusion experiment in Boom Clay", 329-336. Scientific Basis for Nuclear Waste Management XXIX, Mat. Res. Soc. Symp. Proc. Vol 932, Ed P. Van Iseghem, 2006

[5]. K. Lemmens, M. Aertsens, V. Pirlet, N. Maes, H. Moors, P. Van Iseghem, "Measurement of glass corrosion in Boom Clay disposal conditions : first results of the experimental programme 2000-2003 of SCK•CEN". ICEM'03 Conference, September 21-25, Oxford (U.K.)

[6]. K. Lemmens, M. Aertsens, P. Lolivier, N. Malengreau, V. Pirlet, P. de Cannière, P. Van Iseghem. "Characterization and compatibility with the disposal medium of Cogema and Eurochemic reprocessing waste forms". Final report for the period 1996-2000 with NIRAS/ONDRAF. R-3644, 2002.

[7]. K. Lemmens, M. Aertsens, P. De Cannière, P. Van Iseghem, R.Gens, "The corrosion of nuclear waste glasses in a clay environment: mechanisms and modelling". Final report for the programme 1990-1994 with the EC. EUR 17102, 1997

[8]. V. Pirlet, K. Lemmens, P Van Iseghem, "Influence of the near-field conditions on the mobile concentrations of Np and Tc leached out from vitrified HLW". Scientific Basis for Nuclear Waste Management XXVIII, Mat. Res. Soc. Symp. Proc. Vol 824, Eds J. Hanchar, S. Stroes-Gascoyne, L. Browning, 2004, 385-390.

[9]. Valcke E., Smets S., Labat S., Peeters J., Boven P., Thomas P., Dupuis E., Van Iseghem P., Godon N., Jollivet P., Parisot G., Jockwer N. and Wieczorek K. "CORALUS: an integrated *in situ* corrosion test on alpha-active HLW glass", Scientific Basis for Nuclear Waste Management XXIX, Mat. Res. Soc. Symp. Proc. Vol 932, Ed P. Van Iseghem, 2006, 67-78

[10]. Valcke E., Van Iseghem P., Gysemans M., Van Bree P., Moors H., Godon N. and Jollivet P. "Leaching and migration of Np, Pu and Am from α-doped SON68 HLW glass in contact with dense clay", Scientific Basis for Nuclear Waste Management XXIX, Mat. Res. Soc. Symp. Proc. Vol 932, Ed P. Van Iseghem, 2006, 999-1007

[11]. E. Valcke, P. Van Iseghem, S. Smets, S. Labat, N. Godon, N. Jockwer, K. Wieczorek, "CORALUS. An integrated *in situ* test on α-active HLW glass". Final Report 1997-2000 to the EC. R-3494 (2001)

[12]. Jacques D., Lemmens K., "Obtaining solubility constants to describe the incongruent dissolution of SON68 waste glass by an equilibrium ideal solid solution model approach". Scientific Basis for Nuclear Waste Management XXIX, Mat. Res. Soc. Symp. Proc. Vol 932, Ed P. Van Iseghem, 2006, 337-344

[13]. M. Aertsens, K. Lemmens, P. Van Iseghem, “Fitting element profiles for predicting glass dissolution rates in synthetic interstitial claywater”. Mat. Res. Soc. Symp. Proc. Vol 757, Eds R. Finch and D. Bullen, 167-174 (2003)
[14]. M. Aertsens, P. Van Iseghem, "Estimating the life time of a glass container in clay", TOPSEAL '99- Commitment to the future environment. (Antwerp, Belgium, 10-14.10.99). Ed. Belgian Nuclear Society, 1999, ISBN 3-9520691-4-0, Vol II, 339-343
[15]. P. Van Iseghem, M. Aertsens, S. Gin, D. Deneele, B. Grambow, P. McGrail, D. Strachan, G. Wicks. "GLAMOR - A critical evaluation of the dissolution mechanisms of high level waste glasses in conditions of relevance for geological disposal". Final Report to the EC, to be published.
[16]. I. Ribet et al, "GLASTAB – Long term behaviour of glass: improving the glass source term and substantiating the basic hypotheses". Final Report to the EC, to be published.
[17]. N. Maes et al, "Migration Case Study: Transport of radionuclides in a reducing Clay Sediment (TRANCOM-II)". Final report of the EC project TRANCOM-II. BLG-988 (2004)
[18]. C. Cachoir, K. Lemmens, S. Van den Berghe, P. Van Iseghem, "UO_2 dissolution in Boom Clay conditions". Journal of Nuclear Materials 321 (2003), 49-59
[19]. S. Sunder and D. Shoesmith, "Chemistry of UO_2 fuel dissolution in relation to the disposal of used nuclear fuel". AECL-10395 (1991)
[20]. Salah S., Cachoir C., Lemmens K., Maes N., "Static dissolution tests of □-doped UO_2 under repository relevant conditions: Influence of Boom Clay and □-activity on fuel dissolution rates", Scientific Basis for Nuclear Waste Management XXIX, Mat. Res. Soc. Symp. Proc. Vol 932, Ed P. Van Iseghem, 2006, 481-488
[21]. C. Cachoir, K. Lemmens, "Static dissolution of □-doped UO_2 in Boom Clay conditions: Preliminary results". Scientific Basis for Nuclear Waste Management XXVII, Mat. Res. Soc. Symp. Proc. Vol . 807 (2004), Eds V. Oversby and L. Werme, 59-64.

Additional literature

Scientific Basis for Nuclear Waste Management XXIX, Mat. Res. Soc. Symp. Proc. Vol 932, Ed P. Van Iseghem, 2006

1. Gonzales J. L. and Van Iseghem P . "IAEA's Coordinated Research Programmes on Performance of High Level Wastes in Deep Geological Repositories", 33-42
2. P. Van Iseghem, K. Lemmens, M. Aertsens, S. Gin, I. Ribet, B. Grambow, J.L.Crovisier, M. Del Nero, E. Curti, B. Schwyn, B. Luckscheiter. "Chemical durability of high-level waste glass in repository environment: main conclusions and remaining uncertainties from the GLASTAB and GLAMOR projects", 293-304
3. Aertsens M., "An overview of simple basic equations used in HLW glass dissolution modelling: consequences for long term leaching and element profiles", 401-410

Euradwaste ’04. "Radioactive waste management Community - Policy and research initiatives". Ed. C. Davies, 2004, EUR 21027

1. I. Ribet, P. Van Iseghem, E. Valcke, J-L Crovisier, E. Curti, M. Del Nero, B. Grambow, B. Luckscheiter, K. Lemmens, B. Schwyn, “GLASTAB, CORALUS II, GLAMOR Projects: Long-term behaviour studies of vitrified high-level waste”, 161-172

2. P. Van Iseghem, M. Aertsens, S. Gin, D. Deneele, B. Grambow, P. McGrail, D. Strachan, G. Wicks, T. McMenamin, “GLAMOR. A critical evaluation of the dissolution mechanisms of high-level waste glasses in conditions of relevance for geological disposal”, 381-386
3. E. Valcke, S. Smets, S. Labat, P. Van Iseghem, N Godon, P. Jollivet, N. Jockwer, K. Wieczorek, “CORALUS : an integrated *in situ* corrosion test on α-active HLW glass”, 387-392

P. Van Iseghem, K. Lemmens, V. Pirlet, “Assessment of the compatibility of vitrified high-level waste with geological disposal in a Boom Clay formation: remaining uncertainties”. In Radioactive Waste Products – RADWAP 2002, Proceedings of an International Seminar, Eds R. Odoj, J. Baier, P. Brennecke and K. Kühn, 229-235 (2003).

P. Van Iseghem, B. Kursten, E. Valcke, H. Serra and J. Fays, "In situ testing of waste forms and container materials: contribution to the identification of their long-term behaviour". In

Prediction of Long Term Corrosion Behaviour in Nuclear Waste Systems. European Federation of Corrosion Publications Nr 36, Ed D. Féron and D.D. Macdonald, 2002, 36-48.

Glass in its Disposal Environment. Proceedings of the International Workshop on Glass in its Disposal Environment, Bruges (Belgium), April 11-14, 2000. Journal of Nuclear Materials, Vol 298 (2001), Nos 1,2.. Guest Editor P. Van Iseghem.

1. K. Lemmens, "The effect of clay on the dissolution of nuclear waste glass", 11-18
2. M. Aertsens and D. Ghaleb, "New techniques for modelling glass dissolution", 37-46
3. V. Pirlet, "Overview of actinides (Np, Pu, Am) and Tc release from waste glasses: influence of solution composition", 47-54
4. P. Van Iseghem, E. Valcke and A. Lodding, "*In situ* testing of the chemical durability of vitrified high-level waste in a Boom Clay formation in Belgium: discussion of recent data and concept of a new test", 86-94
5. A. Lodding and P. Van Iseghem, "In depth distributions of elements in leached layers on two HLW waste glasses after burial in clay: step-scan by SIMS", 197-202

K. Lemmens, M. Aertsens, V. Pirlet, H. Serra, E. Valcke, P. De Cannière, P. Van Iseghem, "Measurement of glass corrosion in Boom Clay disposal conditions" *8th International Conference on Radioactive Waste Management and Environmental Remediation* (ICEM'01), September 30 – October 4, 2001, Bruges (Belgium). Proceedings published on CF-Rom by ASME,

V. Pirlet, K. Lemmens, P. Van Iseghem, "Leaching of Np and Tc from doped nuclear waste glasses in clay media: the effects of redox conditions". Scientific Basis for Nuclear Waste Management XXV, Mat. Res. Soc. Symp. Proc. Vol 713, Eds P McGrail and G. Cragnolino, 2002, 563-570

K. Lemmens and P. Van Iseghem, "The effect of gamma radiation on the dissolution of high-level waste glass in Boom Clay". Scientific Basis for Nuclear Waste Management XXIV, Mat. Res. Soc. Symp. Proc. Vol 663, Ed. K. Hart, G. Lumpkin, 2001, 227-236

E. Valcke, P. Van Iseghem, S. Smets, S. Labat, N. Godon, N. Jockwer, K. Wieczorek. "An integrated *in situ* corrosion test on α-active HLW glass". EUR 19795 (2001)

L. Noynaert et al. "Heat and radiation effects on the near field of a HLW or spent fuel repository in a clay formation (CERBERUS project)". Final report. EUR 19125 (2000)

EURADWASTE '99, Radioactive Waste Management Strategies and Issues. EUR 19143, 2000, Ed. C. Davies.

1. K. Lemmens, V. Pirlet, M. Aertsens, N. Malengreau, P. De Cannière, P. Van Iseghem, "Experimental and modelling studies to formulate a nuclear waste glass source term in representative geological disposal conditions", 403-406
2. K. Lemmens, C. Cachoir, P. Van Iseghem, "Research related to the direct disposal of spent fuel at SCK•CEN", 411-414
3. E. Valcke, P. Van Iseghem, N. Godon, N. Jockwer, "CORALUS: an integrated in situ corrosion test on α-active HLW glass", 427-430
4. L. Noynaert, P. De Cannière, B. Kurten, D. De Bruyn, P. Van Iseghem, G. Volckaert, C. Beaucaire, H. Pitsch, A. Bouchet, *et al*, "Study of the effect of heat and radiation on the near field of a HLW or spent fuel repository in clay – the CERBERUS project

A. Lodding, P. Van Iseghem, L. Werme, "Progress of corrosion and element kinetics of HLW glasses in geological burial: evaluation by SIMS". In Surface-Active Processes in Materials, Ceramic Transactions, vol 101, 2000 (Publ. The American Ceramic Society), 123-139

T. Advocat, P. Jollivet, Y. Minet, B. Luckscheiter, B. Grambow, R. Gens, K. Lemmens, P. Van Iseghem, M. Aertsens, V. Pirlet, E. Curti, "Experimental and modelling studies to formulate a nuclear waste glass source term in representative geological disposal conditions", Final Report, EUR 19120, 1999

C. Moulin, Jiang Wei, P. Van Iseghem, I. Laszak, G. Plancque, V. Moulin, "Europium complexes investigation in natural waters by Time-Resolved Laser-Induced Fluorescence". Analytica Chimica Acta Vol 396 (1999), 253-261

P. Van Iseghem, M. Aertsens, K. Lemmens, N. Malengreau, V. Pirlet, E. Valcke, "The long-term stability of nuclear waste glass in geological disposal conditions- the Belgian approach" Glass Science and Technology for the 21th Century, 21-24.06.99, Prague (Czech Republic)

P. Van Iseghem, E. Valcke, B. Kursten, A. Lodding, "In situ testing of the chemical durability of vitrified high-level waste in a Boom Formation in Belgium: the effect of gamma radiation"

7th Int. Conference on Radioactive Waste Management and Environmental Remediation (ICEM 99), 26-30.09.99, Nagoya (Japan)

Scientific Basis for Nuclear Waste Management XXII, Mat. Res. Soc. Symp. Proc. Vol 556, Mat. Res. Soc. Publ., Eds. D.J. Wronkiewitz and J.H. Lee, 1999

1. V. Pirlet, P. Van Iseghem, A. Dierckx, C. Marquardt, "The investigation of the Np complexes formed upon interaction of high level waste glass and Boom Clay media", 993-1000
2. K. Lemmens, C. Cachoir, P. Van Iseghem, "Static dissolution of UO_2 in interstitial Boom Clay water", 1009-1016

V. Pirlet, P. Van Iseghem, A. Dierckx, J.-F. Desreux, "The investigation of the Neptunium complexes formed upon interaction of high-level waste glass and Boom Clay media". Journal of Alloys and Compounds 271-273 (1998), 267-271

P. De Cannière, H. Moors, A. Dierckx, F. Gasiaux, M. Aertsens, M. Put, P. Van Iseghem

"Diffusion and sorption of ^{32}Si-labelled Silica in Boom Clay". Radiochimica Acta, Vol 82, 191-196 (1998)

CHEMICAL DURABILITY AND PERFORMANCE ASSESSMENT OF HLW FORMS UNDER REPOSITORY CONDITIONS

SHANGGENG LUO

China Institute of Atomic Energy, Beijing

Authors and Contributors: Hua Zhanghang, Jianwen Yang, Chuanzhi Zhang, Baojun Li, Xi Chen

Abstract

This study covers five parts, including: (1) simulated HLW glass form (waste loading 16 wt%), and pyrochlore–rich synroc (actinides waste loading 46.8 wt%) durability under repository condition, such as the physical properties, leaching behavior and surface corrosion, radiation resistance (tested by S-32 ion of HI-13 accelerator); (2) Perovskite-rich, zirconolite-rich synroc and natural zircon synroc immobilization of actinides (waste loading up to 30-35wt%, 68wt% and 20wt%, respectively) and their product characterization, durability assessment; (3) Perovskite synroc and rutile synroc immobilization of technetium (Tc) waste (loading up to 35wt%) and its product characterization: (4) Self-propagating high temperature synthesis immobilization of SrO (up to 35 wt%): (5) Immobilization of actinides by using uranium tailing which showed the solidification form (loading 15 wt% of waste) has fair properties.

1. INTRODUCTION

The high level wastes (HLW) is stored in the stainless steel tanks and expects to be solidified earlier in China.

At moment, nine units of nuclear power reactors are in operation, another two units will be put operation soon. China is planning expansion of its nuclear power and nuclear technology utilization in order to meet the rapid economical development and large electricity demand. More radioactive wastes will be generated in the coming years.

China adopts the strategy of reprocessing and geological disposal of HLW. The Chinese government pays great attention to the public safety and the environmental protection. The HLW solidification technologies and the long-term behavior of HLW disposal are investigated and developed widely. The cold vitrification demonstration facility (VDF) has tested already. The geological repository site is selecting now. Besides, in order to find the alternative technologies of HLW treatment and disposal, the P-T (Partitioning and Transmutation) technology for HLW is studied in China, such as immobilization of actinides and Tc, Sr ,Cs separated from HLW by using synroc is also investigated.

According to the contract plan the following parts was performed during the past five years.

1. Glass form durability assessment

2. Synroc solidification and its durability assessment

   - Zirconolite-rich, pyrochlore-rich and pervskite-rich synroc solidification of actinides;
   - Natural zircon solidification of actinides;
   - Perovskite-rich synroc solidification of technetium;
   - Rutile-rich synroc solidification of technetium

3. Alternative solidification technology and its product characterization

   - Self-propagating high temperature synthesis of waste forms;
   - Uranium Tailing matrix solidification

2. EXPERIMENTAL

2.1. Glass sample

2.1.1. Glass sample fabrication and its test method

The glass formulation is listed in Table I. The glass sample was melted at 1150^{o}C and kept in this temperature for 3h, then annealed at 500^{o}C for 1h, afterwards cooled to room temperature[1].

TABLE I. COMPOSITION OF BOROSILICATE GLASS MATRIX (WASTE LOADING 16WT%)

SiO_2	B_2O_3	Na_2O	Al_2O_3	Li_2O	CaO	MgO	TiO_2	SrO	Y_2O_3	MoO_3
50.23	18.48	11.21	3.38	2.94	4.54	0.84	0.99	0.037	0.016	0.19
MnO_2	Cs_2O	BaO	Nd_2O_3	Cr_2O_3	Fe_2O_3	NiO	K_2O	P_2O_5	SO_3	
0.014	0.12	0.021	2.03	0.30	3.24	0.59	0.094	0.071	0.66	

The fabricated glass was cut into specimens of 10×2×2mm, then polished and cleaned.

2.1.2. Durability tests

The adopted medium assemblages to simulate the geological disposal condition were:

G1 granite(100%)

G2 granite(80%) + Fe_3O_4(20%)

G3 granite(80%) +cement(20%)

G4 bentonite(100%)

G5 bentonite(80%) + Fe_3O_4(20%)

The granite used in this study was generated from Baishan Area(a candidate disposal site in Gansu Province, China and the composition of granite is shown in the Table II. The cement was 525# common cement produced by Beijing Hancuihe Cement Factory; the bentonite was produced in Weifang, Shangdong Province, and the composition is listed in the Table III. Fe_3O_4 was chemical reagent produced by Beijing Chemical Factory. All those materials were crushed and passed through the 100 mesh sieves before used in the experiment.

TABLE II. OXIDE COMPOSITIONS OF GRANITE

Oxides	SiO_2	TiO_2	Al_2O_3	Fe_2O_3	FeO	MnO_2	MgO	CaO	Na_2O	K_2O	P_2O_5
wt%	67.20	0.61	15.98	0.71	2.48	0.24	0.04	3.51	3.76	3.36	0.13

TABLE III. OXIDE COMPOSITIONS OF BENTONITE

Oxides	SiO_2	TiO_2	Al_2O_3	Fe_2O_3	FeO	MnO_2	MgO	CaO	Na_2O	K_2O
wt%	71.12	0.13	14.16	1.77	0.39	0.03	2.63	1.51	2.21	1.37

The powdered medium were sieved through 100 mesh sieve, and mixed according to designed assemblages.

The deionized water was used as leachant, media/leachant=1:1, at 90 ^oC, $SA/V=20m^{-1}$, where SA is the sum surface areas of three specimens and V is the leachant volume. The test time was 90 days, 0.5, 1, 2 years, respectively.

The assembling of the media/leachant and specimens are shown in Fig.1. Using three specimens as a group, and separating the media/leachant to four parts, put the first part of media/leachant into the vessel, then place the first specimen above of the media/leachant. This process did continuously until all three specimens and four parts of media/leachant were put into the vessel which was made by PTFE. Then, the vessels were put into the preheated (90±2□) oven; weighing the vessels to check its tightness in 2, 5, 15, 30 days at the beginning of the experiment, then weighing it each 30 days.

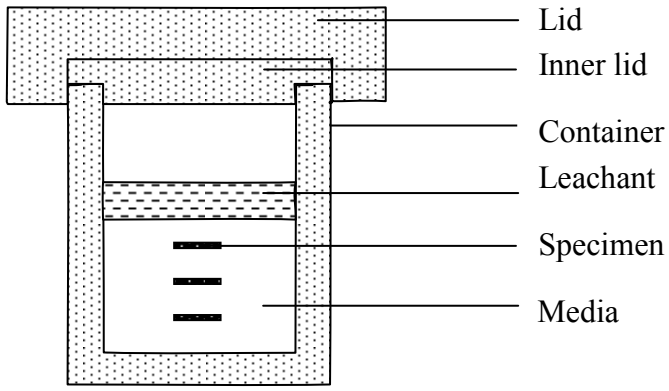

FIG. 1. The leaching containers set

At the end of experiments, took out the vessels and cooled it to room temperature. The specimens were washed by deionized water, then dried (at 100 ^{o}C) and weighed. The media/leachate was centrifuged and filtrated (10,000-30,000 rpm, 0.45μm micro-membrane) to separate the media and leachate.

The leached surface of specimens were analyzed by using Rigaku D/max-RB X-ray Diffractrometer(XRD), CuK_{α}(λ=0.15406nm), and Cambridge S250MK3 Scanning Electron Microscopy with Link AN 10000 Energy Dispersive Spectrometer (SEM/EDS).

2.2. Zirconlite(Z), pyrochlore(Py) and perovskite(P) synroc fablication and characterization

The three types of synroc samples were fabricated as the following steps. First, put the metal salt, which contained Zr, Al and Ti ion, into anhydrous ethanol solution, stir the mixture to make them melt, and then drop the turbid liquid of barium and calcium hydroxide into the mixture, at the same time, drop the dense ammonia into the mixture to keep pH = 9. After dropped all the solutions into the mixture, heated up the stirring container until the mixture became ropy, and then put the ropy mixture into the oven at 90 ^{o}C to dry, after that triturated and sifted out dry mixture, and calcined them at 750 ^{o}C for 1h, and hot pressed them at 1200 ^{o}C/20MPa for 2 hrs, at last, put them into anneal oven at 900 ^{o}C and cool to room temperature[2,3]. Nd and U were used as the simulacrum for trivalent and tetravalent actinides, respectively[4] .

The adopted phase assemblage was 85 wt% main phase (Z,Py or P) and 5 wt% holladite, 10 wt% rutile. The minor phase of hollandite and rutile were used to accommodate any possible residual fission products and maintain chemical flexibility to the slight variations of waste composition and loading. The composition of those three types of synroc is listed in Table IV.

The synroc fabrication technology and XRD, SEM, TEM, ED's determination was as same as mentioned above. The hydrothermal durability of the samples were determined by using the PCT-B (Product Consistency Test)[5] leach test.

Table 4 Composition of synroc samples

Sample no*	Waste loading (wt%)**	Composition (wt%)						
		Al_2O_3	BaO	CaO	TiO_2	ZrO_2	Nd_2O_3	UO_2
1	20	2.5	1.0	9.5	49.5	24.2	13.5	—
2	25	3.2	1.0	8.2	47.2	23.2	17.2	—
3	30	4.0	1.0	6.7	44.7	22.4	21.0	—
4	35	4.8	1.0	5.2	42.8	21.1	25.1	—
5	20	1.6	1.0	11.5	47.5	18.4	—	20.0
6	25	1.9	1.0	11.0	45.9	15.2	—	25.0
7	30	2.1	1.0	10.6	43.4	12.9	—	30.0
8	20(1)	2.0	1.0	10.5	48.0	21.5	6.6	10.4
9	20(2)	1.6	1.0	11.0	48.2	20.2	4.3	13.7
10	20(5)	1.3	1.0	11.5	48.4	18.8	2.0	17.0
11	25(1)	2.4	1.0	10.0	45.9	19.2	8.3	13.2
12	25(2)	2.0	1.0	10.5	46.1	17.6	5.4	17.4
13	25(5)	1.5	1.0	11.0	46.2	16.3	2.7	21.3
14	30(1)	2.8	1.0	9.5	44.0	16.6	10.0	16.1
15	30(2)	2.3	1.0	10.0	44.1	15.2	6.5	20.9
16	30(5)	1.7	1.0	10.5	44.4	13.5	3.2	25.7
17	32.2	0.7	1.0	11.2	45.1	9.8	—	32.2
18	40.2	0.7	1.0	10.4	43.0	4.6	—	40.2
19	47.2	0.7	1.0	9.8	41.2	—	—	47.2
20	37.6(5)	0.7	1.0	10.3	44.4	8.1	3.9	31.5
21	46.8(5)	0.7	1.0	9.4	42.2	2.7	4.9	39.1
22	50.9(5)	0.7	1.0	8.9	41.2	0.2	5.3	42.6
23	68.6	0.7	1.0	—	40.6	—	57.6	—

* Sample $1^{\#}$~$16^{\#}$ are zirconclite-rich synroc samples; sample $17^{\#}$~$22^{\#}$ are pyrochlore-rich synroc samples; Sample $23^{\#}$ is perovskite-rich synroc sample, the waste loading of this sample is adjustable, for Nd is not only a waste element, but also a matrix element.

** The number in parenthesis is the molar ratio of An^{4+}/An^{3+}.

2.3. Pyrochlore-rich synroc

2.3.1. Pyrochlore-rich synroc sample fabrication

The pyrochlore-rich synroc sample was fabricated as the above steps. And its compositions is listed in Table V.

TABLE. V. OXIDE COMPOSITIONS OF THE SYNROC SAMPLES (WASTE LOADING 46.8%)

Composition	Al_2O_3	BaO	CaO	TiO_2	ZrO_2	Nd_2O_3	UO_2
wt%	0.7	1.0	9.4	42.2	2.7	4.9	39.1

2.3.2. Simulated disposal medium test

The experiments designed five experimental systems to simulate the disposal condition. The mediums of five systems were as follows:

P1, granite (100%);
P2, granite (80%) + cement (20%);
P3, granite (80%) + Fe_3O_4 (20%);
P4, bentonite (100%);
P5, bentonite (80%) + Fe_3O_4 (20%)

The granite, cement, bentonite and Fe_3O_4 used in the experiment as well as the experimental vessel, experimental condition and experimental method were as same as described in section 2.1.2. The experiment lasted 91 d, 182 d, 364 d and 728 d, respectively.

2.4. Zircon synroc

2.4.1 Zircon synroc sample

The precursor material used for the synthesis of the zircon waste form was natural gem grade zircon from Gansu Province, China. It mainly consisted of pure zircon with a small amount of SiO_2 through XRD and SEM/EDS analyses. The natural zircon was crushed and sieved through a 200-mesh sieve. The powder was mixed with a nitric acid solution of simulated actinides. Neodymium (Nd) and uranium (U) were used as stimulants of trivalent and tetravalent actinides, respectively, with a molar ratio of An^{3+}/An^{4+} of 1/5. The adopted waste loading was 20 wt%. The mixture dried and calcined was hot- pressed to produce a zircon waste form.

The physical properties, such as density, open porosity and hardness of the zircon waste form as well as XRD , SEM/EDS, TEM/EDS were analyzed. The durability of the sample was tested by the MCC-1 method. The leachate was analyzed by inductive coupled plasma mass spectroscopy (ICP/MS) and the leached surface was investigated by SEM/EDS.

2.4.2. Radiation test

The heavy-ion bombardment provides a fast and simple method for the simulation of α–recoil damage, and many ions (e.g. Ne, Ar, Kr, Xe, Pb, Bi) have been used in heavy ion irradiation study, but S ion used has not seen in the literature. In this study, 100 MeV ^{32}S bombardment using an tandem accelerator was used to study radiation damage effects of pyrochlore-rich synroc.

The positron annihilation technique (PAT) has been widely used in studying the structure defects, phase transformations and radiation effects of the semiconductor and metal materials. It is very sensitive to vacancy defects (mono-vacancy, di-vacancys and voids) in the range of 1-100 Å in the ionic solid materials, so it can be used to study the radiation defects in the synroc waste forms.

FIG. 2 HI-13 tendom accelerator

The heavy ion irradiation was performed at the HI-13 tandem accelerator by using 100MeV ^{32}S and an ion beam current of up to 100nA. The TRIM-91[6]. calculation gives the ion implantation depth of 25μm for 100 MeV ^{32}S in the sample. Based on the TRIM-91 calculation, the Kingchin-Pease model and assumed displacement energy of 25 eV, the average number of displacements produced per incident ^{32}S ion was calculated to be 4600. The displacements calculated with TRIM-91 are shown in Fig.3 as a function of depth. The specimens were irradiated at room temperature with fluencies ranging from 4.76 to 38.1 ions/nm^2 (corresponding to 0.2 ~ 1.6 dpa, damage rate of 1.03×10^{-4} dpa/s, to see Table VI).

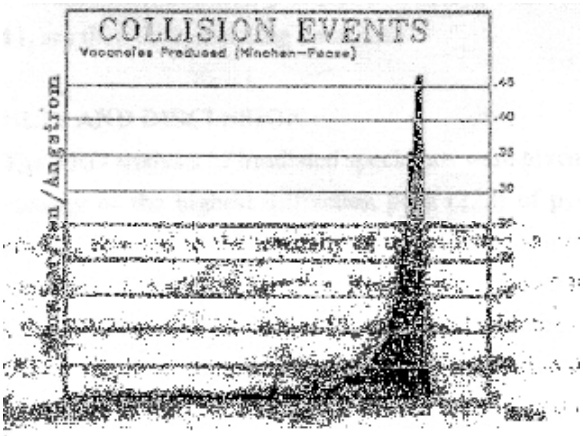

FIG. 3. Distribution of displacements for 100MeV ^{32}S ion implantation

The defects produced by irradiation were studied by using the positron annihilation technique (PAT). The measurements were performed at room temperature by using a standard fast-fast coincidence BaF_2 positron lifetime spectrometer with a ^{22}Na positron source sandwiched between the two pieces of samples. The time resolution of the spectrometer is 210ps. The lifetime spectra each contained 10^6 counts. The lifetime spectra were analyzed by means of a LT program. Two components (τ_1 and τ_2) were employed to fit the positron annihilation spectra, the mean lifetime (τ_{av}) is given by

$$\tau_{av} = \tau_1 I_1 + \tau_2 I_2 \qquad (I_1 + I_2 = 1)$$

Where τ_{av} is the average lifetime of the bulk lifetime and the lifetime of positrons trapped at small vacancies, I_1 and I_2 are their corresponding intensities.

TABLE VI. IRRADIATION CONDITION

Irradiation dose (dpa)	Irradiation time (minute)	Ion fluencies (ion/cm^2)
0.2	32.3	4.76×10^{14}
0.4	64.6	9.53×10^{14}
0.6	96.9	1.43×10^{15}
1.0	161.5	2.38×10^{15}
1.6	258.4	3.81×10^{15}

2.5. Tc- solidification by perovskite-rich and rutile-rich synroc

Synroc immobilization of Tc is a potentioal measurement[7-9]. Based on the valence, ion radii and chemical properties, Mn was selected to simulate Tc. The designed formulae for immobilization Tc are as follows:

85wt% perovskite (P) + 10wt% zirconolite(Z) + 5wt% hollandite(H)

85wt% rutile(R) + 10wt% zirconolite(Z) + 5wt% hollandite(H).

The adopted phase assemblage was 85% main phase (P or R) and 15wt% zirconlite(Z) and hollandite(H). The minor phases (Z and H) were used to accommodate any possible residual composition and maintain the chemical flexibility to the slight variations of waste composition and loading.

The composition of these two type synroc samples are listed in Table VII. and Table VIII.

TABLE VII. COMPOSITION OF PEROVSKITE-RICH SYNROC

Sample No.	Waste Loading(wt%)	Composition (wt%)					
		CaO	ZrO_2	Al_2O_3	BaO	TiO_2	MnO_2
1	20	36.20	3.63	0.69	1.04	44.28	14.20
2	25	36.07	3.63	0.69	1.04	40.39	18.18
3	30	35.93	3.63	0.69	1.04	36.51	22.20
4	35	35.97	3.63	0.69	1.04	32.45	26.40

TABLE VIII. COMPOSITION OF RUTILE-RICH SYNROC

Sample No.	Waste Loading(wt%)	Composition (wt%)					
		CaO	ZrO_2	Al_2O_3	BaO	TiO_2	MnO_2
5	20	1.65	3.63	0.69	1.04	78.77	14.20
6	25	1.65	3.63	0.69	1.04	74.79	18.18
7	30	1.65	3.63	0.69	1.04	70.77	22.20
8	35	1.65	3.63	0.69	1.04	66.57	26.40

The synroc fabrication and characterization processes, the open porosity, density determined methods were the same as above. The X-ray diffraction (XRD) analysis was conducted by D/MAX-RB X-ray Diffract Meter, Cu Kα (λ =1. 54Å), 2 θ =20-80^{o}. The SEM/BEI measured by S250Mk3 scanning electron microscopy. The hydrothermal durability of the samples was measured by using the MCC-1 leach test.

2.6 Self-propagating high temperature synthesis (SHS)

The self-propagating high temperature synthesis of waste form has been reported in references [10-11]. The matrix was composed of TiO_2, CaO, Ti and Cr_2O_3. The nuclide ^{90}Sr was instead of by inactive Sr^{2+}, adding 10, 20, 30, 35 and 40 wt% SrO, respectively. The SHS device scheme is shown in Fig.4. After mixing, the matrix and

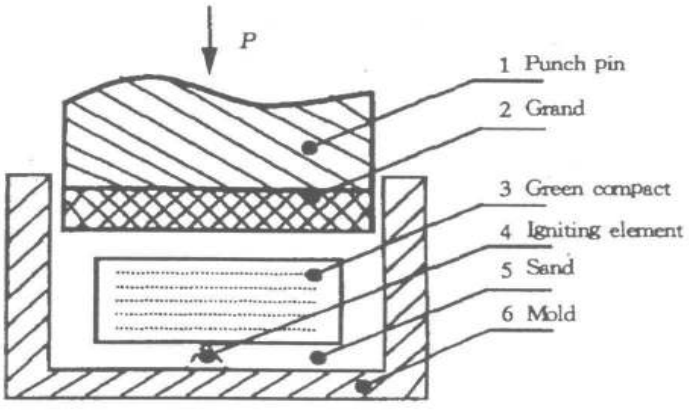

Fig.4 Scheme of SHS device

SrO was pressed into the green compact, then put it into the sands in a steel model. The tungsten filament is served as igniting element. After pressing, the

compact was ignited and combusted. The full pressure was loaded to densify the synthesized ceramic material.

2.7. Solidification of actinides by uranium tailing matrix

The composition of matrix-uranium tailing is listed in Table IX.

TABLE IX. COMPOSITION OF MATRIX-URANIUM TAILING (WT%)

SiO_2	Al_2O_3	K_2O	Na_2O	Fe_2O_3	CaO	MgO	FeO	TiO_2	MnO_2	P_2O_5	Ignition mass loss
73.20	13.95	3.14	2.05	1.86	0.80	0.35	0.32	0.28	0.08	0.05	3.95

The trivalent and tetravalent actinides were instead by Nd^{3+} and U^{4+}. The designed formulation are shown in Table X.

TABLE X. TEST FORMULATION

Sample	Waste loading wt%	Composition (wt%)		
		Nd_2O_3	UO_2	Matrix(tailing)
U-5	5	0.52	4.20	95.28
U-10	10	1.05	8.40	90.55
U-15	15	1.57	12.56	85.87

The fabrication process includes: matrix milling and sieving (200 mesh), mixing with simulated waste, calcining at 750 ^oC for 1 hour, then hot pressing at 900-1200 ^oC and 5～20 MPa for 2 hours.

3. RESULTS AND DISCUSSION

3.1. Glass form durability

3.1.1. Mass loss of leach test

After designed static leaching tests, the specimens were weighed. The mass loss was calculated by the following equation.

$$R=(W_0-W_e)/SA$$

In the equation, R is the mass loss; and SA is the surface area of the specimens; W_0 is the weight of the specimens before leaching test; W_e is the weight of the specimens after leaching test. The results s shown in Table XI.

TABLE XI. MASS LOSS AFTER LEACHING TEST

Time(a)	Mass loss of glass in different medias ($\times10^{-1}gm^{-2}$)				
	G1	G2	G3	G4	G5
0.5	28.78	97.19	192.74	125.44	130.93
1	58.62	158.56	244.21	227.9	230.37
2	61.46	301.74	316.42	378.31	374.34

From Table XI it is found, the mass losses of the four tested systems are decreased with the leaching time.

(1) The bentonite system has higher mass losses. This phenomenon is occurred in other reference[12]. It may by caused by the high ion exchange and adorption ability of bentonite.

(2) The existence of Fe_3O_4 has no obvious effect on the bentonite system, but it enhanced obviously the mass loss in the granite system.

(3) The existence of cement caused increasing of mass loss for granite system.

3.1.2. Surface analyses of leached glasses

The leached sample surfaces were analyzed by SEM/EDS. The element concentrations of Al, Ca, Si and Na were found:

(1) Some elements, such as Ca, Al were enriched on the sample surfaces along with leaching time, but the Ca element came gradually to a equilibrium state.

(2) Some elements such as Na, Si showed opposite trend with Ca, Al. The Na concentration is mostly depleted on the sample surfaces after 2 years leaching test.

(3) The SEM pictures show that there are pitting corrosion and precipitation on the leached glass surfaces.

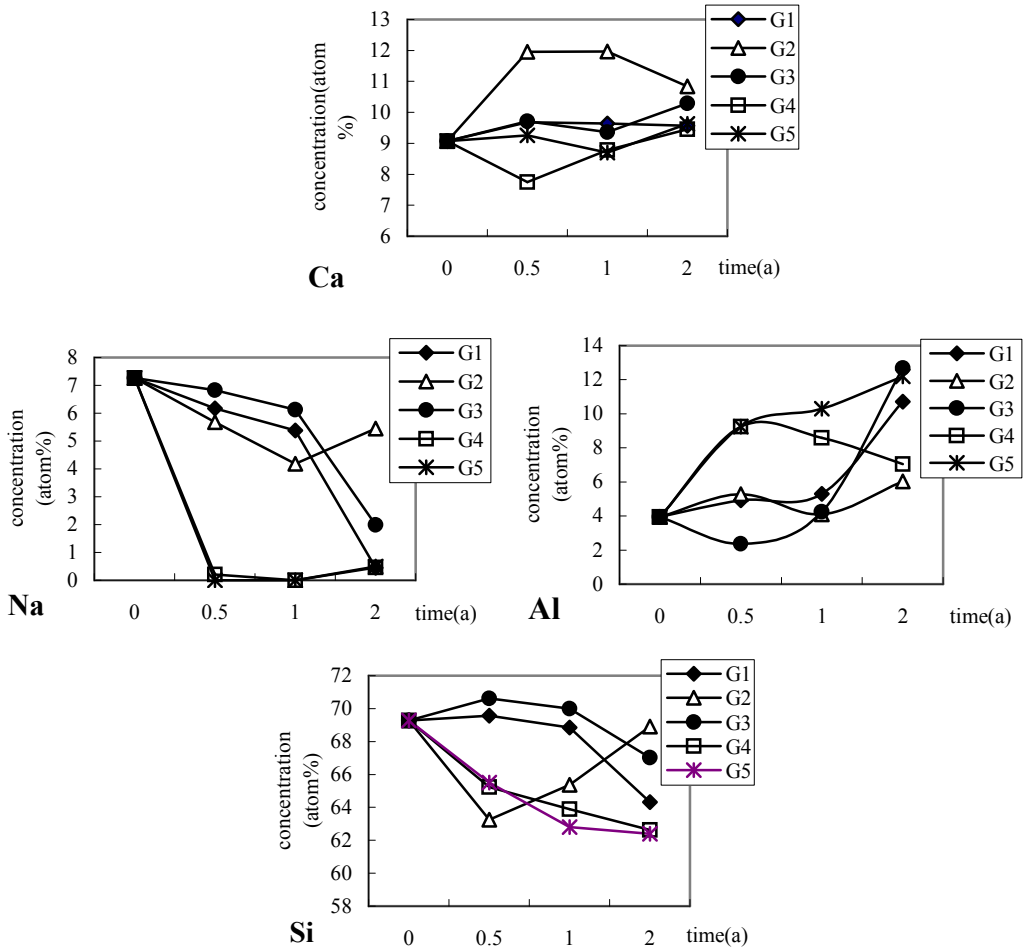

FIG. 5. Concentration of elements Na, Si, Al , Ca after two years leaching

3.1.3. XRD analyses of leached glasses

The XRD patterns show that there is a small peak on the leached glass G1 .This crystal phase needs further investigation.

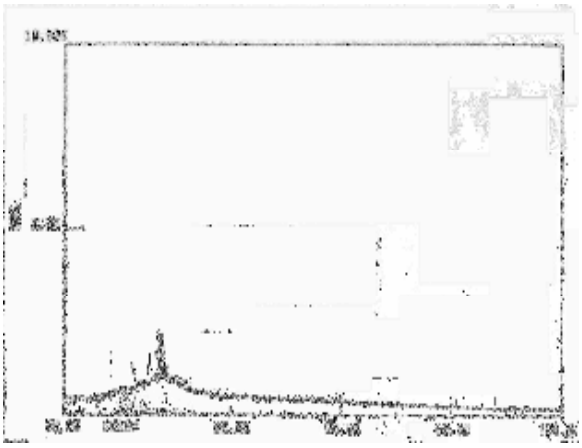

Fig.6 XRD patern of specimen G1 after leaching

3.2 . Zirconolite, pyrochlore and perovskite-rich synroc

3.2.1. Physical properties

The Measured density and open porosity of the synroc samples are listed in Table XII. For comparison, synroc-c reference sample N.0 (PW-4b-D) was also produced and analyzed, the measured density was similar with 4.35-4.50g/cm^3 of Ringwoods' results [13].

Table 12 Physical properties of synroc samples

Sample no.	Density (g/cm^3)	Open porosity (%)	Sample no.	Density (g/cm^3)	Open porosity (%)
0	4.51	0.06	12	4.76	0.11
1	4.56	0.08	13	4.85	0.12
2	4.67	0.12	14	4.86	0.23
3	4.80	0.15	15	4.96	0.28
4	4.89	0.05	16	5.03	0.18
5	4.84	0.10	17	5.15	0.21
6	4.91	0.11	18	5.31	0.07
7	5.05	0.14	19	5.47	0.09
8	4.59	0.19	20	5.16	0.13
9	4.76	0.24	21	5.37	0.06
10	4.71	0.16	22	5.41	0.13
11	4.70	0.19	23	5.28	0.07

3.2.2. Phase assemblages

Phases identified by XRD are summarized in Table XIII, with phases in patterns. The synroc has the phase assemblages as designed.

Table 13 Phase assemblages of synroc samples

Sample no.	Existing phases	Sample no.	Existing phases
1	Z, (R)	13	Z, (R, Py, B)
2	Z, (R, Py)	14	Z, (R, Py, B)
3	Z, (R, Py)	15	Z, (R, Py, B)
4	Z, (R, Py)	16	Z, (R, Py, B)
5	Z, (R, Py, B)	17	Py, (U, H)
6	Z, (R, Py, B)	18	Py, (U, H)
7	Z, (R, Py, B)	19	Py, (U,H)
8	Z, (R, Py, B)	20	Py, (U, H)
9	Z, (R, Py, B)	21	Py, (U, H)
10	Z, (R, Py, B)	22	Py, (U, H)
11	Z, (R, Py, B)	23	P, (Py)
12	Z, (R, Py, B)		

Z(Zirconolite), R(Rutile), Py(Pyrochlore), H(Hollandite), B(Brannerite), U(Uraninite), P(Perovskite)

3.2.3. Microstructure and phase chemistry

SEM analyzed the microstructures of samples; several backscattered electron images (BEI) are listed in Fig. 7. The low-magnification BEI revealed that the samples had very few micro voids in accordance with measured density and open porosity data. The high-magnification BEI of samples shows that the grain size was less than 1μm.

For some Z-rich samples TEM (Fig.8) indicated that zirconolite (Z) was the major phase, minor phases included the expected phase such as rutile (R). Some unexpected phases, like pyrochlore(Py), brannerite (B) and other neodymium or barium titanates (BT) also appeared in the samples. The average chemical composition of the samples were determined by TEM/EDS (TabLE XIV). These data can be used to calculate the structural formula based on the number of oxygen atoms. The structural formula of some Z-rich synroc samples are listed in Table XV.

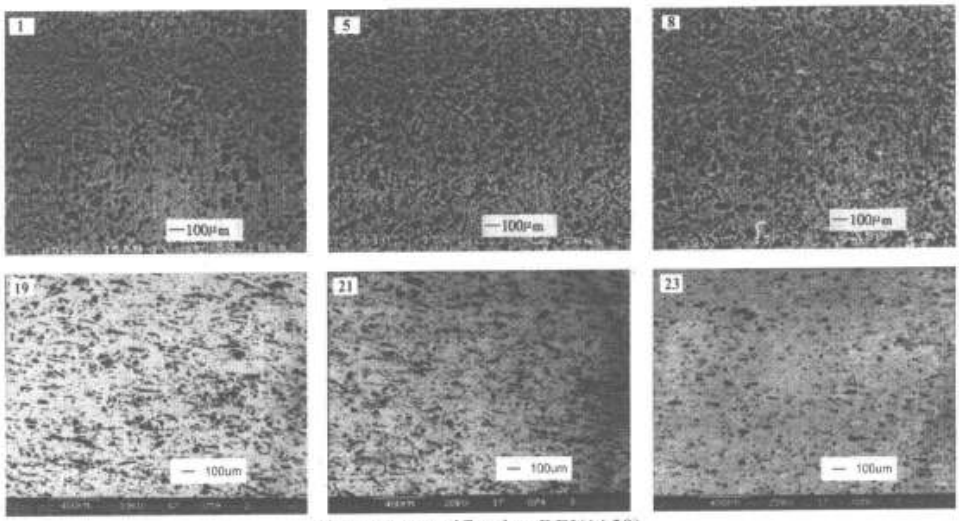

a) Low- magnification BEI(×50)

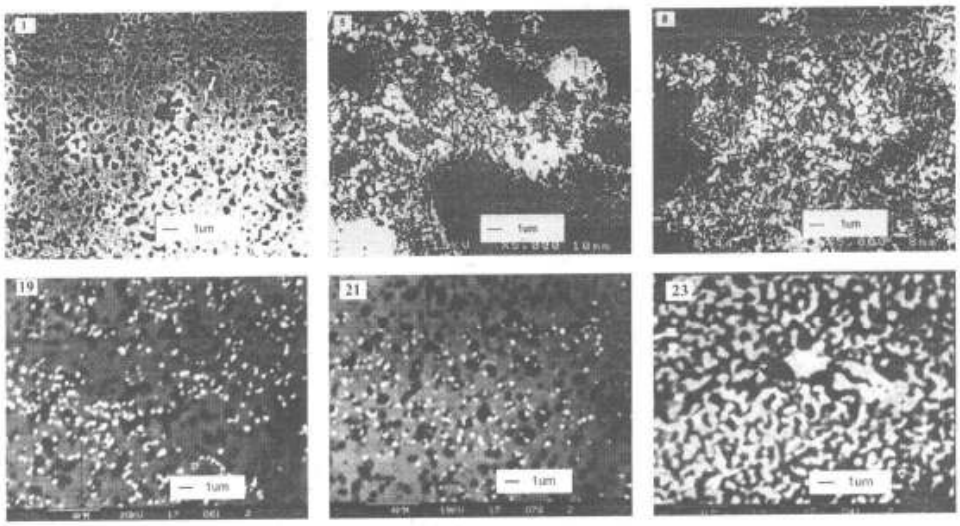

b) High- magnification BEI(×5000)

Fig. 7 Backscattered electron images of synroc samples

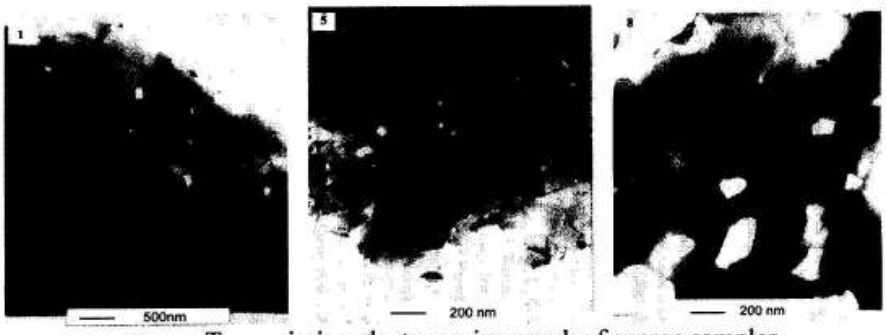

fig. 8 Transmission electron micrograph of synroc samples

Table 14 Phase chemical composition of some Z-rich synroc samples

Sample no.	Phase	Chemical composition (wt%)						
		Al_2O_3	BaO	CaO	TiO_2	ZrO_2	Nd_2O_3	UO_2
1	Z	2.2	—	10.4	45.4	23.4	18.5	—
	R	0.3	—	0.5	90.6	8.0	0.6	—
5	Z	1.9	—	14.8	45.1	27.5	—	10.8
	R	0.2	—	0.3	95.3	3.6	—	0.7
	Py	0.1	—	13.3	38.2	7.8	—	40.6
	B	0.3	—	0.8	40.4	4.0	—	54.4
8	Z	1.9	0.3	11.9	42.2	28.2	9.9	5.5
	R	0.1	—	0.3	94.8	4.1	0.3	0.4
	Py	0.2	0.6	9.9	35.3	6.4	16.2	31.2
	B	0.4	0.7	0.3	40.6	5.3	6.6	46.0

Table 15 Phase structural formulae of some Z-rich synroc samples

Sample no.	Phase	Nominal formula	Phase structural formula
1	Z	$CaZrTi_2O_7$	$(Ca_{0.67}Nd_{0.30})_{0.97}(Zr_{0.69}Nd_{0.10}Ti^{3+}_{0.04}Ti_{0.17})_{1.00}(Ti_{1.84}Al_{0.16})_{2.00}O_7$
	R	TiO_2	$[Ti_{0.94}Zr_{0.05}(Al, Ca, Nd)_{0.01}]_{1.00}O_2$
5	Z	$CaZrTi_2O_7$	$(Ca_{0.94}U_{0.06})_{1.00}(Zr_{0.80}U_{0.08}Ti_{0.12})_{1.00}(Ti_{1.88}Al_{0.12})_{2.00}O_7$
	R	TiO_2	$[Ti_{0.97}Zr_{0.02}(U, Al, Ca)_{0.01}]_{1.00}O_2$
	Py	$CaUTi_2O_7$	$Ca_{1.02}(Zr_{0.27}U_{0.64}Ti_{0.09})_{1.00}(Ti_{1.97}Al_{0.01})_{1.98}O_7$
	B	UTi_2O_6	$(U_{0.80}Ca_{0.02}Zr_{0.13})_{0.95}(Ti_{2.02}Al_{0.02})_{2.04}O_6$
8	Z	$CaZrTi_2O_7$	$(Ca_{0.78}Ba_{0.01}Nd_{0.20})_{0.99}(Zr_{0.84}U_{0.07}Nd_{0.02}Ti^{3+}_{0.04}Ti_{0.03})_{1.00}(Ti_{1.85}Al_{0.14})_{1.99}O_7$
	R	TiO_2	$[Ti_{0.97}Zr_{0.03}]_{1.00}O_2$
	Py	$Nd_2Ti_2O_7$ $CaUTi_2O_7$	$(Ca_{0.80}Ba_{0.02}Nd_{0.44}U_{0.53}Zr_{0.24})_{2.03}(Ti_{1.99}Al_{0.02})_{2.01}O_7$
	B	UTi_2O_6	$(U_{0.67}Ba_{0.02}Ca_{0.02}Nd_{0.16}Zr_{0.17})_{1.04}Ti_{2.00}O_6$

3.2.4. Hydrothermal durability

The hydrothermal durability of Z-rich and P-rich samples was teste3d by using the PCT-B test method. The test condition was 90 °C, 7 days, deionzed water SA/V =1000 m^{-1}. The leachates were analyzed for Ca by atomic absorption spectroscopy and for Ti, Zr, Ba, Al, Nd, and U by inductive coupled plasma mass spectroscopy (ICP/MS). Mass loss and nominalized elemental release rates are listed in Table XVI.

Table 16 PCT results

Sample no.	Mass ($g \cdot m^{-2} \cdot d^{-1}$)	Nominalized leach rate ($g \cdot m^{-2} \cdot d^{-1}$)				
		Ca	Ti	Zr	Nd	U
0	2.5×10^{-2}	8.5×10^{-3}	1.5×10^{-5}	5.7×10^{-5}	9.4×10^{-5}	—
1	1.2×10^{-2}	4.6×10^{-3}	7.8×10^{-6}	2.9×10^{-5}	2.3×10^{-5}	—
2	1.4×10^{-2}	5.5×10^{-3}	9.2×10^{-6}	3.4×10^{-5}	2.9×10^{-5}	—
3	1.6×10^{-2}	6.5×10^{-3}	9.9×10^{-6}	2.8×10^{-5}	2.5×10^{-5}	—
4	1.1×10^{-2}	4.5×10^{-3}	8.9×10^{-6}	2.3×10^{-5}	2.3×10^{-5}	—
5	1.4×10^{-2}	4.7×10^{-3}	8.3×10^{-6}	2.7×10^{-5}	—	2.4×10^{-6}
6	1.6×10^{-2}	4.9×10^{-3}	8.4×10^{-6}	3.1×10^{-5}	—	4.5×10^{-6}
7	1.3×10^{-2}	4.8×10^{-3}	1.1×10^{-5}	2.6×10^{-5}	—	3.2×10^{-6}
8	1.8×10^{-2}	6.6×10^{-3}	1.0×10^{-5}	3.5×10^{-5}	3.1×10^{-5}	6.2×10^{-6}
9	2.1×10^{-2}	6.2×10^{-3}	1.1×10^{-5}	3.1×10^{-5}	5.4×10^{-5}	5.9×10^{-6}
10	2.3×10^{-2}	5.2×10^{-3}	9.8×10^{-6}	3.8×10^{-5}	7.5×10^{-5}	3.8×10^{-6}
11	2.2×10^{-2}	7.0×10^{-3}	9.9×10^{-6}	3.6×10^{-5}	5.4×10^{-5}	6.1×10^{-6}
12	1.6×10^{-2}	5.3×10^{-3}	1.1×10^{-5}	3.1×10^{-5}	7.8×10^{-5}	5.6×10^{-6}
13	1.7×10^{-2}	7.9×10^{-3}	1.0×10^{-5}	3.3×10^{-5}	7.1×10^{-5}	3.0×10^{-6}
14	2.0×10^{-2}	7.2×10^{-3}	1.1×10^{-5}	3.6×10^{-5}	3.7×10^{-5}	6.0×10^{-6}
15	2.5×10^{-2}	7.6×10^{-3}	1.3×10^{-5}	4.0×10^{-5}	4.9×10^{-5}	4.7×10^{-6}
16	1.9×10^{-2}	6.4×10^{-3}	1.2×10^{-5}	3.9×10^{-5}	7.3×10^{-5}	4.4×10^{-6}
		Ba	Ti	Al	Nd	
23	1.9×10^{-2}	3×10^{-5}	5×10^{-7}	6×10^{-5}	3×10^{-7}	
23*	—	3×10^{-3}	7×10^{-7}	8×10^{-4}	3×10^{-7}	

* The test results of ANSTO (Australia Nuclear Science & Technology Organization) for the same sample 23# under the same PCT conditions.

3.3. Pyrochlore synroc durability test

3.3.1. Dissolution rate

When the designed experiment time reached, the containers were taken out from the oven, washed the specimens with deionized water and dried them in oven at 110 ℃, and then weighted the mass weight of the dried specimens.

The mass loss rate was calculated according to the following equation:

$$NL=(W_0-W_e)/SA\cdot t$$

NL: the mass loss rate(g/cm^2·d); W_0: the weight of specimens before leach test; We: the weight after leach test; SA: the surface area of the specimens; t: the leaching time. Figure 9 shows relation between the mass loss rate and the leaching time.

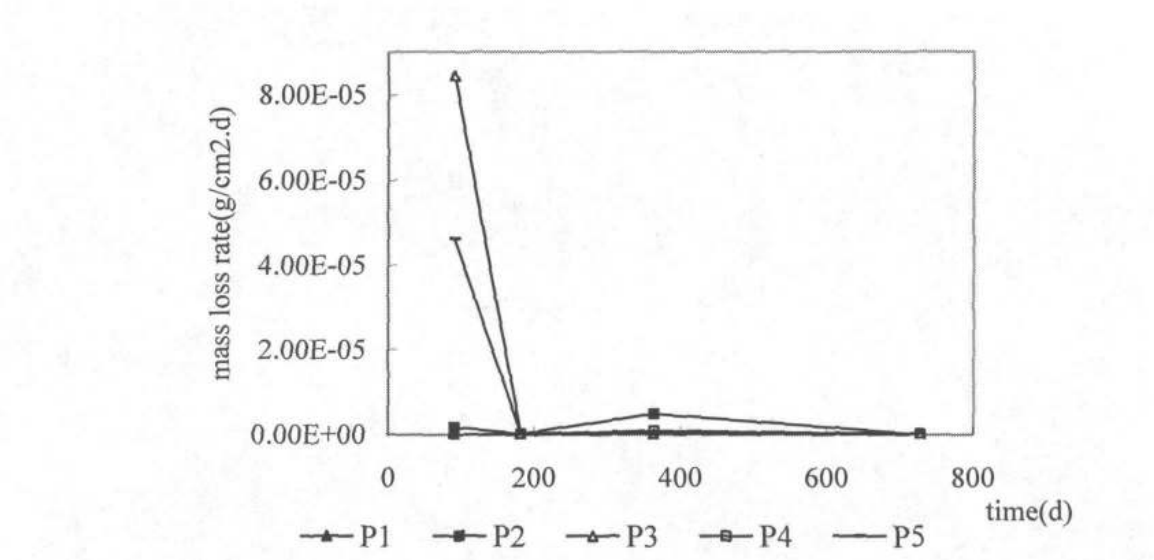

Fig. 9 The dissolution rate of specimens at 90 ℃ for 728d

The Figure 9 shows: (1) The specimens reached the leaching equilibrium after 182 days with 10^{-7} (g/cm^2·d) of the mass loss rate, which suggests pyrochlore-rich synroc has a very low mass loss rate; (2) The mass loss rate of system (P3,P5) with Fe_3O_4 were higher than other systems before 182 days, which indicates that Fe_3O_4 is disadvantage to durability of pyrochlore-rich synroc and causes the mass loss rate increasing.

3.3.2. XRD analysis

The analyses were conducted by the Rigaku D/MAX-RB X-ray diffract meter. The incident particle is Cuk$_\alpha$ (λ =1.54 Å ,2 θ =20−80°). The Figure 10 shows:

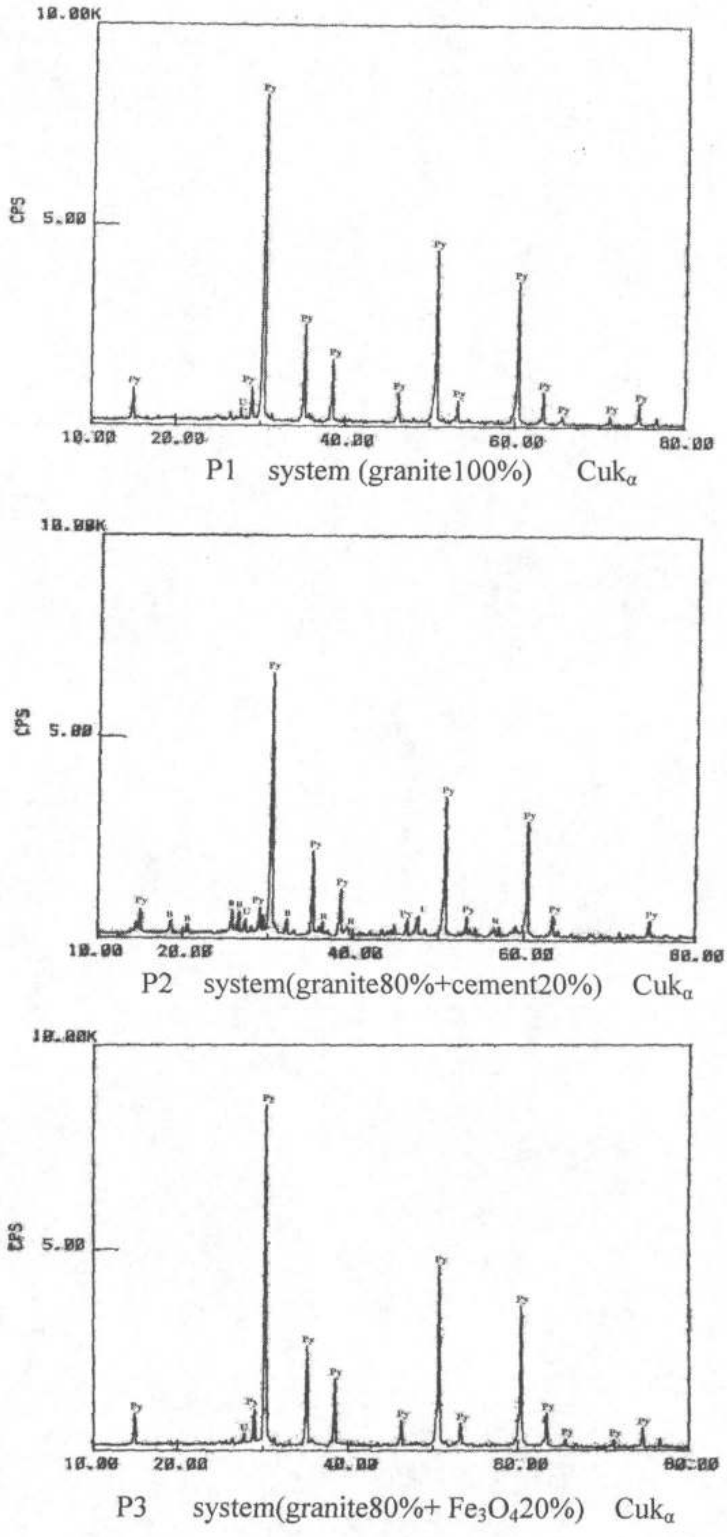

FIG.10. X-ray diffraction patterns of samples in five system (for P1, P2, P3)

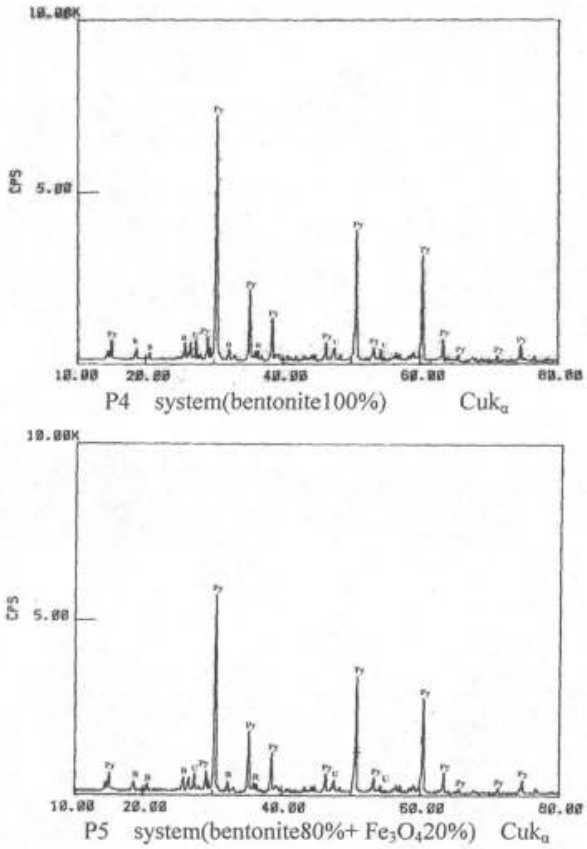

Fig. 11 X-ray diffraction pattern of sample in five systems at 90 ℃ for 728d

(Py: pyrochlore synroc, U: crystal uranium mineral, B: betafite, R: rutile)

— The specimens (bentonite system P4,P5) has two new phase peaks (B,R) on the XRD mapping, and the intensity of new phase peaks were increased with test time. which may be caused by some sediment formed on the sample surface;

— The specimens in P2 had the two new phase peaks on the mapping at the 91th day, but the intensity of the new phase peaks were not increased at the 728th day;

— The peak intensity of pyrochlore in P5 (bentonite 80%+ $Fe_3O_4$20%) is lower than that in P4 (bentonite100%), which suggests that Fe_3O_4 can promote the leaching behavior of synroc.

3.3.3. SEM analysis

SEM/EDS analyses used S-250 MK3 spectrometer with Link AN10000 energy diffraction system. The map of the specimen surface leached for 728d are showed in Fig 12.

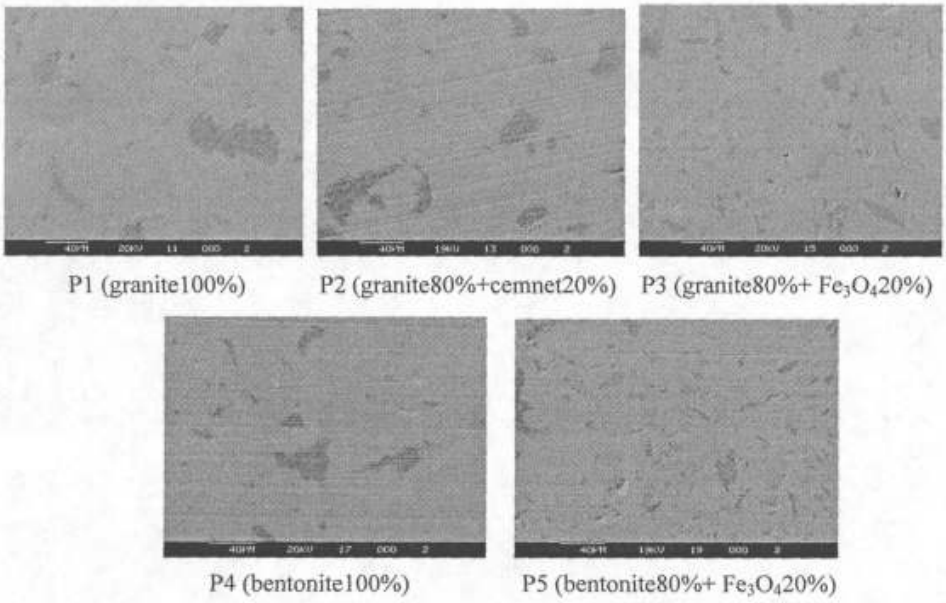

Fig.12 The SEM mapping for the aspects of the specimens at 90℃ for 728d

The Figure 12 indicated: There were some dark materials appeared on the surface, it may be produced by the inhomogeneous mixing in the pyrochlore-rich synroc fabrication process. Some corrosion pits were existed on the surface of P5 and P3, which may be caused by Fe_3O_4. that is consisting with the results of mass loss rate.

3.3.4. EDS analysis

The equipment used is the same as SEM analysis. The determined element (in atom%) on the specimen surface is shown in Fig. 13. It indicted:

— U ion were enriched in the five systems during the test times, which is consisting with the crystal uranium mineral formed on the specimen surfaces found in the XRD mapping;

— Ti ion was depleted on the surfaces after leaching 728 days; The atom percent of Ti ion in P4, P5 and P2 systems were lower than that in P1 and P3 systems. Ti ion is most depleted in granite system (P1) among the five systems. The system with cement and bentonite can retard Ti ion leaching, and Fe_3O_4 had no an effect on Ti ion leaching;

— Ba ion was enriched on the surfaces after leaching 182 days, and there is an enrichment order P3>P1>P5>P4>P2 at leaching 728 days; Fe_3O_4 can enrich Ba ion on the specimen surfaces;

— Ca ion was enriched in bentonite system P4, and most depleted in granite system P1 than other systems;

— The Zr ion was enriched on the specimen surfaces and had an enrichment order P3>P5>P4>P2>P1; Zr ion has an obviously enrichment in the systems with Fe_3O_4; bentonite and cement can speed the enrichment;

— Al ion was enriched in P1 and P2 systems at 728 days, and slightly depleted in P3, P4 and P5 systems; the media with bentonite and Fe_3O_4, can speed the depleted trend.

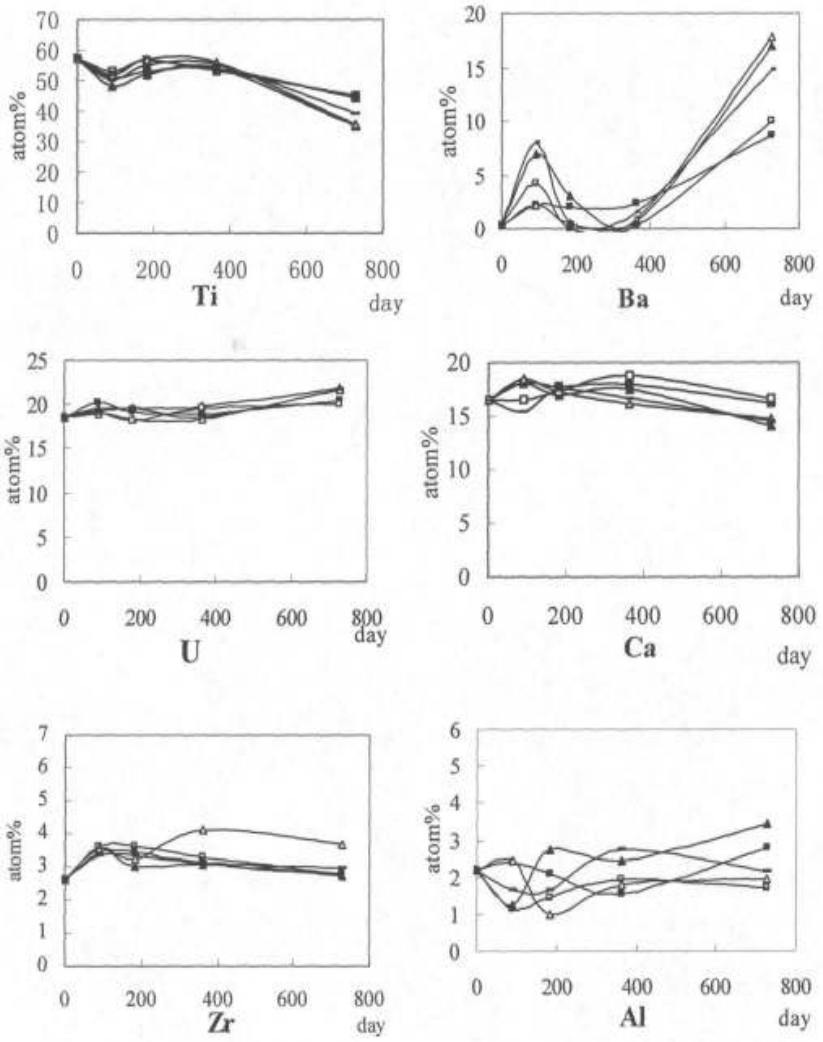

Fig.13 EDS mapping of the element concentration on the leached surfaces 90℃ for 728d
(P1 -▲-, P2-■-, P3-△-, P4 -□-, P5 —)

3.3.5. Leachate analyses

The leachates were analyzed by using MCC-1. The concentrations of Ca, Ti and U element in different medium were given in Fig. 14.

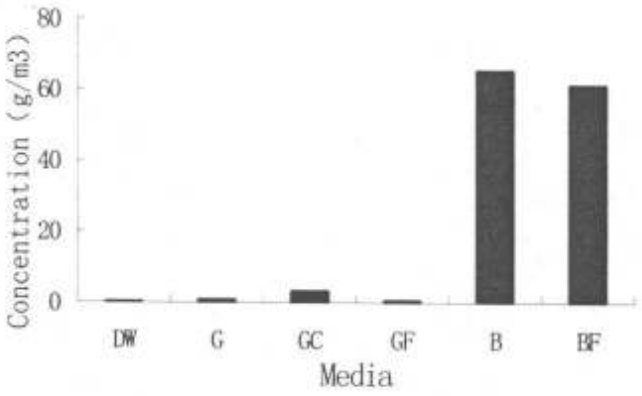

(a) Ca element

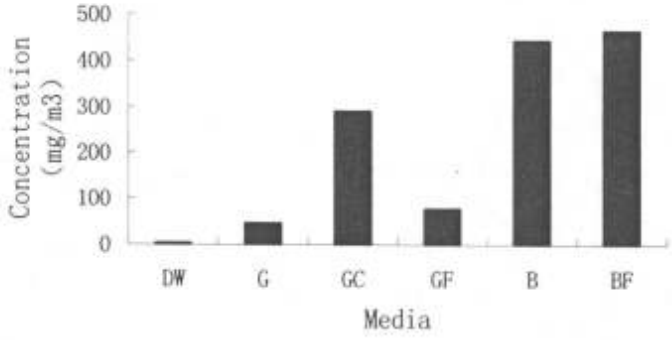

(b) Ti element

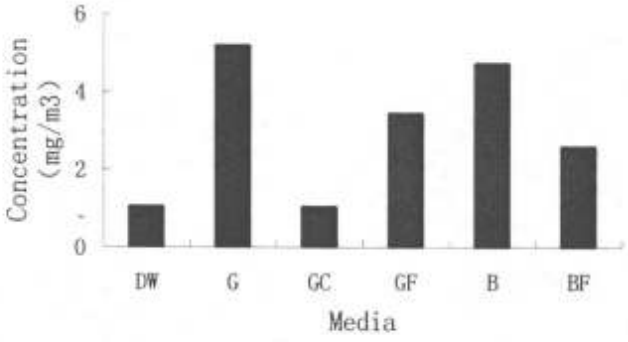

(c) U element

Fig.14 Elemental concentrations in leachate

(DW-deionized water, G-granite, GC-granite+cement, GF-granite+Fe_3O_4, B-betonite, BF-betonite+ Fe_3O_4)

It was found from Fig.14 :

(1) Ca-concentration is the highest in the betonite media leachate. The corrosion product (Fe_3O_4) existence can reduce the Ca-concentration in leachate. Ca-concentration is the lowest in granite media leachate and the cement existence can enhance the Ca-concentration leachate.

(2) Ti-concentration is the highest in the betonite media leachate, but the corrosion product existence can increase the Ti-concentration. Ti-concentration is the lowest in granite media leachate and the cement existence can enhance the Ti-concentration in leachate.

(3) Uranium showed different behavior. U-concentration in leachate has the following order:

- In granite media > in betonite media > in granite + Fe_3O_4 media
- In betonite + Fe_3O_4 media > in granite + cement media

3.3.6. Leached surface analyses

The leached surfaces were analyzed by using SEM/EDS. The concentration of Ca, Ti, U element on leached surface are showed in Fig. 15.

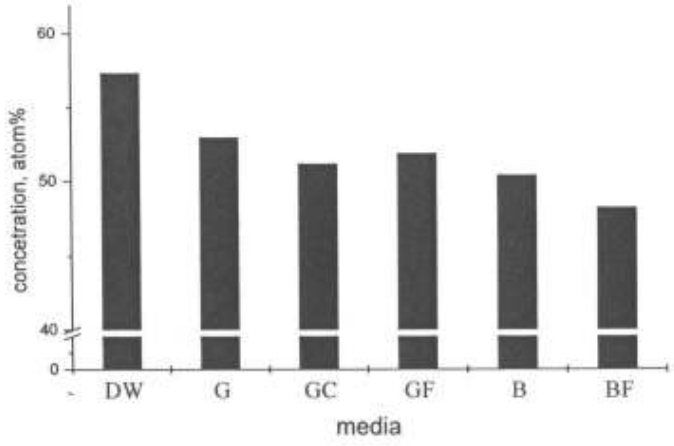

(a) Ti-element

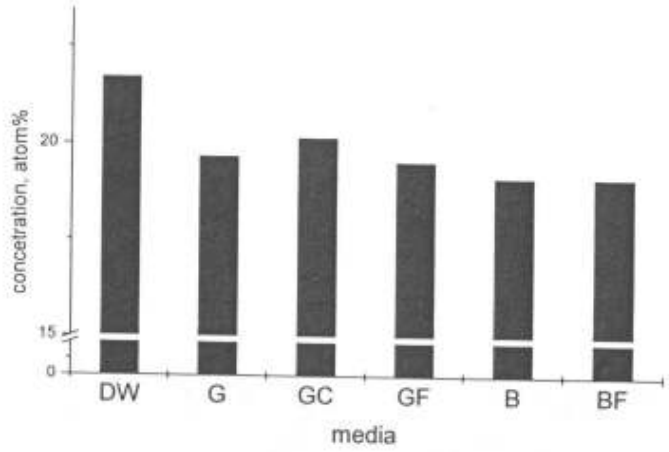

(b) U-element

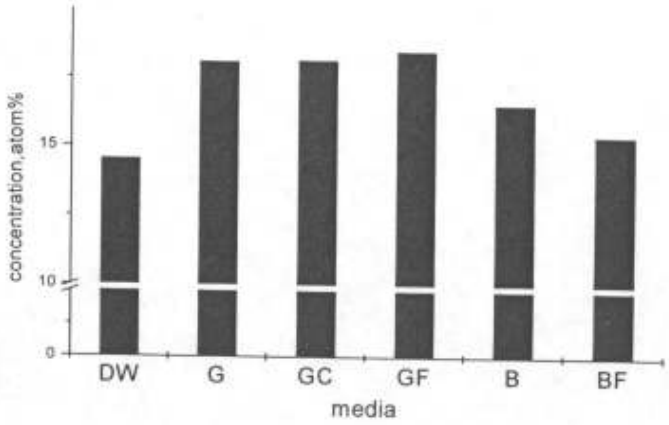

(c) Ca-element

Fig.15Concentration of Ca, Ti, U elements on leached surfaces

It is found that the Ti-concentration and U-concentration on leached surface in medium is decreased. The Ca-concentration on leached surface in medium is increased . It indicated the existence of geological media would enhance the leaching amount of Ti and U elements, but could retard the leaching of Ca element.

3.3.7. XRD analyses of leached surfaces

The XRD patterns of leached pyrochlore-rich synroc are given in Fig. 16. It proves there are no new phases on the leached specimens' surface.

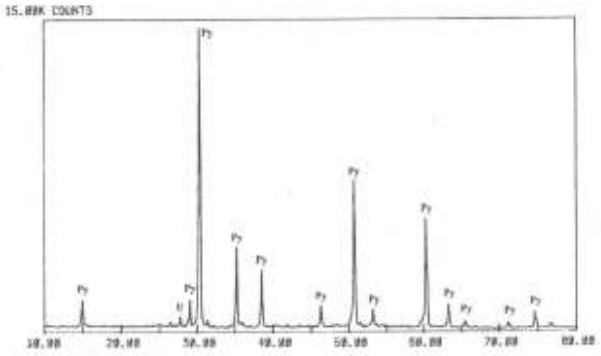

(a) deionized water (90 days)

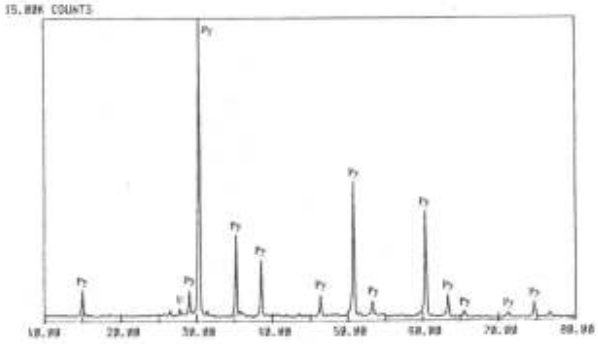

(b) granite media (90 days)

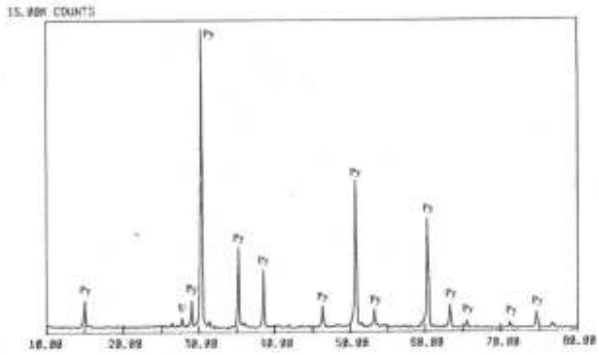

(c) betonite media (90 days)

Fig. 16 XRD patterns of leached specimens

3.3.8.. XRD patterns of irradiated specimens

The XRD patterns of irradiated pyrochrole-rich synroc specimens are showed in Fig.17. The relationship of I/I_0 and irradiation dose are showed in Table XVII and Fig.18.

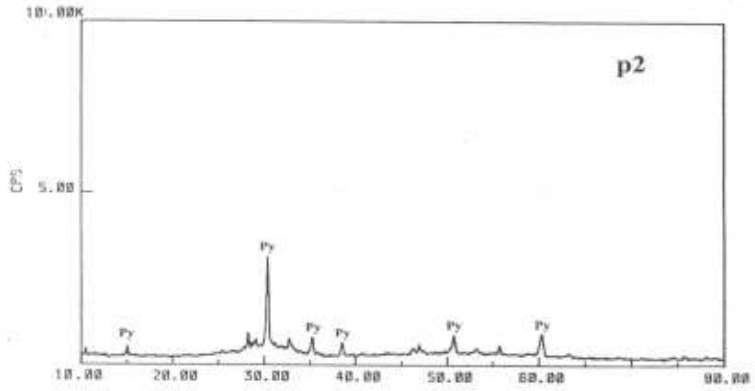

(c) irradiation dose 0.4dpa

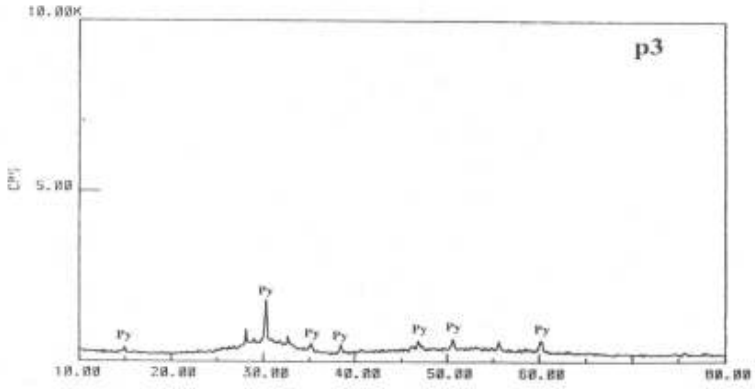

(d) irradiation dose 0.6dpa

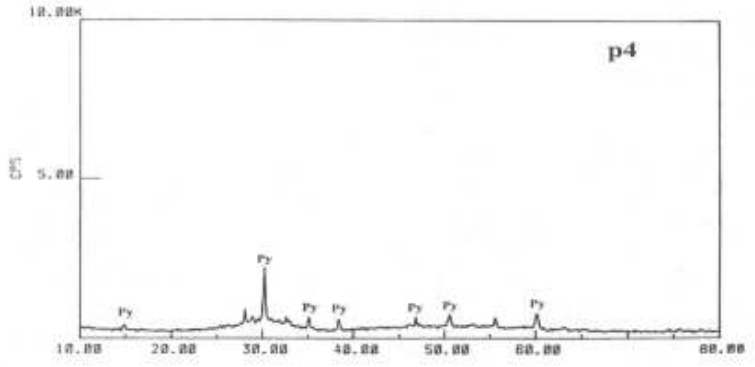

(e) irradiation dose 1.0dpa

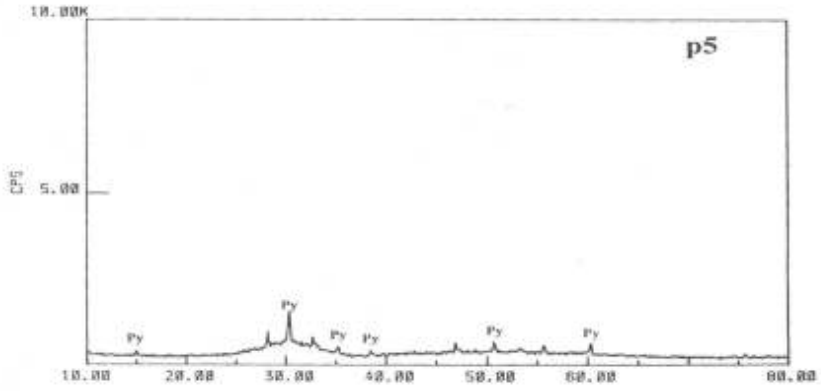

(f) irradiation dose 1.6dpa

Fig. 17 XRD patterns of irradiated specimens

Table 17 Intensity change with irradiation dose

Irradiation dose (dpa)	Diffraction peak intensity (cps)	Relative intensity, I/I_0
0	14218	1
6.2	4057	0.285
0.4	3153	0.222
0.6	1790	0.126
1.0	1673	0.132
1.6	1549	0.112

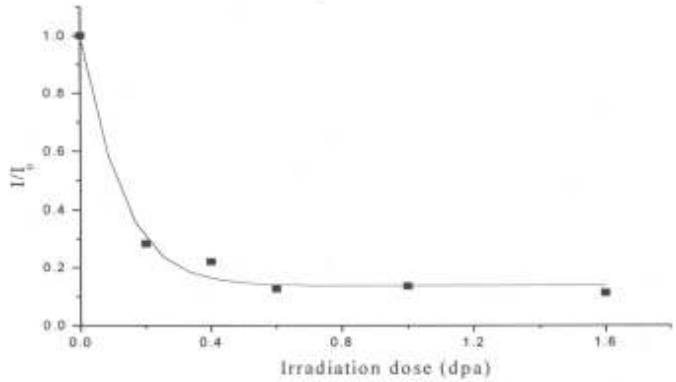

Fig. 18 I/I_0 *vs* Irradiation dose

It is indicated that the amorphous dose is 0.5 dpa for pyrochlore-rich synroc. Its irradiation resistance is better than zirconolite-rich synroc.

3.3.9. Electron diffraction analyses of irradiated specimens

The electron diffraction images are showed in Fig. 19

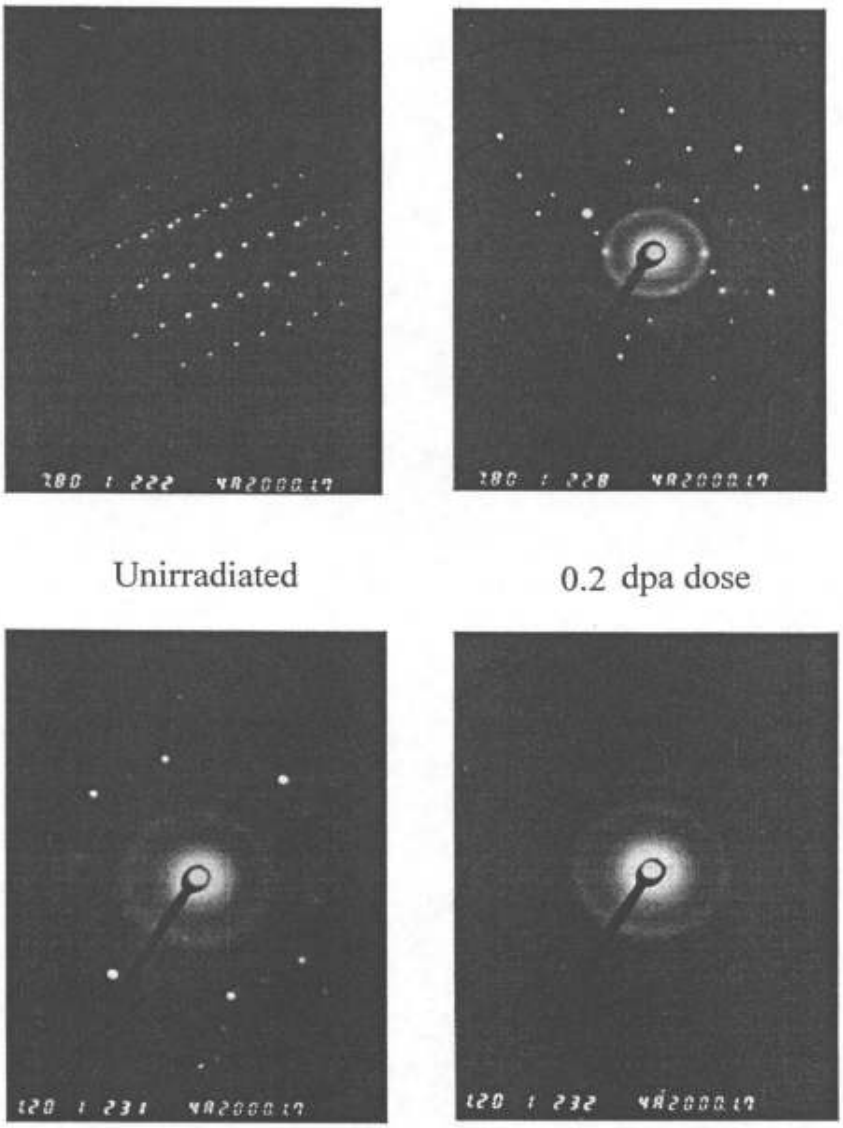

Unirradiated 0.2 dpa dose

0.4 dpa dose 0.6 dpa dose

Fig. 19 Electron diffraction of irradiated specimens

It is cleared that the pyrochlore-rich synroc would lose its crystal structure at the irradiation dose of 0.4 ~ 0.6 dpa.

3.4. Zircon synroc

3.4.1. Physical properties

The physical property test results are listed in Table XVIII.

TABLE.XVIII. PHYSICAL PROPERTIES OF NATURAL ZIRCON AND ZIRCON WASTE FORM

Samples	Density (g/cm^3)	Open porosity (%)	Vickers hardness (kg/mm^2)
Natural zircon	5.27	0.51	846
Zircon waste form	5.09	4.0	715

From the results listed in Tab. 18, the fabricated zircon waste form has better physical properties with open porosity less than 5% to compare with the synthetic zircon wasted form from oxides[6].

3.4.2. Phase assemblages and microstructure

The XRD pattern of zircon waste form (Fig.20) indicated that the major phase was zircon, and the minor phase was uranite (UO_2).

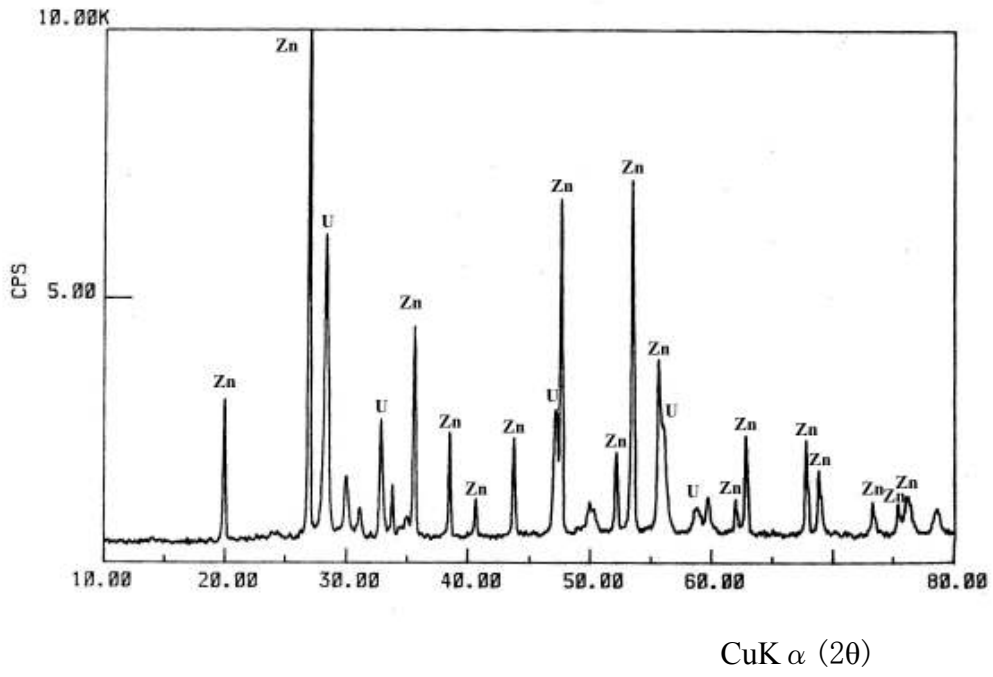

FIG. 20. XRD pattern of zircon waste form (Zn-Zircon, U-Uranite)

The SEM and TEM images of zircon waste form are given in Fig. 21.

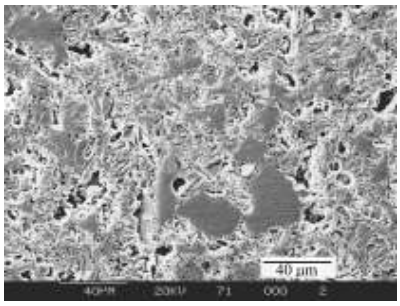

(a) SEI(×500)

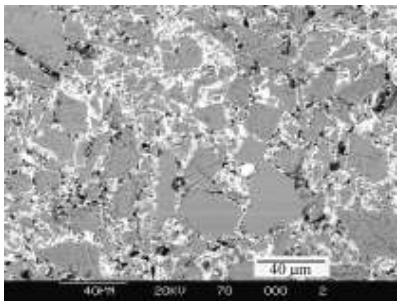

(b) BEI(×500)

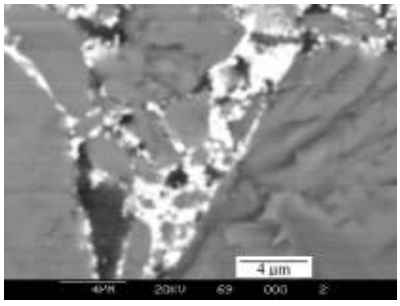

(c) BEI(×5000)

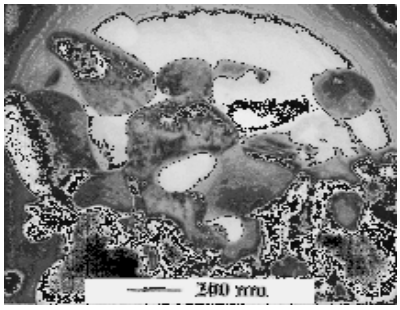

(d) TEM(×60,000)

FIG. 21. SEM and TEM images of zircon waste form

Secondary electron image (SEI) showed that the sample had micro voids, in accordance with physical property test results (Fig. 21a). The backscattered electron image (Fig. 21b) indicated that some of the large zircon grains (10～100 μ m), did not fully participate in the solid state reaction. This was one reason that the physical properties of the zircon waste form were not good as natural zircon. The solid state reaction mainly took place in the matrix between the zircon grains, as can be seen in Fig. 21c. The bright contrast phase is uranite, the gray phase is zircon and the black phase is SiO_2.

The chemical compositions of the phases in the area among the un-reacted zircon grains were analyzed by TEM/EDS (Fig.21d). The results were shown in Tab.19 along with the inferred phase formulae.

The solid-state reaction and Nd/U entering the Zr site cause the difference of Si stoichiometry in zircon phases. The charge balance may be maintained by a fraction of U^{6+} ions in Zr site when Nd^{3+} is included in Zr site of zircon.

The TEM/EDS analyses results confirmed that through the solid state reaction the zircon phase containing the waste elements U and Nd $[(Zr_{0.10}Nd_{0.18}U_{0.60})_{0.88}Si_{1.12}O_4]$ was obtained. The presence of the uranite phase was

due to incomplete reaction with the un-reacted zircon grains. The few SiO_2 phases that existed were due to inclusions in the natural zircon.

TABLE.XIX. RESULTS OF TEM/EDS ANALYSES

Phase	Elemental composition (atm. %)***				Formula
	Si	Zr	Nd	U	
Zircon(A)*	47.70	51.36	0.00	0.95	$(Zr_{1.03}U_{0.02})_{1.05}Si_{0.95}O_4$
Zircon(B)**	55.91	5.06	9.05	29.98	$(Zr_{0.10}Nd_{0.18}U_{0.60})_{0.88}Si_{1.12}O_4$
Uranite	6.73	17.77	8.63	66.87	$(U_{0.67}Zr_{0.18}Nd_{0.09}Si_{0.07})_{1.01}O_2$
SiO_2	95.97	2.00	1.08	0.95	$(Si_{0.96}Zr_{0.02}{}^{Nd}{}_{0.01}U_{0.01})_{1.00}O_2$

* Zircon(A) is the un-reacted natural zircon phase;

** Zircon(B) is the synthesized zircon phase formed by solid state reaction;

*** Elemental composition is the average value of 10 analytical results.

3.4.3. Hydrothermal durability

The hydrothermal durability of the zircon waste form was tested by the MCC-1 method (at 90□, for 3, 7, 14, 28, 90 days, in deionized water, SA/V=10m^{-1}). The leachate was analyzed for Zr, Nd and U by ICP/MS. The mass loss rates and elemental normalized leach rates are listed in Table XX.

TABLE XX. MASS LOSS RATES AND ELEMENTAL NORMALIZED LEACH RATES

Elements	Mass loss rate and elemental normalized leach rate ($g.m^{-2}.d^{-1}$)				
	3 days	7 days	14 days	28 days	90 days
Zr	3.24×10^{-6}	1.39×10^{-6}	6.94×10^{-7}	6.94×10^{-7}	2.16×10^{-7}
Nd	1.75×10^{-4}	4.40×10^{-4}	2.33×10^{-4}	1.19×10^{-4}	1.50×10^{-4}
U	2.22×10^{-5}	3.53×10^{-5}	4.00×10^{-5}	1.31×10^{-5}	1.30×10^{-5}
mass	1.80×10^{-1}	1.2×10^{-1}	8.1×10^{-2}	4.8×10^{-2}	1.60×10^{-2}

The results listed in Table XX indicated that the fabricated zircon waste form was durable with low mass loss rate and elemental normalized leach rates compared with typical synroc[14]. The surface of the leached samples were tested using XRD and SEM. The SEM image of 7, 14, 28 and 90 days leached samples are showed in Fig. 22. From these four images we found there was no significant alteration on the surface under experimental conditions.

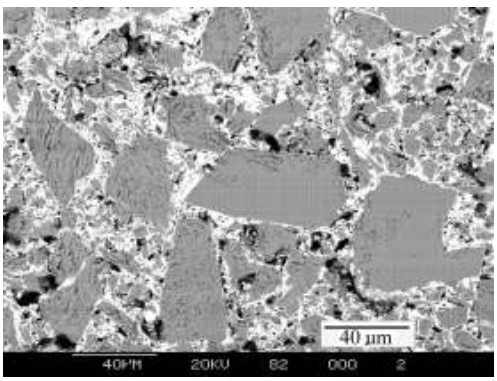

(a) 7 days leaching

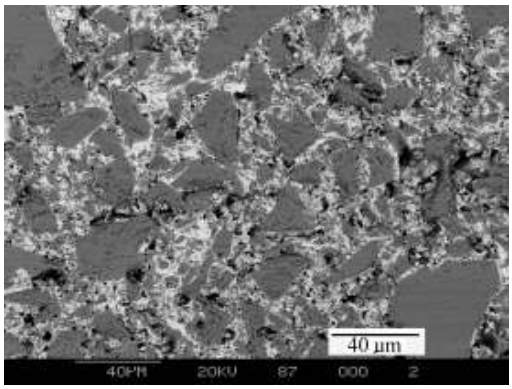

(b) 14 days leaching

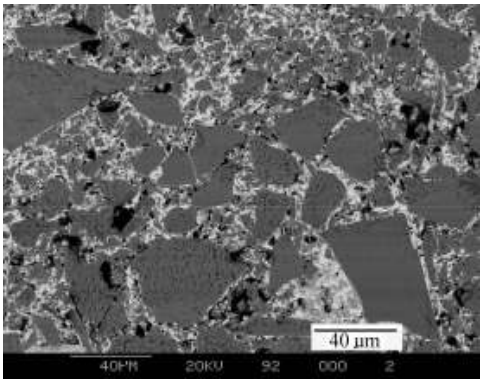

(c) 28 days leaching

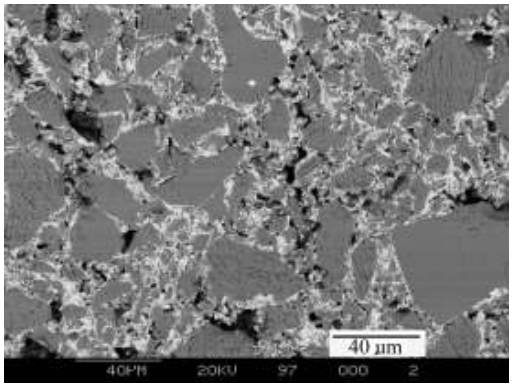

(d) 90 days leaching

FIG. 22 SEM images of leached zircon waste forms

3.4.4. Irradiation test

The samples were irradiated by 100 MeV ^{32}S ion beam on the HI-13 tandem accelerator at National Nuclear Physics Laboratory, China Institute of Atomic Energy (CIAE). The depth of ^{22}S ion implantation was 18.7 μ m, as calculated by the TRIM-91 program[6]. The adopted ion influence was 2.46×10^{11}(ions/cm^2), and the irradiation dose rate was 1.62×10^{-4}(dpa/s). The samples of the zircon waste form were irradiated up to the dose of 1.6 dpa (displacement per atom) at room temperature.

The amorphization dose of the zircon waste form was determined by XRD. The highest diffraction intensity peak (200), I_0, refers to the intensity of an un-irradiated sample. I referred to the intensity of the irradiated samples. The figure of I/I_0 with irradiation dose is shown in Fig. 23.

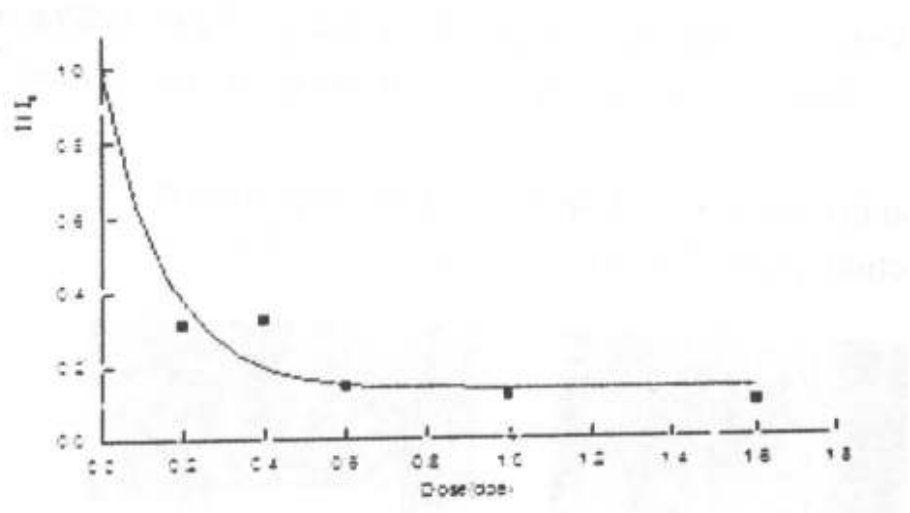

Fig. 23 Zircon I/I_0 *vs* Irradiation dose

From Fig. 23, the zircon phase X-ray amorphous state was reached at the irradiation dose of 0.7 dpa. Because un-irradiated regions existed, the I/I_0 did not fall to zero. This value is comparable with 0.7dpa of 10 wt% ^{239}Pu doped zircon[15] and 0.55dpa of 1.5MeV Kr^+ ions irradiated zircon[16].

3.5. Tc-Immobilization by synroc and its product characterization

3.5.1. Physical properties

Table XXI shows the density and open porosity data of the samples. For comparison, synroc-C reference sample No.0 (PW-46-D) was also fabricated and tested.

TABLE XXI. PHYSICAL PROPERTIES OF SYNROC SAMPLES

Sample No.	Waste loading (wt%)	Density (g/cm^3)	Open porosity (%)
0	20	4.51	0.05
1	20	4.06	0.03
2	25	4.09	0.04
3	30	4.14	0.04
4	35	4.18	0.08
5	20	4.32	0.03
6	25	4.36	0.01
7	30	4.37	0.03
8	35	4.41	0.06

The density data (4.06-4.51g/cm^3) and open porosity data (<1%) indicated that the produced samples are highly densified and have few micro-voids.

3.5.2. Phase assemblages

The phases identified by XRD are summarized in Table XXII where the minor phases are listed in parenthesis. Some XRD patterns show in Fig.24. It indicated that the fabricated synroc samples have the phase assemblage as designed

TABLE XXII. PHASE ASSEMBLAGES OF SYNROC SAMPLES

Sample No.	Existing phases	Sample No.	Existing phases
1	P (Z,H)	5	R(Z,H)
2	P (Z,H)	5	R(Z,H,M)
3	P (Z,H,M)	7	R(Z,H,M)
4	P (Z,H,M)	8	R(Z,H,M)

P(perovskite), R(rutile), Z(zirconolite), H(hollandite), M(metal alloy)

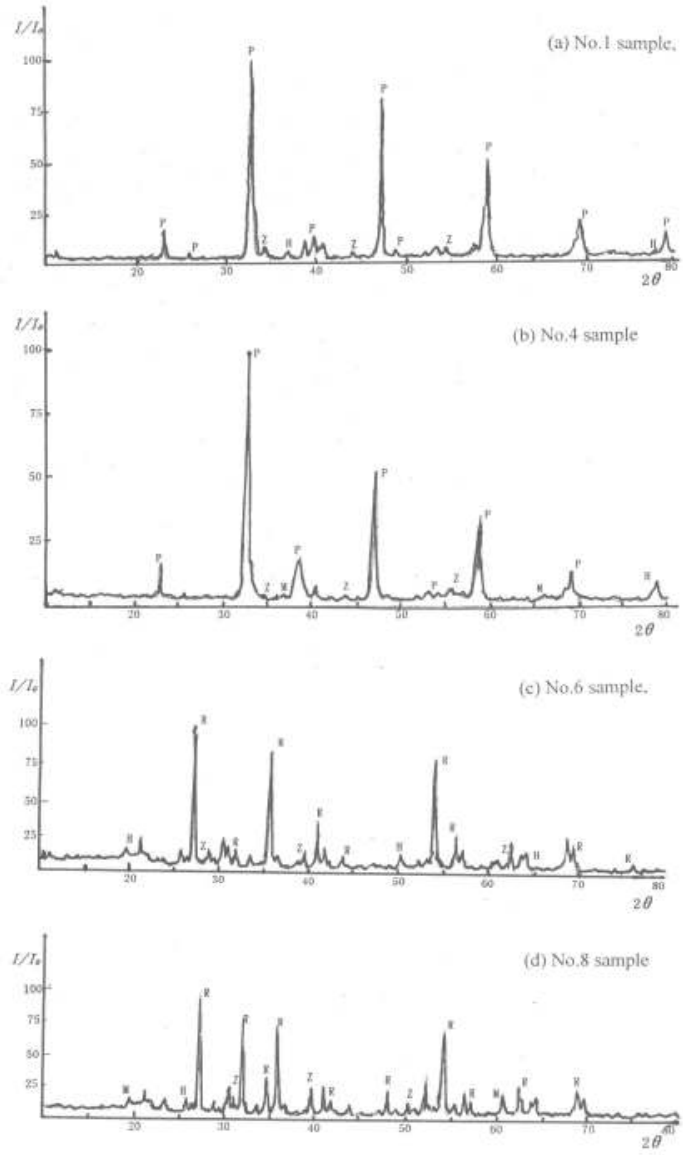

Fig.24 XRD-Pattern
No.1 and No.4 ---perovskite-rich synroc
No.6 and No.8 --rutile-rich synroc

3.5.3. Microstructure analyses

The microstructure of samples were analyzed with SEM. Some SEM and backscattered electron images (BEI) are shown in Fig.25 and Fig. 26.

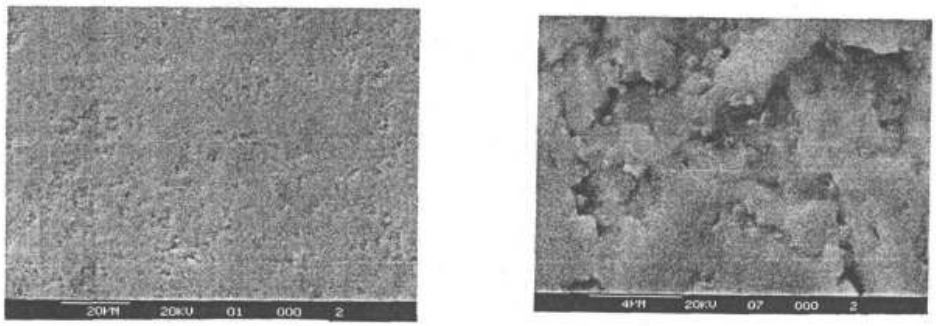

Fig.25 SEM and BEI of perovskite-rich synroc sample (No.1)

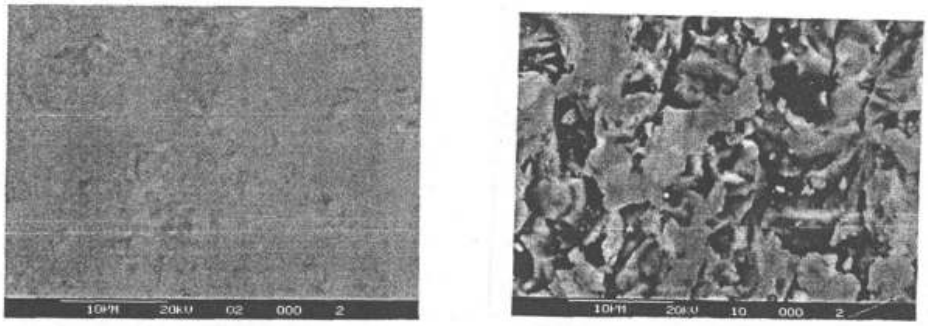

Fig. 26 SEM and BEI of rutile-rich synroc sample (No.5)

The SEM/BEI analyses confirmed the samples are highly densified and homogenous.

3.5.4. Hydrothermal durability

The hydrothermal durability of perovskite-rich and rutile-rich synroc samples were tested by using the MCC-1 method (90℃, 28 days, deionized water, SA/V=10m^{-1}). The Mn, Ti, Zr concentrations were analyzed by inductive coupled plasma mass spectroscopy (ICP/MS). Its mass loss and nominalized element leach rates are listed in Table XXIII.

TABLE XXIII. MCC LEACHING TEST RESULTS

Sample No.	Mass loss (g/m^2 /d)	Nominalized element leach rate (g/m^2 /d)		
		Mn	Ti	Zr
1	1.2×10^{-3}	$<2.8\times10^{-5}$	$<3.0\times10^{-5}$	$<2.4\times10^{-5}$
2	1.3×10^{-3}	$<2.3\times10^{-5}$	$<2.4\times10^{-5}$	$<1.9\times10^{-5}$
3	1.6×10^{-3}	$<1.9\times10^{-5}$	$<2.0\times10^{-5}$	$<1.6\times10^{-5}$
4	2.5×10^{-3}	$<1.6\times10^{-5}$	$<1.7\times10^{-5}$	$<1.4\times10^{-5}$
5	1.3×10^{-3}	1.0×10^{-3}	$<3.0\times10^{-5}$	$<2.4\times10^{-5}$
6	1.3×10^{-3}	1.1×10^{-3}	$<2.4\times10^{-5}$	$<1.9\times10^{-5}$
7	2.1×10^{-3}	1.4×10^{-3}	$<2.0\times10^{-5}$	$<1.6\times10^{-5}$
8	3.3×10^{-3}	1.6×10^{-3}	$<1.7\times10^{-5}$	$<1.4\times10^{-5}$

The data given in Table 23 indicated that, the fabricated samples have good leach resistance, at level of 10^{-5} $g/m^2/d$~10^{-3} $g/m^2/d$, particularly, perovskite-rich synroc has lower leaching rate. In fact, the concentrations of Mn, Ti, Zr in leachate were less than the detection limitation of ICP/MS, so the leach rate may be more lower..

3.6. Study on self-propagating high temperature synthesis of waste form

Using chromium oxide (Cr_2O_3) as an oxidant, immobilization of simulated waste in perovskite ($CaTiO_3$) by the self-propagating high-temperature synthesis (SHS) method was tested. The combustion synthesis of perovskite is based on the following formula:

$$2Cr_2O_3+3Ti+4CaO+TiO_2 \rightarrow 4CaTiO_3+2Cr+Q$$

The heat released from the reaction makes the reaction self-sustaining. Meanwhile, the waste is melted and the simulating nuclide (Sr^{2+}) is immobilized in the perovskite. The tungsten filament was served as igniting element. After pressing, the compact was ignited and combusted. The full pressure was loaded to density the synthesized ceramic material.

3.6.1. Physical properties of synthetic product

The bulk density and hardness of SHS synthetic products were measured. The results are listed in Table XXIV.

TABLE XXIV. DENSITY AND HARDNESS OF SYNTHETIC PRODUCT

Density g/cm^3	Hardness (HV) GPa
4.10	9.2

3.6.2. XRD composition

The synthetic product was analysed by XRD. The XRD patterns are showed in Fig. 27

From Fig.27 it was found that a perovskite structure with a pseudocubic crystal lattice was formed and Sr is existed in the perovskite lattice.

Comparing the XRD patterns of different amount of SrO added, it was found the synthetic products are composed of single $CaTiO_3$ phase when SiO_2 content is less than 35%, but SrO increases up to 40%, free SrO appears in the product (to see Fig.27).

It proves that immobilization limitation of SrO can be up to 35% with this SHS method.

3.6.3. SEM microstructure analyses

The SEM shows perovskite phase is irregular polgon. The grain size ranges from 30 to 40 μm. It proves that Sr is well distributed in the grain and SrO is combined with $CaTiO_3$ to form the uniform solid solution.

3.6.4. Synthesis mechanism discussion

$$\Delta H^{o}_{298} = 4\Delta fH^{o}_{298}(CaTiO_3) - 2\Delta H^{o}_{298}(CrO_3)$$
$$- \Delta fH^{o}_{298}(CaO) - \Delta fH^{o}_{298}(TiO_2)$$
$$\Delta H^{o}_{298} = -1995.79 kJ \cdot mol^{-1}$$
$$Tad = 2945K$$

Because the adiabatic temperature is so high as 2945K, the matrix and SrO can be well molten. In addition, the solid solution can be formed in an ultra-short time. Thus, the synthesis reaction is accomplished in liquid state. It can increase the product density and improve well-distributing nature. The nuclide Sr can be well immobilized in the perovskite lattice by SHS method.

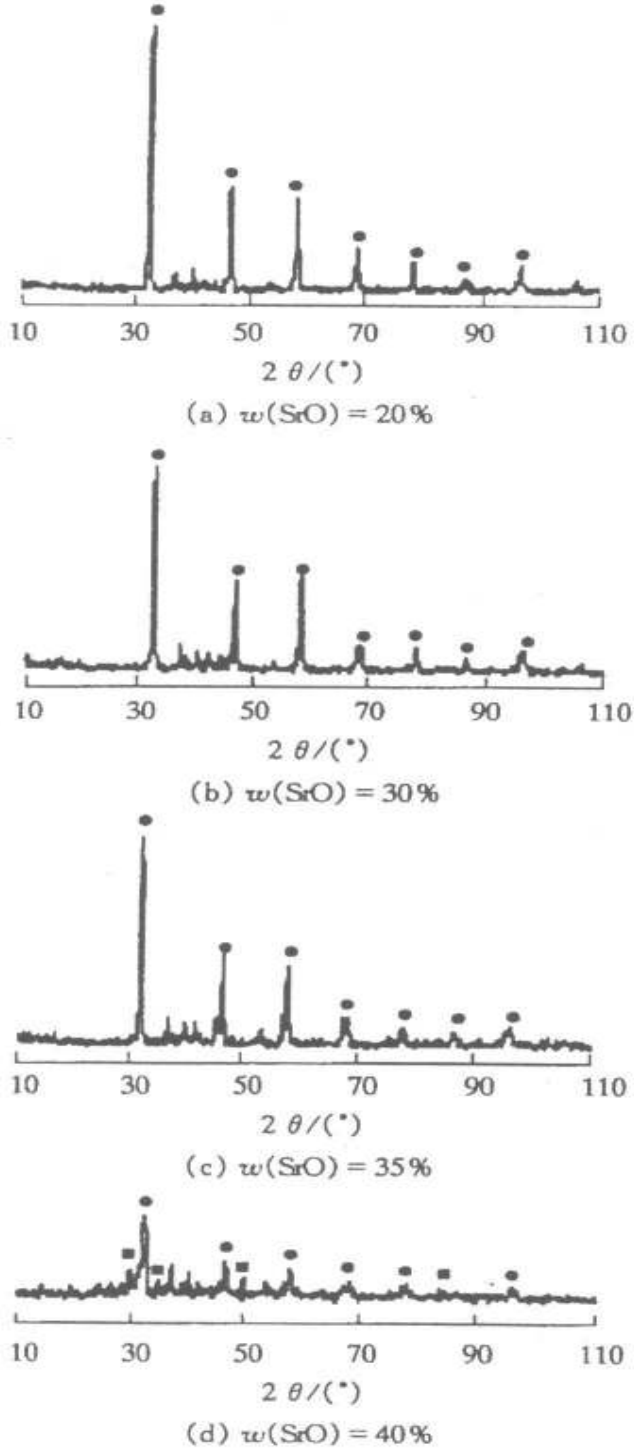

Fig.27 XRD of SHS samples

■ **SrO, • CaTiO3**

3.7. Uranium tailing matrix solidification

Zerconolite and pyrochlore solidify actinides have been studied in our previous reports[5,6]. Owing to it requires higher temperature and higher pressure and the matrix cost is also high, this study extends to try solidification it by uranium tailing.

The density, porosity and mass loss (measured by MCC-1) of fabricated products are listed in Table XXV.

TABLE XXV. CHARACTERIZATION OF FABRICATED PRODUCTS

Sample		Fabrication condition	Sample properties			Remark
			density, g/cm^3	porosity %	Mass loss radio $g/m^2.d$	
U5	1	1050 °C, 6.5MPa				Test material melted, model broken
	2	1200 °C	1.08			A honeycomb-like thing
U10	1	1050 °C, 9MPa				Test material melted, model broken
	2	1000 °C, 6MPa	2.71	0.60	2.45×10^{-2}	
	3	1050 °C, 6MPa				Test material melted, model broken
U15	1	900 °C, 5MPa	2.73	1.75	7.65×10^{-2}	
	2	900 °C, 5MPa	2.76	1.05	4.10×10^{-2}	
Synroc-C		1200 °C, 20MPa	4.43	0.003	3.19×10^{-3}	
Zerconolite		1200 °C, 20MPa	4.46	0.08	3.90×10^{-3}	
Pyrochlore		1200 °C, 20MPa	5.31	0.07	3.80×10^{-3}	

Uranium tailing contains more amount of Si and Al. From Tab.25. it was found that a glass-like product can be obtained at 900 °C 5MPa by using matrix uranium tailing. The solidified form has loadage of 15 wt% actinides with fair properties.

4. CONCLUSION

4.1. The glass durability test using simulated repository condition showed:

- Mass losses of the four tested systems are decreased with the leaching time.
- The bentonite system has higher mass losses. This phenomenon is occurred in other reference[16]. It may by caused by the high ion exchange and adoption ability of bentonite.
- The existence of Fe_3O_4 has no obvious effect on the bentonite system, but it enhanced obviously the mass loss in the granite system.
- The existence of cement caused increasing of mass loss for granite system.
- Some elements, such as Ca, Al were enriched on the sample surfaces along with leaching time, but the Ca element came gradually to a equilibrium state.
- Some elements such as Na, Si showed opposite trend with Ca, Al. The Na concentration is mostly depleted on the sample surfaces after 2 years leaching tests.
- The SEM pictures show that there are pitting corrosion and precipitation on the leached glass surfaces.

4.2 Results obtained for Synroc

The present research work shows that zirconolite rich, pyrochlore-rich and perovskite-rich synroc are suitable for the immobilization of actinide wastes.

Based on their product properties and leach test results, these three kinds of synroc samples can accommodate actinide loading up to 30 –35 wt%,47 –50 wt% and 68.6 wt% for Z-rich synroc, Py-rich and P-rich synroc, respectively.

4.2.1. For the Pryochlore-rich form:

- The mass loss rate reached the leaching equilibrium after 182days with 10^{-7} $g/cm^2 \cdot d$ of the mass loss rate, the mass loss rate is very low and indicates that pyrochlore-rich synroc has good resistibility to leach;
- The mapping of XRD showed two new peaks appeared on the leached surface in the system with bentonite and cement (P2, P4 and P5 systems).
- SEM mapping showed some corrosion pits on the specimen surfaces in the system with Fe_3O_4; so that, Fe_3O_4 can speed the corrosion and it is consistent with the result of mass loss rate;
- The analytical results of EDS suggest that the system with bentonite and cement can speed the enrichment of Zr ion, and slow down the leaching of Ti ion. And in the five simulated disposal media, expect that Ti ion was depleted on the surface, U, Zr, Al and Ca ion were in equable states and Ba was enriched, which indicated the simulated disposal media can effectively retard the leaching behavior.

4.2.2. For the Zirconolite-rich form:

- The zircon waste form bearing 20wt% simulated actinides using natural zircon powder as precursor material indicated. This formulation is feasible.
- Through solid state reaction, the zircon phase containing U and Nd was obtained.
- The fabricated zircon waste form had acceptable physical properties including density (5.09 g/cm^3), open porosity (4.0%) and hardness (715 kg/mm^2). It was durable; the elemental normalized leach rate for Nd was (10^{-4}), for U was (10^{-5}), for Zr was (10^{-6}-10^{-7}) $g.m^{-2}.d^{-1}$ and the mass loss rate was (10^{-1}-10^{-2}) $g.m^{-2}.d^{-1}$. There was no significant alteration on the surfaces under these experimental conditions.
- The amorphization dose of the zircon waste form was 0.7 dpa, indicating that the zircon waste form was relatively stable under the simulated irradiation condition.
- Due to the large grains of natural zircon which inhibited the solid state reaction, the properties of the zircon waste form were not good enough. However, the reduction of grain size and adjustments in the fabrication process, would improve its properties.

4.2.3. For the perovskite-rich form:

- Perovskite-rich synroc and rutile-rich synroc is suitable for the immobilization of Tc.. Tc^{4+} can substitute the Ti^{4+} position in the perovskite or form the stable rutile phase as Ti^{4+}.
- Based on their physical properties and leach rate data, the perovskite-rich synroc and the rutile-rich synroc can accommodate Tc up to 35wt%.
- In comparison, Tc immobilization by using perovskite-rich synroc is more favorable approach.
- The self-propagating high temperature synthesis technology has immobilization limitation of SrO up to 35-wt%. The nuclide Sr can be well in the perovskite lattice by this method.

4.2.4. For Uranium tailings matrix:

- Uranium tailing contains more amount of Si and Al. It was found that a lass-like product can be obtained at 900˚C, 5MPa by using matrix uranium tailing. The solidified form has loading of 15 wt% actinides with fair properties.

ACKNOWLEDGEMENT

This research work is supported by International Atomic Energy Agency, Commission of Science Technology and Industry for National Defense, China.. It should be appreciated.

The authors also thank Dr. E. R. Vance ANSTO, Australia for his valuable advice.

The authors also express appreciation to Prof. Shenyun Zhu, Mr. Yunjun Xu for their support in irradiation experiment, also many thanks to Dr. E. R. Vance, ANSTO, Australia, for his valuable advice.

REFERENCES

[1] Shanggeng Luo, Jiawei Sheng, Baolong Tang, A comparison of PWR-glass and HLW-glass, J. Nuclear Materials, 298(2001)180

[2] Shanggeng Luo, Xinzhang Zhu, Baolong Tang, Actinides containment by using zirconolite-rich synroc, Proceedings of SPECTRVM'98. International Conference on Decommissioning and Decontamination and on Nuclear and Hazardous Waste Management, Vol.2, 829(1998).

[3] Liyu Li, Shanggeng Luo, Balong Tang and Dex Wang , Immobilization of sodium-bearing high-level radioactive waste in synroc containing $Na_{0.5}Nd_{0.5}TiO_3$-type perovskite, J.Am. Ceram. Soc., 80(1), 250(1997).

[4] E. R. Vance, B. D. Begg, R.A. Day and C. J. Bayne, Retention of Actinides in natural pyrochlores and zirconolites, Radiochemica Acta, 66/67 ,469(1994).

[5] Standard Test Method for Static Leaching of Monolithic Waste Forms for Disposal of Radioactive Waste, ASTM Designation: C 1220-98.

[6] J.R.Biersack, L.G.Haggmark, A monte carlo computer program for the transport of energetic ion in amorphous targets, Nuclear Instruments and Methods, 107,577 (2000).

[7] K. P. Hart et al., Immobilization of separated Tc and Cs/Sr in synroc, Mat. Res. Soc. Symp., Proc., Vol. 412, 1996, Materials Research Society, P. 261.

[8] E. R. Vance et al., Synroc derivatives for the Hanford waste remediation task, Mat. Res. Soc. Symp. Proc., Vol. 465, 1997, Materials Research Society, P.341.

[9] E. R. Vance et al., Further studies of synroc immobilization of HLW sludges and Tc for Handord tank waste remediation, Mat. Res. Soc. Symp. Proc., Vol.506, 1998, Materials Research Society, P. 269.[10] I. P. Borovinskaya, et al., Consolidation of radioactive wastes into mineral-like materials by the SHS method, Inter. J. Self-propagating High-temperature Synthesis, Vol.7, Number 1,129(1998).

[10] M. I. Ojovan, et al., Processing of large-scale radwaste-containing blocks using exothermic metalic mixtures, Mat. Res. Soc. Symp. Proc., Vol. 556,239(1999).

[11] R. C. Ewing, W. Lutze, W. J. Weber, Zircon: A host-phase for disposal of weapons plutonium, J. Mater. Res., 120(2),242(1995).

[12] W. J. Weber, R. C. Ewing, C. R. A. Catlow, T. Diaz de La Rubia, L. W. Hobbs, C. Kinoshita, et al., Radiation effects in crystalline ceramics for the immobilization of high-level nuclear waste and plutonium, J. Mater. Res., 13(6),1434(1998).

[13] J.Yang, X.Zhu, B.Tang, S..Luo, Incorporation of actinides in zirconolite-rich,pyrochlore-rich and perovskite-rich synroc, Environmental Issues and Waste Management Technologies in the ceramic and Nuclear Industries V, Ceramic Transaction, 107, 577(2000).

[14] W.J.Weber, R.C.Ewing, L.M.Wang, The radiation induced crystalline to amorphous transition in zircon, J. Mater. Res., 9(3), 688(1994).

[15] K. Lemmens, et al., Measurement of Glass Corrosion in Boom Clay Disposal Condition, SCK·CEN, Bortrysnh 200, B-2400, Mol, Belgium.

CHEMICALLY DURABLE IRON PHOSPHATE GLASSES FOR VITRIFYING SIMULATED NUCLEAR WASTE

A. MOGUŠ-MILANKOVIĆ

Ruđer Bošković Institute, Division of Materials Physics, Zagreb, Croatia

Abstract

The work described below is being conducted under the Research Contract No: 10638, "Chemically Durable Iron Phosphate Glasses for Vitrifying Simulated Nuclear Waste", where iron phosphate glasses are being investigated as alternative glasses for vitrifying selected nuclear wastes. The results of our research have shown that the iron phosphate glasses (IPG) containing from 25 to 40 mol% Fe_2O_3 are highly effective for vitrifying HLW. A very good chemical durability of IPG is attributed to the presence of Fe-O-P bonds, which are more hydration resistant than the P-O-P bonds usually present in other phosphate glasses. In addition to their excellent chemical durability, IPG can be melted between 950^{o}C and 1150^{o}C.

IPG waste forms obtained by adding different amounts of various simulated nuclear waste components (such as Cs_2O, Na_2O, Al_2O_3, PbO, Bi_2O_3, MoO_3 and SrO) to the base iron phosphate glass whose composition is $40Fe_2O_3$-$60P_2O_5$ (mol%) showed that it is possible to have a waste form with a corrosion rate one thousand times lower than that of one of a comparable borosilicate glass.

IPG with an O/P ratio of 3.5 are based on pyrophosphate groups and these glasses are chemically more stable in aqueous solutions compared to phosphate glasses with O/P ratio less than 3.5. Because of their unusually high chemical durability and other properties the IPG are potential candidates for the nuclear waste immobilization.

Our next activity was focused on the detailed examination of PbO-Fe_2O_3-P_2O_5 glasses combined with simulated nuclear waste. Some of the high level nuclear wastes (HLW) at Hanford, such as the waste from tank B-110 contain high percentages of P_2O_5 and Fe_2O_3 besides other oxides.

Further activity emphasized the IPGs containing high waste loading of up to 75 wt% of high chrome HLW at Hanford WA. Hanford high chrome wastes are being investigated since iron phosphate glasses are expected to have a higher solubility limit for chrome oxide and, therefore, potentially higher waste loadings than can be achieved in borosilicate glasses.

A major objective of the present study was to investigate the vitrification of the high chrome wastes at Hanford in IPG. An important part of the present work was to determine the maximum waste loading and the chemical durability of the high-chrome iron phosphate waste forms by different methods. The chemical durability of both glassy and deliberately crystallized waste forms was determined from dissolution rate (D_R).

1. RESULTS

1.1. Structure and properties of IPG glasses

A study of the structure and crystallization of binary IPG are presented in papers [1] and [2], which are integral part of this report.

The binary IPG, Table I, can be melted at relatively low melting temperature, up to 1000^{o} C. When IPG are melted in air they contain both Fe(II) and Fe(III) ions and equilibrium between them depends upon melting temperature, time and atmosphere.

The systematic evolution of the nature of the phosphate network from metaphosphate based on $(PO_3)^-$, (Q^2), units through the pyrophosphate structure based on dimeric $(P_2O_7)^{4-}$, (Q^1), units to the orthophosphate structure based on monomeric $(PO_4)^{3-}$, (Q^0), units with increasing iron content is shown in Figs. 1 and 2.

With the addition of iron oxide content the non-bridging oxygen ions with the formal charge $(P\text{-}O^-)$ form P-O-Fe bonds. It was found that good chemical durability is due to the formation of more hydration resistant Fe-O-P bonds with increasing Fe_2O_3, Fig. 3.

The best chemical durability has been determined for the glasses with an O/P ratio of 3.5 and for this ratio the structure consists of pyrophosphate units that are strong cross-linked with iron in the glass network. The chemical durability of the iron phosphate waste forms increases as the total number of Fe-O-P bonds increases in the waste forms, Fig. 6.

When up to 20 mol% one or more common nuclear waste component such as Cs_2O, Na_2O, Al_2O_3, PbO, Bi_2O_3, MoO_3 and SrO was added to binary IPG of approximately 40Fe-60P composition, Tables II and III, the glasses could be melted also on relatively low melting temperature. This is very important especially for the Cs-IPG because such a low melting temperature reduces the probability of evaporization of Cs during vitrification. Another fact important for the Cs-IPG is that CsCl can be directly immobilized in IPG [3].

It was found that the chemical durability for sodium and Cs-IPG is high (10^{-9} g/cm^2/min) whereas for mixed alkali oxide is lower at (10^{-7} g/cm^2/min) after 20 days at 90ºC, Figs. 4 and 5. The chemical durability for these IPG is not dependent on type of content of alkali oxides, depends only on Fe_2O_3 content.

Figure 6 shows the dissolution rate of iron phosphate glasses containing waste oxides. The data points plotted fit two lines where the upper one is for phosphate glasses contain either iron or alumina whereas the lower line is for glasses containing both iron and alumina. These results indicate the benefit of an increase of chemical durability when phosphate glasses contain both simulated waste oxides and iron oxide.

Since there was a controversy if lead should or should not be used in iron phosphate glasses for waste form application, and on the role of Fe in the inhibition of corrosion, our investigation was focused on $PbO\text{-}Fe_2O_3\text{-}P_2O_5$ glasses [4].

Table IV shows composition and selected properties of $PbO\text{-}Fe_2O_3\text{-}P_2O_5$ glasses and partially crystallized compositions. The compositions containing <33.7 mol% Fe_2O_3 form glass as no crystalline phases were detected by XRD. Samples A4, A5 and A6, containing more than 33.7 mol% Fe_2O_3 were partially crystallized.

The Raman spectra of glassy and crystallized compositions are shown in Figs. 7(a) and (b). The spectra of the PbO-Fe_2O_3-P_2O_5 glasses are similar, with the most prominent bands related to the pyrophosphate groups. Some barely detectable bands are attributed to metaphosphate structure.

The Raman spectra for partially crystallized PbO-Fe_2O_3-P_2O_5 samples are shown in Fig. 7(b). The spectrum of the A4 crystallized sample shows a Raman pattern typical for an orthophosphate composition. With increasing Fe_2O_3 content, bands related to pyrophosphate units and barely detectable metaphosphate structures, respectively, appeared in Raman spectra for the A5 and A6 compositions.

The dissolution rate, (D_R), of the glass and partially crystallized PbO-Fe_2O_3-P_2O_5 samples, measured from their weight loss in distilled water at 363ºK, are given in Fig. 8. For glasses with O/P ratio <3.95 dissolution is almost constant for a given immersion time. The D_R gradually increased for the compositions partially crystallized. Glasses with O/P <3.95 and (Fe+P)/P <1.0 had a D_R value more less than the window glass, depicted by the area between the dashed lines, and comparable to the D_R of a lead-free IPG. For the crystallized compositions whose O/P ratio exceeds 3.95, the difference in D_R is small compared to that for glasses. The dissolution rates for crystallized compositions are slightly higher than that for glasses suggesting that the chemical durability of the crystalline $Fe_3(P_2O_7)_2$ and $Fe_7(PO_4)_6$ phases identified in these samples, is comparable to previously investigated binary IPG.

1.2. Properties of PbO-Fe_2O_3-P_2O_5 nuclear waste forms

The chemical durability of PbO-Fe_2O_3-P_2O_5 waste forms (both glassy and crystalline) is a function of their composition and relate these properties to the structure of the waste forms [5].

The batch composition in wt% and properties of PbO-Fe_2O_3-P_2O_5 waste forms containing simulated B-100 waste from Hanford is shown in Table V. The samples containing less than 16 wt% of simulated B-110 nuclear waste formed glass as no crystalline phase was detected by XRD. Some of the samples, which contain more than 16.5 wt% waste content, were partially crystallized. The compositions with the O/P ratio less than 3.91 tended to form glass. The glass-forming tendency decreases with the increasing O/P ratio.

1.2.1. DTA and XRD

Fig. 9 shows the DTA patterns for the base glass and glass samples containing 11wt%, 14wt%, 19wt% simulated B-110 nuclear waste, respectively. The sample A9 was partially crystallized. The exothermic peaks at ~ 596°C, 611°C, 644°C and 618°C are attributed to crystallization of the pyrophosphate waste forms. $Fe_3(P_2O_7)_2$.

The resulting XRD patterns shown in Fig.10 indicate that $Fe_2Pb(P_2O_7)_2$ and $Fe_3(P_2O_7)_2$ are the main phases present in the samples containing less than 14 wt% simulated B-110 nuclear waste. As the waste content increased the lead-iron-pyrophosphate phase ($Fe_2Pb(P_2O_7)_2$), decreased and the crystalline $NaFeP_2O_7$ and SiP_2O_7 phases became dominant in the XRD spectra. The presence of the crystalline ferrous-ferric pyrophosphate ($Fe_3(P_2O_7)_2$) phase in all of the samples is related to the higher concentration of Fe_2O_3 and P_2O_5 for these compositions.

1.2.2. Dissolution rate

The chemical durability of the glassy and crystallized PbO-Fe_2O_3-P_2O_5 waste forms is shown in Fig. 11. For glasses with simulated B-110 waste content <8 wt%, the dissolution rate is approximately constant for a given immersion time. The D_R of the glasses with simulated nuclear waste contents between 8 to 12 wt% was the smallest for the samples studied. The D_R gradually increased for samples as the waste content increases above 14 wt%. These samples were partially crystallized and had (Fe+Pb)/P molar ratio of ~ 1.0. Glasses with molar (Fe+Pb)/P ratio of ~ 0.90 had a D_R value 100 times less than the D_R for window glass and is comparable to the D_R of glass iron phosphate (lead-free) waste forms with a simulated B-100 waste content of 35 wt%. In general, the D_R increased with increasing of waste content, however, most of the samples investigated sill had a D_R similar to window glass. This indicates that the chemical durability of the crystalline $Fe_2Pb(P_2O_7)_2$, and $Fe_3(P_2O_7)_2$ phases present in the crystallized samples is as good as that of the glasses.

1.3. High chrome nuclear waste in IPG

A major objective of the further study was to investigate the vitrification of the high chrome wastes at Hanford in iron phosphate glasses [6]. An important part of the present work was to determine the maximum waste loading and the chemical durability of the high chrome-iron phosphate waste forms. The chemical durability of both glassy and deliberately crystallized waste forms was determined from dissolution rate (D_R) and product consistency test (PCT) measurements.

1.3.1. Glass preparation

Batches that produced 50 to 100 g of glass of the general wt% composition $x(W)\bullet(100\text{-}x)P_2O_5$, where W denotes the simplified waste and x ranged from 35 to 90 at 5 % intervals were prepared by mixing the appropriate amounts of the oxides listed in the right hand column of Table VI.

Each glass was identified as “IP(x)W”, where “IP” stands for iron phosphate and “x” is the mass % of simulated waste, W. Thus, a designation as IP70W means an iron phosphate glass with a simulated waste (W) loading of 70 mass %. The volatilization of P_2O_5 and Na_2O during melting appears to be small.

1.3.2. XRD

The XRD results indicated that all waste forms containing ≤ 65 mass % waste were glassy. Those containing ≥ 70 mass% wastes contained small amounts (<1.5 mass %) of crystalline Cr_2O_3, see Fig. 12. On the basis that the IP65W composition contains a total of 2.6 mass % Cr_2O_3, but is free of crystalline Cr_2O_3, it is concluded that the solubility limit of Cr_2O_3 in these iron phosphate melts (for 2 h melting) is about 2.6 mass %. This is at least 2.6 times larger than the amount of Cr_2O_3 that can be dissolved in borosilicate melts, (solubility of Cr_2O_3 in borosilicate glasses is < 1 mass %).

1.3.3. Dissolution rate

As shown in Fig. 13, the dissolution rate for all the iron phosphate waste forms containing 55 to 80 mass % waste is up to 50 times smaller than that for soda-lime-silica window glass, even though, those waste forms containing 70 to 80% waste contain nearly 20

mass % Na_2O. The IP65W waste form, had the lowest dissolution rate (5.9×10^{-10} g/cm^2/min) or highest chemical durability in water at 90 °C. The presence of a small amount (up to 1.5 mass%) of crystalline Cr_2O_3 in these glasses does not appear to adversely affect their chemical durability to any measurable degree.

1.3.4. Product consistency test (PCT)

The PCT measured from the amount of ions released from powders immersed in deionized water at 90 °C for 7 days (ASTM C-1285-97).

The PCT was measured only for the IP70W and IP75W glasses in the present study. The pH value of the leachate was 9.03 and 9.51 for IP70W and IP75W glasses respectively. Concentration (ppm) of ions found in leachate by ICP-ES after PCT of glassy and crystallized samples is given in Table VII.

The average total normalized mass release for IP70W (Table VII) from PCT is only 1.33 g/m^2. The average total normalized mass release (1.86 g/m^2) for the IP75W sample is a little higher than that of IP70W but is still quite low.

1.3.5. Raman spectra

Raman spectra for the IPG containing high waste loading of up to 80 wt% of high chrome HLW are shown in Fig.14. There is an evidence of the structural evolution of glasses as a function of waste content.

The Raman spectrum of IPG containing 35 wt% waste consists of the bands related to the metaphosphate glass structure. In Raman spectra for glasses containing up to 50wt% along with bands due to the metaphosphate chains some bands associated with pyro- and orthophosphate groups are also present in glass structure. The barely detectable bands related to the uranium oxides present in simulated nuclear waste. With increasing waste content up to 80 wt%, the uranium oxide (U_3O_8) content increases. Since the uranium oxides generate intense fluorescence the conventional laser Raman instrumentation cannot be used. However, some barely detectable bands could be recognized in our spectra. Raman spectra of the glasses containing from 55 to 80 wt% wastes show the changes of phosphate network structure from that based on pyrophosphate structure to those based on orthophosphate groups suggesting a shortening of the length of phosphate units.

To obtain more information about the phosphate network in these waste forms the Raman spectra of glasses containing no uranium oxides are measured. Raman spectra of IPG containing 65 to 80 wt% no uranium wastes are shown in Fig.15. The Raman spectra for 65 and 70 mol% waste content show that these two structures consists predominantly pyrophosphate structure with some metaphosphate chains.

With further increase of waste content the observed bands are related to the orthophosphate units. The Raman spectrum for the glass containing 80 mol% wastes content shows bands that are sharp and more intense suggesting crystallization for this glass.

2. VITRIFICATION OF SODIUM BEARING WASTE (SBW) IN IPG USING COLD CRUCIBLE INDUCTION MELTING TECHNIQUES (CCIM)

The main objective of this study was to investigate the suitability of iron phosphate glasses (IPG) for vitrifying the SBW with an aim to producing a waste form with high waste loading and acceptable chemical durability. Melting these IPGs by the Cold Crucible Induction Melter (CCIM) technique has also been explored in a preliminary fashion, since this technique eliminates many materials and operating constraints, such as the chemical corrosion of the melter refractories and metal electrodes, which is inherent in the joule-heated melter (JHM) now being used to vitrify nuclear waste [7].

A simulated sodium bearing waste (SBW) was successfully vitrified in iron phosphate glasses (IPG) at a maximum waste loading of 40 wt% using a cold crucible induction melter (CCIM) as well as an electric furnace. No sulfate segregation or crystalline phases were detectable in the IPG when examined by SEM and XRD.

IPG waste forms are melted at a relatively low temperature (1000°C) and for short times (< 6 h) compared to borosilicate glasses. These advantages combined with those of a significantly higher waste loading and the feasibility of CCIM melting offer a considerable savings in time, energy, and cost for vitrifying the SBW.

The IPG waste forms containing 40 wt% SBW satisfy all of the known requirements for aqueous chemical durability as evaluated from their bulk dissolution rate (D_R), product consistency test (PCT), and vapor hydration test (VHT).

2.1. Chemical durability

2.1.1. Dissolution rate (D_R)

The D_R of the iron phosphate IP40WG and IP40WG-CCIM glasses and the borosilicate Environmental Assessment glass is shown in Fig. 16. The D_R of the present IP40WG and IP40WG-CCIM iron phosphate glasses was ~25 and ~5 times, respectively, lower than that of the EA glass in DIW at 90°C. It should be noted that the increase in the pH of the leachate for the IPGs was much less (from only 5.8 to 6.9) than the increase for the EA glass (from 5.8 for the DIW to 8.9).

2.1.2. Product consistency test (PCT)

The PCT results for the iron phosphate glasses (IP40WG and IP40WG-CCIM) and some borosilicate glasses are given in Fig. 17. The PCT protocol was designed specifically for borosilicate glasses and the established representative elements for PCT release for BS glasses are B, Na, and Li. There has not been any established PCT specification for phosphate glasses and both IP40WG and IP40WG-CCIM glasses do not contain either B (very little, 0.1 wt% B_2O_3, for IP40WG) or Li.

The r_{Na} released from IP40WG and IP40WG-CCIM was only 1.0 g/L (0.5 g/m^2) and 3.5 g/L (1.8 g/m^2), respectively. This PCT release (r_{Na}) from the IP40WG and IP40WG-CCIM iron phosphate glasses was ~14 and ~4 times, respectively, less than the r_{Na} leached from the EA borosilicate glass. The r_{Na} (0.5 g/m^2) released from IP40WG was also less than

or comparable to the r_{Na} released from the CVS-IS (1.5 g/m^2) and LD6-54-12 (0.4 g/m^2) standard BS glasses.

The chemical durability of the IP40WG-CCIM was not quite as good as that of the conventionally melted IP40WG, but was still better than that of the EA glass and comparable to that of the CVS-IS glass. The pH of the DIW used for the PCT increased considerably more for the borosilicate glasses (from 5.9 to 10.3 and from 5.7 to 11.4 and 11.9) than for the iron phosphate glasses (from 5.7 to 9.1 and 9.4). This small change in pH for iron phosphate glasses is due to their larger buffering action, compared to silicate glasses, in the solution.

The absence of any visually noticeable corrosion of the iron phosphate glass particles during the PCT is confirmed by their surface morphology after testing. The appearance of the as made IP40WG and IP40WG-CCIM glass particles as seen by SEM is shown in Fig. 18(a) and (c), respectively, while the appearance of the particles after the 7 day PCT is shown in Fig. 18(b) and (d), respectively. The sharp corners and edges of the particles after PCT in Fig. 18(b) and (d) and the absence of any detectable corrosion layer on the surface are clear evidence of the excellent chemical durability of the IP40WG and IP40WG-CCIM waste forms.

2.1.3. Vapor hydration test (VHT)

Figure 19 shows the appearance of the cross section (a, c) and external surface (b, d) of the IP40WG and IP40WG-CCIM, respectively, after 7-day VHT at 200°C. There was hardly any detectable corrosion on the surface of the IP40WG glass (Fig. 19(a)).

The small particles (corrosion products) were identified by XRD to be $Na_3Al(PO_4)_2 \cdot 1.5H_2O$ (Fig. 19(a)).

The chemical durability measured by three independent techniques (D_R, PCT, and VHT) for the IP40WG and IP40WG-CCIM waste forms produced results that are in excellent agreement with each other and showed that both waste forms meet all current DOE requirements for chemical durability. The chemical durability of the IP40WG-CCIM glass was not as good as that of the conventionally melted IP40WG glass, possibly due to the presence of significant amounts of Fe(II) and the different raw materials and procedures used to prepare the batch.

3. CONCLUSION

- IPG containing from 25 to 40 mol% Fe_2O_3 are highly effective for vitrifying HLW. A very good chemical durability of IPG is attributed to the presence of Fe-O-P bonds, which are more hydration resistant than that P-O-P bonds usually present in other phosphate glasses In addition to their excellent chemical durability, IPG can be melted between 950^{o}C and 1150^{o}C.
- IPG waste forms obtained by adding different amounts of various simulated nuclear waste components (such as Cs_2O, Na_2O, Al_2O_3, PbO, Bi_2O_3, MoO_3 and SrO) to the base iron phosphate glass whose composition is $0.40Fe_2O_3$-$0.60P_2O_5$ (mol%) showed that it is possible to have a waste form with a corrosion rate one thousand times lower than that of one of a comparable borosilicate glass.
- IPG with an O/P ratio of 3.5 are based on pyrophosphate groups and these glasses are chemically more stable in aqueous solutions compared to phosphate glasses with O/P

ratio less than 3.5. Because of their unusually high chemical durability and other properties the IPG are potential candidates for the nuclear waste immobilization.

— dissolution rate of the IPG containing nuclear wastes from tank B-110 at Hanford is comparable to that for borosilicate glasses.

— high chrome (up to 4.5 mass %) waste at Hanford can be vitrified by simply adding about 30 mass % phosphate to the waste and melting the mixture at 1250 °C for 2 h. The solubility limit of Cr_2O_3 in these iron phosphate melts is about 2.6 mass%, compared to < 1 mass % in common borosilicate glasses. Iron phosphate waste forms having waste loading of 55 to 75% of the high chrome HLW have an exceptionally high chemical durability.

— the successful melting of small amounts (~1 kg) of the IP40WG glass in the CCIM is highly encouraging since any potential problems involving glass contact refractories and metal electrode materials needed for joule heated melting are avoided. Based on the present results, CCIM appears to be a viable technique for melting iron phosphate glasses on a large-scale. This viability was also suggested by the high electrical conductivity measured in the IPG melts over their melting range.

— the chemical durability of the IP40WG and IP40WG-CCIM vitrified waste forms meets current DOE requirements.

— IPG containing 40 wt% SBW can be melted as low as 950-1000°C without sulfate segregation. Because these melts have a high fluidity (low viscosity at the melting temperature) and become rapidly homogeneous, melting times can be as short as a few hours (< 6 h) compared to the ~48 h needed for borosilicate glasses. The high waste loading, low melting temperature, rapid furnace throughput (short melting times), and potential for melting iron phosphate glasses in a CCIM offer a means to significantly reduce the cost of vitrifying the Sodium Bearing Waste.

REFERENCES

[1] A. Moguš-Milanković, Delbert E. Day, B. Pivac and K. Furić, *Structural Study of Iron Phosphate Glasses*, Phys. Chem. Glasses, 38 (1997) 74.

[2] A. Moguš-Milanković, M. Rajić, A. Drašner, R. Trojko and D. E. Day, *Crystallization of iron phosphate glasses, Phys. Chem.Glasses*, 39 (1998) 70.

[3] A. Moguš-Milanković, B. Šantić, K. Furić and D. E. Day, *TSC and dc conductivity in cesium iron phosphate glasses*, Phys. Chem. Glasses, 40 (1999) 305.

[4] A. Moguš-Milanković, A. Šantić, S. T. Reis, K. Furić, D. E. Day*, Studies of lead-iron phosphate glasses by Raman, Mössbauer and Impedance spectroscopy*, J. Non-Cryst. Solids, accepted for publication

[5] S.T. Reis, M. Karabulut, D. E. Day, *Structural features and properties of lead-iron-phosphate glasses*, J. Nucl. Mater. 304 (2002) 87.

[6] W. Huang, D. E. Day, C. S. Ray, C. W. Kim, A. Moguš-Milanković, *Vitrification of High Chrome Oxide Nuclear Waste in Iron Phosphate Glasses,* J. Nucl. Mater., 327 (2004) 46.

[7] C.W. Kim, C.S. Ray, D. Zhu, D.E. Day, D. Gomber, A. Aloy, A. Moguš-Milanković, M. Karabulut, *Chemically durable iron phosphate glasses for vitrifying sodium bearing waste (SBW) using conventional and cold crucible induction melting (CCIM) techniques*, J. Nucl. Mater., 322 (2003)

TABLE I. BATCH AND ANALYZED COMPOSITION OF BINARY IPG (MOL%)

Code	Batch composition		Glass composition*				Density
	Fe_2O_3	P_2O_5	Fe_2O_3	P_2O_5	Na_2O	Al_2O_3	(g/cm^3)
F-15 H	14	86	25	75	-	-	2.68
F-27	24	76	22	71	6	1	2.83
F-30 H	28	72	28	70	-	2	2.73
F-38	35	65	30	61	9	-	3.07
F-43	40	60	32	55	13	-	2.98
F-50 Z							

* as determined by EDAX. Some of the glasses contained less than 2 mol% Al_2O_3 dissolved from the alumina crucible during glass melting.

TABLE II. THE COMPOSITION OF IPG CONTAINING DIFFERENT CS_2O CONTENT

Code	mol % Cs_2O	mol % Fe_2O_3	mol % P_2O_5	$Fe(II)/Fe_{tot}$ (%A)	O/P ratio	CS/P ratio
F38	0	35.3	64.7	0.20	3.32	0
FCs17	17.4	29.1	53.5	0.15	3.48	0.32
FCs24	24.0	26.8	49.2	0.15	3.56	0.49
FCs28	28.0	23.4	48.7	0.15	3.57	0.57

TABLE III. BATCH COMPOSITION AND SELECTED DATA FOR MOO_3-FE_2O_3-P_2O_5 AND SRO-FE_2O_3-P_2O_5 GLASSES.

Sample Cod.	**Batch composition (mol%)**				**Mo/P**	**O/P**	**Fe/P**	**Sr/P**	**Tg (±5 K)**	**α^*(±3.0×10^{-7}/K)**	**Fe(II)/Fe$_{tot}$**
	MoO_3	**Fe_2O_3**	**SrO**	**P_2O_5**							
SERIES A											
A1	5	38		57	0.044	3.632	0.667		489	67.7	nm
A2	10	36		54	0.093	3.778	0.667		460	70.0	0.18
A3	15	34		51	0.147	3.941	0.667		451	69.0	0.17
A4	20	32		48	0.208	4.125	0.667		438	74.2	0.15
SERIES B											
B1	5	35		60	0.042	3.500	0.583		487	61.0	nm
B2	10	30		60	0.083	3.500	0.500		463	71.6	0.14
B3	15	25		60	0.125	3.500	0.417		469	72.1	0.11
B4	20	20		60	0.167	3.500	0.333		nm	nm	nm
SERIES C											
C1	5	40		55	0.045	3.727	0.727		475	67.6	nm
C2	10	40		50	0.100	4.000	0.800		460	74.1	nm
C3	15	40		45	0.167	4.333	0.889		444	80.2	0.26
SERIES M											
M1		38	5	57		3.544	0.667	0.044			nm
M2		36	10	54		3.593	0.667	0.093			0.27
M3		32	20	48		3.708	0.667	0.208			0.25

*Average coefficient of thermal expansion between 298 and 573 K. nm: not measured. Calculated areas of the Fe(II) and Fe(III) doublets in the Mössbauer spectra.

TABLE IV. COMPOSITION AND SELECTED PROPERTIES OF (43.3-X)PBO-(13.7+X)FE_2O_3-43P_2O_5, (0≤X≤30), COMPOSITIONS.

Sample Code	**Composition (mol%)**			**Molar Ratio**		**$Fe(II)/Fe_{tot}$[b] (± 0.03 %)**	**Log D_R[c]**	**T_g (±2 K)**	**T_c (±2 K)**	**D (g cm^{-3}) (± 0.02 g cm^{-3})**	**R_{Fe-Fe} (Å)[d] (± 0.5 %)**
	PbO	**Fe_2O_3**	**P_2O_5**	**O/P[a]**	**(Fe+Pb)/P[a]**						
A0(G)[a]	43.3	13.7	43.0	3.48	0.82	0.14	-8.6	771	869	4.1	3.83
A1(G)	38.3	18.7	43.0	3.60	0.88	0.18	-8.6	785	933	4.7	3.30
A2(G)	33.3	23.7	43.0	3.71	0.94	0.28	-8.6	810	951	4.5	3.09
A3(G)	28.3	28.7	43.0	3.83	1.00	0.27	-8.4	804	946	4.4	2.93
A4(C)	23.3	33.7	43.0	3.95	1.05	0.32	-8.2	779	864 / 918	4.1	-
A5(C)	18.3	38.7	43.0	4.06	1.11	0.38	-8.1	-	864 / 919	4.0	-
A6(C)	13.3	43.7	43.0	4.18	1.17	0.41	-8.3	-	864 / 919	3.8	-

[a] Molar ratios of O/P and (Fe+Pb)/P were calculated from the batch compositions.

[b] $Fe(II)/Fe_{tot}$ ratio was calculated from the Mössbauer data.

[c] Dissolution rates (g/cm^2min) for glass and crystalline samples were measured from the weight loss experiments in distilled water at 363 K for 32 days.

[d] R_{Fe-Fe} (Å) was calculated for glasses, where Fe ions are randomly distributed.

TABLE V. BATCH COMPOSITION IN WEIGHT PERCENT AND PROPERTIES OF PBO-FE_2O_3-P_2O_5 WASTE FORMS.

Glass Composition (wt%)	**A0**[a]	**A1**	**A2**	**A3**	**A4**	**A5**	**A6**	**A7**	**A8**	**A9**
P_2O_5	33.99	36.76	38.63	39.27	39.89	40.51	41.76	43.00	44.26	45.47
Fe_2O_3	12.18	17.22	20.96	22.21	23.46	24.72	27.23	29.73	32.26	34.80
PbO	53.82	42.82	34.80	32.12	29.45	26.77	21.42	16.07	10.70	5.35
Bi_2O_3	-	1.22	2.14	2.44	2.74	3.05	3.66	4.27	4.87	5.48
SiO_2	-	1.10	1.94	2.21	2.49	2.76	3.32	3.87	4.42	4.97
Na_2O	-	0.68	1.19	1.36	1.53	1.70	2.04	2.38	2.72	3.06
Al_2O_3	-	0.13	0.22	0.26	0.29	0.32	0.38	0.45	0.51	0.57
CaO	-	0.07	0.12	0.14	0.16	0.18	0.21	0.25	0.28	0.32
Waste loading (wt%)	-	4.72	8.28	9.45	10.63	11.81	14.17	16.54	18.88	21.24
Properties										
O/P ratio[b]	3.50	3.62	3.71	3.74	3.78	3.81	3.84	3.91	3.96	4.00
(Fe+Pb)/P ratio[b]	0.83	0.75	0.70	0.67	0.67	0.64	0.63	0.61	0.60	0.57
D_{RG}[c] ($g/cm^2/min$)	1.7×10^{-9}	1.4×10^{-9}	1.8×10^{-9}	6.2×10^{-10}	8.1×10^{-10}	3.0×10^{-9}	1.8×10^{-9}	3.6×10^{-9}	5.9×10^{-9}	4.1×10^{-9}
D_{RC}[c] ($g/cm^2/min$)	2.8×10^{-9}	1.0×10^{-9}	4.4×10^{-10}	7.6×10^{-10}	1.1×10^{-8}	1.2×10^{-7}	4.0×10^{-7}	-	-	-
ρ (g/cm^3)	4.1	4.1	4.2	4.4	4.1	3.6	3.6	3.4	3.3	3.3
Tg (^oC)	498	nm	516	519	508	486	507	504	503	474
Tc (^oC)	596	nm	631	617	611	593	644	632	618	599

[a] Starting lead-iron-phosphate glass

[b] Molar ratio of oxygen to phosphorus and (Fe+Pb)/P molar ratio were calculated from the batch compositions.

[c] Dissolution rates for glass (D_{RG}) and crystalline (D_{RC}) samples was measured from the weight loss experiments in distilled water at 90^oC for 32 days.

TABLE VI. BATCH COMPOSITION IN WEIGHT PERCENT OF HIGH CHROME IPG

#	Spl.ID.	Al_2O_3	Bi_2O_3	CaF_2	Cr_2O_3	Fe_2O_3	Na_2O	P_2O_5	SiO_2	U_3O_8	ZrO_2	La_2O_3
15	IP35W	7.35	1.05	1.05	1.40	3.15	9.10	66.75	5.60	3.15	1.05	0.35
10	IP40W	8.40	1.20	1.20	1.60	3.60	10.40	62.00	6.40	3.60	1.20	0.40
6	IP45W	9.45	1.35	1.35	1.80	4.05	11.70	57.25	7.20	4.05	1.35	0.45
3	IP50W	10.50	1.50	1.50	2.00	4.50	13.00	52.50	8.00	4.5	1.50	0.50
1	IP55W	11.55	1.65	1.65	2.2	4.95	14.3	47.75	8.8	4.95	1.65	0.55
21	IP60W	12.60	1.80	1.80	2.40	5.40	15.6	43.00	9.6	5.4	1.8	0.6
23	IP65W	13.65	1.95	1.95	2.6	5.85	16.9	38.25	10.4	5.85	1.95	0.65
24	IP70W	14.7	2.1	2.1	2.8	6.3	18.2	33.5	11.2	6.3	2.1	0.7
25	IP75W	15.75	2.25	2.25	3	6.75	19.5	28.75	12	6.75	2.25	0.75
26	IP80W	16.8	2.4	2.4	3.2	7.2	20.8	24	12.8	7.2	2.4	0.8

BATCH COMPOSITION IN WEIGHT PERCENT OF HIGH CHROME IPG WITHOUT U_3O_8

#	Spl.ID.	Al_2O_3	Bi_2O_3	CaF_2	Cr_2O_3	Fe_2O_3	Na_2O	P_2O_5	SiO_2	U_3O_8	ZrO_2	La_2O_3
231	IP65W	14.7		2.75		4.03	29.94	29.58	19.01			
241	IP70W	15.56		2.90		4.26	31.69	25.47	20.12			
251	IP75W	16.39		3.06		4.49	33.38	21.49	21.20			
261	IP80W	17.19		3.21		4.70	35.02	17.65	22.23			

TABLE VII. CONCENTRATION (PPM) OF IONS FOUND IN LEACHATE BY ICP-ES AFTER PCT OF GLASSY AND CRYSTALLIZED IP70W AND IP75W SAMPLES

Element	Concentration (ppm)*			
	IP70WG	IP70WX	IP75WG	IP75WX
Al	39.3	31.2	73.5	55.7
Bi	<0.1	0.2	<0.1	0.8
Ca	<0.1	0.1	<0.1	0.2
Cr	0.5	<0.1	0.3	<0.1
Fe	0.3	0.2	0.3	0.7
Na	138	130	184	190
P	73	55.1	90	74
Si	22.5	32.8	30.0	44.2
U	0.2	1.84	0.3	3.27

* Average of duplicate samples, estimated error is ± 3 %

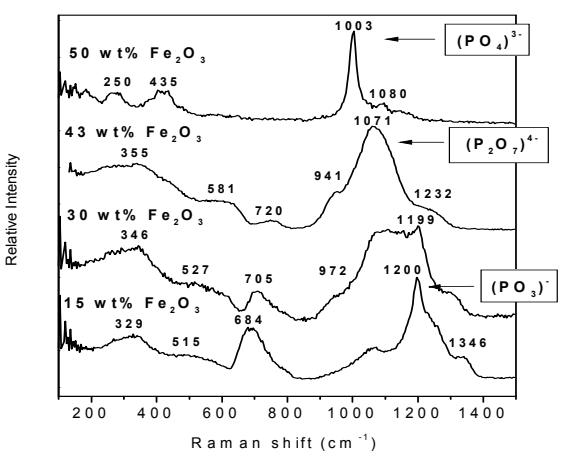

FIG. 1. Raman spectra of iron phosphate, xFe_2O_3 $(100-x)P_2O_5$ glasses ($15 \leq x \leq 50$). The Raman bands for 15 wt% Fe_2O_3 glass are characteristic for the structure containing chains of PO_4 tetrahedra, which share their corners to form P-O-P bonds. With increasing Fe_2O_3 up to 43 wt% the Raman spectra consist of pyrophosphate structure containing only one P-O-P bond.

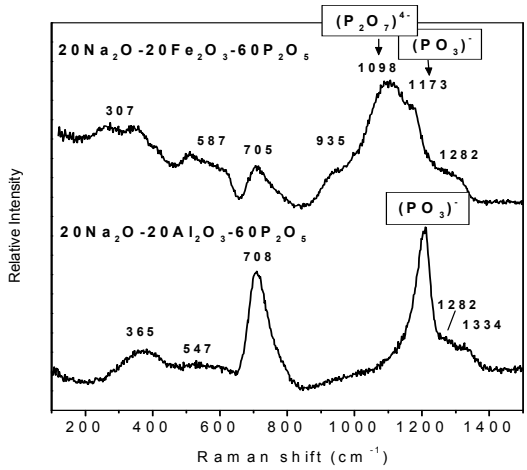

FIG. 2. Raman spectra for the $20Na_2O$-$20Al_2O_3$-$60P_2O_5$ and $20Na_2O$-$20Fe_2O_3$-$60P_2O_5$ glasses. The structural changes show the decrease in the relative intensity of the $(PO_3)^-$ non-bridging oxygens in Q^2 structure and an increase of the $(P_2O_7)^{4-}$ non-bridging oxygens in Q^1 structure.

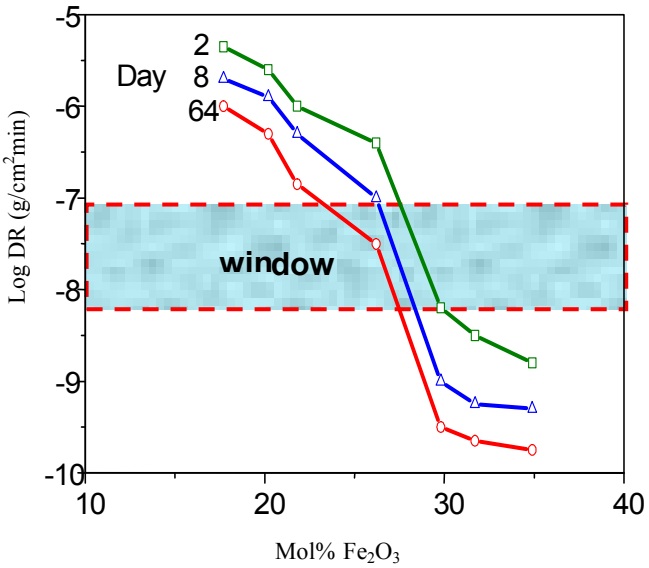

FIG. 3. Dissolution rate of iron phosphate glasses in distilled water at 90 °C for 2, 8 and 64 days.

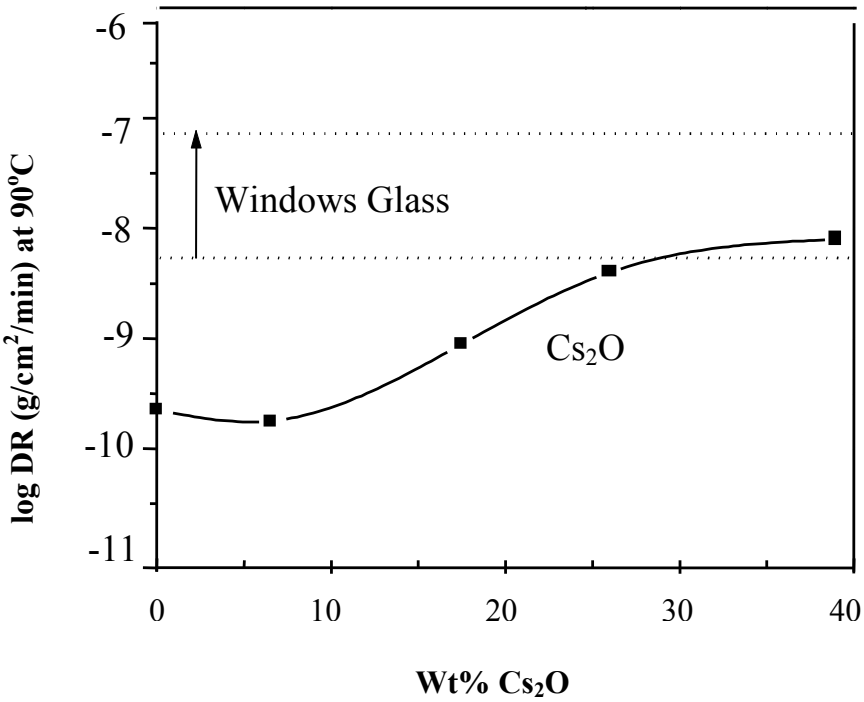

FIG. 4. Dissolution rate (DR) for IPG in distilled water at 90°C for 16 days as a function of Cs_2O content. Dashed lines denote DR for windows glass.

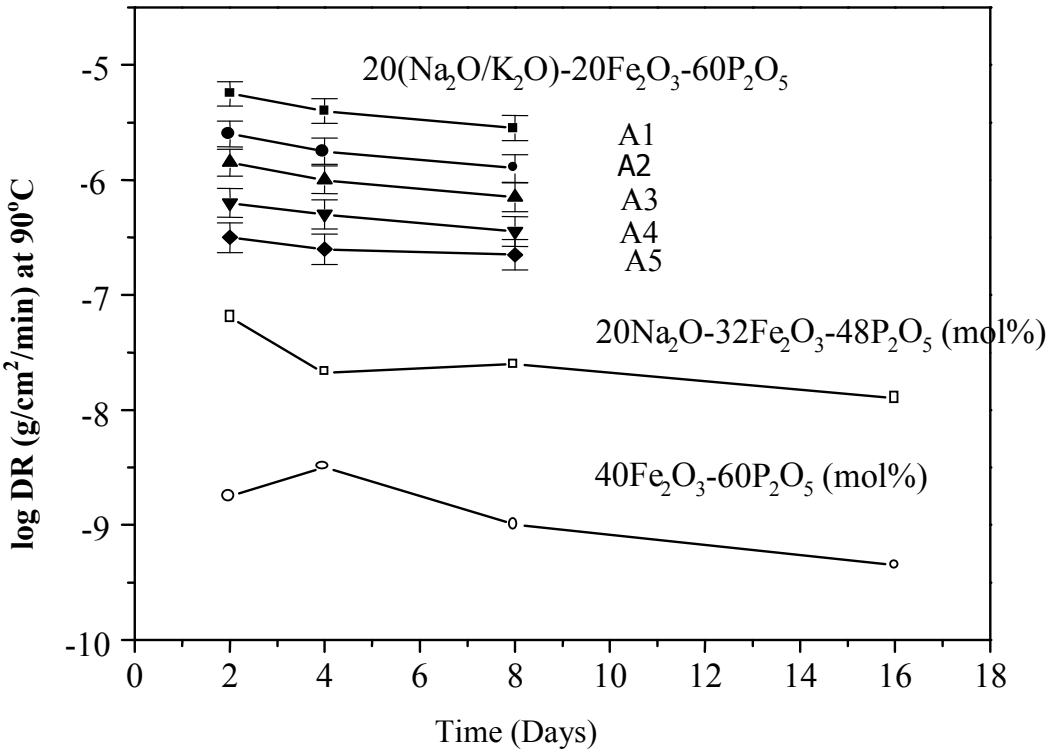

FIG. 5. Dissolution rate (DR) of the IPG containing different alkali oxides in distilled water at 90°C.

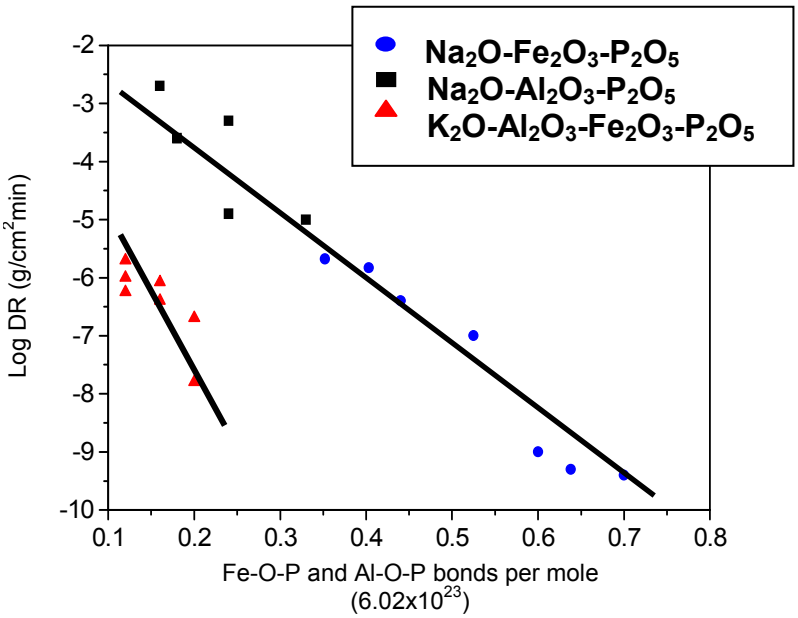

FIG. 6. Dissolution rate (DR) of iron phosphate glasses containing waste oxides measured in distilled water at 90°C plotted vs. total number of Fe-O-P and Al-O-P bonds calculated from the batch.

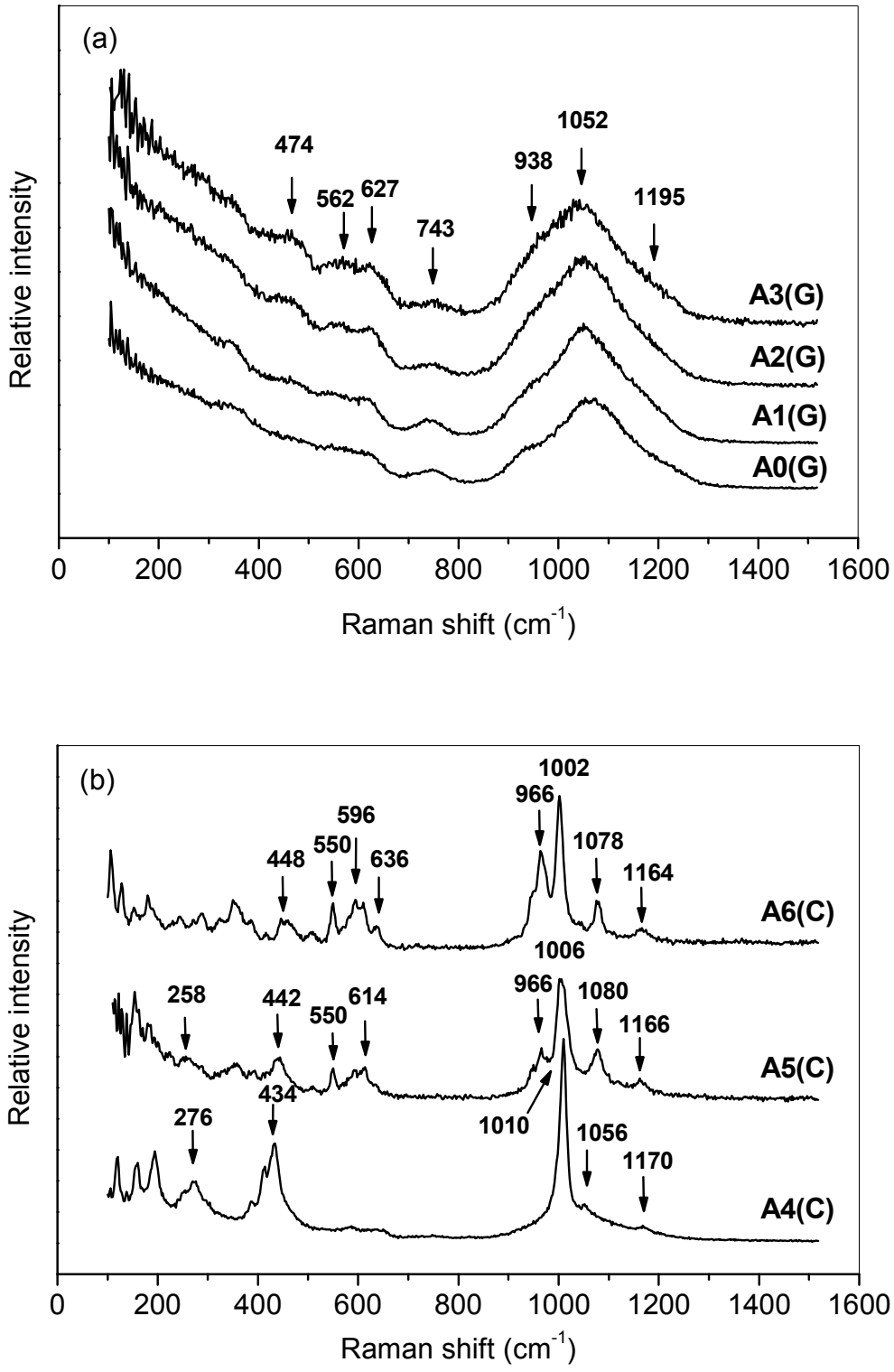

FIG. 7. The Raman spectra of lead-iron phosphate glasses (a) and partially crystallized samples (b)

.

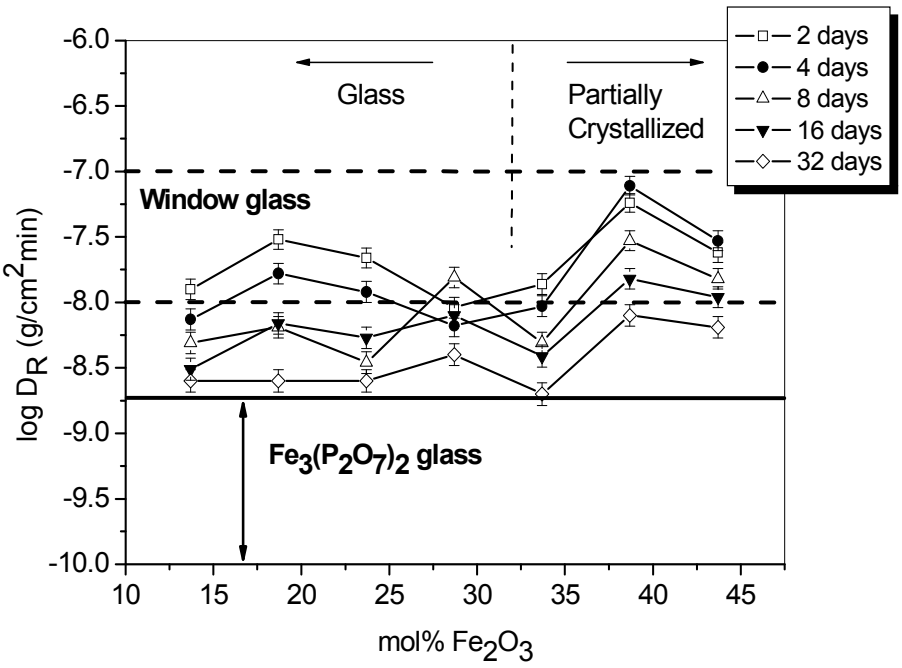

FIG. 8. Dissolution rate (D_R) for glassy and crystallized lead-iron phosphate samples as a function of the Fe_2O_3 content after immersion in distilled water at 363 K for 2, 4, 8, 16, and 32 days.

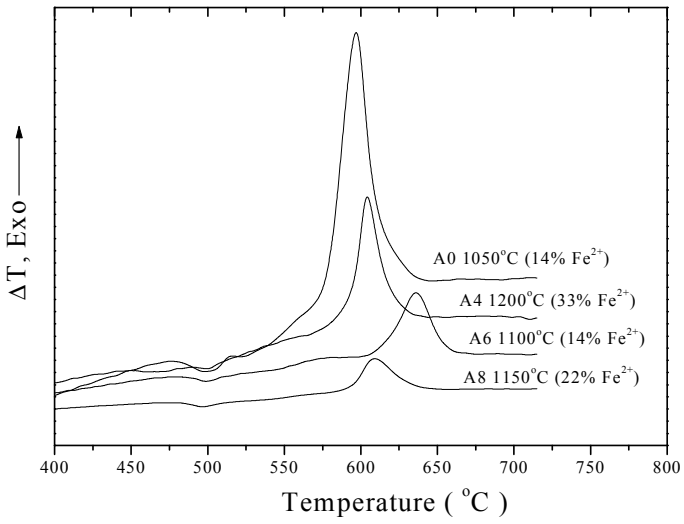

FIG. 9. Differential thermal analysis (DTA) curves forIPG with simulated waste content of 0 to 19 wt%.

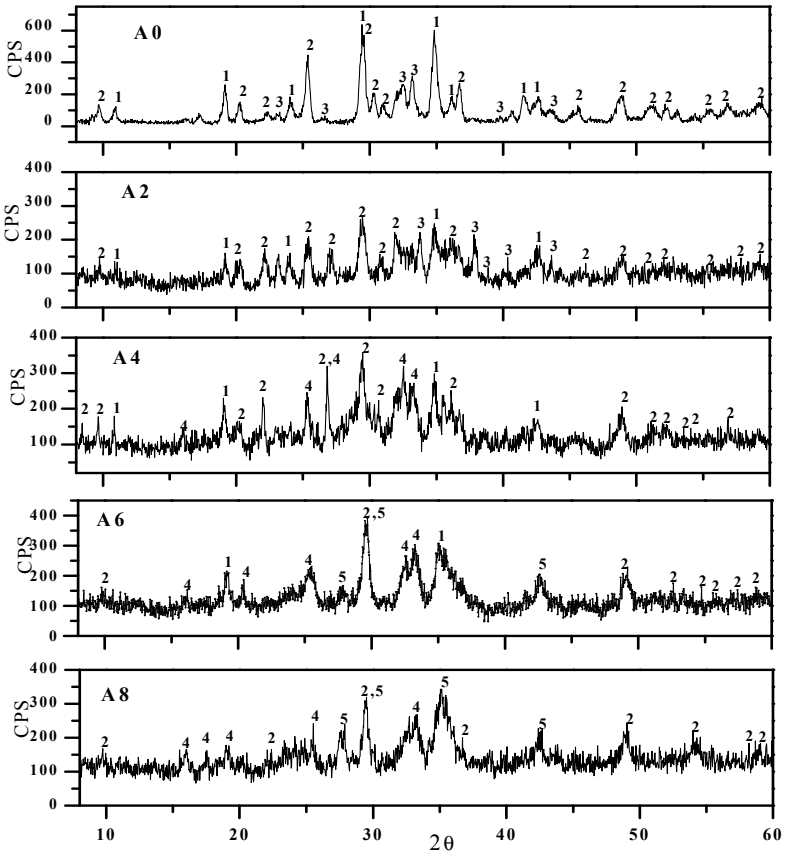

FIG. 10. X-ray diffraction patterns for IPG waste forms after crystallization treatment for 24h in air. Crystallized phases identified by XRD were #1 $Fe_2Pb(P_2O_7)_2$, #2 $Fe_3(P_2O_7)_2$, #3 $Pb_2P_2O_7$, #4 $NaFeP_2O_7$, and #5 SiP_2O_7.

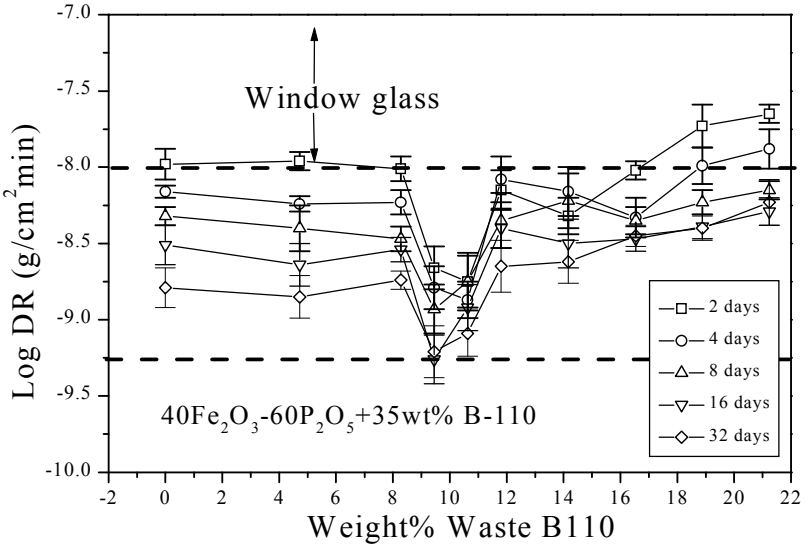

FIG. 11. Dissolution rate (D_R) for glassy and crystallized IPG waste forms as a function of the wt% of waste B110 after immersion in distilled water at 363 K for 2, 4, 8, 16, and 32 days.

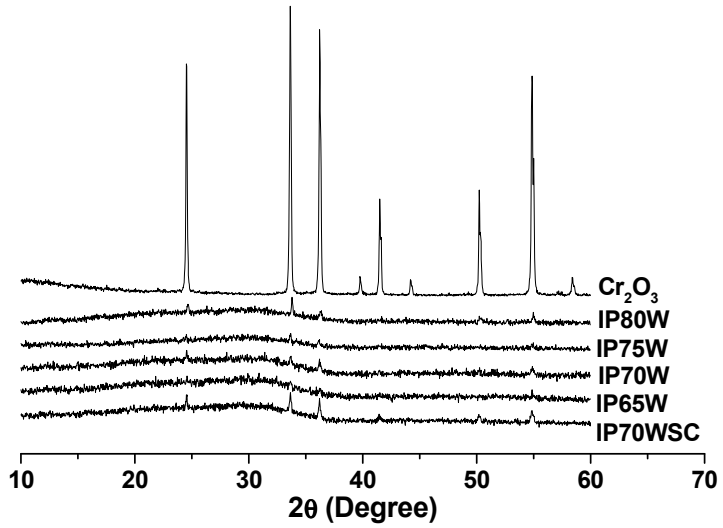

FIG. 12. XRD patterns for Cr_2O_3 containing iron phosphate waste forms, annealed. Trace amounts of crystalline Cr_2O_3 are evident in the samples with ≥ 70 mass % waste loading. The curve IP70WSC is for a sample cooled at 2 ˚C/min from its melting temperature.

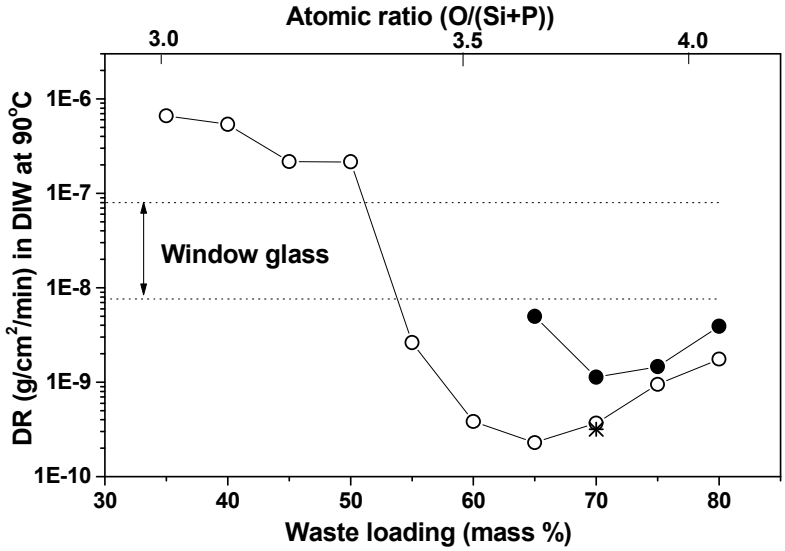

FIG. 13. Dissolution rate (DR) of iron phosphate waste forms after 128 days in deionized water at 90 ℃ for glassy (open circles), Crystallized at 650 ℃ for 48 h (solid circles), and sample slowly cooled at 2 ℃ / min from its melting temperature (star). Estimated error in DR is ±15 %.

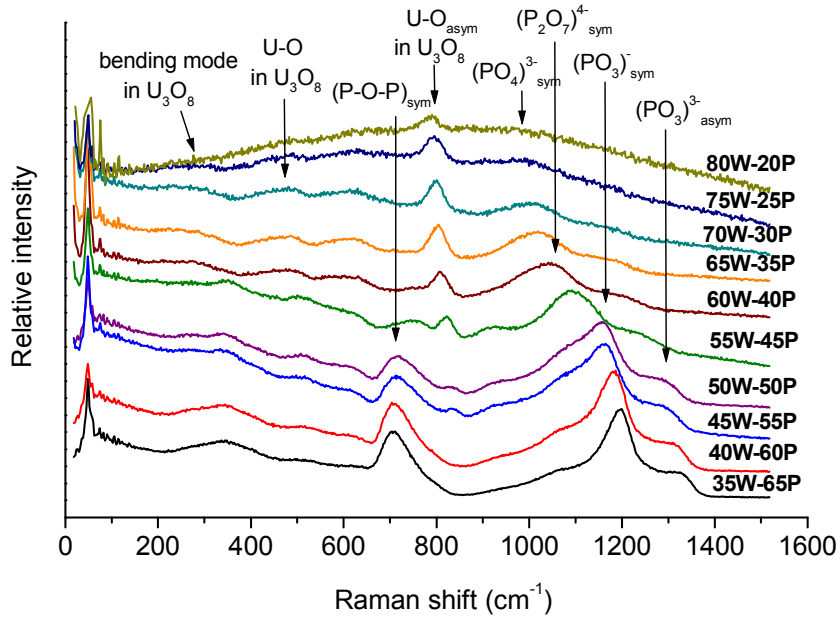

FIG. 14. Raman spectra of iron phosphate waste forms containing the percent waste shown for each curve.

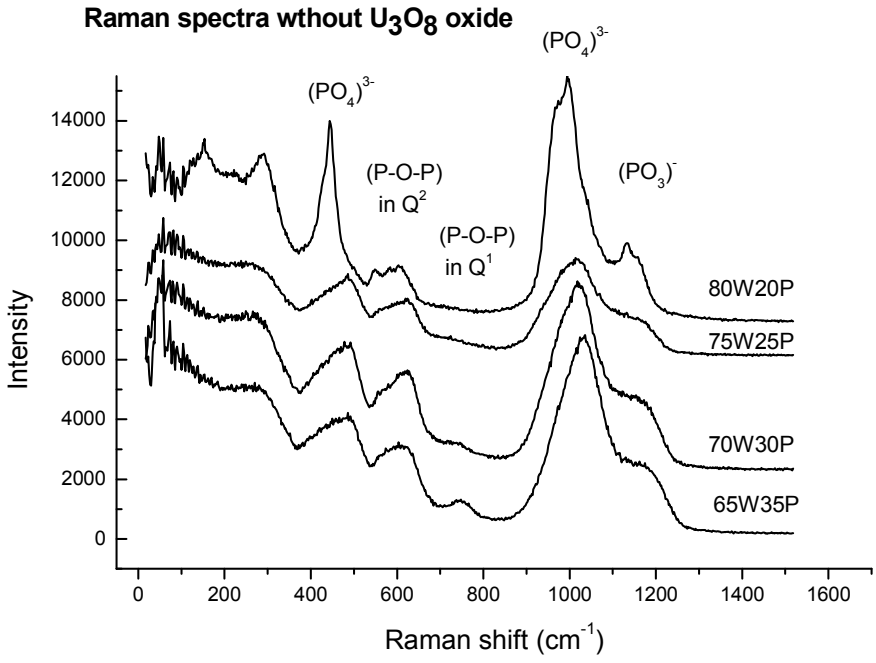

FIG. 15. Raman spectra of iron phosphate waste forms without U_3O_8.

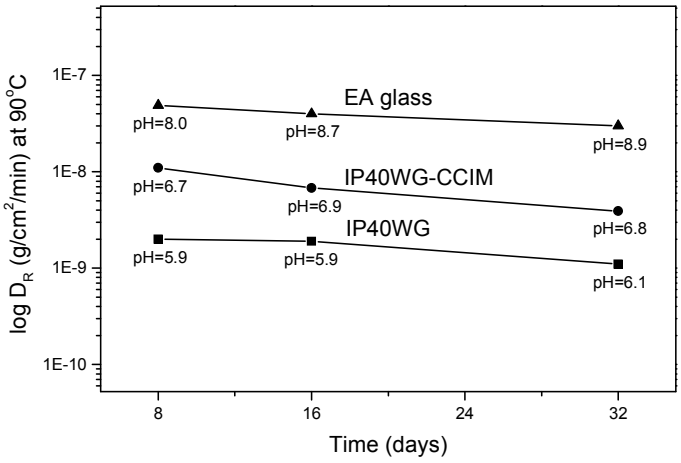

FIG. 16. Dissolution rate (D_R = g/cm^2/min) in DIW at 90°C for iron phosphate glasses (IP40WG and IP40WG-CCIM) and EA glass Initial pH of DIW was 5.8. Note the nearly constant pH of the leachate for the IP40WG and IP40WG-CCIM samples which is due to the larger buffering action (compared to silicate glasses) of phosphate glasses.

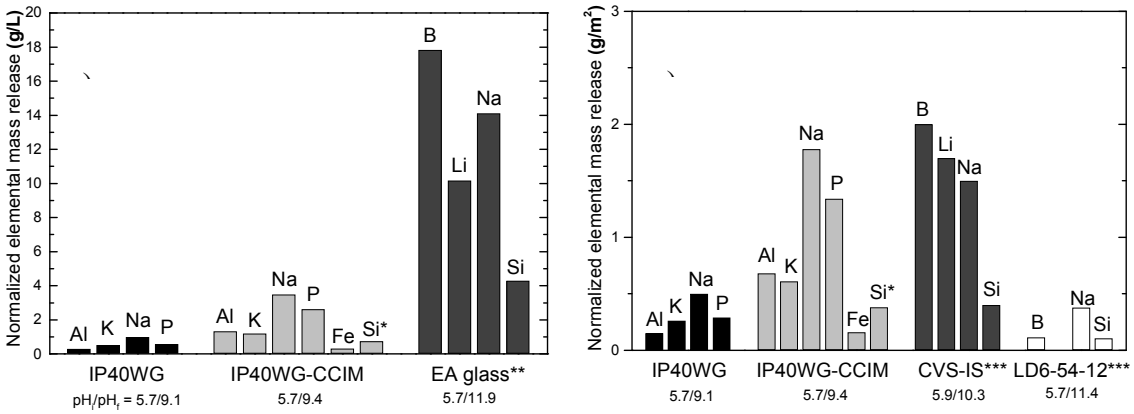

*FIG. 17. Normalized elemental mass release (g/L (a) or g/m^2 (b)) from iron phosphate glasses and standard borosilicate glasses after PCT in DIW at 90°C for 7 days. Elements for which the mass release is less than 0.01 g/L or g/m^2 are not shown. The initial (pH_i) and final (pH_f) pH of the leachate is given for each glass. * Arbitrary Si from the sacrificial conductive silicon carbide. ** Averaged data of selected EA glasses produced at the Savannah River Site. *** CVS-IS and LD6-54-12 are standard borosilicate glasses made by PNNL, and averaged data is listed here.*

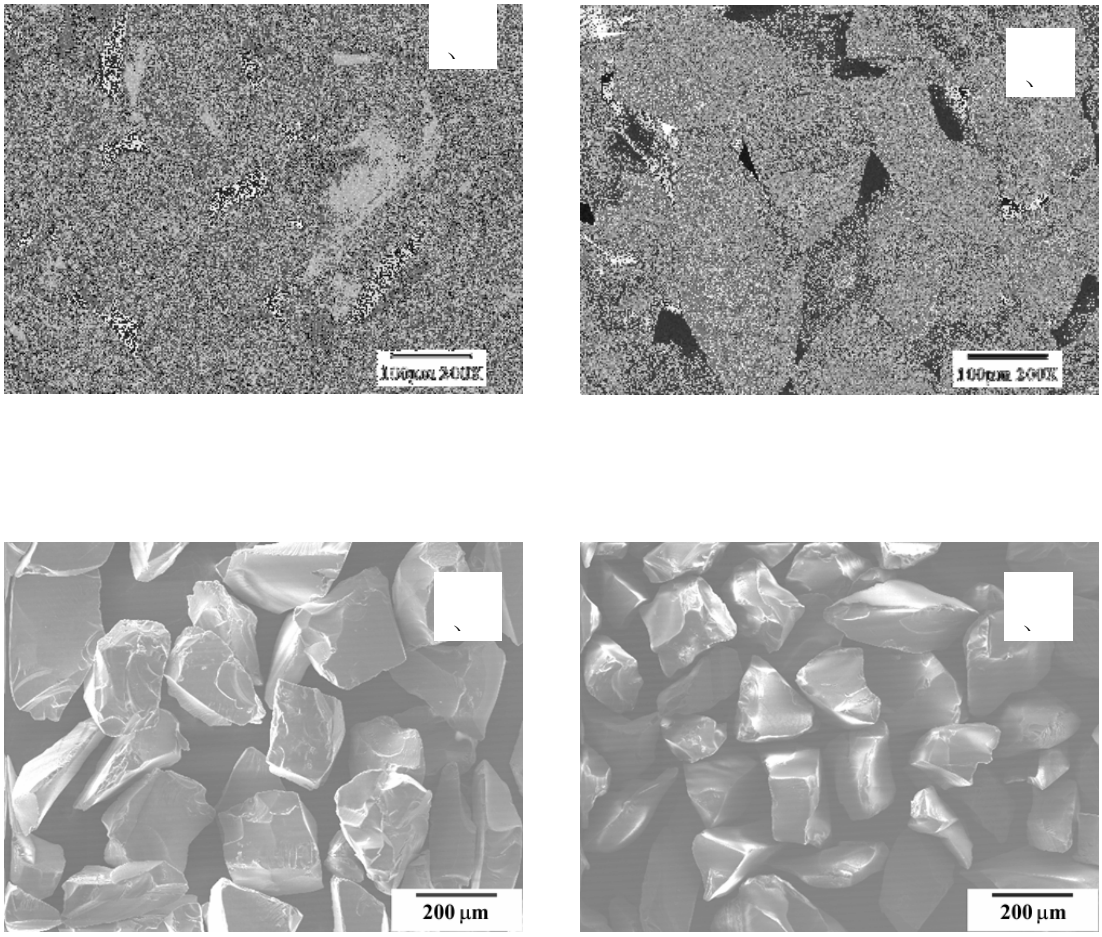

FIG. 18. SEM photomicrographs of uncorroded IP40WG glass particles (a) and after immersion in deionized water at 90℃ for seven days (PCT) (b). Uncorroded IP40WG-CCIM glass particles (c) and after PCT (d).

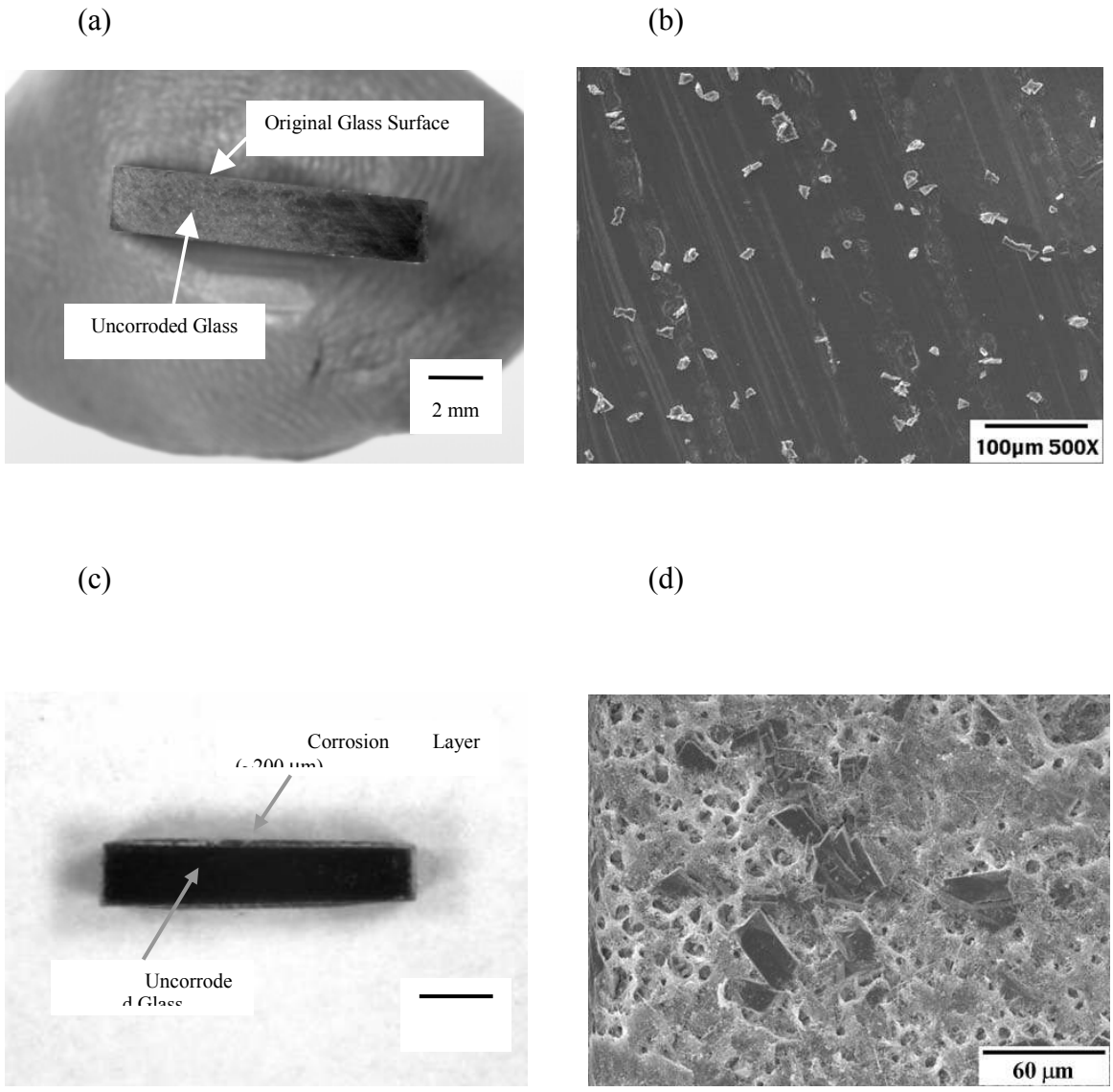

FIG. 19. Optical photo- (a), (c) and SEM photomicrographs (b), (d) of the IP40WG and IP40WG-CCIM specimens after the VHT (200℃ for seven days). (a) cross sectional view of IP40WG: no corroded layer was detectable on the surface; (b) external surface of IP40WG: polishing features still remained and only a few visible corrosion products were heterogeneously distributed on the surface; (c) cross sectional view of IP40WG-CCIM: very thin corrosion layer was seen on the surface, but still compares favorably with borosilicate glasses such as LAW-A33 and LD6-54-12; (d) external surface of IP40WG-CCIM.

EFFECT OF MICROSTRUCTURE CHANGES ON THE MOBILITY OF RADIONUCLIDES IN SIMULATED HLW CERAMICS

V. BALEK
Nuclear Research Institute Řež, Czech Republic

Abstract

Ceramic matrices for immobilization of HLW (e.g. perovskite, zirconolite, brannerite, zircon mineral based ceramics), prepared at ANSTO and C.I.A.E., respectively were characterized at the NRI Rez from the viewpoint of their microstructure and transport property changes caused by leaching. Scanning electron microscopy (SEM) and diffusion structural analysis (DSA) techniques were used. The thermal behavior of "as leached" and "as prepared" samples were compared. The DSA was used for the evaluation of atomic transport properties of the ceramic matrices. The effect of leaching on the thermal stability of the ceramics microstructure was characterized. The behaviour of the ceramic HLW matrices in simulated repository conditions was predicted by using the results of the mathematical modeling.

1. CHARACTERIZATION OF MICROSTRUCTURE CHANGES AND ASSESSMENT OF TRANSPORT PROPERTIES BY USING RADON (^{220}RN) AS DIFFUSION STRUCTURAL PROBE

Transport properties of ceramic matrices and their alteration products were characterized by using radon as a diffusion structural probe .The solid samples were labeled by radionuclides of ^{224}Ra and ^{228}Th as the parent nuclides of ^{220}Rn .

It was further supposed that the parent ^{228}Th radionuclide was situated on the surface of the sample up to the depth of several nanometers. By using Monte Carlo method and TRIM code the maximal recoil paths for ^{224}Ra and ^{220}Rn in the samples was determined. The calculated maximal penetration depth of ^{220}Rn was: for the zircon based ceramics: 94nm, for the perovskite ceramics ($CaTiO_3$): 119.2nm and for brannerite ceramics (UTi_2O_6) : 60 nm.

In the calculations it was supposed that the recoil energy of both ^{224}Ra and ^{220}Rn is 85 keV/atom. It was further supposed that ^{228}Th and ^{224}Ra do not migrate in the solids at temperatures used for the measurements and that the value of the total emanating rate E_{TOTAL} of a solid is composed of two terms: the emanating rate, E_R, due to recoil, and the emanating rate, E_D, due to diffusion. The total emanating rate E_{TOTAL}, representing the probability of the release rate of radon atoms from a solid, can be expressed in the simplified way as

$$E(T)= E_R + E_D(T) \bullet \Psi(T) \qquad (1)$$

where $E_D(T)$ is characterizing the radon mobility along diffusion paths, and the $\Psi(T)$ characterizing micro-structural changes that influence the number of radon diffusion paths.

In the case that the number of diffusion paths and/or surface area decreases on heating, the structural function $\Psi(T)$ has a decreasing character, whereas if the

number of diffusion paths increases during the heating the structural function $\Psi(T)$ has an increasing character. These assumptions were used in the modeling of the temperature dependencies of radon diffusion that describe the thermal behavior of the solids.

It was supposed that the radon mobility was controlled by the microstructure development. The mobility of radon as a microstructure probe was evaluated by means of the mathematical model. The effect of leaching on the microstructure and atomic transport properties on brannerite ceramics as a matrix for immobilization of HLW is presented as an example in the following paragraphs.

1.1. Characterization of the effect of leaching on brannerite ceramics

Brannerite ceramics (Uranium titanate, UTi_2O_6) was proposed for immobilization of high level radioactive waste (HLW) resulting from the nuclear industry facilities [1-3]. The chemical stability and durability of the ceramics are crucial points for the application. Therefore, natural brannerite mineral as well as synthetic ceramics were the subject of studies dealing with their stability towards leaching in acidic and alkaline fluids [4]. It was found that the presence of phthalate as a buffer component (pH range of 2–6) had a little effect on the uranium release from synthetic brannerite at 40 ^oC. In alkaline conditions of bicarbonate (pH 11) uranium release was increased and the dissolution of brannerite was enhanced. The preferential release of uranium over titanium was observed in acidic conditions (pH 2) at 90 ^oC, and the dissolution of uranium was over 100 times higher than that of Ti. In the alkaline conditions at 90 ^oC the dissolution of brannerite ceramics was congruent (no preferential release) [4].

In order to evaluate the properties of the brannerite ceramics caused by leaching it was of interest to investigate the effect of leaching on surface morphology, microstructure changes and atomic transport properties of brannerite ceramics. For this purpose, “as-prepared” and ”as-leached“ samples in acidic and alkaline fluids were characterized by scanning electron microscopy (SEM) and diffusion structural analysis (DSA) [5]. In the DSA analysis the radon atoms were used as a microstructure probe and as a tracer to model the mobility of the species similar in size to radon atoms e.g. water molecules. The behavior of the ceramic HLW matrices in simulated repository conditions was predicted by using mathematical modeling.

Preparation of samples:

Synthetic brannerite, UTi_2O_6, was prepared by the alkoxide/nitrate route [1]. Stoichiometric mixtures of UO_2 and TiO_2 (anatase) were dried and calcined in argon at 750^oC for 1 hr and subsequently wet-milled for 2 hrs and then dried. The static leaching tests were carried out by 0.01 M solution of HNO_3 (pH 2) and 0.1 M solution of KOH (pH 11) for 7 days at 90 ^oC.

Methods of characterization:

Diffusion structural analysis (DSA) [5], based on the measurement of the release of inert gas atoms form the solids, was used to characterize microstructure changes and transport properties of the samples under *in situ* conditions of heating [6,7]. In this study radon ^{220}Rn atoms were used as inert gas microstructure probe.

Atoms of radon, ^{220}Rn, were formed by the spontaneous α-decay of ^{228}Th and ^{224}Ra. The samples were labeled by ^{228}Th and ^{224}Ra radionuclides. The ^{224}Ra and ^{220}Rn atoms were incorporated into the sample due to the recoil energy (85 keV $atom^{-1}$), which the atoms gained, by α-spontaneous decay. The maximal penetration depths of the recoiled ^{224}Ra and ^{220}Rn atoms in the brannerite ceramics was 59.2 nm as calculated by Monte Carlo method by using TRIM code [8]. The theoretical density 6.35 g/cm^3 was considered in the calculation.

1.2. Results and discussion

From SEM micrographs in Fig.1 it is obvious that similar surface morphology was observed for the samples before and after leaching at pH 2 and pH 11, respectively. To better characterize the surface and subsurface structure irregularities of the brannerite ceramics the diffusion structural analysis (DSA) was used. The experimental DSA results were obtained on heating of the brannerite ceramics in argon in the temperature range from 20 to 1200°C. From DSA results in Fig. 1 it is obvious that the leaching at pH 2 and pH 11 influenced the thermal behavior of the brannerite ceramics.

We assumed that the increase of the radon release rate in the temperature range 20ºC to 250°C was controlled by random "single jump" mechanism in surface and subsurface structure irregularities, that served as a radon diffusion paths. The break observed at about 250 °C and the subsequent decrease of the radon release rate in the interval 250-500°C was due to the annealing of the radon diffusion paths in the sample surface and subsurface. The most important decrease of E(T) was observed with the as-prepared ceramics sample. On further heating above 500°C the increase of E(T) was supposedly due to the radon diffusion along grain boundaries. The break observed at approximately 800 °C and the subsequent decrease of E(T) could be ascribed to the sintering of the solid particles prepared by milling of the calcined ceramic body. The increase observed in the range 1000–1250°C was due to the radon diffusion by the bulk diffusion mechanism in the sintered brannerite ceramics.

1.3. Assessment of the leaching effect on brannerite ceramics

The experimental DSA data were evaluated using mathematical model proposed recently [9]. The DSA results obtained by the mathematical modeling are presented in Fig. 1 as full line curves. Taking into account the good agreement between the model curves and the DSA experimental results of the brannerite ceramics presented in Fig. 1, the model curves were used to evaluate the effect of leaching on thermal behaviour of brannerite ceramic. From the model DSA curves in Fig. 2 it was decided to compare the differences in thermal behaviour of the samples in following temperature intervals: 50-250°C, 250-500°C, 500-800°C and 800-1000°C.

In the temperature range 20-250°C where the radon release rate was controlled by random "single jump" mechanism, differences in the radon mobility in the as leached samples and the as prepared sample were supposed (see the slope of the temperature dependences of radon release rate E(T) in Fig.2).

Similarly, in the range 500–800°C where we supposed that the radon release was controlled by the diffusion along grain boundaries, the differences in the radon mobility in the as leached samples and the as prepared sample were also supposed.

From the slope of the temperature dependence of radon release rate E(T) observed in Fig.2, curve 2, we assumed that in the sample leached at pH 2, the number of structure irregularities that served radon diffusion paths decreased in comparison with the "as prepared" brannerite ceramics sample. Radon diffusion parameters, calculated from the DSA results in the respective temperature intervals 50-250 ^{o}C, 800-1000 ^{o}C, are presented in Table 1.

2. CONCLUSIONS

DSA results enabled us to assess the thermophysical properties of brannerite ceramics samples and to characterize the effect of leaching in the solutions of various pH used in this study. Radon atoms were used as a microstructure probe and as tracer of the samples permeability in their subsurface up to approximately 60nm. Additional information about thermal stability of the structure irregularities was obtained by DSA. In general, the DSA results gave supplementary information about annealing of the sub surface layers of the ceramis and enabled us to deeper understand effect of microstructure on mobility of radionuclides in the HLW forms. It was demonstrated that microstructure changes strongly influence the radon mobility on sample heating. The radon (atom size 0.38nm) served a diffusion structural probe to characterize the atom mobility and microstructure changes of the ceramics matrices.

ACKNOWLEDGMENTS

This work was carried out in the frame of the IAEA Coordinated Research Programme under Research Agreement No. CZR-10,646.

REFERENCES

[1] A.E. Ringwood, S.E. Kesson, K.D. Reeve, D.M. Levins, E.J. Ramm, in: W. Lutze, R.C. Ewing (Eds.), Radioactive Waste Forms for the Future, 1988, p. 233.

[2] B.B. Ebbinghaus, R.A. VanKonynenburg, F.J. Ryerson, E.R. Vance, M.W.A. Stewart, A. Jostsons, J.S. Allender, T. Rankin, J. Congdon, Ceramic Formulation for the Immobilization of Plutonium,Waste Management 98 (CDROM), Tucson, AZ, USA, 5 March, 1998.

[3] K.B. Helean, A. Navrotsky, G.R. Lumpkin, M. Colella, J. Lian, C.R. Ewing, B. Ebbinghaus, J.G. Catalano: *J. Nucl. Mater.* **320**(2003)231

[4] Y. Zhang, B.S. Thomas, G.R. Lumpkin, M. Blackford, Z. Zhang, M. Colella, Z. Aly, *J. Nucl. Mater.* **321**(2003)1

[5] V. Balek, J. Toelgyessy, Emanation Thermal Analysis and Other Radiometric Emanation Methods, in: Wilson and Wilson's Comprehensive Analytical Chemistry, Part XIIC, Elsevier Sci. Publ. (1984) pp. 43-71.

[6] V. Balek, *Thermochim. Acta* **192**(1991)1

[7] V. Balek, J. Subrt, T. Mitsuhashi, I.N. Beckman, K. Gyoryova, *J. Therm. Anal. Cal.* **67**(2002)15.

[8] J. F. Ziegler, J. P. Biersack: The stopping and range of ions in solids, Pergamon Press, New York, 1985

[9] I.N. Beckman, V. Balek, *J. Therm. Anal. Cal.* **67**(2002)49.

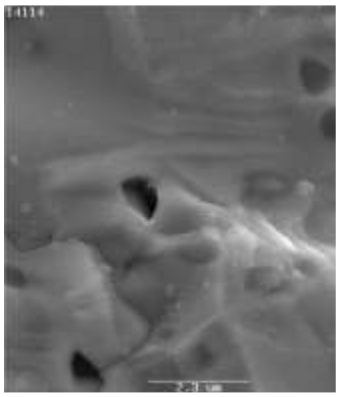

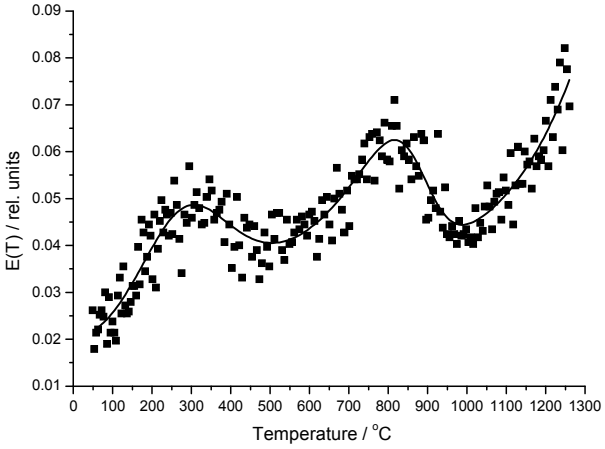

a

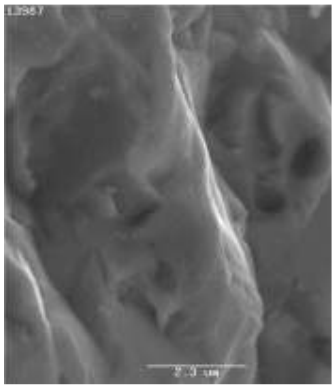

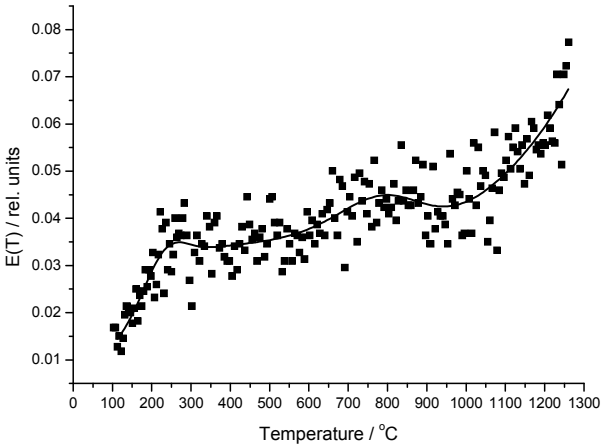

b

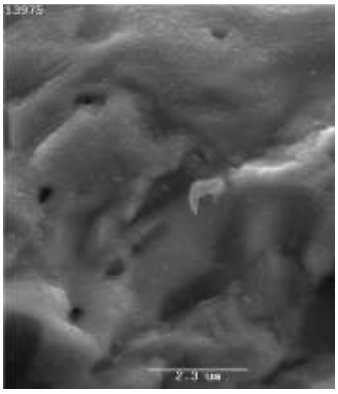

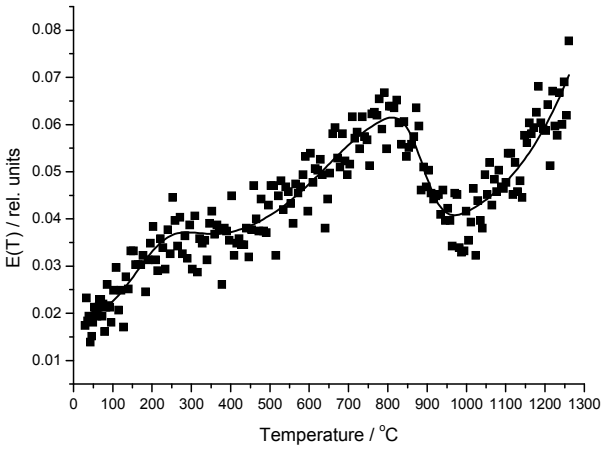

c

FIG. 1 Characterization of brannerite ceramics samples (a) "as-prepared", (b) "as-leached" at pH 2 and (c) "as-leached" at pH 11 by means of SEM and DSA. In the comparison of model curves with the experimental DSA data of the brannerite ceramics. Full points represent experimental data and full lines correspond to the model curves of radon release rate E(T). .

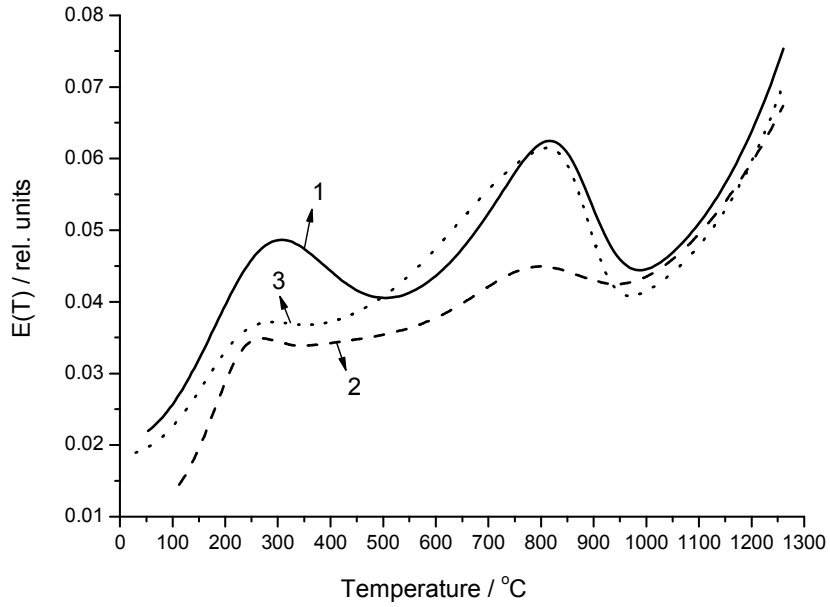

FIG. 2. Temperature dependences of radon release rate obtained by mathematical modeling of the experimental DSA data that characterized thermal behavior of brannerite ceramics as affected by leaching. Curve 1 "as-prepared" sample; curve 2 "as-leached" sample at pH 2; curve 3 "as-leached" sample at pH 11.

TABLE I ATOMIC TRANSPORT PROPERTIES OF BRANNERITE CERAMICS SAMPLES AS AFFECTED BY LEACHING.

Sample of brannerite ceramics	**Temperature range 20-500 °C**			**Temperature range 500-1000 °C**			**Temperature range 1000-1250 °C**	
	Radon mobility		**Maximum rate of defects annealing [^{o} C]**	**Radon mobility**		**Maximum rate of sintering [o C]**	**Radon mobility**	
	D_0 [cm^2/s]	**Q_D [kJ/mol]**		**D_0 [cm^2/s]**	**Q_D [kJ/mol]**		**D_0 [cm^2/s]**	**Q_D [kJ/mol]**
as-prepared	$2.2 \cdot 10^{-9}$	40	320	$6.2 \cdot 10^{-6}$	142.5	861	$1.3 \cdot 10^{-5}$	230
as-leached at pH 2	$2.4 \cdot 10^{-7}$	58	243	$1.5 \cdot 10^{-6}$	149.8	785	$1.2 \cdot 10^{-7}$	173
as-leached at pH 11	$4.5 \cdot 10^{-9}$	44	247	$7.0 \cdot 10^{-8}$	112.5	888	$2.4 \cdot 10^{-5}$	240

NUCLEAR GLASS WASTE FORMS: PHYSICAL AND CHEMICAL PROPERTIES

J. L. DUSSOSSOY
CEA-VRH, DEN-DTCD, Bagnols/Cèze, France

Authors and Contributors: O. Pinet, S. Peuget, I. Bardez, T. Advocat

Abstract

The production of nuclear energy in France has been associated with the optimization of radioactive waste management, comprising the partitioning and the recycling of recoverable energetic materials, volume reduction, the conditioning, and the disposal of the end waste. The public's concern regarding its long-term management caused the French Government, in 1990, to delay the implementation of the geological disposal and to prepare a law, passed on December 30, 1991, requesting in particular the study of solutions and processes for:

— minimizing the quantity and the hazardousness of waste, via partitioning and transmutation,
— either reversibly or irreversibly disposing the waste in deep geological formations,
— waste conditioning and long-term interim storage.

An update on the progress made in research conducted pertaining to the third bullet will be discussed in the paper. Developments made in the area of waste treatment and conditioning were targeted at ensuring the availability of qualified processes that could be applied to historic waste to be recovered or to improve (e.g. by volume reduction) a number of existing treatment processes.

The objective of the conditioning being to ensure durable confinement for all the steps in the package management, it is necessary to establish the scientific and technical grounds for the prediction of the package long-term behavior, and to confirm that the relevant functions are provided, in particular confinement, handling, and recovery. The work done in recent years has provided the scientific base of a true science on long-term behavior, with detailed modeling and experimental validation of the principal phenomena at work considering all the different types of packages (glass, concrete, bituminized, compacted waste, spent fuel).

Important results are now available concerning both the possibility of significantly reducing the quantity and the radiotoxicity of long-lived waste, and for the modes of waste conditioning applicable to long-term interim storage facilities [1].

Data on new glass waste forms devoted to fission products immobilization will be described in more detail in this paper.

1. GLASS MATERIALS STUDIES

Since 1978 in France, HLW arising from spent fuel reprocessing operations, have been vitrified into borosilicate glasses, using the two step calcination - vitrification technology in a metallic hot melter.

These vitrified waste forms had proven to be durable and easy to process in metallic induction-heated melters, at typical operating temperatures of 1100 to 1150°C. More than 12000 glass canisters were produced in France up to now, cumulating up to 10^{20} Bq ($\beta\gamma$). The major basic physical, chemical and thermal properties of existing borosilicate glass formulations are reported in the Table I.

These glasses have complex compositions since they contain approximately 30 elements. In addition to the fission products and transuranics, some chosen elements are introduced during sintering to meet the specific qualities required in the final material:

- Silicium, aluminium and boron are introduced to form vitreous network,
- Alkaline and alkaline-earth elements are introduced for modifying the matrix by lowering the melting point and thus facilitating the preparation of the glass; boron also acts as a flux and enables incorporating molybdenum,
- Zirconium and aluminium confer good chemical properties upon the final material.

The vitreous state is defined by its structural and thermodynamic characteristics.

The feasibility of designing and producing via cold crucible melter (CCM) new glass and glass-ceramic waste forms for immobilising other high level wastes is currently being investigated. Two examples are discussed into details in the present paper :

1) the formulation and vitrification of Umo fission product solutions,
2) the formulation of glass to vitrify fission product solutions arising from higher burn-up UO_2 fuels (60 GWd/t)

TABLE I. BASIC PROPERTIES OF THE R7T7 FRENCH BOROSILICATE GLASS WASTE FORM

oxydes	Nominal comp.	Specified Range of composition	Major properties	For the Nominal Comp.	For the specified range of Comp.
SiO_2	45,1	42,4 - 51,7			
B_2O_3	13,9	12,4 - 16,5	Viscosity	110 dPa.s (1100°C)	87 - 310 dPa.s (1100°C)
Al_2O_3	4,9	3,6 - 6,6			
Na_2O	10,1	8,1 - 11,0			
CaO	4,0	3,5 - 4,8	Tg	502°C	500 - 533°C
MgO	-	-			
Fe_2O_3	3,0	< 4,5			
NiO	0,4	< 0,5	r_0 (100°C)	2 $g.m^{-2}.d^{-1}$	1,6 - 4,1
Cr_2O_3	0,5	< 0,6	R_f (35-90°C)	<$10^{-4}g.m^{-2}/d$	Identical
P_2O_5	0,3	<1,0			
Li_2O	2,0	1,6 - 2,4	Thermal stability	$CaMoO_4$, CeO_2, spinelles	
ZnO	2,5	2,2 - 2,8			Identical
Ox.PF+ZrO_2+NM	12,9 + 0,37	4,2 - 18,5	Radiation stability		
Ox.actinides					

1.1. Formulation of a glass matrix for containment of UMo-MoSnAl solutions

Considering elements present in the UMo-MoSnAl High level waste feed solutions, (legacy solutions derived from the reprocessing in the seventies of spent Mo-Sn-Al fuels), the molybdenum and phosphorus loading capacity of the glass is unquestionably decisive for the waste loading capability of the containment matrix. Molybdenum loading is limited to about 4 wt% in conventional nuclear borosilicate glasses. At higher values a water-soluble segregated yellow molybdic phase could appear in the glass. Phosphorus cannot be loaded to above a few percent in this type of glass because it forms silicates liable to diminish the chemical durability of the residual glass. It was therefore decided to investigate a different composition range than R7/T7 glass also to take into account the radioactive specificity of UMo solution.

It was chosen to begin with a range based on SiO_2, Na_2O, Al_2O_3, P_2O_5, B_2O_3 and MoO_3. Tests were also conducted with various additives: CaO to stabilize molybdenum in the form of durable calcium molybdate crystals, ZrO_2 to enhance the chemical durability of the final glass, and ZnO. The limits of the composition range were determined from the results obtained during CEA tests in the 1960s and 1970s with compositions capable of being fabricated at temperatures below 1200°C; the target value is now between 1200°C and 1300°C, however, made possible by the use of a cold crucible melter. The following weight percentage composition range was investigated:

SiO_2	:	32	-		44
Al_2O_3	:	<			5
B_2O_3	:	15	-		22
Na_2O	:	12			
MoO_3	:	10	-		12

Tested additives: CaO, ZnO, ZrO_2.

Over 100 glass samples were fabricated and characterized in this range. The results (Figure 1) for each composition are normalized for the three constituents with the greatest impact on the final material within the studied range: SiO_2, Al_2O_3, P_2O_5. Three glass families were identified within the domain, in addition to highly refractory matrices unsuitable for fabrication at 1300°C:

— Glasses that are translucent after quenching,

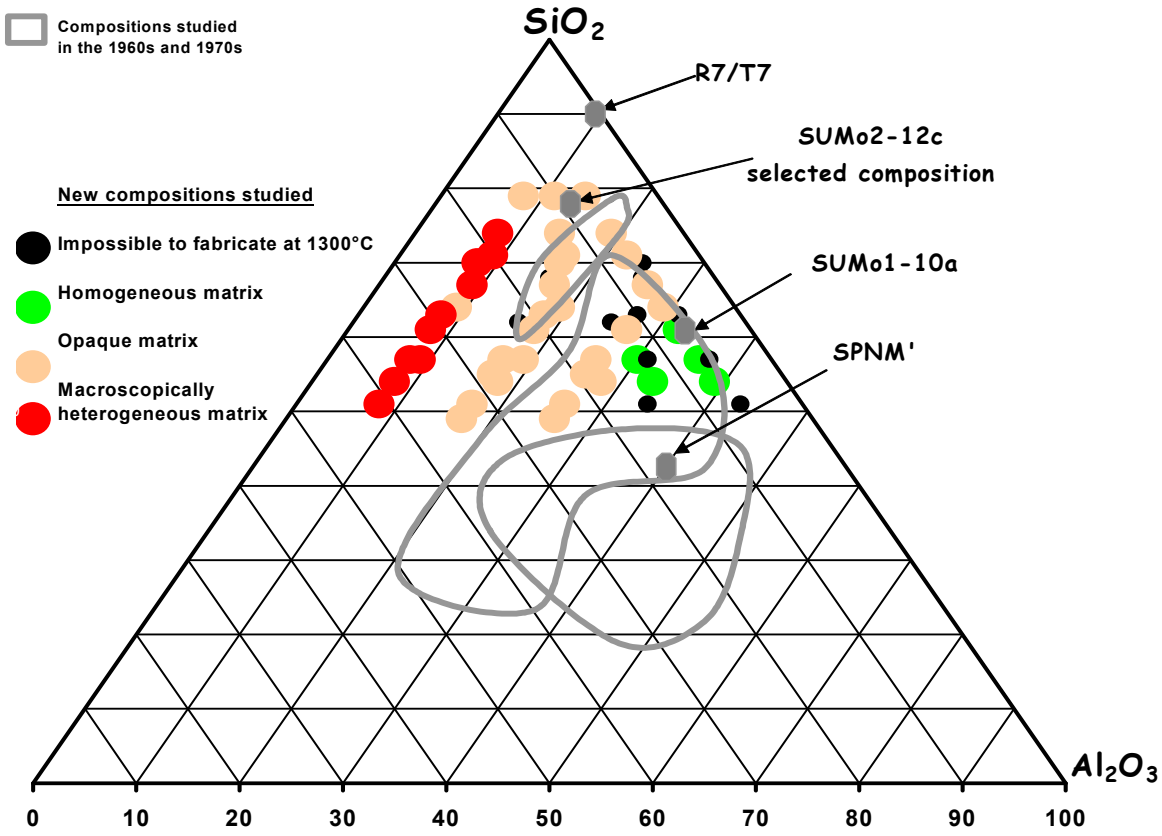

— Opaque glasses,
— Macroscopically heterogeneous matrices.

FIG. 1. Various Glass composition ranges for the vitrification of Umo-solutions.

SUMo1-10a and SUMo2-12a glasses from the first and second families, respectively, were selected for further optimization, together with reduced SPNM′ glass. The qualities of reduced SPNM′ glass for vitrification of UMo-MoSnAl solutions were observed during another formulation study; although this composition is not part of the selection range, its advantageous chemical durability and viscosity characteristics are related to the oxidation state of molybdenum, which is reduced to +IV [(4)]. Following this optimization and characterization phase, SUMo2-12c glass (optimized from SUMo2-12a) was selected as the reference formulation. The compositions of the reference glass is indicated in Table II. The reference glass was also fabricated in a pilot cold crucible melter at Marcoule (scale one copy of the further hot Vitrification cell). Samples were taken at different positions along a vertical cross section of the canister.

The reference UMo glass, SUMo2-12c, is a vitreous material fabricated at 1250°C [2]. It is opaque, as it contains microbeads uniformly distributed in the glass. The microbeads containing molybdenum, phosphorus, calcium and zinc are capable of stabilizing molybdenum and phosphorus, which are difficult to incorporate in a silicate network. Some of the beads appear to be crystallized and contain calcium molybdate.

Chemical durability tests in Soxhlet mode at 100°C yielded r_0 values of 3 $g \cdot m^{-2} d^{-1}$; PCT tests in pure water at 90°C at a glass-surface-area-to-water-volume ratio of 80 cm^{-1} indicated a maximum boron leach rate of 2.5 10^{-2} $g \cdot m^{-2} d^{-1}$ between 91 and 120 days. The molten glass properties are also compatible with fabrication in a cold crucible melter: a viscosity of 38 dPa·s at 1250°C and an electrical resistivity of about 6 Ω·cm at 1250°C. The glass fabricated in the laboratory based on the cooling scenarios expected in the waste canister exhibited the same properties as the glass sampled from the canister.

Considering the possible amplitude of the variations affecting the matrix fabrication parameters described above, the parameters determining the limits of the acceptability range are the molybdenum and phosphorus concentrations in the final glass. For the purposes of this formulation study, the sensitivity study has thus consisted in determining the extreme acceptable variations for these three parameters.

TABLE II. REFERENCE UMO-GLASS COMPOSITION (IN OXIDE WT.%).

	SUMo2-12c
SiO_2	35,99
Na_2O	8,79
B_2O_3	12,96
Al_2O_3	6,18
P_2O_5	3,69
MoO_3	12,00
ZnO	5,62
ZrO_2	7,14
CaO	5,67
others	1,96
total	100,00

1.2. Formulation of a glass matrix for high waste loading containment

New nuclear fuels with high burn-up rates (60 000 MWd/t) have been under study for some years in France and should allow a use about twice as long as what is currently achieved in power reactors. Reprocessing of this nuclear spent fuel will generate highly radioactive liquid wastes (HLW) more concentrated (fission products

and minor actinides) than nowadays. Therefore, new glass compositions have to be developed, able to immobilise the wastes as a whole. These matrices must show high chemical durability and larger glass transformation temperatures (T_g) than those of the current borosilicate nuclear glasses.

As the actinides and lanthanides quantity is expected to increase in the spent fuel with higher burn-up, we oriented our research on glassy matrices rich in rare earths. Previous investigations on lanthanide aluminoborosilicate glasses (LaBS) or lanthanide aluminosilicate glasses (SiAlO), which are glasses containing high rare earth amounts, showed that they both display high glass transformation temperatures and considerably high chemical durabilities, probably because of the presence of the rare earth in the glass [3, 4, 5, 6, 7]. Nevertheless most of these compositions were not chosen in this work because of their high melting temperatures ($T_m \geq 1450°C$), which could induced problems of volatility of some fission products during melting and problems during melt casting into the stainless steel containers. In fact, a possible glass composition, able to incorporate the new HLW, could be close to the LaBS one, including additional quantities of sodium and boron oxides (known as fluxing agents) such as to decrease the melting temperature below 1300°C.

Compositions were tested in the simplified seven-component glass system SiO_2 – B_2O_3 – Na_2O – Al_2O_3 – CaO – ZrO_2 – RE_2O_3 (RE = rare earth : La, Ce, Pr and Nd). In this simplified system more than 75 wt. % of the new HLW were simulated (the other 25 wt. % did not play a fundamental role in the properties of the glass and were thus eliminated for the structural study). Moreover, low amounts of calcium and zirconium oxides were introduced such as to improve glass chemical durability ([3, 4].

Glass formulation has shown the role of alumina content on the glass stability.

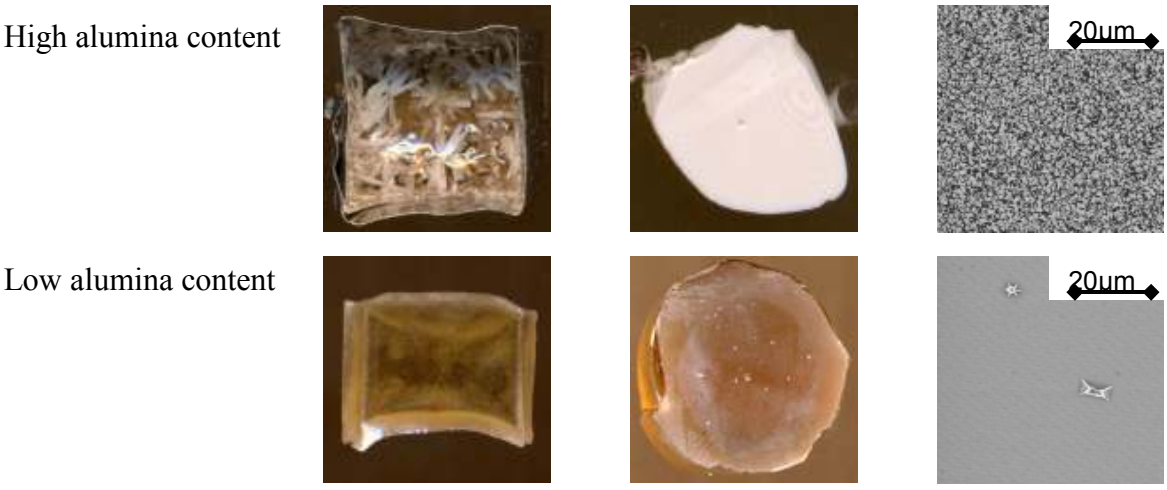

FIG. 2. Influence of Al_2O_3-content in the glass formulation on the crystallization.

Glasses with high alumina content crystallised in apatite $Ca_2TR_8(SiO_4)_6O_2$

The following baseline glass composition chosen for this study is (Glass 1, wt. %) : 51.0 SiO_2 – 8.5 B_2O_3 – 12.2 Na_2O – 4.3 Al_2O_3 – 4.8 CaO – 3.2 ZrO_2 – 16.0 RE_2O_3 (with RE = La, Ce, Pr and Nd).

Chemical durability tests in Soxhlet mode at 100°C yielded r_0 values of 0.4 $g \cdot m^{-2} d^{-1}$ and PCT tests in pure water at 90°C at a glass-surface-area-to-water-volume ratio of 80 cm^{-1} indicated a maximum boron leach rate of about 2.5 10^{-3} $g \cdot m^{-2} d^{-1}$ between 14 and 56 days. The molten glass properties are also compatible with fabrication in a cold crucible melter: the viscosity is equal to 62 dPa·s at 1300°C.

EXAFS experiments were performed by I. Bardez [3], to determine the evolution of the neighbouring of the rare earth in the glass according to its concentration. EXAFS can also give information on the occurrence of Nd-Nd clusters, particularly for high [Nd_2O_3] concentration in the glass.

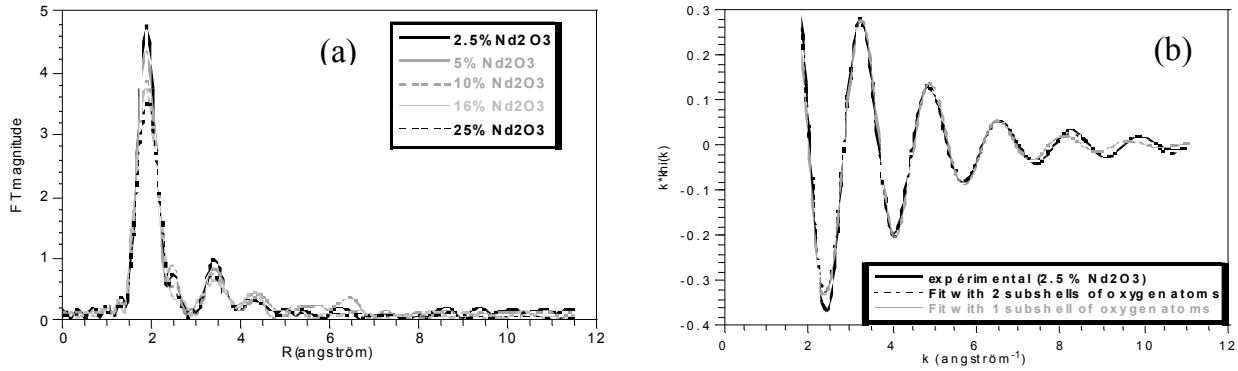

FIG. 3. (a) Fourier transforms of Nd L_{III}-edge EXAFS spectra of glasses containing 2.5, 5, 10, 16 and 25 wt. % Nd_2O_3 (T=77 K), (b) Comparison of the experimental EXAFS spectra of the glass containing 2.5 wt. % Nd_2O_3 with a fit realised thanks to 1 subshell of oxygen atoms and a fit realised with 2 subshells of oxygen atoms first nearest neighbours (from [3]).

The Fourier transforms of the EXAFS spectra display a linear decrease of intensity as [Nd_2O_3] increases (FIG. 3(a)). The results of curve fits are summarized in Table III. In such matrices, neodymium appears always surrounded by 9 ± 1 oxygen atoms distributed in two subshells (Figure 3(b)) (5 at 2.37 Å ± 0.03 Å and 4 at 2.55 Å ± 0.03 Å). These distances are close to those found for model compounds. Moreover, the neodymium ions have approximately 3.5 second neighbours silicon at 3.90 Å. In fact, no phenomena of Nd-Nd clustering at less than 4 Å were detected in these glasses, even for high neodymium contents.

TABLE III. QUANTITATIVE RESULTS OF THE EXAFS ANALYSIS OF THE 2.5, 5, 10, 16 AND 25 WT. % ND_2O_3 GLASSES. (N_I, σ_I, R_I) CORRESPONDS RESPECTIVELY TO THE NUMBER OF NEIGHBOURS, THE DEBYE-WALLER AND THE DISTANCE (ND-NEIGHBOURS).

		2.5 %	***5 %***	***10 %***	***16 %***	***25 %***
Nd–O	N1	5	5	5	5	5
	σ1 (Å)	0.04	0.05	0.065	0.07	0.08
	R1 (Å)	2.36	2.36	2.37	2.37	2.38
Nd–O	N2	4	4	4	4	4
	σ2 (Å)	0.07	0.07	0.09	0.09	0.10
	R2 (Å)	2.55	2.54	2.55	2.55	2.56
Nd–Si	N3	3.5	3.5	3.5	3.5	3.5
	σ3 (Å)	0.09	0.10	0.10	0.11	0.11
	R3 (Å)	3.92	3.92	3.92	3.91	3.89
	Goodness of fit	98.4 %	98.3 %	98.9 %	98.1 %	98.8 %

1.3. Radiation stability of borosilicate glass

1.3.1. Radiation processes and associated questions

The main sources of irradiation in nuclear glasses result from α decay due to actinides (Am, Cm, Pu, …), β decay due to Fission Products (137Cs, 90Sr, …), and γ transitions accompanying the b and αdecay.

The α decay, characterized by the creation of a recoil nucleus (energy ~0.1 MeV, deposited on ~30 nm) and the emission of an α particle (energy of 4 to 6 MeV deposited on ~20 μm) which eventually generates a helium atom, are the principal sources of the creation of atom displacement.

The β decays engender high-energy electrons (0.1 to 3.5 MeV) often accompanied by γ radiation. These radiations are in great part responsible for the electronic excitations and ionisations that take place in the material.

The properties of actinide glasses are studied in the framework of the high level waste management programs. In particular, the reprocessing of high burn-up fuels will increase the minor actinide content in the glass package. Consequently, studies are in progress to understand actinides solubility in the borosilicate glass matrix, and to determine the effects of alpha decays on the glass properties.

To study the damage engendered by self-irradiation, three main approaches were implemented [8, 9, 10]:

1) The first approach is focused on atomistic modeling. Until now, most of the studies looked at molecular dynamics to understand the ballistic effects induced by the deceleration of the Recoil Nuclei (RN) emitted following αdecay, the main objective of those studies being to understand the structural behaviour of the matrix and identify the mechanisms following the cascade of displacements engendered.
2) The second approach is based on the use of inactive glasses, irradiated by external irradiation techniques (neutrons, heavy ions, electrons, g, etc.). It should be fairly easy, by means of experimentation, to achieve the objective of accessing the macroscopic and microscopic changes taking place in the material. By characterising the glasses at the atomic scale using fine analysis spectroscopy, (RPE, Raman, EXAFS, RMN, ...) this approach should enable experimentally accessing the structural changes in the matrix. Perturbatory effects due to the high doses injected, and the small volumes irradiated (temperature rise, charge effect, effects of segregation, etc.) are the major drawbacks involved in this type of experiment.
3) The third approach focuses on the study of the macroscopic changes (density, alteration, stored energy, mechanical properties, etc.) taking place in the active materials. This is the reference, since it is the most representative of the real case. To study the effect of α decay, we usually use glasses doped with actinides. Preparing glasses doped with ^{244}Cm provides us with glasses that in just a few years are capable of integrating doses equivalent to those integrated over several thousands of years in the actual nuclear glasses. This simulation method is the most representative of the long-term effect of α decay. This method is adopted by the majority of the scientific community and the International Standard Organisation to test the stability of matrices for the containment of high-level nuclear waste subject to α decay. Concerning study of the effect of β–γ radiation, the technique consists of manufacturing an active glass of a composition very comparable to real glass. Although it does not achieve accelerated ageing, this technique has the advantage that it represents the real case and enables significant observations on the human scale (10 to 30 years). Indeed, with this type of radiation, most of the energy is deposited in the first 30 years.

1.3.2. Experimental results obtained with 244Cm-doped glass

"R7T7" borosilicate glasses have been doped with different curium contents (0,04wt%, 0,4wt% and 1,5wt% of $^{244}CmO_2$). The macroscopic properties (density and initial dissolution rate) of the glasses were characterized up to 2.10^{18}α/g.

Overall, at macroscopic scale we have a fairly good and realistic grasp of the effect of α decay in R7T7 nuclear glasses.

In a range of doses corresponding to a maximum ageing of approximately 10^4 years for R7T7 type glass (~ 4 to 5 10^{18} α decay / g of glass), the experimental studies provide at the macroscopic scale with a reassuring set of observations:

— Little variation in volume, in terms of amplitude, 0.6% max, which limits the risks of breakdown due to the tension exerted on the glass (Figure 4),
— No fundamental decrease in resistance to aqueous corrosion (Figure 5).

These results generally corroborate the studies performed on other types of glass (American, German, Japanese glass).

The saturation phenomena observed on certain properties (density, etc.) cause us to think that a balance between the creation and remedying of flaws could be achieved at around 2 10^{18} decays/g of glass. For some properties (density, mechanical properties) those saturation phenomena have been confirmed at very high dose (~10^{19} α decays/g on a Japanese glass similar to R7T7, which corresponds to approximately 5 10^{5} years' ageing of R7T7).

The helium produced as a result of α decay is a possible source of the formation of bubbles. However, it must be emphasised that the results obtained on the behaviour of helium in other types of glass are fairly contradictory. Indeed, the Japanese revealed the presence of gas bubbles (~10^{17} bubbles/m3) of fairly significant diameter (~0.23µm) on doped glass at ambient temperature, whereas on an inactive glass injected with a high concentration of helium, the Germans did not observe the formation of bubbles. Lastly, the results obtained on doped glasses with a considerable accumulation of helium do not, at ambient temperature, show any particular fragilisation (on the contrary, the strength increased noticeably).

Concerning β-gradiation, simulations of ageing were studied essentially using external irradiation techniques (electron bundles, γ radiation). Techniques that engender perturbatory effects make it difficult to interpret the results. Concerning the structure of the glasses, our recent spectroscopic studies highlight, during external irradiation, a slight increase in the connectivity of the reticulated network, slight migration of the sodium and the occurrence of oxygen bubbles. However, for French glass irradiated with electrons to an integrated dose exceeding 10^{9} Gray, no evolution of the macroscopic properties (density, mechanical properties, stored energy, alteration by water) was observed.

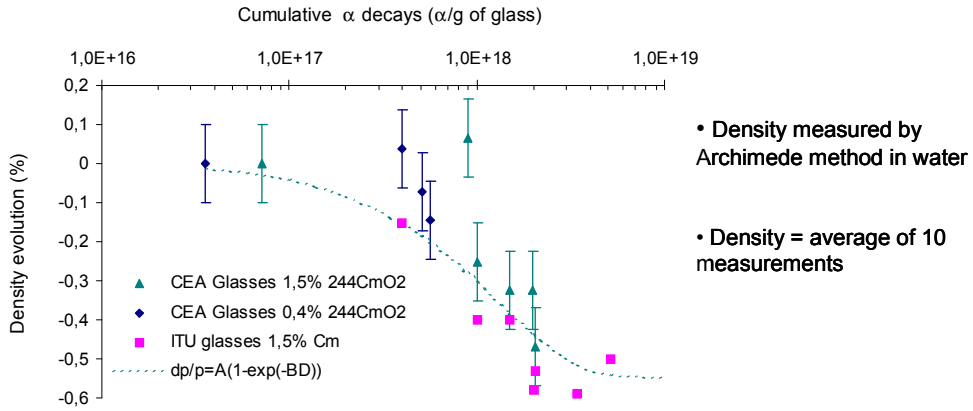

FIG. 4. Evolution of the Specific weight of Cm-doped borosilicate glasses as a function of the cumulative alpha decays.

Generally, unless the received dosages are considerably higher than those we anticipate in the containment glass, the studies performed on other types of glass corroborate these results fairly well.

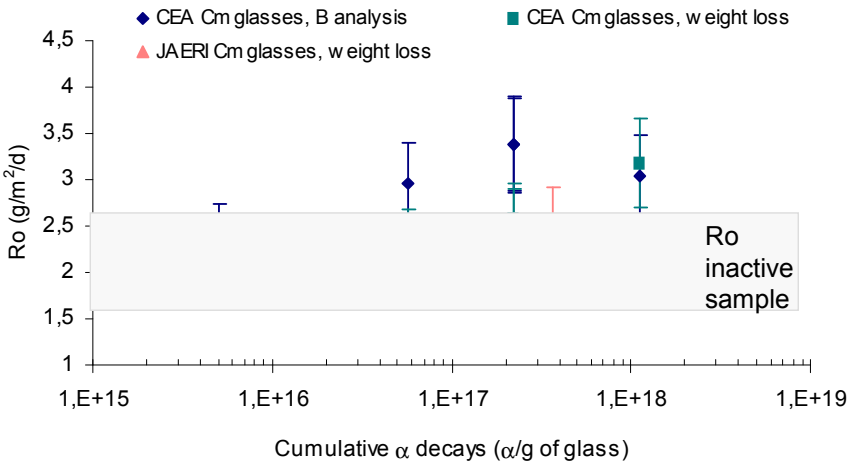

FIG.5. Initial glass dissolution rates at 100°C (soxhlet test, 28 days, glass coupons) measured on Cm-doped borosilicate glasses as a function of the alpha cumulative decays.

2. CONCLUSIONS

Material intended for conditioning solutions of fission products and actinides must have a multitude of properties because of the complexity of the problem posed. Glass was chosen for the containment material because of:

— the flexibility required for containing wastes composed of a variety of elements,
— its thermal stability,
— its excellent chemical durability
— its good resistance to self-irradiation αβγ
— its mechanical properties.

Finding a suitable composition of glass is a compromise between the properties and quality of the material, technical feasibility and safety criteria for definitive disposal.

REFERENCES

[1] C. Courtois, JM. Cavedon, M.Tallec, D. Warin. « Research on Waste Conducted in the Framework of the Law of December 30 1991", Global Conference, Nov.2001, New Orleans. (in press).

[2] R. Do Quang, V Petitjean, F. Hollebecque, O. Pinet, T.Flament, A.Prod'homme, Virtrification of HLW produced by uranium molybdenum fuel reprocessing in COGEMA'cold crucible melter, Waste Management Conf., Tucson, 23-27 feb., 2003.

[3] I. Bardez, D. Caurant, F.Ribot, P. Loiseau, J.L. Dussossoy, F.Villain, N. Baffier, C. Fillet. « Structural Characterisations of Rare Earth-Rich Glasses for Nuclear Waste Immobilisation », MRS-Kalmar, Sweden, june '03, SBNWM symp. Proceeding, (in press).

[4] F. Meaker, D. K. Peeler, J. C. Marra, J. M. Pareizs and W. G. Ramsey, Mat. Res. Soc. Symp. Proc 465, 1281, (1997).

[5] G. Leturcq, G. Berger, T. Advocat and E. Vernaz, Chemical Geology 160, 39 (1999).

[6] L. Li, D. M. Strachan, H. Li, L. L. Davis and M. Qian, J. Non-Cryst. Solids 272, 46 (2000), L. Li, H. Li, M. Qian, D. M. Strachan and J. Non-Cryst. Solids 283, 237 (2001).

[7] L. Li, D. M. Strachan, H. Li, L. L. Davis and M. Qian, Ceram. Trans. 107, 131 (2000).

[8] Delaye, J.M. and Ghaleb, D. (2002) Volume change origin in glasses submitted to ballistic collisions, molecular dynamics simulations. Nuclear Instruments & Methods in Physics Research, Section B B191 10-16.

[9] Abbas, A., Delaye, J.M., Ghaleb, D., and Calas, G. (2001) Molecular Dynamics Study of the Structure and Dynamic Behaviour at the Surface of a Silicate Glass. Journal of Non Crystalline Solids.

[10] Boizot, B., Petite, G., Ghaleb, D., and Calas, G. (2001) Dose, dose rate and irradiation temperature effects in b-irradiated simplified nuclear glasses by EPR spectroscopy. Journal of Non-Crystalline Solids 283 (1-3), pp. 179-185.

VITRIFICATION OF SULPHATE BEARING HIGH LEVEL WASTE (HLW)

P.K. WATTAL
Bhabha Atomic Research Centre, Mumbai, India

Authors and Contributors: MAHESH CHANDER, P. SHEKHAR, RAJEEV RANJAN

Abstract

The Indian strategy for the management of spent fuel is based on Reprocessing-Conditioning-Recycle (RCR) option.

Reprocessing of spent fuel by the PUREX process leads to the generation of high-level radioactive liquid waste. Strategy for the management of high-level waste in India involves:

a) Immobilization of HLW in borosilicate matrices
b) Interim storage of vitrified HLW for a period of about 50 years
c) Ultimate disposal of vitrified HLW in deep geological repository

Borosilicate matrices have found wide acceptance for immobilization of high level wastes. Suitable glass compositions within the borosilicate family have been formulated and characterized for sulphate bearing high-level radioactive waste[1]. Presence of sulphate in HLW, generated earlier, is on account of ferrous sulphamate as a reducing agent, added during partitioning stage of reprocessing. Solubility of sulphur in the form of sodium sulphate is very less (<1% wt) in normally deployed borosilicate melts for vitrification of HLW [2]. The soluble alkali sulphate gets phase separated in the glass melt and its presence is not desirable since this phase is enriched with radio Cs and has high solubility in water. In addition, volatility of sulphates during glass formation is another area of concern. Attempts to address this problem were made and alternative glass forming systems based on lead and barium borosilicate systems were studied for immobilization of this sulphate bearing waste.

1. CHOICE OF GLASS MATRIX

It is well recognized that thermal stability of sulphate compounds is enhanced if the associated cation has a large ionic radius and a low charge. Vitreous melt formulations in the lead and barium borosilicate systems were tried on plant scale with actual high-level waste [3]. Plant scale vitrification runs with lead based glass matrix showed presence of an undesirable separate yellow phase, which not only affected homogeneous distribution of radionuclides but also caused problems during pouring of vitreous product. Hence, barium borosilicate system has been successfully adopted on the plant scale for vitrification of actual HLW.

1.1. Matrix formulation and comparison

Glasses were prepared based on lead borosilicate system (WTR-62) and barium borosilicate system (SB-44) by weighing and mixing known amount of glass forming chemicals and waste constituents. The mix was charged in the furnace at 750^{O}C and temperature was increased gradually at an interval of 50^{O}C and kept for one hour at each temperature, till the glass became pourable. The molten vitreous mass was soaked for 2 hours at a temperature 50^{O}C above the pour temperature. Table I gives the composition of HLW.

Compositional details of lead borosilicate and barium borosilicate systems studied are given in Table II. Table III compares their product properties [4]. In view of the difficulties faced during plant scale runs using lead borosilicate systems, detailed evaluation with regard to optimum waste loading and phase separation were carried out on barium borosilicate systems [2].

TABLE I. COMPOSITION OF HLW

Principal Waste Oxides	**Concentration (gm/litre)**
UO_2	**34.03**
SO_4	**3.0**
Na_2O	18.2
CeO_2	0.0025
Fe_2O_3	3.95
CrO_3	1.1
NiO	0.38
Cs_2O	0.068
SrO	0.0062
RuO_2	0.0169
BaO	0.215

TABLE II. COMPOSITIONAL DETAILS OF GLASS FOR PLANT RUNS

Oxides	**Lead Borosilicate, WTR-62 (wt%)**	**Barium Borosilicate, SB-44 (wt%)**
SiO_2	30	30.5
B_2O_3	20	20
Na_2O	5	9.5
PbO	25	--
BaO	--	19
Waste Oxide	20	21

TABLE III. PROPERTIES OF VITRIFIED WASTE PRODUCT (VWP)

Product Property	**Lead Borosilicate (WTR-62)**	**Barium Borosilicate (SB-44)**
Pouring Temperature (^{0}C)	900-930	925-950
Homogeneity	Not Homogeneous Yellow Coloured Phase Separation observed	Homogeneous No Phase Separation
Density (gm/cc)	3.35 - 3.50	3.0 - 3.20
Viscosity (Poise) at 950^{0}C	135	55
Swelling (Relative Volume of Swelled Mass w.r.t Dried Powder)	3.14	2.56
Wt. Loss at 1000^{0}C	BDL	BDL
Leach Rate (gm/cm^2/day) i) NA released basis (110 days) (as Fission Product constituents) ii) U released basis (as Actinide constituents)	 2.79 x 10^{-5} BDL	 8.71 x 10^{-6} BDL

1.2. Waste loading

Studies were undertaken to find out the optimum waste loading in barium based systems[2]. Glasses were prepared with different waste loading (21-27 wt %) and the product pour temperature and phase separation were noted. Details of the experimental observations are presented in Table IV. In order to understand the limiting step for increasing the waste loading, a few glasses were also made without sulphate keeping the other constituents intact and increasing the waste loading as high as 30 % by weight. Studies have not indicated any noticeable presence of separated phase even up to 30 wt % waste loading without sulphate. Waste loading up to 21 wt % for sulphate bearing HLW can well be accommodated in barium based glass system without having any phase separation. Glass composition, SB-44, has been adopted in the plant scale vitrification with actual HLW.

TABLE IV. EFFECT OF WASTE LOADING ON BARIUM BASED GLASS

Code	**Composition in weight percentage**					**Pour Temp (^{0}C)**	**Visual observation**
	SiO_2	**B_2O_3**	**Na_2O**	**BaO**	**W.O**		
SB44	30.5	20	9.5	19	21	925	Dark Brown colour, No Phase Separation
SB44B	28.96	18.98	9.02	18.04	25	925	Phase Separation
SB44C	28.18	18.48	8.78	17.56	27	925	Phase Separation

1.3. Phase separation

As mentioned earlier, a yellow coloured separated phase was observed in lead borosilicate glass formulation, which was normally absent up to 2.5 wt % sulphate in barium borosilicate glass (Fig. 1). The concentration of sodium and sulphate in the separated phase from both the glasses is given in Table V. The compositional variations of glass formers (SiO_2+B_2O_3) and glass modifiers (Na_2O+PbO+BaO+CaO) with waste oxide loading are also given. While lead based borosilicate glasses gave very high concentration of sodium and sulphate in the separated phase, their concentrations in different compositions of barium borosilicate matrices were substantially low. Barium was found to be more effective than lead in retaining the sulphate within the glass matrix. Chemical analysis of the soluble fraction on the top surface of the glass product indicated very small amount of sodium and sulphate indicating a better retention potential for sulphate.

FIG. 1. Vitrified waste product based on barium borosilicate & lead borosilicate glass

TABLE V. CHEMICAL ANALYSIS OF SEPARATED PHASE ON THE SURFACE OF VITRIFIED WASTE PRODUCT (VWP)

Type	**Composition of the Glass (wt %)**			**Chemical Analysis of Separated Phase (mg/100g of VWP)**	
	Glass Formers	Glass Modifiers	Waste Oxide	Na Conc.	SO_4 Conc.
Lead Borosilicate					
WTR-62	50	30	20	335	589
Barium Borosilicate					
SB15	47.5	32.5	20	58	150
SB22	54	24	22	15	26
SB33	54	25	21	21	47
SB44	50.5	28.5	21	07	14

2. LEACHING

Leaching of Vitrified Waste Product (VWP) based on both lead and barium borosilicate systems were evaluated. While lead borosilicate glasses have been studied under repository conditions as well, leaching of barium based borosilicate glasses under this environment has been initiated

2.1. Leaching behaviour with distilled water

Vitrified waste products obtained from Leach rate of the vitrified product after 110 days at 100^{O}C using distilled water as leachant on sodium release basis are 2.79 x 10^{-5} and 8.71 x 10^{-6} gm/cm^2/day for lead and barium borosilicate systems respectively and are comparable. Leaching behaviour of the vitrified product after 110 days at 100^{O} C with distilled water on sodium release basis is presented in Figure 2.

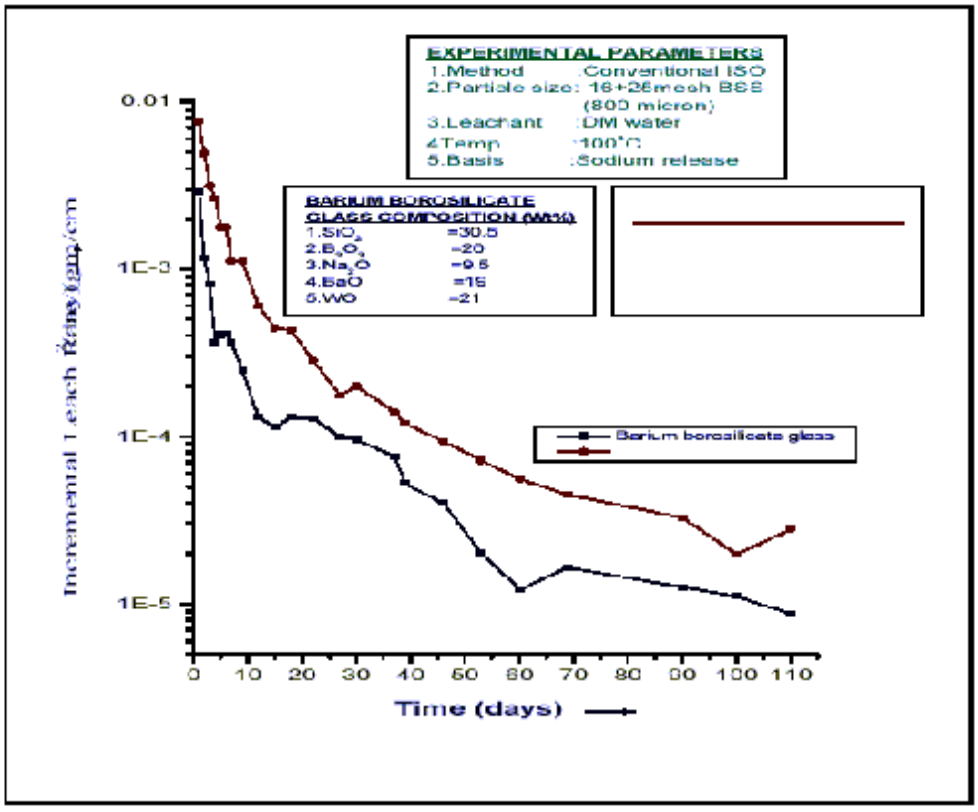

FIG. 2. Leaching pattern of vitrified waste product (VWP)

2.2. Leaching behavior under repository conditions

The normalised leach rates for lead borosilicate (WTR- 62) glass matrix based on silica, boron and sulphate analyses of leachates were of the order of 10^{-3} to 10^{-5} gms/cm^2/day for 45 days test period in presence of synthetic ground water as well as in presence of other materials likely to be present along with synthetic ground water. The effect of granite, bentonite and

ferric oxide in contact with synthetic ground water on the leach rates of WTR-62 glass matrix was studied.

The leachate samples were analysed for pH, sodium, silica, boron, and sulphate content. These analyses were carried out by pHmetry, ion chromatography and spectrophotometry.

Results of pH measurement

The analysis of leachates in distilled water and synthetic ground water containing humic acid indicated that the leachate pH increased with time (Figure-3). The pH of synthetic ground water initially decreased in about 25 days and then increased in 90 days. The pH of the leachate from the experiments in presence of bentonite, granite and ferric oxide showed an initial decrease and subsequent rise in pH similar to synthetic ground water leachate.

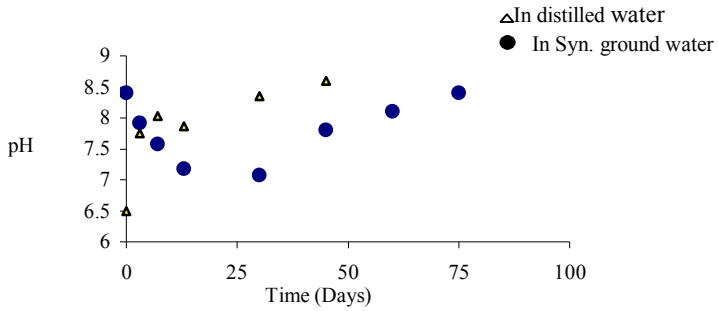

FIG. 3. Leachate pH during leaching of Lead Borosilicate Glass, WTR-62

Element Mass Loss (NL_i) of Glass Matrix

The elemental mass loss (NL_i) from 1.0 gm of glass matrix was calculated based upon the analysis of leachate samples for sodium, silica, boron and sulphate. The NLR_{is} were expressed in units of $gm/cm^2/day$. The observed values are given in Table VI.

TABLE VI. ELEMENTAL MASS LOSS (NL_I) FROM GLASS MATRIX

NLR_i, $gm/cm^2/day$	**Distilled water**	**Synthetic Ground water**	**Synthetic Ground Water + additives**			
			Granite (0.1 gm)	**Bentonite (0.1 gm)**	**Bentonite (0.1gm) + Ferric Oxide (0.06 gm)**	**Humic Acid**
Sodium	2.7E-4	Not analysed				
Silica	2.0E-4	2.4E-3	1.8E-3	2.1E-4	6.9E-5	5.2E-4
Boron	1.1E-4	8.7E-4	1.6E-4	5.3E-3	1.7E-4	6.3E-5
Sulphate	ND	1.8E-5	3.1E-5	8.5E-5	3.7E-4	2.7E-4

During the initial period of leaching, the exchange of Na^+ ions of glass matrix with hydronium ions of water is fast since the Na^+ ions near the glass matrix-water interface get exchanged. The exchange rate slows down, as the hydronium ions have to diffuse through the

exchanged layer. Thus, after about 15 to 20 days, the high initial leach rates stabilise to a lower value and are mainly controlled by matrix dissolution mechanism. A formation of leached layer on the glass matrix surface retards the ion exchange as well as matrix dissolution mechanisms of glass leaching. The NLR_{Sodium} for the distilled water leachant stabilised at 2.7 x 10^{-4} gm/cm^2/day after 45 days.

The NLR_{Silica} and NLR_{Boron} in synthetic ground water leachant and ground water containing granite were higher than distilled water leachant. This is due to higher initial pH of 8.4 of synthetic ground water as compared to 6.5 for distilled water. The difference of an order of magnitude between NLR_{Silica} compared to NLR_{Boron} under above conditions was probably due to saturation of leachant by silica from granite.

The observed NLR_{Silica} in presence of granite was higher by about an order of magnitude than that in presence of bentonite and with additional ferric oxide because of silica leaching to synthetic ground water from granite and uptake of silica by bentonite and iron oxide.

The leach rates in presence of synthetic ground water containing bentonite and also with additional ferric oxide were an order of magnitude higher than NLR_{Silica} under similar conditions due to uptake of leached ions by bentonite. Also, NLR_{Silica} and NLR_{Boron} in synthetic ground water containing bentonite and also with additional ferric oxide were lower than values for synthetic ground water.

NLR_{Boron} represents more realistic leach rates of glass matrix as compared to NLR_{Silica} because boron is not the component of both granite as well as bentonite,

The $NLR_{Sulphate}$ increased in synthetic ground water containing bentonite and with additional ferric oxide compared to synthetic ground water alone and ground water containing granite. $NLR_{Sulphate}$ was found maximum in presence of bentonite and ferric oxide with synthetic ground water. $NLR_{Sulphate}$ was higher in synthetic ground water containing humic acid as compared to synthetic ground water alone.

Besides this, microstructural characterization studies with respect to homogeneity, yellow phase formation and its characterization, leach layer analysis have also been conducted.

3. HOMOGENEITY AND MICRO-STRUCTURAL CHARACTERISATION

Studies using Scanning Electron Microscope (SEM) and line scans using PET crystal have been carried out to investigate the homogeneity of these glasses. The Back-scattered Electron (BSE) images of the lead borosilicate glass and barium borosilicate glass samples show that these glasses are quite homogeneous (Figure 4).

In order to confirm any compositional variations in the major constituents of lead boro-silicate glass (Si, Pb and Fe), line profiles across a distance of 50 μm and at 1000 regular intervals were taken. These profiles confirm the observation (BSE image) that there are no inhomogeneities in the glass (Figure 5). WDS spectra of glass samples based on barium borosilicate formulation are presented in Figure 6. As seen from the above figures, products are homogeneous in nature and have by and large uniform distribution of the elements within the glass. Overlapping of the images and spectra also reveals that Ba and S are not always together, thereby, minimizing the possibility of segregation and settling of $BaSO_4$ at the bottom.

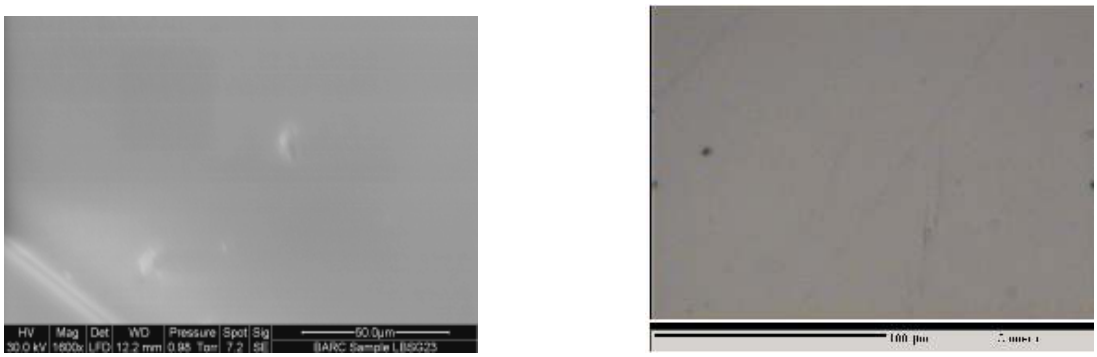

a. Lead Borosilicate Glass (WTR-62) **b. Barium Borosilicate Glass (SB-44)**

FIG. 4. SEM image indicating homogeneous nature of glass

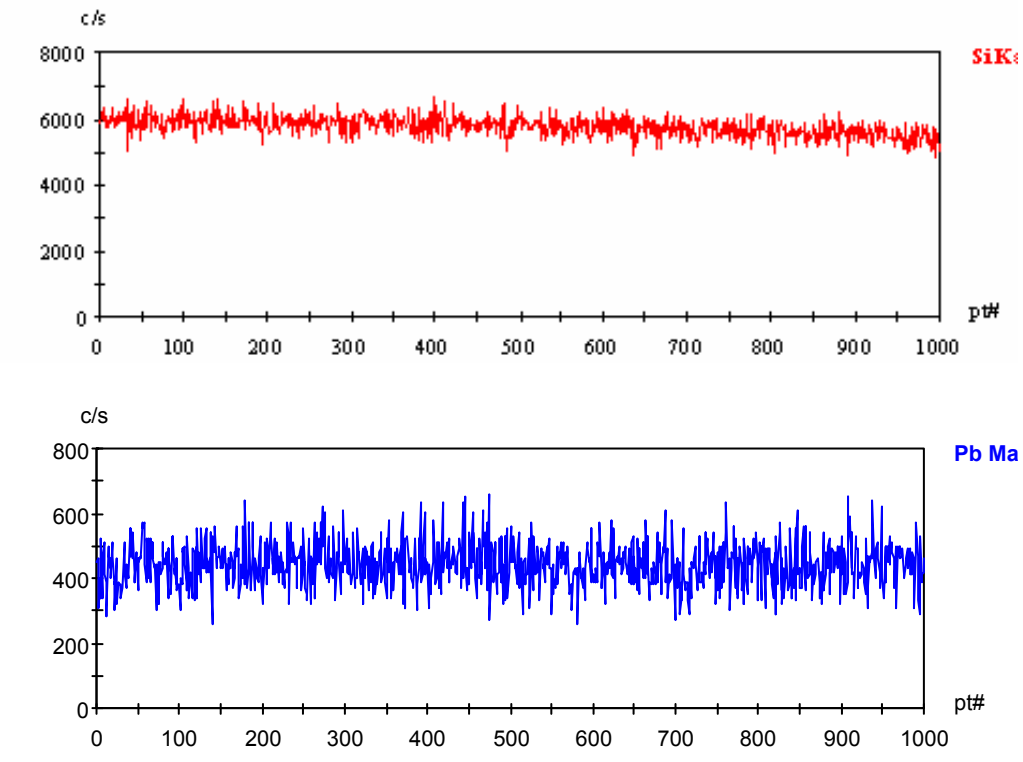

FIG. 5. Line Scans of Si using TAP crystal and of Pb using PET Crystal over a distance of 50 μm (1000 points)

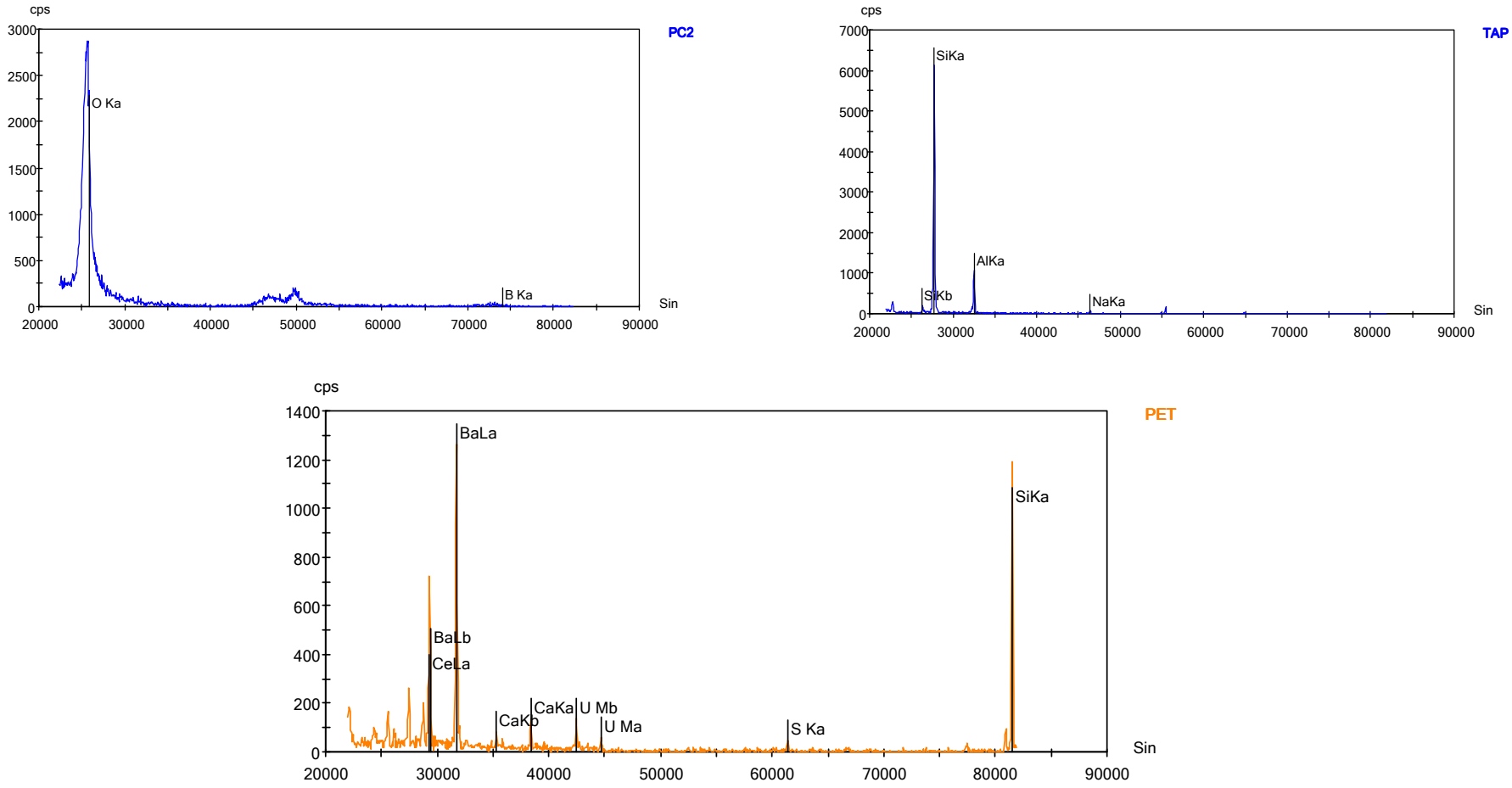

FIG. 6. WDS Spectra of barium borosilicate waste glass (SB-44)

4. PLANT SCALE VITRIFICATION USING LEAD BASED BOROSILICATE SYSTEM

The HLW waste tried out on plant scale is characterized by relatively higher concentration of uranium, sodium and sulphate [3]. This waste is acidic (1-1.5 M HNO3) with average density of 1.13 gm/cm^3. After extensive inactive trials with lead borosilicate glass matrix (WTR-62), nearly 5000 litres of actual HLW were vitrified.

Vitrification at plant scale employed a semi-continuous rising level glass process carried out in a metallic melter located inside a shielded cell having 1.5 m thick concrete wall. The metallic melter is a multizone induction furnace with 4 main heating zones for production of molten vitrified mass and a separate heating zone for draining molten glass into stainless steel canister. Melter and susceptor pots are made of high nickel chromium alloy (Inconel-690). Power levels were maintained so as to achieve maximum evaporation rate keeping in view the upper limit of the susceptor temperature, which should not exceed 1100^0 C.

The key processing steps involved are feeding, evaporation, calcination, glass melt formation, soaking and subsequent draining of molten glass in storage canister. Feeding of waste and glass forming additives in the form of slurry at a pre-determined rate is started after process pot bottom zone temperatures reach nearly 600^0 C. Feeding is continued till the solids (calcined cake) build up to a pre-determined level indicated by temperature of nearly 600^0 C. The calcined mass is then fused to form glass. This mass is soaked for 6-8 hours to achieve better homogeneity. Finally, VWP is drained by energizing the freeze valve into a storage canister positioned under the furnace. Draining is confirmed by indications of change in weight using load cell as well as by in-cell camera. Whenever drainage is to be stopped, freeze valve is de-energized and air-cooling is started.

Waste and inactive glass forming additives in the form of slurry was fed to the melter, through a single feed line. Precipitation of lead sulphate was observed in the feed header resulting in choking of this feed line. Waste and slurry feed lines were, thereafter, separated and choking due to lead sulphate precipitation was overcome. However, problem of occasional choking of slurry feed line was still persisting. System modifications helped to minimize this problem.

The maximum operating temperature of the glass during vitrification was limited to 950-1000^0 C. This was on account of the limitations imposed by material of construction of the melter pot (Inconel-690). At this operating temperature, the viscosity of the molten glass was good enough for pouring. Pouring patterns as viewed with the in cell camera are illustrated in Figure-7. Initially, normal pouring as a thin stream was observed (Figure-7.A). Subsequently, towards the end, the pouring was not normal and went through various stages resembling rod formation (Figure-7.E&F), pouring through hollow cylinder (Figure-7.C), multiple streams (Figure-7.D) etc. The most difficult situation encountered during the pouring was the choking at the bottom of the susceptor (Figure-7.H). The choke was followed by filling of the glass, in annular space between the process pot and susceptor.

It was concluded that a separate sulphate layer was getting formed in the process pot, which would float on the top of the molten glass due to the density difference. During complete pouring of the molten glass form the process pot, this separated sulphate layer (yellow phase) would drain vigorously, resulting in off normal pouring and subsequent choking of the susceptor pot.

Based on these difficulties, barium based borosilicate system was adopted, as against lead borosilicate glass, for this HLW. Experiences using barium borosilicate glass system indicate that this glass formulation is able to accommodate sulphate effectively without impairing the other properties of the product and there were no difficulties observed during pouring of these glasses.

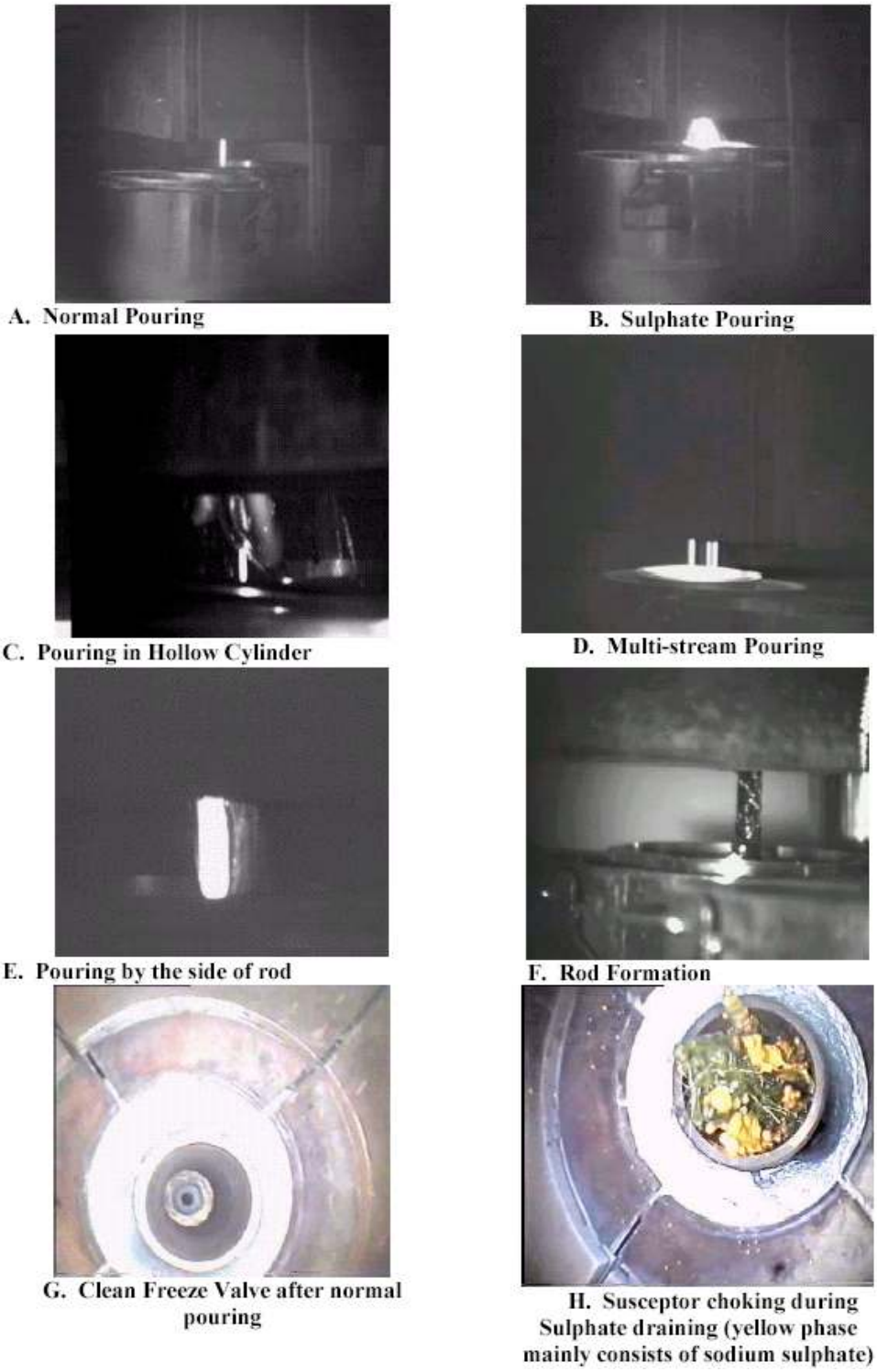

FIG. 7. Pouring Patterns observed using Lead Borosilicate Glass Matrix

ACKNOWLEDGEMENTS

I wish to express my deep appreciation to Shri D. S. Deshingkar, Shri Tejas Morzaria, Shri Darshit Mehta, Shri Aniruddha D., Shri B.B. Verma, Shri P.D. Ozarde, Shri Kanwar Raj, Shri Vidya Thorat, Shri Soudamini N., Shri R. K. Mishra and Shri C. P. Kaushik of Nuclear Recycle Group, BARC for providing information valuable to the present work through their research on stable borosilicate systems and subsequent implementation on plant scale.

REFERENCES

[1] JAHAGIRDAR, P.B., WATTAL, P.K., Vitrification of sulphate bearing high level wastes in borosilicate matrix", Journal of Waste Management (18), 265-273, 1999

[2] KAUSHIK, C.P., MISHRA, R.K., KATARNI, V.G., THORAT, VIDYA, SOUDAMINI, N., OZARDE, P.D., RAJ, KANWAR, Performance Evaluation of Vitrified Waste Product based on Barium-Borosilicate Matrix deployed for Vitrification of Sulphate Bearing High Level Radioactive Liquid Waste, BARC Report, BARC/2004/E/019

[3] MORZARIA, TEJAS, MEHTA, DARSHIT, D., ANIRUDDHA, VERMA, B.B., OZARDE, P.D., RAJ, KANWAR, Engineering Scale Processing of Sulphate Bearing HLLW by Vitrification – an Operating Experience", 14th Annual Conference of Indian Nuclear Society and 1st BRNS Conference on Nuclear Fuel Cycle, INSAC–2003, IGCAR, India

[4] THORAT, VIDYA, SOUDAMINI, N., MISHRA, R.K., KAUSHIK, C.P., RAJ, KANWAR, Studies on Barium and Lead Borosilicate systems for Immobilization of Sulphate bearing High Level Radioactive Liquid Waste, 14th Annual Conference of Indian Nuclear Society and 1st BRNS Conference on Nuclear Fuel Cycle, INSAC–2003, IGCAR, India

STUDIES ON APPLICABILITY OF THERMODYNAMIC DATABASE OF RADIOACTIVE ELEMENTS AND GLASS ALTERATION BEHAVIOR FOR PERFORMANCE ANALYSIS OF HLW DISPOSAL IN JAPAN

MIKAZU YUI

Japan Nuclear Cycle Development Institute, Tokai-mura, Japan

Abstract

Japan Nuclear Cycle Development Institute (JNC) has developed an in-house thermodynamic database of radioactive elements (JNC-TDB) and has performed glass durability studies for high-level radioactive waste (HLW) disposal in Japan. This paper presents the related studies on availability of the JNC-TDB, co-precipitation/solid-solution, glass alteration under high-pH condition, and natural analogue studies.

1. AVAILABILITY OF THE JNC-TDB (YUI, ET AL., 2003)

We have developed an in-house thermodynamic database of radioactive elements (JNC-TDB) for the recent H12 performance assessment (JNC, 1999) of HLW geological disposal in Japan, especially focused on reducing conditions expected in the repository (Yui et al., 1999). Applicability of thermodynamic databases means the relevance for predicting aqueous speciation and solubility of radioactive elements for performance assessment. The JNC-TDB can be accessed through URL: http://migrationdb.jnc.go.jp/. The quality has been checked partly through independent experiments by JNC. This paper presents the recent studies on applicability of the JNC-TDB, co-precipitation/solid-solution, glass alteration under high-pH condition, and natural analogue studies.

1.1. Applicability of thermodynamic data for more stable solid phases

Thermodynamic data show that the crystalline phases are more stable and less soluble than the amorphous phases, and that at elevated temperature, such as those expected in the high-level waste repositories, amorphous phases are expected to transform to crystalline phases. The crystalline tetravalent actinides oxides in general are about eight orders of magnitudes less soluble than the amorphous phases (Fig. 1, Rai et al., 1987).

Previously, a study on the transformation of amorphous to crystalline phases was carried out by using ThO_2 phases as a representative of actinides(IV) oxides (Rai et al., 2000) and showed that ThO_2(am) readily converts to extremely insoluble ThO_2(cr) at 90ºC in a few weeks.

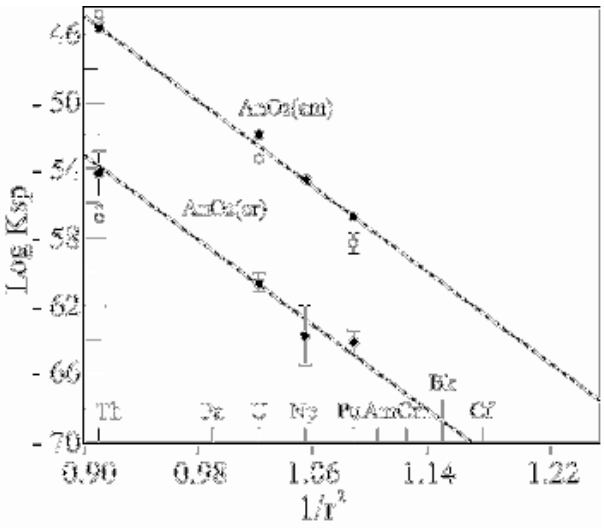

FIG. 1 Variation of solubility products of actinide oxides[1]. Rencent data (○) for U*[2], Th*[3] and Pu*[4] are also shown.*

*1: Rai et al., 1987, *2: Rai et al., 1997, *3: Rai et al., 2000, *4: Rai et al., 2002

Following the previous study, we conducted solubility measurements at higher temperature to study the transformation of UO_2 amorphous to crystalline phases (Rai et al., 2003a). These studies are conducted under rigidly controlled redox conditions maintained by $EuCl_2$ as a function of pH and from the over saturation direction where UO_2(cr) was precipitated at 90ºC in the low pH region. X-ray diffraction analyses of the solid phases with the observed solubility behavior as shown in Fig. 2, identified UO_2(cr) as the dominant phase pH<~1.2 and UO_2(am) pH>~1.2. Based on this study, the data for UO_2(cr) solubility product as a maximum will be adopted in the JNC-TDB, but it's relevant only in low pH region at lower temperature.

We have also studied the dissolution behavior of the Th-doped glasses, phosphate-free borosilicate glass, to validate the JNC-TDB. The Th composition of the glass is 0.99%. Powdered glass at <80 mesh was used to accelerate the equilibration rate. All experiments were conducted at room temperature (23±2ºC). Experiments were conducted by adding 1g of ground glass to 30ml solutions in plastic tube by continuously adjusting pH by adding HCl. The comparison with Th concentrations predicted by using the JNC-TDB showed that the observed aqueous Th concentrations are lower than those expected in equilibrium with ThO_2(am) or ThO_2(cr) in the very acidic range shown in Fig. 3. The Th concentration-controlling phases in these glasses might result from a combination of phases involving ThO_2(cr) or Th reaction with silicate both in the aqueous and solid phases. Further studies with Th-containing glasses are required to improve the JNC-TDB by the relevant data for Th-silicate.

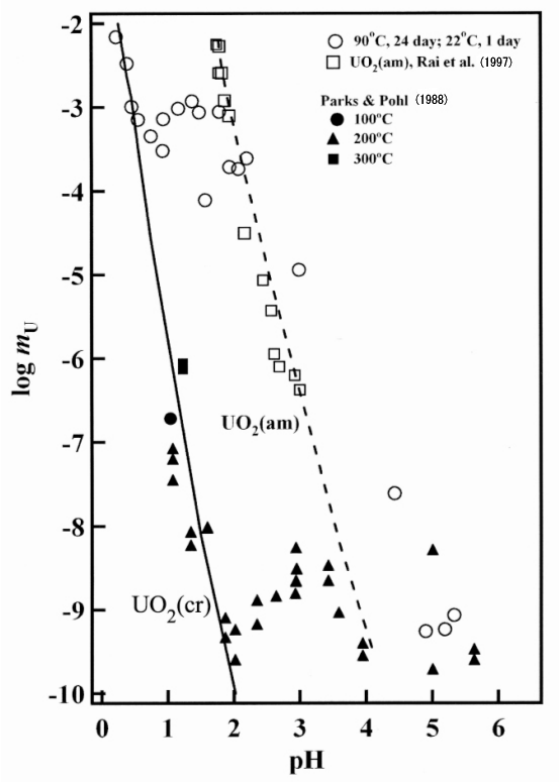

FIG. 2 Uranium concentrations as a function of pH resulting from heating U(IV) aqueous solutions or UO_2(am) suspensions in $EuCl_2$ at 90°C. Lines depict predicted concentrations in equilibrium with UO_2(cr) (solid line) and UO_2(am) (dashed line).

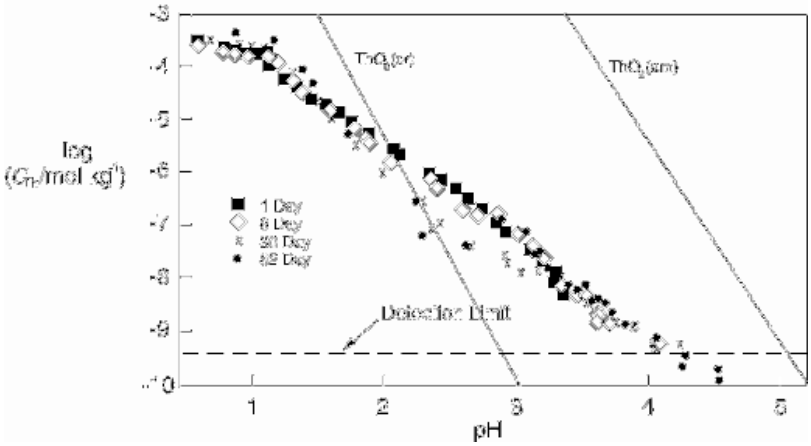

FIG. 3. Aqueous Th concentration in glass/water suspensions. Lines represent predicted solubilites for Th-solids.

1.2. Applicability of thermodynamic data for Redox State of Pu

The reliability in the JNC-TDB is important for redox equlibria of actinides, especially for Pu, due to debates about which redox state is dominant, trivalent or

tetravalent in the neutral pH range under reducing conditions. The difference in redox states of Pu affects the setting of its migration parameters.

The PuO_2(am) solubility measurements were conducted as a function of time, for pH values from 5 to 11, and in the presence of 0.001M $FeCl_2$ or 0.00052M hydroquinone as reducing agents relevant under geological conditions (Rai et al., 2002). All experiments were conducted at room temperature (23±2ºC) in an atmospheric controlled chamber (Ar 99.99%, with <10ppm O_2). The observed PuO_2(am) solubilities as an example shown in Fig. 4 in 0.001M $FeCl_2$ solution were several orders of magnitude higher than the Pu(IV) concentrations predicted by using thermodynamic data. The combination of techniques involving UV-Vis-NIR spectroscopy and solvent extraction with thenoyltrifluoroacetone in toluene, and thermodynamic analyses of data showed that Pu(III) was dominat aqueous oxidation state. The related thermodynamic data in the JNC-TDB is a little bit different from the value, and is to be revised.

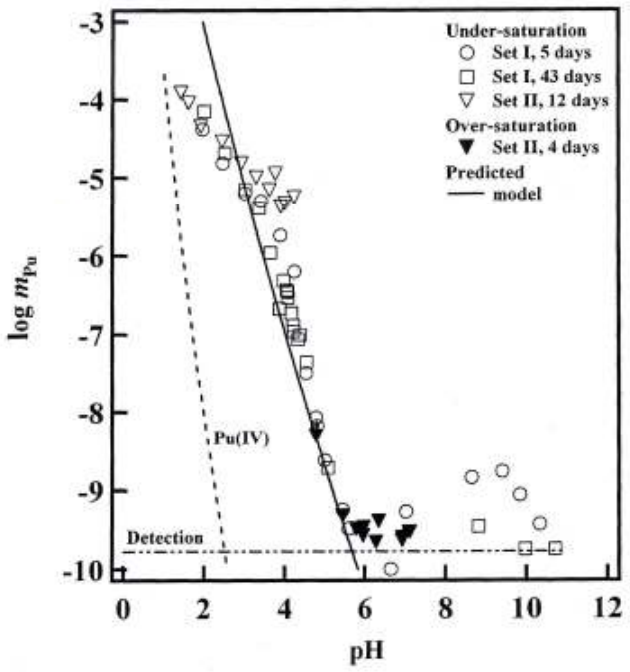

FIG. 4. Aqueous Pu concentration as a function of pH from PuO_2(am) suspensions in 0.001 M $FeCl_2$. Lines represent Pu concentrations in equilibrium with PuO_2(am) predicted from the thermodynamic data: dashed line-concentration of Pu(IV) species; solid line-total Pu concentrations (Set I, II; different sets of experiments).

1.3. Applicability of thermodynamic data in cementitious conditions

The applicability of the JNC-TDB to highly alkaline environment needed to be checked, because the use of cement material is expected for tunnel mechanical support in soft rock in the context of HLW disposal. The applicability of the JNC-TDB was checked preliminarily by comparison between reliable measured solubilities of some radioactive elements(Am, Th, Sn and Ni) in cement waters and calculated

values using the JNC-TDB(Yui et al., 2003). Based on these comparison, the JNC-TDB appears to be quite reliable and applicable to different systems, however, data improvement is needed such as data for not only pure phases but also solid-solutions in cement-water system.

2. STUDIES ON CO-PRECIPITATION

As indicated above by the study on Th-doped glass dissolution behavior and the JNC-TDB availability in cementitious conditions, solid-solution/co-precipitation studies are required. The H12 performance assessment also adopted co-precipitation of Ra as the source of the waste glass. We have initiated a co-precipitation studies for Ra(Ba)-Ca-CO_3 system and solid-solution studies of $(U_x, Np_{1-x})O_2$(am) system.

A co-precipitation study has adopted the free-drift method for Ba-Ca-CO_3 and Ra-Ca-CO_3 system by variable CO_2 concentration.

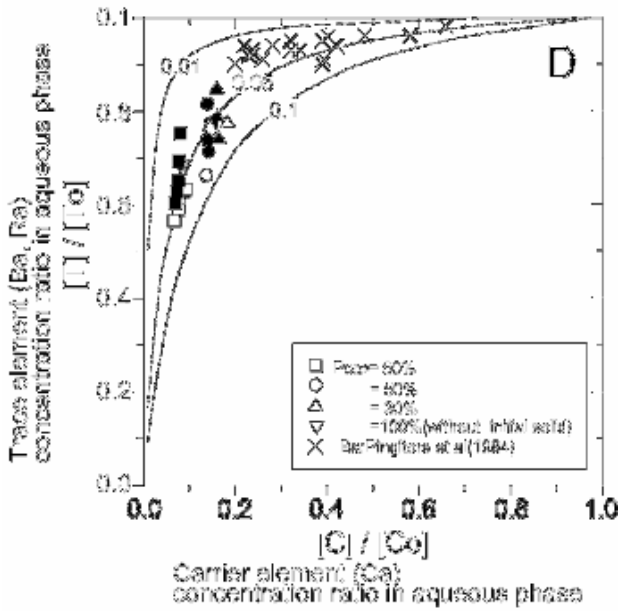

FIG. 5. Experimental result of Ba and Ra-226 coprecipitation with $CaCO_3$ and calculated line by homogeneous partition law

D:howogeneous partition coefficient,
Black symbol: Ra-226, white symbol: Ba

The co-precipitation behavior of Ba and Ra is modeled by homogeneous partition law, which is described: $\frac{[T]_{solid}}{[C]_{solid}} = D\frac{[T]_{aq}}{[C]_{aq}}$

where, $[T]_{solid}$: tracer element(Ba or Ra) concentration in solid phase, $[T]_{aq}$:tracer element concentration in aqueous pahse, $[C]_{solid}$: carrier element (Ca) concentration in solid phase, $[C]_{aq}$: carrier element concentration in aqueous phase, D: homogeneous partition coefficient. The calculated distributions by this simple model are also shown in Fig. 5 by varying the D value. There are many models to describe, however, in this study, it was found that very simple homogeneous partition law can be applied with the rough by estimated D value of 0.05.

The formation of a solid-solution can significantly affect the solubility of radioactive elements, however, the thermodynamic data for the end members are often not so reliable, especially under reducing environment. We have carried out the experiments to determine the nature of U(IV) and Np(IV) solid-solutions and their thermodynamic properties under consideration of the reliable thermodynamic data for UO_2(am), NpO_2(am) and related aqueous species (Rai et al., 2003b). For this purpose, $(U_x, Np_{1-x})O_2$(am) precipitates with values of x varing from 0.05 to 0.95 were prepared, characterized, and used to determine their solubility in dilute to concentrated K_2CO_3 and $KHCO_3$ solutions.

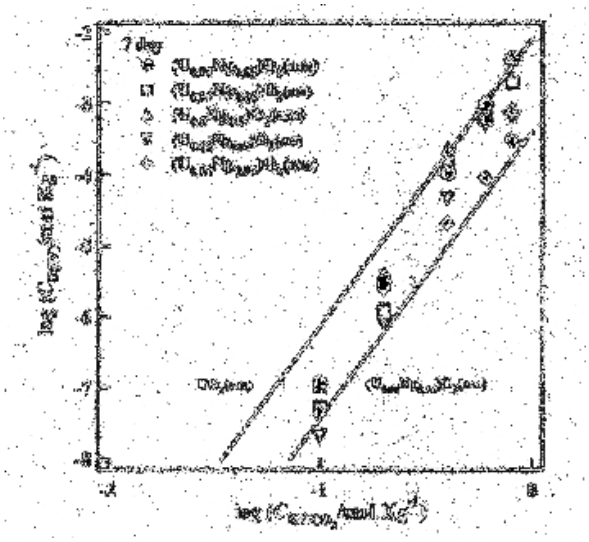

FIG. 6. Uranium concentrations in solutions contacting different solid-solutions equilibrated with $KHCO_3$ solutions (bottom figure). Upper solid line is bestfit to UO_2 (am) solubilities reported. Lower solid lines is predicted based on the solubility of UO_2 (am) and assuming an ideal solid-solution behavior for an amorphous solid containing 0.05 mole fraction of U.

Aqueous U(IV) concentration in equilibrium with $(U_x, Np_{1-x})O_2$(am) solid-solution of five different compositions in the concentrated $KHCO_3$ solutions shown in Fig. 6 show that 1) the solubility of UO_2(am) (Rai et al., 1998) sets an upper limit on the observed concentrations, in agreement with the expected solubilities for the solid-solutions of very high mole fractions (e.g., X_U=0.95), and 2)the solubility predicted for X_U =0.05, based on ideal solid-solution, sets lower limit for the observed solubility. Similar conclusion can be drawn for Np(IV). These data clearly show that the experimental solubility data are consistent with the formation of an ideal solid-solution behavior and that the non-ideal solid-solution behavior can be ruled out.

3. STUDIES ON GLASS ALTERATION UNDER HIGH-PH CONDITION

The experiments were conducted to understand qualitatively and quantitatively the secondary phase formation and associated elemental release during HLW glass dissolution under highly alkaline condition. Static dissolution experiments were adopted with a simulated HLW glass, P0798 under highly alkaline condition by using NaOH, KOH at elevated temperature to accelerate the reaction as a function of temperature, time and alkaline concentration. Crystalline secondary phases during glass dissolution were analyzed by XRD and electron microscopies and the dissolved

element concentrations were analyzed by ICP-MS. Normalized mass loss as a function of time and observed secondary minerals are shown in Fig. 7.

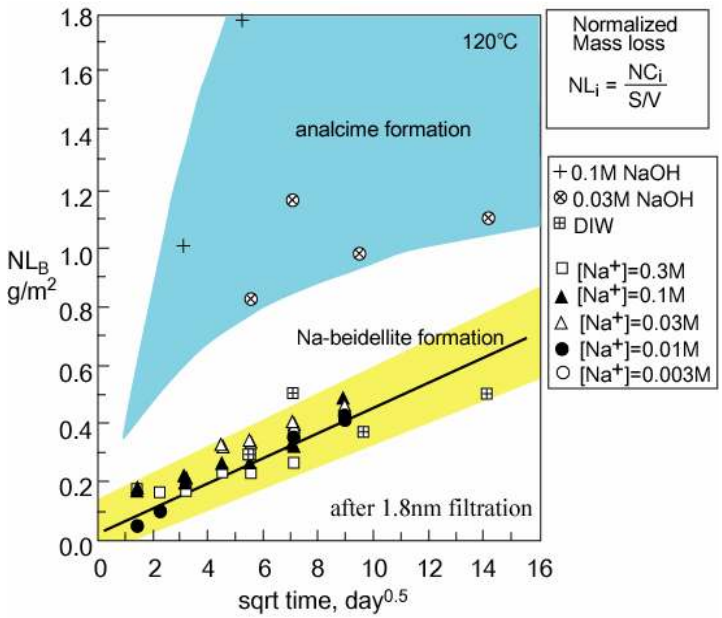

FIG. 7. Normalized mass loss as a function of time

These results indicated that;

1) Thermodynamic calculation based on published equilibrium constants cannot evaluate the empirical secondary phase formation,
2) At conditions where only Na-beidellite forms, the glass dissolution rate is slow, while at conditions where analcime forms, the glass dissolution rate is extremely fast,
3) At conditions where only Na-beidellite forms, the glass dissolution rate is propotional to suare root of time, which suggests the process is diffusion-controlled,
4) Most of Cs in the glass is retained in the secondary phases by sorption onto Na-beidellite or incorporation into analcime.

4. NATURAL ANALOGUE STUDIES

Natural analogue studies on volcanic glasses in the Kanto region have been continued and indicated that volcanic glasses in deep underground are altered to montmorillonite and clinoptilolite for about 0.5My. For example, the mineralogy of the core samples are shown in Table I by the XRD analysis.

TABLE. I. MINERALOGY FOR NATURAL ANALOGUE SAMPLES BY XRD

sample \ mineral		montmorillonite	chrolite	illite	quartz	phgioclase	clinoptilolite	hornblend	Estimated temperature
Yokohama borehole	1003.47~1003.53m					△			43℃
	2000.12~2000.18m	△				○	•		70℃
	2006.34~2006.37m	•	•	•	◎	○	△		70℃
Ichihara borehole	2038.17~2038.20m					△		△	50℃
Somaoki borehole	1000m						△		45℃
	1300m						○		51℃

relative amount : □much, ○medium, △little, • trace

The main conclusion of the observation of the volcanic glasses is as follows.

— Volcanic glasses buried at 50°C sampled from Ichihara boreholes are found to be not altered.
— Volcanic glasses buried at 70°C sampled from Yokohama boreholes are found to be completely altered to montmorillonite and clinoptillolite for about 0.5My in saline type of groundwaters.
— The analysis of volcanic glasses sampled from Somaoki boreholes has supplied the activation energy of alteration rates. Based on the observation, it was found that it takes more than 5My at 41°C and more than 2My at 50°C to convert the volcanic glasses to clinoptillolite.

5. CONCLUSION

The JNC in-house thermodynamic database (JNC-TDB) for radioactive elements has been developed for performance assessment in H12 report. The applicability of the JNC-TDB has been checked to perform the realistic analysis of solubilities of radioactive elements concerning more thermodynamically stable solubility limiting solid phases such as crystalline phase, to predict redox states of Pu in neutral pH range under reducing conditions and to estimate solubilities in cementitious conditions. Based on these studies, the present JNC-TDB is almost applicable.

Co-precipitation studies for Ra(Ba)-Ca-CO_3 and $(U_x, Np_{1-x})O_2$(am) system have been studied and interpreted by using the simple homogeneous partition law and the ideal solid-solution model, respectively.

The glass alteration study under highly alkaline conditions at the elevated temperature has indicated that the alteration products depend on pH. The glass

dissolution rate, where analcime is formed, is higher than that where Na- beidelite is formed. A latter rate is likely dominated by the diffusion.

Natural analogue studies of volcanic glasses in the sea bed indicated that it takes more than 5My at 41ºC and more than 2My at 50ºC to transform the glass to clinoptilolite.

REFERENCES

[1] Japan Nuclear Cycle Development Institute (1999): H12 Project to Establish Technical Basis for HLW Disposal in Japan, Project Overview Report, JNC TN 1400 99-010.

[2] Parks, G. A. and Pohl, D. C. (1988): Hydrothermal Solubility of Uraninite, Geochim. Cosmochim. Acta, 52, 863.

[3] Pingitore, N. E. et al. (1984): The Experimental Partitioning of Ba^{2+} into Calcite, Chemical Geology, 45, 113.

[4] Rai, D. et al. (1987): Solubility of $NpO_2.xH_2O$(am) in the Presence of Cu(I)/Cu(II) Buffer, Radiochim. Acta, 42, 35.

[5] Rai, D. et al. (1997): The Solubility of Th(IV) and U(IV) Hydrous Oxides in Concentrated NaCl and $MgCl_2$ Solutions, Radiochim. Acta, 79, 239.

[6] Rai, D. et al. (1998): A Thermodynamic Model for the Solubility of UO_2(am) in the Aqueous K^+-Na^+-HCO_3^--CO_3^{2-}-OH^--H_2O System, Radiochim. Acta, 82, 17.

[7] Rai, D. et al. (2000): Thermodynamic Model for the Solubility of Thorium Dioxide in the Na^+-Cl^--OH^--H_2O System at 23□ and 90□, Radiochim. Acta, 88, 297.

[8] Rai, D. et al. (2002): Reductive Dissolution of PuO_2(am): The Effect of Fe(II) and Hydroquinone, J. Solution Chemistry, 31(6), 433.

[9] Rai, D. et al. (2003a): Solubility and Solubility Product of UO_2(c) Precipitated from Aqueous U(IV) Solutions at 90□, J. Solution Chemistry, 32, 1.

[10] Rai, D. et al. (2003b): Thermodynamics and Solubility of $(U_x, Np_{1-x})O_2$(am) Solid-Solution in the Carbonate System, submitted to Migration03.

[11] Yui, M. et al. (1999): JNC Thermodynamic Database for Performance Assessment of High-level Radioactive Waste Disposal System, JNC Technical Report, TN8400 99-070.

[12] Yui, M. et al. (2003): Applicability of Thermodynamic Database of Radioactive Elements Developed for the Japanese Performance Assessment of HLW Repository, J. Nuclear Science and Technology, 40(5), 356.

LONG-TERM DISSOLUTION BEHAVIOR OF SPENT FUEL IN COMPACTED BENTONITE AND SYNTHETIC GRANITIC GROUNDWATER

KWAN SIK CHUN

Korea Atomic Energy Research Institute, Daejon, Rep. of Korea

Abstract

This contribution describes experimental work which aims to get the information on corrosion behaviour of Spent Fuel, and to obtain the release rate of radionuclides from the fuel within domestic bentonite and synthetic granitic ground water. Specimens of fuel with burn-up up to 39 GWd/tU, with and without bentonite, have been subjected to leaching. The effects of bentonite on the dissolution rate, and of structural materials, copper and stainless steel on caesium release have been identified and are reported.

1 INTRODUCTION

The R&D for the disposal of spent fuels accumulated up to our NPPs' lifetime at the Korea Atomic Energy Research Institute (KAERI) has been performed since the early 1997 in order to develop a reference repository system in Korea by 2006. The relevant R&D activities are carried out on three topical areas: geoscience environment research, system development and performance assessment and radionuclide migration study. Work on the second topical area was terminated at the end of March in 2003. In the third topical area, system demonstration has been added to support partly the validation of a reference repository system. Now the first year R&D of the third area is almost completed. The results suggest that the repository system should be located in plutonic rock and consist of vertical emplacement boreholes in separate disposal panels for spent CANDU and PWR fuels. Other features should include corrosion resistant containers, into which PWR and CANDU spent fuels are encapsulated, and domestic Ca-bentonite buffer layers[1].

Many experimental results have been reported for the dissolution behavior of spent nuclear fuel and unirradiated UO_2 in water under various conditions [2-8]. Most of the studies on the dissolution of UO_2 pellet with bentonite have been concerned about the formation of alteration phase and precipitates which are solubility-limiting solid phase of uranium in bentonite water. A few experiments have been tried for the identification of dissolution mechanism of spent nuclear fuel in a repository condition [9,10], which is not well known with the lack of real data.

In KAERI, the long-term dissolution experiment of spent PWR fuel has been carried out under the compacted bentonite and synthetic granitic groundwater since June of 1998. The purpose of this experiment is to get the information on corrosion behavior of spent nuclear fuel and release rate of radionuclides from the fuel within our domestic bentonite and synthetic granitic groundwater in order to support the development of radionuclide release models from spent nuclear fuel in the near-field to identify the release mechanism, and finally to support the performance assessment

of our reference disposal concept. Under this program KAERI has joined the Coordinated Research Project (CRP) on “the Chemical Durability and Performance Assessment of Spent Fuel and High-level Waste Forms under Simulated Repository Conditions” in March of 1999.

2. EXPERIMENTAL

2.1. Status of the specimens loaded for their leaching

Except one specimen, all the specimens have been dismantled, as shown in Table I.

TABLE I. LEACHING PERIODS AND BURN-UPS OF THE SPECIMENS LOADED INTO EACH LEACH CELL

Sample number	Weight (g)	Leaching period	Burnup (MWD/MTU)	Remarks
#1	1.86850	98.06.27 – 04.03.19	39,089	Without molder Dismantled
#2	1.70938	98.06.27 – 04.03.19		Without molder Dismantled
#5	1.93256	98.06.27 – 04.03.19		With Cu/SS plates, and without molder and bentonite; Dismantled
#7	1.73027	98.06.27– 02.07.15		Without molder Dismantled
#10	4.09839	98.06.27 – 02.12.27		Without bentonite Dismantled
#51	1.92894	99.12.04 – 02.12.27		Without molder and Bentonite; Dismantled
#55	7.49033	99.05.29 – 04.03.19		Dismantled
#56	7.38966	99.05.29 – 02.07.15		Dismantled
#57	6.87454	99.05.29 – 04.03.19		Dismantled
#58	1.59284	99.12.04 – 04.12.04	37,805	Without molder and Bentonite
#59	7.15128	98.05.29 – 02.12.27		Dismantled
#61	8.41754	00.12.06 – 02.12.27		Dismantled

2.2. Analysis

About 10ml of the leachates from all the baths (related to Table 1) were sampled after 1566 and 2092days. The activities of these leachates were measured by using γ-spectrometer (EG&G ORTEC ADCAM-100) and low-background α/β counter (LB-5100). The copper and stainless steel sheets from the leach cell for the specimen No.5 were taken out, settled into the 5M HNO_3 solution for one day, and then the activities of the solution has been measured. The amounts of U-238 in the leachates were also measured by ICP-MS. And the leach cell for the specimen No.1 was dismantled after 2092days and then the bentonite blocks in contact with this specimen was sliced at a

certain thickness as around 7 pieces. And the sliced bentonite layers will be dissolved to measure cesium and gross activity of alpha-emitters adsorbed on the bentonite.

2.3. Measurement of gap inventory and instant release fraction

Two 2-mm thickness specimens included with a clad were prepared by cutting the spent PWR fuel rod of C15-I08 with diamond saw without cooling water for the measurement of gap inventory. Each of them had been put in a bottle with 50 ml of distilled water for 149 days. About 5mls of the solution were collected at certain periods up to that period and filtered with 0.2㎛ filter, and their cesium detected by γ-spectrometer. The amounts of Sr in the gap was analyzed by liquid scintillation counting of eluted solution of Sr separated on SR-resin (Eichrom Co.)[11].

The spent fuel powder, which was produced by cutting G23-J11 spent fuel rod with a diamond blade, was used for the measurement of an instant release fraction. This powder put into 50ml of 0.1M HCl solution. After several tens minutes, the dissolved solution was replaced. This replacement was repeated several times. Finally, the collected solution was filtered and analyzed.

3. RESULTS AND DISCUSSION

The fractional release rate and the cumulative release fraction of cesium from spent fuel specimens up to 2092days are illustrated in Fig. 1 and 2. The release rates in case of the specimen in contact with bentonite and the specimen in contact with the metal sheets of copper and stainless steel without bentonite decreases sluggishly. Their rates at 1866days are approximately 1.35×10^{-8} and 1.55×10^{-6} fraction per day, respectively. However, the release rate of the specimen without bentonite and the metal sheets at 1340days is approximately 4.40×10^{-6} fraction per day, which is about 3 times higher than that without bentonite and with metal sheets.

The empirical formulas of the fractional release rates of cesium are derived from the measured values (see Fig. 1) as the following equations :

In case of bare fuel : $Ro = 2.07 \times 10^{-5} \, Exp[-1.22 \times 10^{-3} * T]$ ……..(1)
and

in case of fuel with bentonite : $Rb = 1.39 \times 10^{-8} \, Exp[-6.02 \times 10^{-5} * T]$ ……..(2)

where R is the fractional release rate, as fraction per day, and T is time, as days. While the calculated values from the equation (1) for bare fuel were not well agreed, the values from the equation (2) for fuel in contact with bentonite were agreed very well. This suggests that some more leaching data for bare fuel without bentonite should be required for the derivation of more reasonable empirical equation.

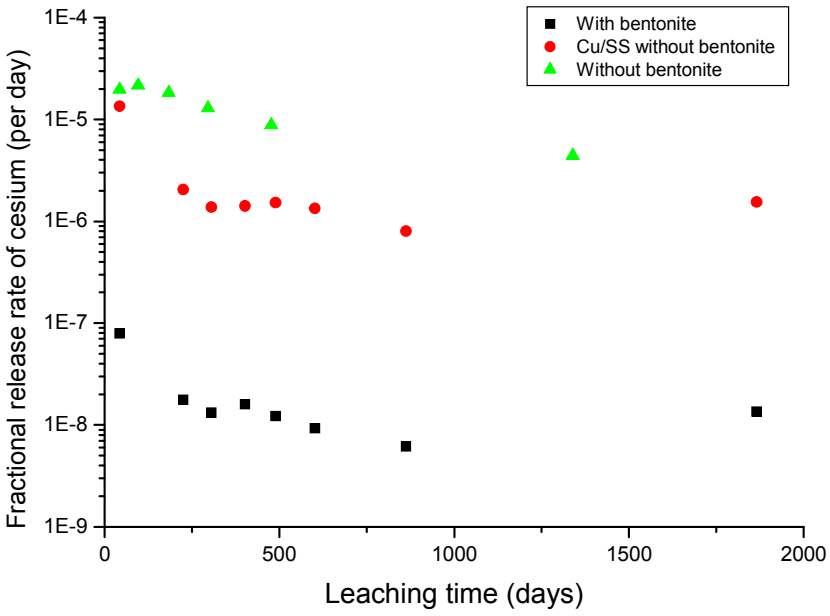

FIG. 1. Fractional release rates of cesium by leaching up to 2092days.

As shown in Fig. 2, the cumulative release fractions of cesium from the specimens in contact with bentonite up to 1480 and 2092days are about 1.82×10^{-5} and 2.20×10^{-5} , respectively. And the cumulative fraction of cesium from the specimen without bentonite and the metal sheets up to 1566days is about 9.73×10^{-3} , which is over 3 times higher than that from the specimen without bentonite and with the metal sheets, 2.55×10^{-3} up to 1480days. These indicate that the dissolution rate of cesium could be controlled by waste package material(s) and bentonite block. The retardation factor of cesium by the bentonite block was more than 400 up to around 1500days.

The apparent diffusivities of cesium in bentonite blocks as a function of time are given in Fig. 3. The diffusivity was suddenly decreased and then nearly constant with the increase of their contact time. The diffusivities derived from the measured values are fitted by the following equation :

$$Da = 2.28 \times 10^{-13} + 3.62 \times 10^{-11} \, Exp[-1.53 \times 10^{-2} * T] \quad \text{.....(3)}$$

where Da is apparent diffusivity, as m^2/sec, and T is time as days. The time when the second term in this Equation (3) would be negligible will be around 400days, after which their diffusivity become nearly constant as shown in Fig. 3. The diffusivity is 2.28×10^{-13} m^2/sec and this is much lower than others[12,13].

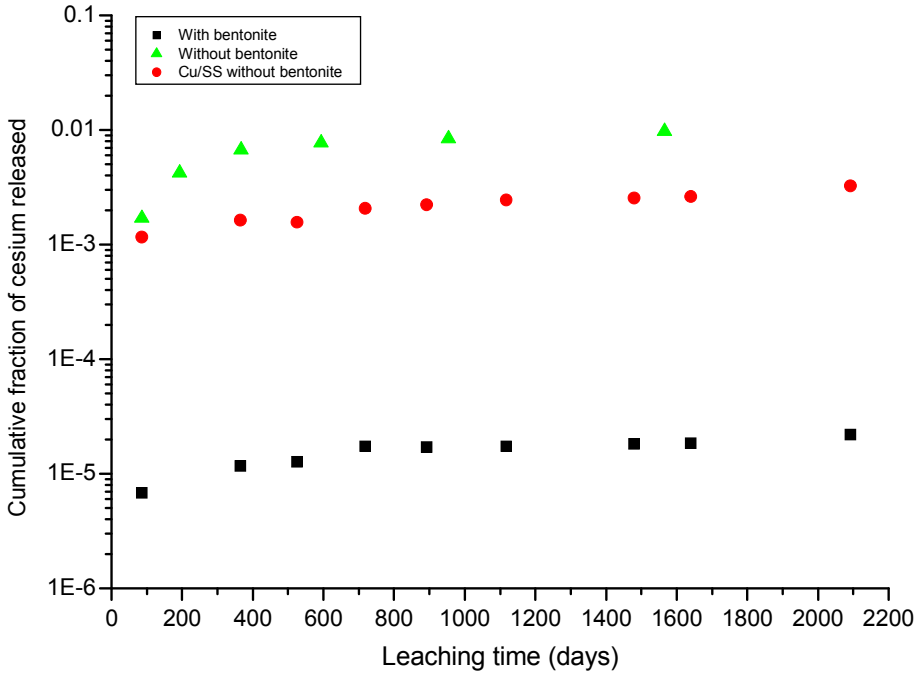

FIG. 2. Cumulative fractions of cesium released by leaching up to 2092days

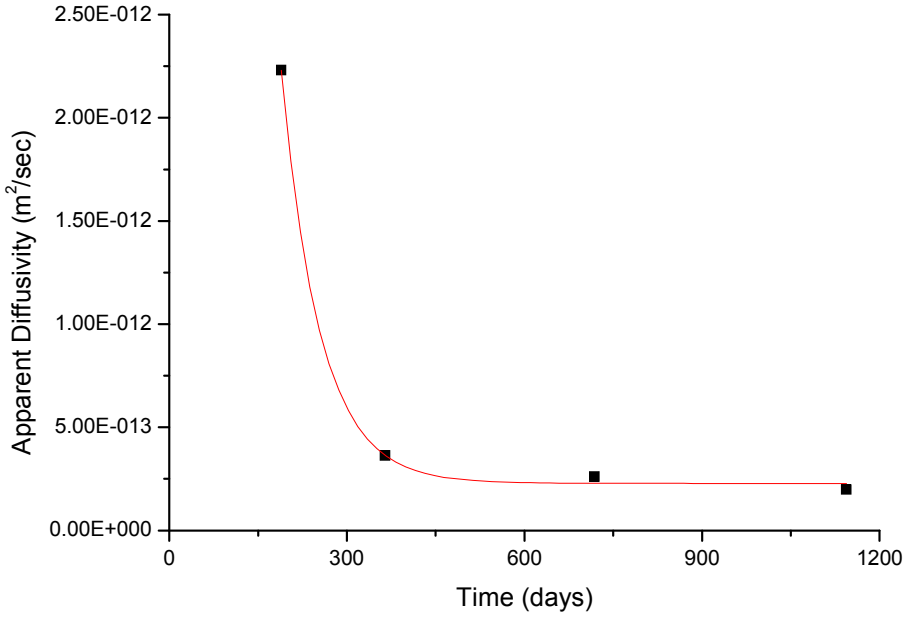

FIG. 3. Apparent diffusivity of cesium in bentonite block as a function of time

The specific activity of cesium contaminated on copper sheets was approx. 0.41μCi/cm^2, which was about ten times higher than that on stainless steel sheets. This means that copper could be more favorable material for the retardation of cesium than stainless steel. On the other hand, the total fraction of the cesium contaminated on the copper and stainless steel sheets was about $3x10^{-5}$, which was at least two order lower than the difference between the release fractions of cesium within and without metal sheets from pure bare fuel. This suggests that other effect(s) by waste package material(s) would control the dissolution rate of spent fuel, and for this identification the further research should be required.

The amount of cesium dissolved from the spent fuel specimens into a demineralized water as a function of time is illustrated in Fig. 4. By this curve fitting, the cumulative fraction of cesium was derived as the following equation.

$$C = 4.03x10^{-3} + 3.39x10^{-5}\ T$$

This indicates that the gap inventory of cesium would be around 0.4%, which is very close to the cumulative fraction of cesium up to 193days (see Fig. 2). This suggests that the initial release amount of cesium from spent fuel into a granitic groundwater could be dependant on its gap inventory.

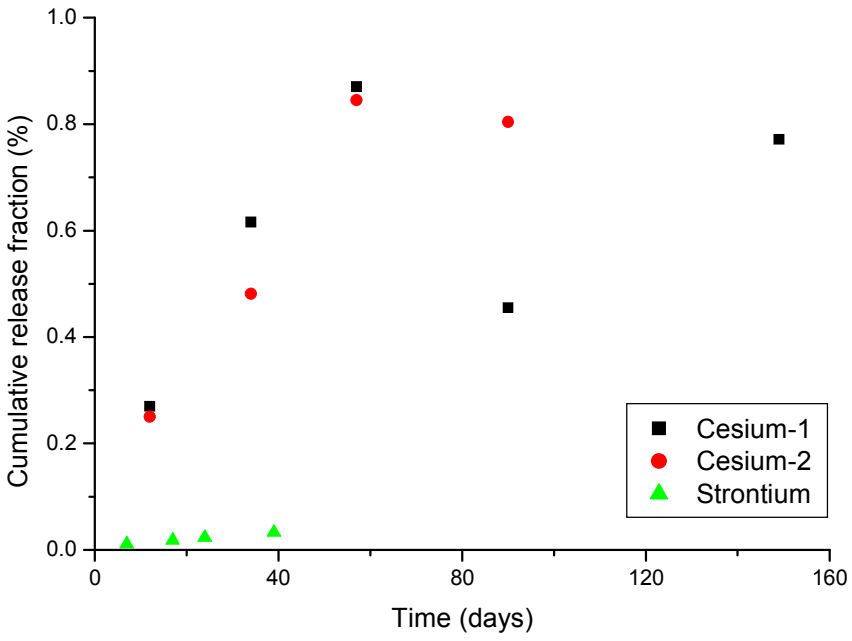

FIG. 4. Gap inventories of cesium and strontium in spent PWR fuel

The instant release fractions of cesium from spent fuel powder were in the range of about 1.2% to 2.9%, as their intercepts given in Fig. 4, of which the high value is equal to that recommended as a reasonable value in SR97[14]. And our results suggest that the cesium inventory in gap and grain boundary of spent PWR fuel would be less than 3%. On the other hand, the instant release fraction of strontium was about

0.4%, as an intercept shown in Fig. 5. This value is much higher than others reported [15].

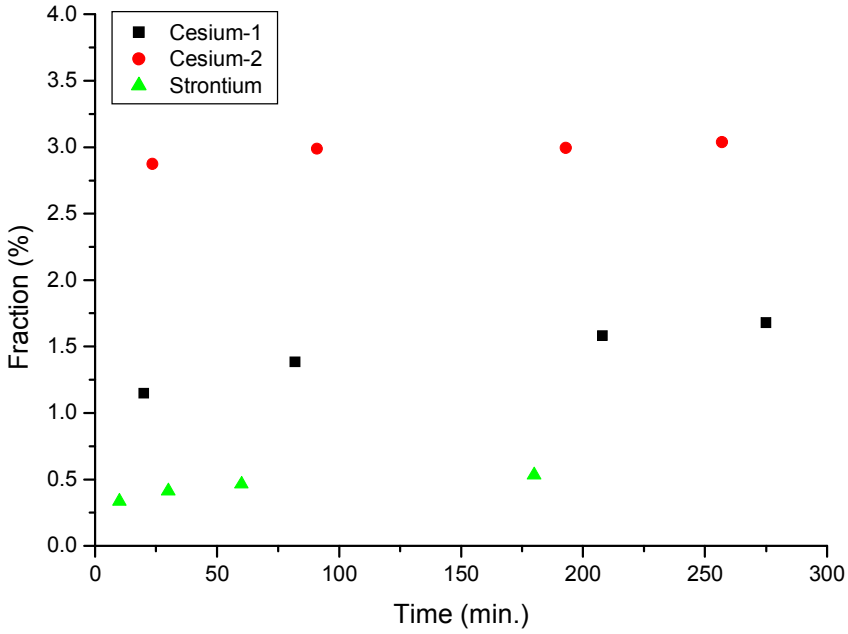

FIG. 5. Instant release fraction of cesium and strontium from spent fuel

The release rate and the cumulative amount of gross alpha emitters are shown in Fig. 6 and 7. The long-term release rate through the bentonite block from spent fuel specimen is about 0.1 Bq per g of spent fuel per day, while the value of the rate without bentonite and with the metal sheets is around 0.8 Bq per g of spent fuel per day. And the value of the release rate from the specimen without metal sheets and bentonite is approximately 3.5 Bq per g of spent fuel per day. As shown in Fig. 7, the cumulative gross alpha activity from the specimen in contact with bentonite block up to 2092days is about 350 Bq, while the activity without bentonite block and with the metal sheets is about 1530 Bq per g of spent fuel. On the other hand, the cumulative gross alpha activity (6280 Bq. Per g of spent fuel) from the specimen without bentonite and the metal sheets up to 1566days is about 20 times higher than that with bentonite block.

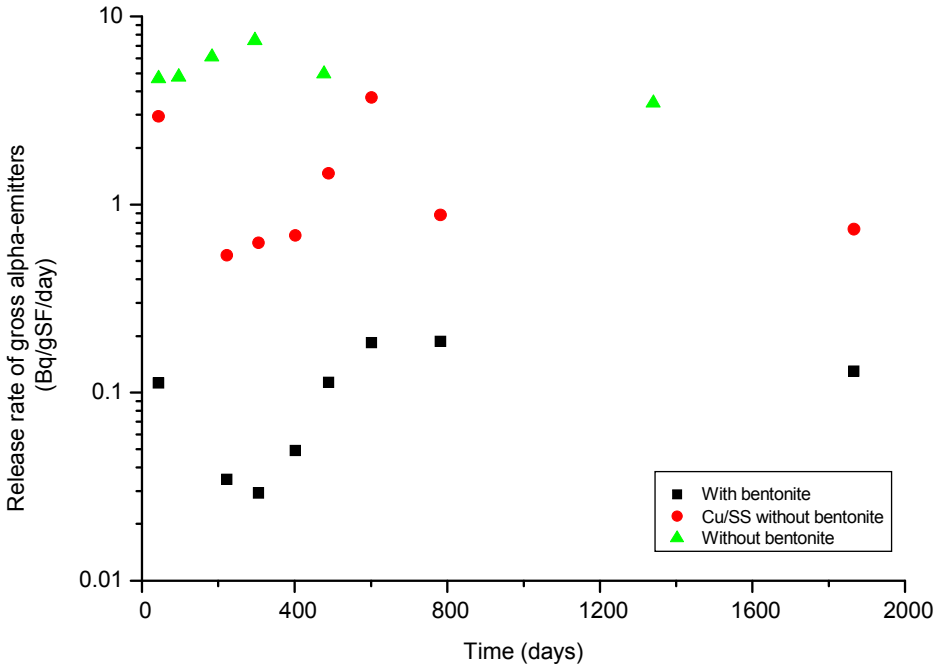

FIG. 6. Release rates of gross alpha activities by leaching up to 2092 days

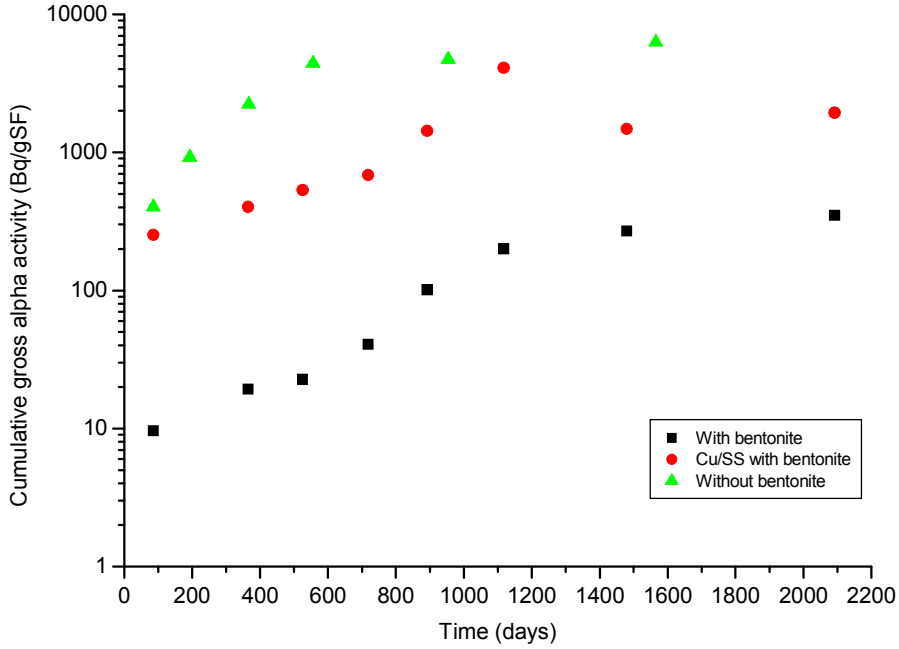

FIG. 7. Cumulative gross alpha activities released up to 2092 days

The concentration of uranium released from spent fuel specimens as a function of exposure time is illustrated in Fig. 8. As shown in this figure, the concentration with the increase of the time was rapidly increased up to around 1000days and then sluggishly increased. The concentration at 2092days was around $3x10^{-6}$ mol/l, which was at least one order higher than the solubility of the unirradiated UO_2 fuel under an anoxic condition in a synthetic granitic groundwater[16]. The dissolution rate derived from the measured values was about $2.7x10^{-6}$ mol/m^2-day. This was much higher than those obtained from unirradiated UO_2 fuels under anaerobic condition[16], while this was very close to the value derived from that dissolved from spent fuel into the saturated NaCl solution under an aerobic condition[17]. To confirm if the dissolution of uranium would be dependent on its solubility limit, the more longer term experiment should be required.

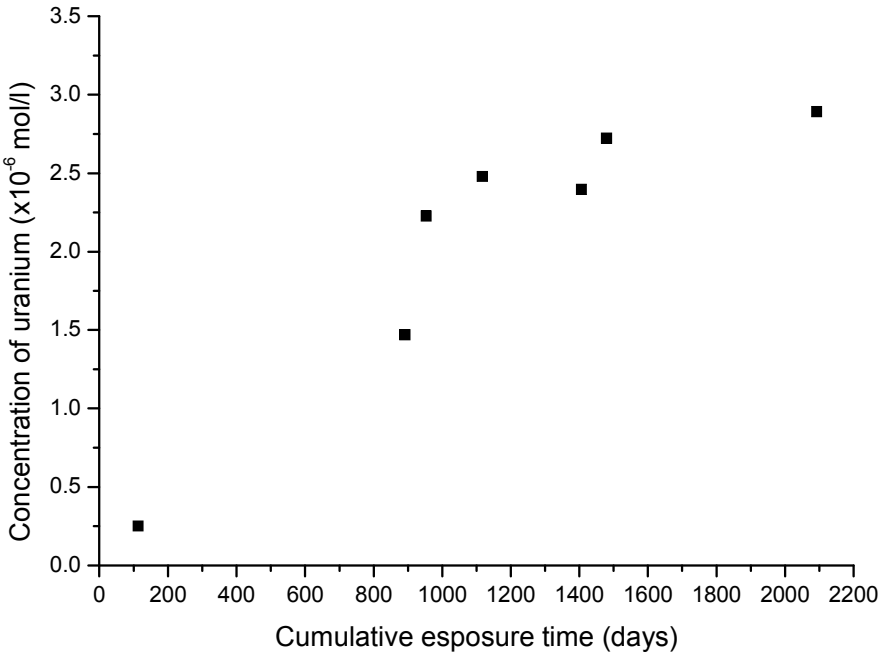

FIG. 8. Concentration of uranium in leachant as a function of exposure time

The activity distribution on the bentonite block related to the specimen No.1 is in analysis. So this result will be finalized up to the middle of May in 2004.

4. CONCLUSIONS

To identify the long-term leaching behavior of spent PWR fuel under a repository, the spent fuel exposed in their leachant up to around 5.7-years and these leachates were collected, and their gamma and gross alpha activities were analyzed.

The empirical formulas of the fractional release rates of cesium are derived from the current measured values as the followings :

In case of bare fuel : $Ro = 2.07 \times 10^{-5} \exp[-1.22 \times 10^{-3} * T]$ ……..(1) and

in case of fuel with bentonite : $Rb = 1.39 \times 10^{-8} \exp[-6.02 \times 10^{-5} * T]$ ……..(2)

The cumulative fraction of cesium released from the specimen from spent fuel without bentonite and the metal sheets up to 1566 days is about 9.73×10^{-3} fraction and the cumulative activity of alpha-emitters is about 6280Bq/g of spent fuel. The cumulative release fraction of cesium and the cumulative gross alpha activity through bentonite block are approximately 1/400 and 1/20 of those without bentonite block, respectively.

The long-term apparent diffusivity of cesium in the domestic Ca-bentonite compacted as its density of $1.4 Mg/m^3$, which is in a granitic groundwater, is about 2.28×10^{-13} m^2/sec.

The concentration of uranium released from spent PWR fuel in the synthetic granitic groundwater under an Ar-atmosphere was rapidly increased up to around 1000days and then sluggishly increased with the increase of the exposure time. To confirm if the dissolution of uranium would be dependent on its solubility limit, the more longer term experiment should be required.

REFERENCE

[1] C.H. Kang et al., “Geological disposal system development”, KAERI/RR-2336/2002 (2003).

[2] Forsyth, R.S. and Werme, L. O. "Spent Fuel Corrosion and Dissolution", J. Nucl. Mat. 190, p.3 (1992)

[3] J.A. Serrano et al., “Comparison of the leaching behavior of irradiated fuel, SIMFUEL, and Non-irradiated UO_2 under oxic conditions”, Radiochimica Acta, vol.82, p.33 (1998)

[4] K. Lelous et al., “Leaching of spent fuel and simulated fuel in the presence of environmental materials : Integral experiments”, Mat. Res. Soc. Symp. Proc., vol.506, p.191 (1998)

[5] D.J. Wronkiewicz et al., “Ten-year results from unsaturated drip tests with UO_2 at 90^{o}C : Implications for the corrosion of spent fuel”, J. Nucl. Mat., vol.238, p.78 (1996)

[6] R.S. Forsyth, L.O. Werne and J. Bruno, “Preliminary study of spent UO_2 fuel corrosion in the presence of bentonite”, J. Nucl. Mat., vol.160, p.218 (1988)

[7] J.C. Tait, S. Stroes-Gascoyne, R.J. Porth,, D. Wood and R.B. Heimann, “Leaching of used CANDU fuel in the presence of clay, titanium, and granite rock”, Mat. Res. Soc. Symp. Proc., vol.127, p.309 (1989)

[8] L.H. Johnson and J.C. Tait, " Release of segregated nuclides from spent fuel", SKB-TR-97-18 (1997)
[9] Y. Albinsson, R. Forsyth, G. Skarnemark, M. Skalberg, B. Torstenfelt and L. Werme, , (Mat. Res. Soc. Symp. Proc. 176, Boston, U.S.A., 1989) pp.559-565.
[10] H. Rameback, M. Skalberg, U.B. Eklund, L. Kjellberg and L. Werme, Radiochimica Acta 82, 167 (1998).
[11] Eichrom Technologies Inc., "Sample preparation using extraction chromatography", 8505 South Cass Avenue, Suite 111 Darien. IL60561 USA, 2001.
[12] W.J. Cho, J.W. Lee and C.H. Kang, "A compilation and evaluation of radionuclide diffusion and sorption properties in the buffer material for the HLW repository", KAERI/TR-2216/2002 (2002).
[13] S. Mukai and S. Kataoka, "Diffusion of some radionuclides in compacted Ca-bentonite under reducing condition", Raiochimica Acta 82, 179 (1998).
[14] B. Grambow, "Review of spent fuel related issues in SKB's SR97", SKI-R-00-47 (2002).
[15] S.S. Kim, K.S. Chun, C.H. Kang and H.S. Suh, leachung of the simulated borosilicate waste glasses and spent nuclear fuel under a repository conditions, KAERI/TR-2351/2002 (2002).
[16] K. Ollilia, Dissolution of unirradiated UO2 fuel in synthetic groundwater – Final report, POSIVA 99-24 (1999).
[17] E. Cera, M. Grive, J. Bruno and K. Ollila, Modelling of UO2 dissolution mechanisms in synthetic groundwater solutions – Dissolution experiments carried out under oxic conditions, POSIVA 2001-03 (2001).

STUDIES OF MINERAL-LIKE MATERIALS BELONGING TO PYROXENE AND GARNET GROUPS FOR HIGH LEVEL WASTE IMMOBILIZATION

P.P. POLUEKTOV

The Federal State Unitarian Enterprise A.A. Bochvar, Russian Scientific Research Institute of Inorganic Materials (VNIINM), Russia

Authors and Contributors: N.V. KRYLOVA, T.V. SMELOVA

Abstract

In this contribution to the CRP, we have investigated the structure of some physical and chemical properties of specimens able to be vitrified in cold crucible melters. They represent two mineral groups, pyroxenes and garnets. Pyroxene minerals are capable of isomorphous incorporation of Alkali, Alkaline-earths elements as well as Al^{+3} and Fe^{+3}. Pyroxene use is suggested for incorporation in HLW as well as fractions of calcium and strontium. In the work performed, a matrix composition that corresponds to natural occurring mineral was studied.

1. INTRODUCTION

HLW from reprocessing is converted into solid forms suitable for transportation, storage, and future disposal in the Russian Federation. All solidification approaches share a common trait, that of a reliable incorporation of radionuclides into solid synthesized matrices. A one-stage solidification process using a direct electric heating furnace to produce phosphate glass is used on an industrial scale at the PO "Mayak". There are good reasons to prefer glass as a matrix. Of fundamental importance is its ability to accommodate and immobilize a variety of radionuclides present in HLW, because of its amorphous structure, and give a product of good performance and reproducibility. The ability to incorporate different waste elements (more than 40 elements) into a durable, high integrity, glass product, and then suppress their mobility, results from the unique random network structure of glass.

An alternative to such a one-stage melter is a two-stage process in a cold crucible induction melter (CCIM), which has the following unique features:

- no direct contact between melter material and molten oxide due to a "skull" formed on the cold crucible walls;
- the possibility of synthesizing the compounds over a wide range of compositions with different melting temperatures;
- the small dimensions;
- the possibility of remote disassembly and replacement.

Each fraction of waste needs a matrix of stable natural minerals including necessary elements (or their analogs) which are stable under radiation. The minerals

ought to be reproducible. With CCIM, the temperature of synthesis should not exceed 2000-2100^{0}C.

A decisive factor in selecting a universal matrix is an ability to include cations of different sizes and charges. There are many minerals, silicates among them, having the necessary anion structure. In silicates, one atom of silicon forms with four atoms of oxygen a tightly adhered tetrahedron SiO_4^{4-}. Silicates as a function of the content of anion tetrahedrons can form crystalline structures in the form of islands, chains, bands, nets, and frameworks. These anion constructions bind together through cations supporting the electrical neutrality of the structure. The above mentioned silicates may include a wide set of cations, but framework structures usually show heterogeneity. The island and chain silicates are useful for homogeneous matrices. Garnet is typical of island silicate, pyroxene of chain silicate.

Garnet is a multicomponent solid solution $A_3^{2+}B_2^{3+}(SiO_4)_3$, where A = Ca, Sr, Mg, Fe^{2+}, Mn^{2+}, B = Al, Fe^{3+}, Cr^{3+}. The tetrahedrons SiO_4^{4-} bind though octahedrons BO_6. Garnet - andradite $Ca_3Fe_2^{3+}(SiO_4)_3$ has the largest size of a cubic elementary cell (12,05 A^o).

Pyroxenes have a general formula XYZ_2O_6, where X = Ca, Sr, Mn^{2+}, Fe^{2+}, Mg^{2+}, Na, Li, Cs, Y = Mn^{2+}, Fe^{2+}, Mg, Fe^{3+}, Al, Cr^{3+}, Ti^{4+} and Z is Si or Al included into anion tetrahedrons. A cation Al^{3+} may substitute for a cation Si^{4+} due to their nearly equal sizes, but only by simultaneous substitution in cations in the neighborhood.

The substitution of Al^{3+} in tetrahedrons produces aluminosilicates and aluminates; also, Ti^{4+}, B^{3+}, Fe^{3+}, Be^{2+}. Titanosilicates (and in limit titanates) are generated by substitutions of Ti^{4+}. They are similar to silicates in immobilizing radiocations but extend the technological and technical capabilities of the latter.

Minerals, namely, jadeite, eguirine, orthite, arfvedsonite, sphene, garnet, zirconolyte were chosen as matrices for the incorporation of high level waste (HLW) fractions. Materials, whose compositions are consistent with those minerals, were produced by the IMCC method as mineral-like materials.

This work discusses the results of the investigations into the structure and some physical and chemical properties of specimens that represent two mineral groups, i.e., pyroxenes and garnets.

Pyroxene minerals (pyroxene group) are capable of isomorphous incorporation of alkali, alkaline-earth elements as well as Al^{+3} and Fe^{+3}. Pyroxenes are suggested for the incorporation of HLW as well as fractions of calcium and strontium. In this work a matrix composition was studied that corresponds to that of the naturally occurring mineral-eguirine.

The garnet group minerals have a large number of mineral types of isomorphous series of andradite and almandine. Garnets may be used to incorporate fractions of REE and TUE. The studies matrix composition corresponds to that of the naturally occurring mineral-andradite. The compositions of the studies materials are summarized in Table I.

TABLE I. COMPOSITIONS OF STUDIED MATERIALS

Suggested material	**Content of oxide, % mass**									
	Na_2O	Fe_2O_3	SiO_2	CaO	BaO	Cs_2O	SrO	CeO_2	La_2O_3	ZrO_2
Eguirine	9.2-13.4	18.3-27.9	48-50	-	0-3.6	0-5.0	0-5.0	3.0	-	-
Andradite	-	10.3-36	29-42.5	8.5-29.5	-	0-5	0-5	4-8	0-15	3.8-6.9

In addition, eguirine based samples were specially prepared so that they contained elements of the platinum group and molybdenum: Na_2O – 13.4, Fe_2O_3 – 17.6, SiO_2 - 50, PdO – 2.7, Cr_2O_3 – 4.0, Rh_2O_3 – 0.6, NiO – 2.7, RuO_2 – 3.1, Nb_2O_3 – 0.7, MoO_3 – 6.5.

Mixed oxides of stable elements were used as simulators of HLW and their fractions. Prior to melting the charge was loaded with radioactive tracers Sr^{90}, Cs^{137}, Ce^{144} in amounts needed to implement the subsequent radiometric analysis.

The structures of the samples were examined using X-ray phase analysis, scanning electron and optical microscopy.

2. EXPERIMENTAL PART

The examinations of the structures of the samples having compositions of the tabulated eguirine, evidence that the materials are 100% glass both homogeneous and isotropic. This is also corroborated by x-ray diffractometry demonstrating the amorphous structure of the samples.

Specially prepared specimens are an exception; they contain 5% oxides of platinum group elements (Ru, Rh, Pd), 4%Cr_2O_3, 2.7%NiO and 6.5% MoO_3. According to the microscopic examinations the prepared specimens contain 60-80% glass and 20-40% crystalline phase.

The scanning electron microscopy clearly identifies three different crystals, in their compositions and forms: crystals of (Ni, Fe, Cr, Pd, Ru) oxides, ruthenium and palladium metals. However, the basis of the specimens is formed by glass; its composition is adequately uniform. Minor variations in the quantitative ratio between the additives do not alter the general structure pattern of the specimens.

The structure of the andradite type matrix is substantially dependent of its composition. The specimens containing oxides of mineral forming cations (% mass) in the ratio of Fe_2O_3:SiO_2:CaO ≈ 4:5:1 have non-uniform structures and contain phases of magnetite, crystoballite and wollastonite as well as a major portion of the glass phase.

A higher content of calcium oxide and the unavailability of mono- and bivalent nuclides make feasible to produce fully crystalline microporous ceramics in IMCC. The ratio between the major mineral-forming oxides in the ceramics is ~ 1:1:1. According to the data of the X-ray phase analysis and electron microscope examinations the specimen

consists of compositions having the structures of garnet, apatite-britholite (below britholite), wollastanite and magnetite in the ratio ~ 70:15:10:5.

The incorporation of 18 - 27% HLW simulators into the matrix, basically at the expense of a lower content of iron oxide, results in a vitreous crystalline material; its crystalline constituent comprises three main mineral phases, namely, garnet (andradite), britholite (calcium silicate and REE of the apatite structure) and wollastonite as well as the vitreous phase. The magnetite phase is observed in individual specimens.

The components of some major phases of andradite are listed in Table II.

TABLE II. COMPONENTS OF MAJOR PHASES OF ANDRADITE

Oxides, % mass	**Garnet**		**Britholite**		**Wollastonite**		**Vitreous phase**	
	1	**2**	**1**	**2**	**1**	**2**	**1**	**2**
SiO_2	24.10	24.00	21.66	21.76	49.62	49.69	37.26	38.31
CaO	25.91	25.02	14.24	14.45	48.55	48.16	13.85	13.66
FeO	-	-	0.58	0.90	1.83	2.15	-	-
Fe_2O_3	32.42	31.44	-	-	-	-	25.88	24.67
ZrO_2	9.93	10.01	5.06	4.41	-	-	6.42	6.06
La_2O_3	0.50	0.50	10.91	10.15	-	-	5.00	5.63
Ce_2O_3	1.19	1.73	16.78	17.63	-	-	5.01	5.51
Nd_2O_3	4.85	4.46	24.11	23.73	-	-	4.83	5.68
EuO	1.09	2.84	6.67	6.96	-	-	1.78	0.47
∑TR	7.63	9.53	58.47	48.47			16.62	17.29

It is evident from table 2 that the main components of garnet comprise oxides of calcium, iron and silicon. Zirconium and REE are encountered to a lesser extent. Garnet is observed as isometric grains and skeleton type crystals (fig.1 (a,b)). The inter-plane distances of the main reflections in the diffraction patterns (2.71; 1.6; 2.48 and 3.04A) are consistent with those of natural andradite.

Britholite forms grains having sections of elongated-prismatic or hexagonal shapes (fig. 1). Their specific feature is the availability of garnet, magnetite and wollastonote inclusions. The diffraction patterns are consistent with the main reflexes inherent in naturally occurring britholite mineral that has a typical apatite type of the lattice. The britholite composition mainly comprises REE, silicon and calcium oxides as well as minor quantities of Zr and Fe.

Wollastonite is available as prismatic or orthorhombic crystals (fig. 1c) in the center of which garnet and magnetite inclusions are observed. Glass fills in the interspaces between the crystalline phases in the crystallized and glass enriched phases.

The composition of the glass is dominated with oxides of silicon, calcium and iron, while REE and Zr are present in much less amounts (Table III).

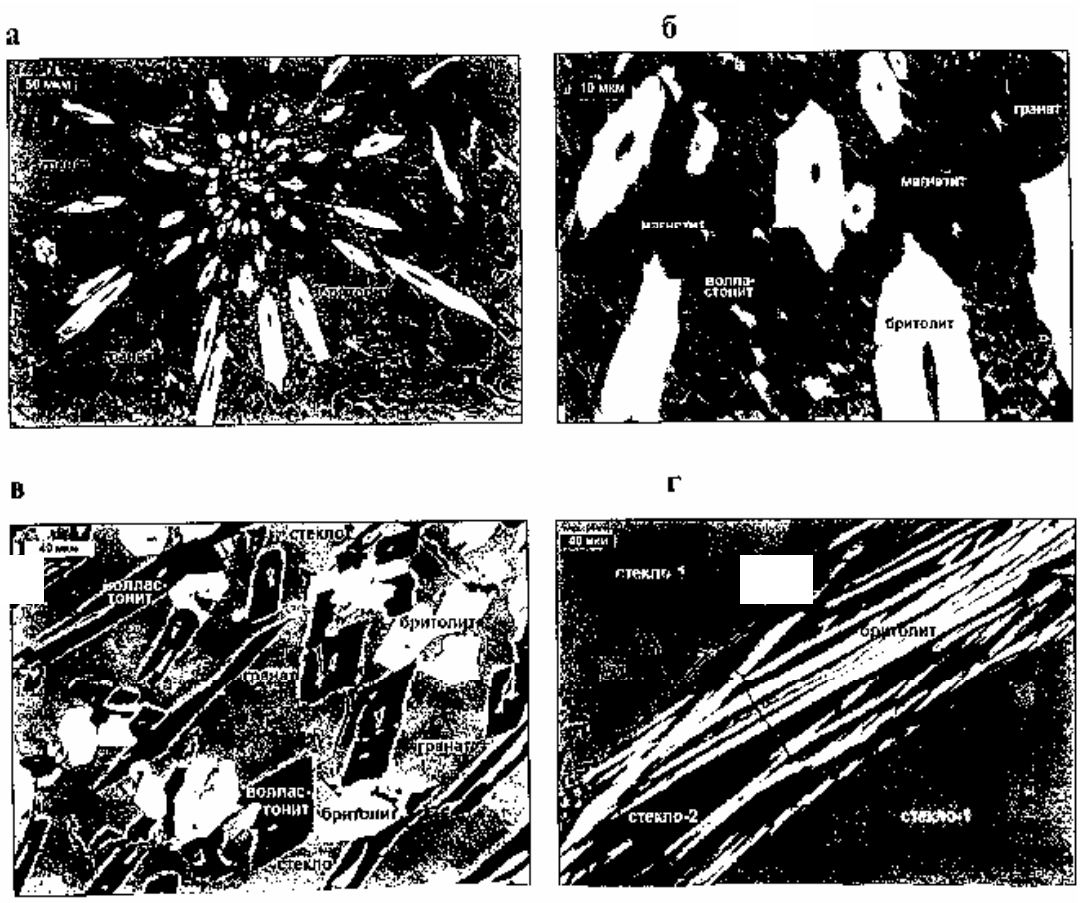

FIG. 1. Scanning electron microscope patterns of specimens:

a, b – general view and detailed structure of specimen N 1; c, d – structure of crystalline and vitreous portions of specimen N 2

TABLE III. COMPOSITIONS OF BRITHOLITE AND GLASS IN VITREOUS

Oxides	**Basic light-grey glass**			**Dark-grey glass near britholite crystals**				**Britholite**
	1	**2**	**mean.**	**1**	**2**	**3**	**mean.**	
SiO_2	32.84	32.48	32.66	35.57	37.42	35.85	36.28	23.98
CaO	22.58	32.65	27.62	32.52	28.22	27.02	29.25	17.56
FeO	-	-	-	-	-	-	-	2.66
Fe_2O_3	19.77	17.51	18.64	21.11	24.46	23.35	22.97	-
ZrO_2	5.37	5.77	5.57	5.73	5.67	5.61	5.67	5.02
La_2O_3	3.06	4.35	3.71	1.23	0.70	2.26	1.40	8.57
Ce_2O_3	4.73	5.39	5.06	1.56	1.18	1.86	1.53	14.08
Nd_2O_3	8.88	8.46	8.67	1.88	1.72	3.63	2.41	21.54
EuO	2.77	2.40	2.59	0.40	0.63	0.37	0.47	6.59
$\sum TR_2O_3$	19.44	20.60	20.03	5.16	4.23	8.16	5.81	50.78

The given results point the fact that garnet and britholite contain the dominant part of HLW simulators in the specimens. Here, lanthanides are basically concentrated in britholite (58-63%) while in garnet $\sum REE_2O_3$ amount to 9-14% mass. On the contrary, the zirconium content of garnet is almost twice higher than that of britholite. The content of zirconium in britholite is lower than in glass (tables 2, 3). The fact that REE are concentrated in britholite brings about a decrease of their contents in glass at sites contacting crystals (table 3). Iron does not essentially enter into the britholite composition; as a consequence, glass is enriched in FeO where it contacts britholite. The same pattern is also characteristic of calcium and silicon the content of which in the specimen is higher than it is required for britholite to form. This results in the growth of their concentrations nearby the britholite. The other crystalline phases, i.e., wollastonite and magnetite, are depleted in REE and Zr.

Actinides are known to be available in glasses as three - (Am, Cu) and four-valent (Np, Pu) cations [1]. In terms of their sizes the former ones are close to lanthanides, particularly, to neodymium and gadolinium, as well as to calcium. The radii of four-valent actinides are less than those of three-valent ones and comparable to ytterbium and lutecium, four-valent cerium and, to a lesser extent, to zirconium [2]. One can expect that the behaviour of americium and curium will be similar to the distribution of calcium, lanthanum and neodymium, while the behaviour of uranium, neptunium and plutonium will be like the one of cerium, zirconium and gadolinium. Previously britholite containing 6% mass Cm^{244} was synthesized [3]. The concentration of uranium and thorium, in naturally occurring britholites, amounts to 20%. Proceeding from this fact and taking into account the comparable behaviour of actinides and lanthanides one can assume that the maximum actinide content of artificial britholite will be not less than 10% by mass.

The results of studying the chemical stability of the synthesized matrices are summarized in Tables IV and V.

TABLE IV. CHEMICAL STABILITY OF EGUIRINE COMPOSITION (LEACHING RATE, G/CM^2 DAY X 10^{-6})

	1 day			3 day			7 day			14 day			21 day		
	Na	**Cs**	**Sr**	**Na**	**Cs**	**Sr**	**Na**	**Cs**	**Sr**	**Na**	**Cs**	**Sr**	**Na**	**Cs**	**Sr**
Initial	2.7-7.6	*	1.2-10	4.8-5.2		0.9-1.11	0.01-4.8	0.6-0.9	0.2-0.9	0.1-0.9	0.06-0.22	0.2-0.6	0.02-0.9	0.01-0.8	0.03-0.06
Annealed	3400-11000	8.4-80		22-2000	2.6-22	3.5-6.2	338-562	0.62-9.8	-	438	6.8	7.7-139	1.7-90	0.30	11.5-58
Irradiated 10^8 rad	-	-	-	7.6-14.2	-	1.6-2.54	0.02-4.8	-	0.54-1.0	0.1-1.7	-	0.4-0.9	0.1-0.3	-	-
Irradiated 10^9 rad	20-184	5.7-6	3.8-5.3	0.013-8.3	0.13-2.5	0.08-0.09	0.012-2.8	0.018-0.022	0.043-0.45	0.07-0.44	0.01-0.013	0.025-0.12	0.007-0.54	0.01-0.013	0.1-0.5
Irradiated 10^{10} rad	84-562	6.7-11	92	2.4-29	-	-	0.01-7.04	-	-	0.01-2.9	*	*	0.01-0.54	*	*

*) - < 10^{-7} g/cm^2 day;
-) - non determined

TABLE V. CHEMICAL STABILITY OF GARNET COMPOSITION (LEACHING RATE, G/CM^2 DAY X 10^{-6})

Treatment	1 day			3 day			7 day			14 day		
	Ca	**Ce**	**Eu,Gd, Nd,La**	**Ca**	**Ce**	**Eu,Gd, Nd,La**	**Ca**	**Ce**	**Eu,Gd, Nd,La**	**Ca**	**Ce**	**Eu,Gd, Nd,La**
Initial	9.66	*	****	5.5	*	****	4.3	*	****	1.5	*	****
Annealed at 650°C 200 h	8.55	*	****	2.9	*	****	1.42	*	****	1.3	*	****
400 h	47.5	*	****		*	****	5	*	****	1.2	*	****
Irradiated 10^8 rad	-	*	****	77.3	*	****	6.3	*	****	2.53	*	****
10^9	54	*	****	10.7	*	****	3.35	*	****	1.93	*	****
10^{10}	136	*	****	5.42	*	****	1.14	*	****	1.46	*	****

*) - < 10^{-7} g/cm^2 day;
-) - non determined

The initial specimens of the studing materials feature a high chemical stability. The rate of leaching of cerium and gadolinium from the minerals assumed to incorporate transuranium element fractions is below the limit of detection, i.e., $<1x10^{-7}$ g/cm^2 day. The rate of calcium and strontium leaching from the materials produced is at the level of that from chemically stable glasses and meets the requirements of ГОСТ 50926-96 placed on solidified HLW.

The irradiation resistance of the matrices was found from the changes in their chemical stability after γ-irradiation to 10^8, 10^9 and 10^{10} rad, respectively. The determined leaching rates are tabulated (tables 4 and 5). The rate of leaching from a pyroxene composed material gradually increases with the radiation dose during the first day of the irradiated material contact with water. The leaching rate of the material irradiated to 10^{10} rad exceeds that of the initial material by approximately 1.5 orders. This is typical of alkali and alkaline earth materials. It is to be noted that upon further contact with water the nuclide release rates from the material decreases drastically and after three and more days it is lower than in the initial specimen.

A similar pattern is also demonstrated by the andradite composition as for as the leaching of calcium that is one of mineral formers with the least resistantance to water. The release of REE does not vary with the radiation dose and as before it is below the detection limit. This kinetics of leaching alkali and alkaline earth nuclides from vitreous materials fully conforms to the effect of the irradiation-chemical destruction detected and comprehensively studied previously in phosphate and borosilicate glasses under irradiation [4, 5]. This effect was shown to result from γ - radiation surface reactions proceeding between radicals and ions of air components and alkali and alkaline earth ions within the compositions of solidified matrices. The soluble compounds easily enter the water in the first minutes of its contact with the specimen, as a result of which during the subsequent contact with water the release of nuclides from a layer depleted in them is decelerated and determined by their diffusion from inner layers of the matrix. This same effect was also noticed under β- and α- radiation.

The above radiation induced damages are only found at the glass surface and do not show up in the bulk which inhibits the formation of a layer by limiting the specimen contact with air.

The thermal resistance of the studied materials was determined from their chemical stability after ~ 200 h at 650^{o}C. It is found (Table IV) that the chemical stability of pyroxene compositions drastically degrades as a result of anneal. The sodium leaching rate increases by two or three orders, the leaching of calcium and strontium also accelerates. In this case the structure of a specimen is also altered.

The section of the specimen have a homogeneous vitreous appearance, however, the electron-microscopic examination identifies a crystalline phase – synthetic eguirine, - in the quantity of < 10% the formation of which is a consequence of the partial crystallization of glass (Fig. 2).

There is a difference between the glass compositions in the central part (Table VI, analysis 1) and at the contact with the crust (table 6, analysis 2,3).

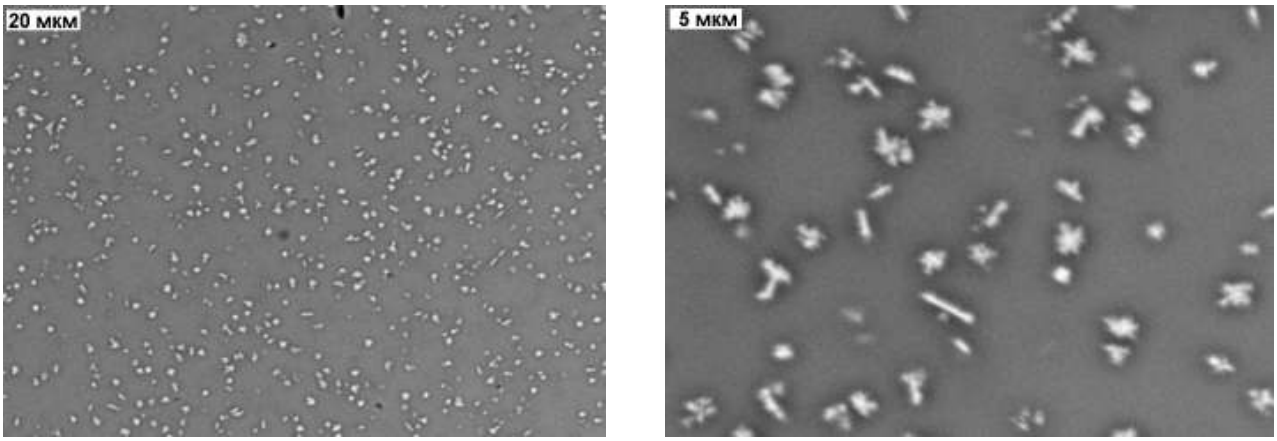

FIG. 2. Reflected electron-microscopic patterns of eguirine vitreous ceramics structure, the central part. White – eguirine, grey – glass.

TABLE VI. PHASE COMPOSITIONS (% MASS) OF EGUIRINE CONSTITUENTS AFTER ANNEAL AT 650^0C FOR 240 H.

Oxides	**Central parts**					**Crust**			
	Glass			**Eguirine**		**Fe-pollucite**	**Pyroxene**	**X-phase**	
	1	**2**	**3**	**1**	**2**			**1**	**2**
Na_2O	8.55	8.29	6.31	6.69	6.62	2.38	10.51	21.99	24.14
Al_2O_3	1.39	1.15	1.24	0.81	0.88	0.81	1.91	1.17	1.18
SiO_2	49.28	49.56	47.38	38.66	34.86	35.93	42.90	44.72	45.38
Fe_2O_3	26.18	23.77	22.96	42.77	48.96	22.04	25.76	25.05	25.64
SrO	2.72	3.66	4.39	3.61	2.60	1.18	5.73	0.79	1.25
Cs_2O	6.08	7.35	12.51	4.75	3.58	35.16	1.14	5.71	1.99
BaO	4.78	5.01	3.87	2.70	2.50	2.50	10.97	0.57	0.42
PbO	1.01	1.22	1.34	-	-	-	1.07	-	-

TABLE VII. COMPOSITION OF WHITE POWDER ON CRUST (THE ANALYSES ARE NORMALIZED TO THE SUM OF 100%)

NN	Na_2O	Al_2O_3	SiO_2	Fe_2O_3	SrO	Cs_2O	BaO	PbO
1	39.57	4.78	23.80	28.69	2.44	0.71	-	-
2	28.10	4.01	14.85	22.48	15.45	-	13.55	1.56
3	13.77	3.19	11.38	4.99	23.95	0.90	26.95	14.87
4	40.30	2.71	51.66	1.61	2.31	-	1.41	-
5	60.00	2.00	36.13	-	-	-	1.88	1.88
6	28.70	-	-	-	-	-	-	71.30

On the reflected electron patterns “the crust” consists of three phases, namely, Fe-pollucite, pyroxene and an unidentified x-phase (Fig. 3, Table VI). Fe-pollucite (the white colour on the patterns) tends to the inner part of “the crust”. It is a synthetic analog of naturally occurring pollucite in which Al^{+3} is substituted by Fe^{+3} and has the formula – $(Cs,Na)Fe[Si_2O_6]$.

Pyroxene develops at the outer surface of the crust and has the formula $(Na,Sr,Ba)_{1,0}Fe_{1,0}(Si,Al)_{2,0}O_{6,0}$.

The x-phase base is formed by oxides of sodium, iron and silicon amounting to ~ 95% mass. The results of the x-phase analysis (Table VI) differ between themselves in the content of calcium which is likely to be explained by the influence of pollucite microinclusions.

The electron microscope was also used to study the white coat of the surface. The results of the analysis are of approximate assessment nature. The composition of the substance was determined in areas that differ in their colour from white to gray.

The semi-quantitative analysis established the abnormally high concentrations of SiO_2, Na_2O, SrO, PbO, BaO in the white powder (Table VII). The most abundant phase is aqueous sodium carbonate ($Na_2CO_3 \cdot H_2O$); oxide of lead is also determined reliably. Aside from these, other phases are available as can be aqueous phases of strontium and barium of the type $Sr_3Si_2O_7 \cdot 4H_2O$ and $BaSiO_3 \cdot 7H_2O$ (Table VII).

The coat is likely to be formed by two routes, diffusion of alkaline nuclides at the surface upon heat treatment and their interaction with atmospheric air both during heat treatment and during the subsequent storage at room temperature (processes of oxidation, carbonization and hydratation).

It is appears that dissolution rate of this layer is higher for releases of alkali and alkaline earth nuclides to water as it was mentioned above.

In pyroxene specimens composed of platinum subgroup elements and molybdenum the crystalline phase amounts to ~ 20-40%. The composition of this phase does not differ from that of the initial material.

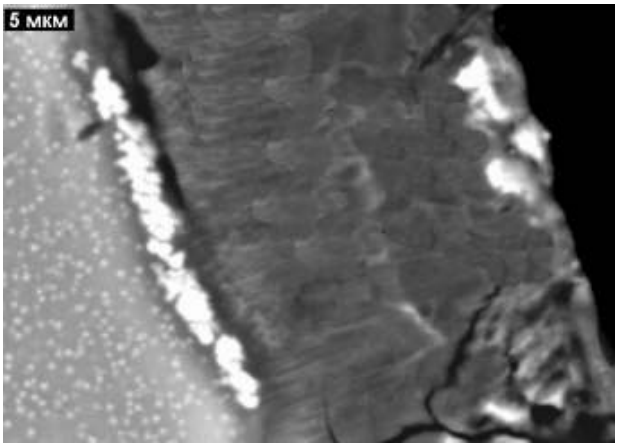

FIG. 3 Reflected electron-microscope patterns of "the crust" structure.

The white coat available at the surface of annealed specimens shows high concentrations of sodium and molybdenum. Similar to the above mentioned specimens the most abundant phase is aqueous sodium carbonate. Molybdenum is present in two phases, namely, MoO_3 and $NaMoO_5$ that is readily soluble in water.

The chemical stability of andradite type specimens defined by calcium releases to water varies insignificantly (a factor of 2 – 4); the rare earth element leaching rate remains below the detection limit.

The studies into the structures of annealed materials evidence that the crystalline part of the specimen, heat treated at 650^{o}C for 224 h, was not subject to any substantial change (Fig. 4a). The base of the crystalline phase is formed by garnet (andradite) having the composition similar to that of garnet of unannealed specimens with the same contents of zirconium and rare-earth elements. Britholite is also present and contains up to 58% REE and interstitial glass (Table VIII).

TABLE VIII. COMPOSITIONS (% MASS) AND FORMULAR OF PHASES FROM VARIOUS PARTS OF SPECIMEN T77

Oxides	**Recrystallized part**			**Vitreous part**				
	garnet	**Britho-lite**	**Interstitial glass**	**Glass**			**Britho-lite-1**	**Britho-lite-2**
				dark	grey	light		
SiO_2	29.01	22.14	44.18	36.39	35.93	33.38	22.85	25.90
CaO	26.40	14.76	23.05	28.03	26.75	23.77	15.03	16.23
Fe_2O_3	27.96	-	14.86	24.27	22.77	17.90	-	-
FeO	-	1.14	-	-	-	-	0.75	2.85
ZrO_2	7.06	3.25	3.80	5.85	6.30	5.50	3.87	4.35
La_2O_3	1.73	9.41	3.95	1.59	1.88	3.76	10.29	9.26
Ce_2O_3	2.33	17.40	3.68	1.76	2.49	5.64	16.84	15.31
Nd_2O_3	3.66	24.72	5.02	1.91	2.60	7.66	23.41	20.84
EuO	1.86	7.18	1.46	0.20	1.28	2.39	6.97	5.26
$\sum TR_2O_3$	9.58	58.71	14.11	5.46	8.25	19.45	57.51	50.67

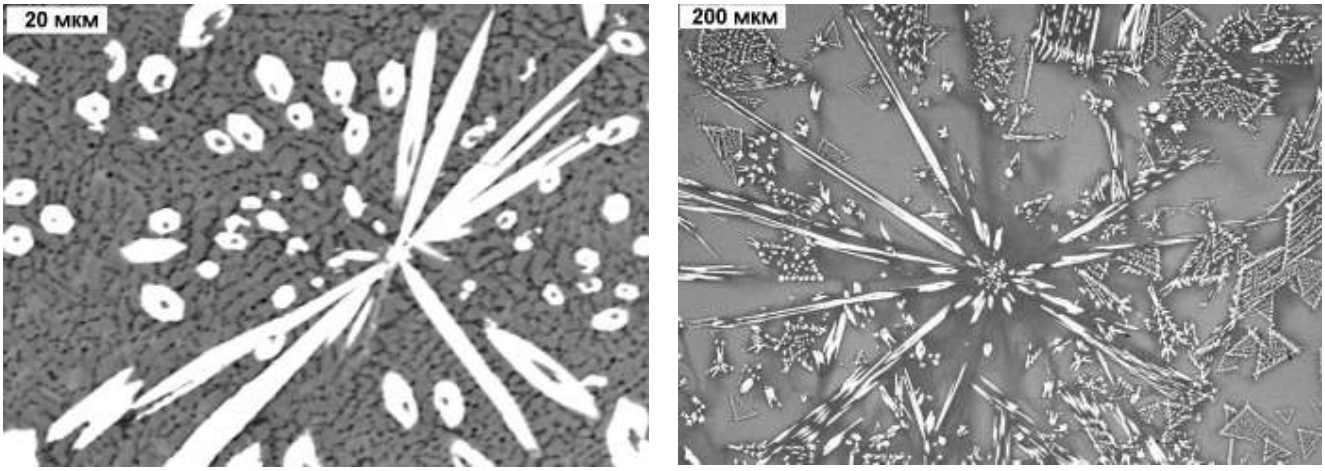

a – crystallized b – vitreous part

FIG. 4.

The vitreous part of the specimens substantially differs from that of the unannealed ones. The difference involves partial devitrification of the basic glass to for britholite (Fig. 4b). Britholite constitutes ~ 30% mass. It has two morphologic versions, namely, asterisk agglomerations of elongated – prism shaped crystals (britholite-1) and skeleton crystals (britholite-2). Both britholites have quite close compositions (Table VIII).

It is to be noted that the colour of the glass is highly inhomogeneous. All transitions from light – to – dark grey colour can be observed. It is characteristic that the so-called crystallization "paints", i.e., dark coloured glass areas much depleted in rare earths, appear near britholite crystals (table 3). No other phases were detected in crystallized glass.

An increase of the time of the heat treatment (up to 400 h) of the vitreous part of the andradite material results in a further decrystallization of glass to form britholite and in the appearance of a novel phase, namely, garnet crystals, in areas highly enriched in britholite (Fig. 5b). The composition of this garnet is very close to that of the dark-grey glass near the britholite crystals (Table 9). The formation of garnet crystals seems to proceed as a result of the crystallization of the dark residual glass that appeared after the formation of britholite upon longer – term heat treatment.

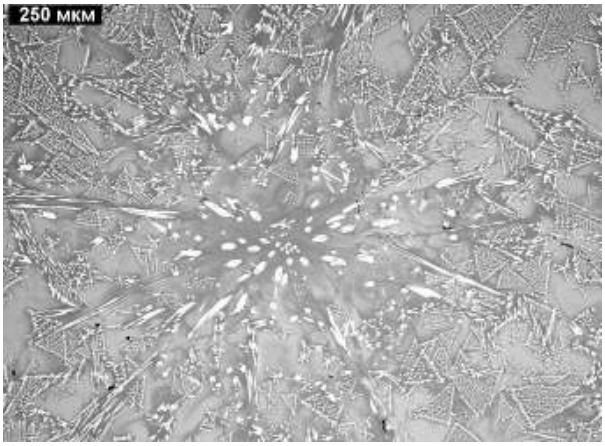

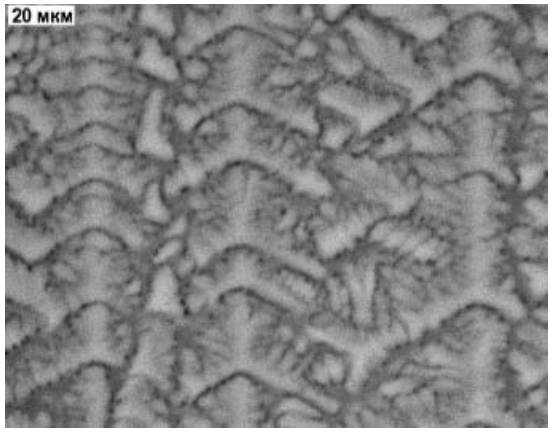

a - britholite – white and all tints of grey glass

b - garnet – grey, dark grey glass

FIG. 5 Reflected electron microscope pattern of a part of andradite specimen heat treated at 650^0C and 400^0C

TABLE IX. COMPOSITIONS AND FORMULAR OF GARNET, BRITHOLITE AND GLASS COMPOSITION IN VITREOUS PART OF SPECIMEN

Oxides	Glass					Britholite-1		Britholite-2		Garnet	
	Light grey	Light grey	grey	grey	Dark grey	1	2	1	2	point	scan
SiO_2	33.96	34.40	34.04	34.69	37.21	23.37	24.39	23.96	25.44	36.12	36.56
CaO	22.43	22.79	23.06	22.85	25.64	14.06	15.52	15.81	17.33	24.31	25.44
Fe_2O_3	19.69	19.83	19.63	21.07	24.08	-	-	-	-	22.11	23.50
FeO	-	-	-	-	-	1.45	2.26	2.11	3.05	-	-
ZrO_2	5.93	6.21	6.48	5.69	6.08	5.30	4.87	4.75	5.96	5.83	6.97
La_2O_3	4.10	3.60	3.87	2.85	1.89	10.30	9.27	9.53	10.26	2.08	1.72
Ce_2O_3	5.01	4.52	5.41	3.93	1.94	16.33	15.26	14.86	14.68	2.79	2.41
Nd_2O_3	7.99	7.74	7.11	6.76	3.20	23.30	22.52	22.34	19.80	3.30	3.38
EuO	2.57	3.02	2.33	2.02	0.75	6.48	6.27	7.42	6.09	1.29	1.03
$\sum TR_2O_3$	19.65	18.88	18.72	15.56	7.78	56.41	53.32	54.15	50.83	9.46	8.54
Sum	101.68	102.11	101.93	99.86	100.79	100.59	100.36	100.78	102.61	97.83	101.01

3. CONCLUSION

— The structure and physico-chemical properties of mineral-like compositions consistent with naturally occurring minerals of the pyroxene and andradite classes were studied, and specimens were prepared at IMCC.

— Pyroxene type material is vitreous. The andradite composition is glass ceramics the crystalline constituent of which consists of three basic phases, namely, garnet (andradite), britholite and wollastonite; the former two containing, respectively, zirconium and basic components of the TUE fraction. Britholite is a mineral from apatite class; it has a very durable structure. Content of britholite in matrix is not less than 60%.

— The materials after preparation were shown to have a high chemical stability. However, the thermal stability of eguirine (pyroxene) materials is not high. After 200 h at 650°C a readily soluble layer is created at the surface of specimens. The layer has abnormally high contents of Na_2O, SiO_2, SrO, Pb, BaO and MoO_3 (if the latter is available in the specimens). The high temperature apparently promotes the devitrification of specimens with the crystalline phase (eguirine) being precipitated. The damage of the glass structure results in releases of non-bound components that readily migrate to the surface and react with the atmosphere. It is believed that the adjustments of the specimen compositions, reduction of the alkali metal quantity (substitution of

eguirine by, e. g., jadeite) will make it feasible to produce materials of this class having higher thermal stability and irradiation resistance.

— Heat treatment of andradite also results in the crystallization of its vitreous phase to form (upon 400 h anneal) the britholite phase which like the previously produced one incorporates up to 60% mass RE fraction. This ability of britholite seems to be very interesting since it allows the immobilization of a wide range of isotopes in the garnet – britholite matrix.

REFERENCES

[1] Haire Rg., Assefa Z., Stump N Sci.Basis for Nuclear Waste Management XXI, edited by J.McKinleg and C.Mc.Combie (Mater.Res.Soc.Proc.506, Pittsburgh, PA, 1998), pp.153-160.

[2] Shanon RD, Acta Cryst.Pt.A. 1976 Vol32 pp.751-767.

[3] Wald JW., Weber WJ.Clinard F.W. Progress in Nuclear Energy, 1995. Vol29, N 2, pp. 63-127.

[4] F.S. Dukhovich, V.V. Kulichenko. Atomnaya Energiya, 1965, v. 18, p. 361.

[5] V.V. Kulichenko, N.V. Krylova, N.D. Musatov et al. Investigations in the field of solidifying liquid, solid and gaseous waste and decontamination of contaminated surfaces. Collect., M., Atomizdat, 1965, p. 361.

IMMOBILIZATION OF HIGH-LEVEL LIQUID WASTES: GENERAL APPROACHES AND METHODOLOGY OF CHOOSING MATRIX MATERIALS AND TECHNOLOGICAL PROCEDURES OF THEIR PRODUCTION

P. P. POLUEKTOV, YU. I. MATYUNIN

The Federal State Unitarian Enterprise
A.A. Bochvar All-Russin Scientific Research Institute of Inorganic Materials (VNIINM), Russia

Abstract

This work discusses experience with a one-stage solidification process using a direct-heating electric furnace to produce phosphate glass on an industrial-scale. The development of a new technology for immobilising liquid radioactive wastes into vitreous and mineral-like compositions employing a two-stage process described as a “Cold Crucible Induction Melter” is presented as a promising direction in the field of radioactive waste management. This is a compact process which avoids direct contact between melter-material and molten oxide and permits synthesis of compounds with a wide range of compositions involving different melting temperatures.

1. INTRODUCTION

The main aim of the management of liquid radioactive wastes is their solidification with the production of compositions that should provide the safe transportation conditions, ecologically safe long-term storage, and final disposal in geological formations. Liquid radioactive wastes can be immobilized using different technologies. However, all of them are based on the concept of a strong radionuclide fixation in a synthetic solid matrix.

Beginning in 1987, high-level liquid wastes (HLLWs), which were accumulated at the PA "Mayak" and formed upon reprocessing of spent nuclear fuel at the operating RT-1 plant, have been processed with the formation of aluminophosphate glass on an industrial scale according to the one-stage technology with the use of a direct Joule-heated melter (EP-500) [1-5] (Fig. 1).

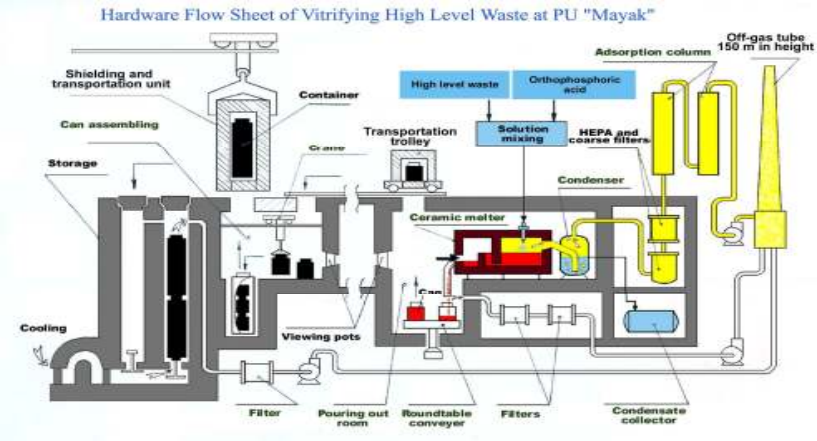

FIG. 1. Hardware flow sheet of vitrifying high-level waste at PA "Mayak"

At present, an EP-500/3 melter has been in industrial operation at the PA "Mayak". More than 17,000m^3 of liquid radioactive wastes with a total activity of more than 400 millions Ci were transformed into the phosphate glass form at the vitrification shop with more than 3000 tons of glass produced and stored in a dedicated storage facility (Fig 2).

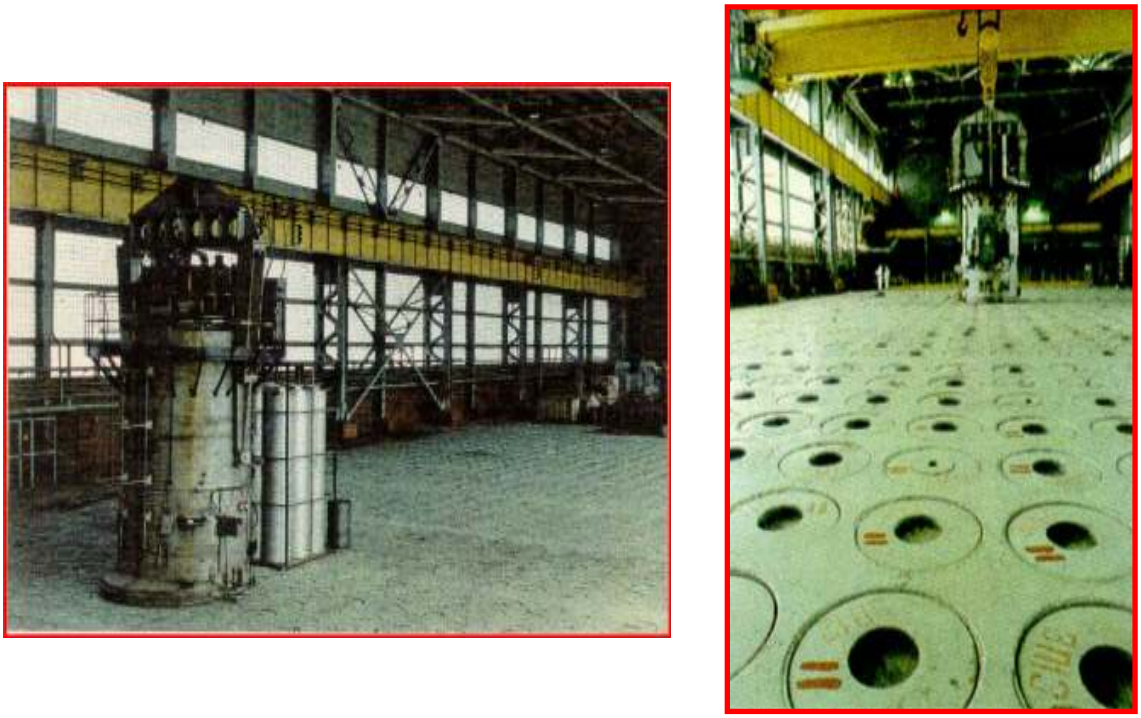

FIG. 2. Storage facility at the PA "Mayak"

An electric melter of the EP-500 type operates continuously, and the composition of HLLWs fed for vitrification is maintained virtually constant and has serious limitations on certain waste components. However, the range of radioactive wastes accumulated and formed at the PA "Mayak" is considerably wider. Moreover, radioactive wastes of unusual

compositions can be formed upon "dry" reprocessing of the fuel of innovative reactors and most of them cannot be reprocessed in electric melters of the EP type.

In order to provide the reprocessing of radioactive wastes of different compositions, equipment and technologies of their immobilization are under development, including

— different variants and modifications of the industrially used direct Joule- heated ceramic melters,
— "cold" crucible induction melters (CCIM),
— microwave melters,
— self-propagating high-temperature synthesis,
— hot pressing,
— hot isostatic pressing,
— cold pressing (sintering),
— superstoichiometric sorption.

At industrial enterprises and research institutes of Minatom RF and the Russian Academy of Sciences, works on matrix compositions are extensively performed in the following directions:

— investigation of the properties of currently used aluminophosphate and promising borophosphate and other glasses for the HLLW immobilization,
— the design of new vitreous and mineral-like matrices for different HLLW fractions and their synthesis with the use of different methods,
— the justification of the criteria for the choice of matrix compositions depending on their properties and the amount and types of radionuclides in radioactive wastes.

Analysis of the works carried out in the field of radioactive-waste management - the transformation of radioactive wastes into a more safe solid form suitable for the subsequent disposal - demonstrates that about ten methods and technologies for fabricating solidified products are under development at different levels. With regard to matrix compositions for the immobilization of radioactive wastes, more than a hundred of materials of different classes and compositions with model and real radioactive wastes have been synthesized and studied in the recent decade.

At present, the EP-500 ceramic melter (the PA "Mayak" (Fig 3) [1-4]) and the "cold" crucible induction melter (lab-scale facilities at the PA "Mayak" and the VNIINM (Fig. 4) [6-11] and a pilot facility at the “Radon” for the vitrification of low-level and medium-level wastes [12-15]) are the best developed technological approaches to the reprocessing of radioactive wastes with the production of solid forms).

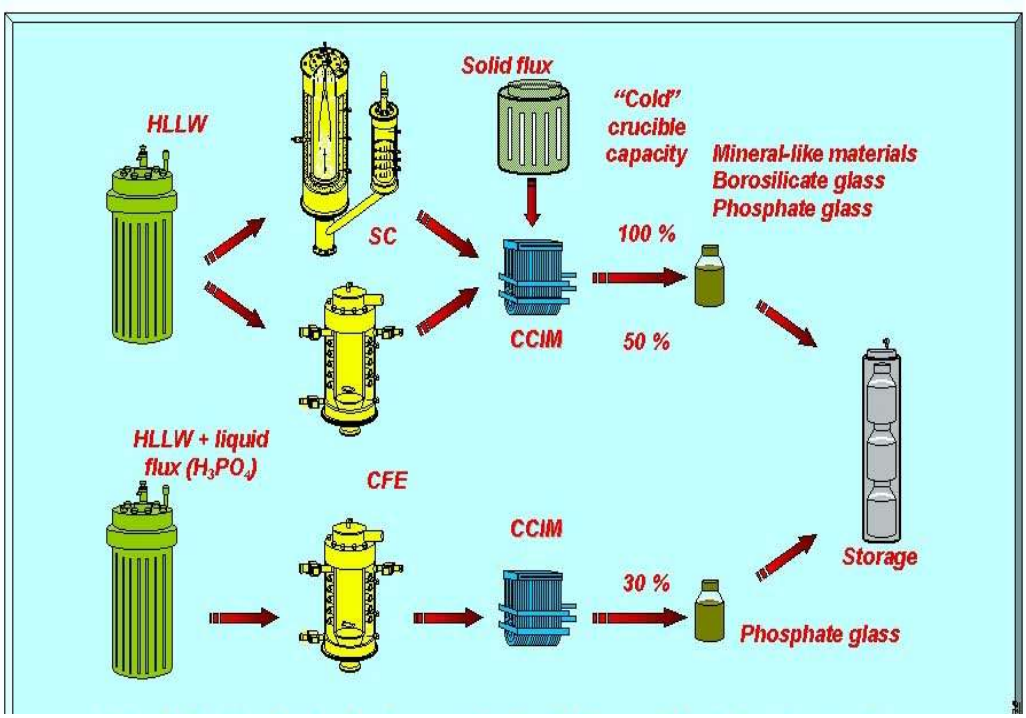

FIG. 3. Technological schemes for "cold" crucible induction melter.

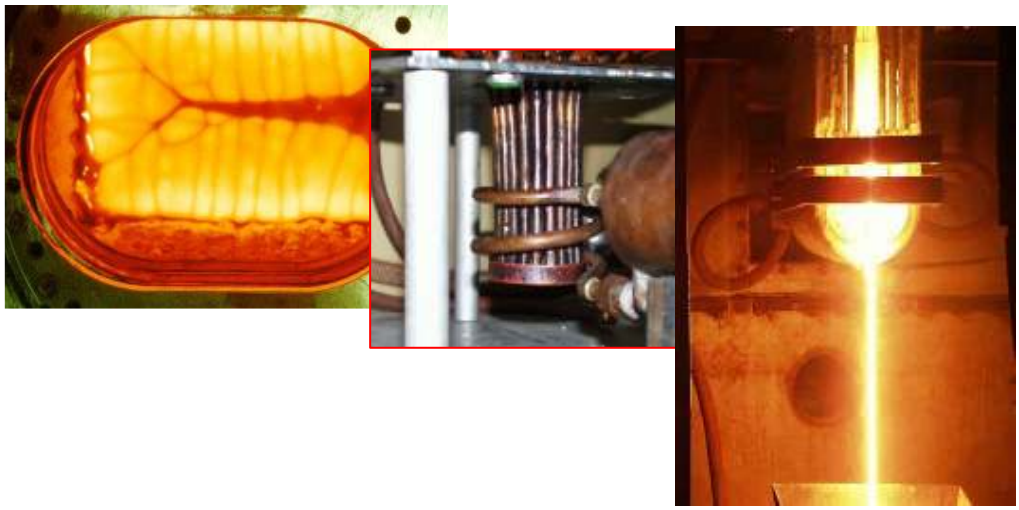

FIG. 4. Laboratory scale "cold" crucible induction melter

Facilities using microwave heating have been approved at the pilot level at the MCC [16-19]. However, these facilities are characterized by a low production rate and a number of

disadvantages that do not make it possible to treat them at present as a technology alternative to the operating EP melter and the CCIM for the immobilization of radioactive wastes with a wide range of compositions.

Other aforementioned methods for immobilizing radioactive wastes, for the most part, are at laboratory development stages and, in prospect, can be used for immobilizing insignificants amounts of specific (including fractionated) wastes or preparing materials suitable for transmutation of long-lived radionuclides whose disposal is not forseen.

The systematization and analysis of the results obtained in synthesis and investigation of products of radioactive-waste solidification and the determination of promising directions in this field of radioactive-waste management is the topical problem associated with providing a justified choice of optimum technologies and matrix compositions for different purposes.

In order to perform the justified choice of matrix compositions for the immobilization of radioactive wastes (whose range is currently wide), it is necessary to carry out the correct comparative analysis of the results of the performed investigations of these materials. This requires a database that would involve the description of the methods for producing any particular composition (with the level of their technological development), the techniques for investigating the properties of these materials, and specific analytical data.

The main characteristics of solidified radioactive wastes are as follows:

— the hydrolytic durability, which is characterized by the leaching rate of nuclides in the course of contact between solidified radioactive wastes and distilled water and underground waters of intended disposal sites (this characteristic also determines a possible quantitative release of radionuclides from solidified radioactive wastes under the conditions of real disposal);
— the thermal and radiation resistances that determine the behaviour of solidified radioactive wastes in the course of storage and the ability of materials to retain or to change their initial properties (primarily, the hydrolytic durability and the structure) in certain ranges of storage temperatures and radiation doses;
— the thermal properties (the thermal conductivity, heat capacity, and thermal expansion coefficient) that determine the conditions of melt cooling and the storage and disposal of solidified radioactive wastes;
— the mechanical (strength) properties (the compression strength, Young modulus, etc.) that provide a garateed mechanical safety of the matrix during transportation, storage, and disposal.

These characteristics describe the main properties of solidified materials during their long-term storage and the subsequent disposal and allow one to predict their behaviour.

The level of the development of the technology for fabricating solidified radioactive wastes and the possibility of producing blocks of these materials with the required properties and geometry are the final factors responsible for the choice of a particular material as a final product of radioactive-waste solidification for the subsequent storage and burial.

The stability of an optimum structure of solidified wastes during their long-term storage is one of the main characteristics. This characteristic is especially important for glasses of different types - the materials that, at present, are used for immobilizing radioactive wastes on the industrial scale.

An initially amorphous structure of a glass matrix can partially or completely crystallize in the course of cooling of glass blocks after pouring a glass melt into containers (cans, barrels) and also during the temporary storage due to the heat released in blocks upon decay of radionuclides.

As regards crystalline (mineral-like) compositions for the HLLW immobilization, the experimental investigations carried out to date demonstrated that, when the immobilization of radioactive wastes is performed with the production of mineral-like compositions (analogs of natural materials), especially, with the use of the melting method, it is not necessarily possible to prepare a final material with a controlled crystalline structure [20].

However, the required result, namely, the preparation of completely crystalline materials with a controlled structure, can be achieved upon additional heat treatment of synthesized materials.

The inverse process - the amorphization of a crystalline structure - can occur under the action of internal irradiation of a radioactive material during its storage. This phenomenon is most frequently observed when studying crystalline materials containing alpha emitters [21-23].

Certain experimental data of investigations into properties of solidified radioactive wastes will be given below. In each specific case (a certain composition of solidification products produced according to a particular technology), it is necessary to predict the properties of final products.

The development of the technology of immobilizing liquid radioactive wastes into vitreous and mineral-like compositions with the use of a "cold" crucible induction melter (CCIM) is a promising direction in the field of radioactive-waste management. The use of this technology makes it possible not only to reprocess radioactive wastes of variable compositions but also to synthesize various matrices that involve radionuclides of different types, including fractionated wastes.

In order to simulate successfully and correctly possible structural transformations in immobilized waste forms produced by melting, it is necessary to consider and determine some technological parameters of the process, which can substantially affect the quality of final solidified products.

These parameters are as follows:

— the synthesis temperature of the final product and the temperature of a melt upon pouring into transport containers (cans),
— the overall dimensions, material, wall thickness, configuration, and other characteristics of transport containers (cans),
— the production rate of the final product and the filling rate of transport containers (cans),
— the conditions of cooling and preliminary (prior to placement in a temporary repository) treatment of transport containers (cans),
— storage conditions of transport containers (cans) or cases in the temporary repository.

Since vitreous and mineral-like compositions of different types can be prepared as final materials with the use of melting, it is necessary to obtain sufficiently complete information on the main physicochemical (primarily, the chemical, phase and radiochemical

compositions; density; etc.) and thermal (the heat capacity, thermal conductivity, softening and melting temperatures, possibility of additional crystallization, etc.) properties of the synthesized compositions.

When other procedures and technologies (self-propagating high-temperature synthesis, pressing, sintering, etc.) are applied to immobilize radioactive wastes with the production of solidified compositions, it is also necessary to simulate possible changes in the physicochemical properties of final products with the aim of predicting their behavior in the course of the subsequent storage and burial with due regard for specific features of technological parameters of their synthesis.

In order to determine possible structural transformations and, as a consequence, the properties of solidified wastes during their cooling, transportation, and temporary and long-term storage, samples prepared under laboratory conditions should be subjected to additional heat treatment corresponding to the storage conditions of real products.

Investigation into the properties of additionally heat-treated samples of solidified wastes allows one to determine and identify changes in their structure and properties and to predict, with a sufficient degree of confidence, the behavior of blocks of solidified products in the course of long-term storage.

It is necessary to simulate and determine more realistically possible changes in the structure and properties of solidified wastes during their cooling, transportation, and temporary and long-term storage with allowance made for the internal heat release and irradiation. For this purpose, the samples prepared under laboratory conditions and doped with alpha emitters (if required) should be subjected to additional heat treatment under external gamma irradiation that correspond to the conditions under which real products will be stored and the dose which they can receive in the course of storage.

Investigations on the properties of these samples of solidified wastes permit to determine and identify the changes in their structure and properties. Subsequently, the experimental data obtained will enable to simulate configurations of zones in blocks of solidified wastes with different properties and to predict their behaviour during long-term storage taking into account the possible crystallization (amorphization) of the final product.

As an illustration of the foregoing, the results of investigations on the properties of borophosphate glasses BP-2 (synthesis of the initial glass at 1000°C for 2 h) and BP-5 (synthesis of the initial glass at 1000°C for 5 h) prepared under different temperature – time conditions are presented in Figs. 5 and 6.

Figure 5 shows the X-ray powder diffraction patterns, the EPR spectra, and the SEM micrographs of borophosphate glass samples (Table I) subjected to heat treatment at the "critical" temperature of their crystallization (630°C) for 0.5-5.0 h. These data clearly demonstrate the transformations occurring in the matrix composition and the successive formation of different crystalline phases. At the first stage, the $Na_3(Al,Fe)_2(PO_4)_3$ iron-containing sodium aluminophosphate phase (2) crystallizes in the glass (1). Then, the sodium aluminophosphate phase (3), most likely, containing boron impurities is formed in the glass. The $(Ce,La,Nd)PO_4$ monazite crystalline phase (4) grows within regions of phase (3).

TABLE I. CALCULATED COMPOSITION OF BOROPHOSPHATE GLASS

Oxide	Oxide content, wt %
Na_2O	24,04
Al_2O_3	18,27
B_2O_3	3,85
P_2O_5	50,00
Fe_2O_3	1,44
NiO	0,29
Cr_2O_3	0,09
La_2O_3	0,48
Nd_2O_3	0,29
CeO_2	0,48
CaO	0,48
MnO	0,29

X-

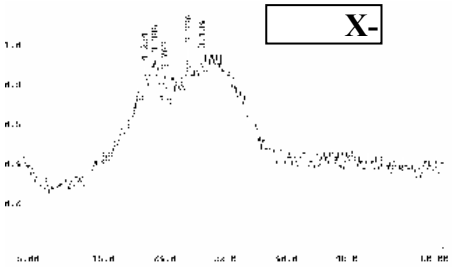

E

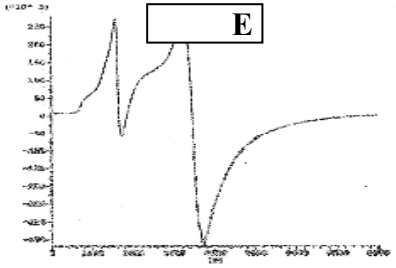

S

630°
C, 0.5 h

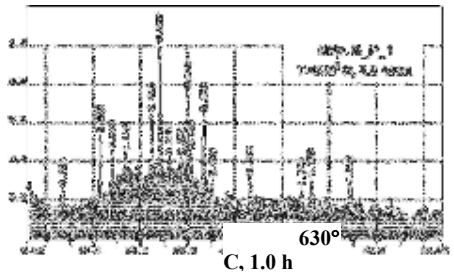

630°
C, 1.0 h

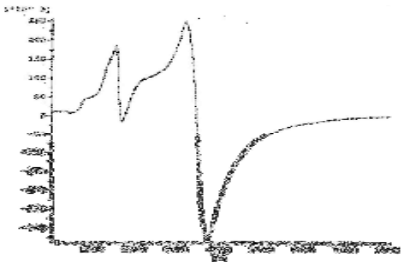

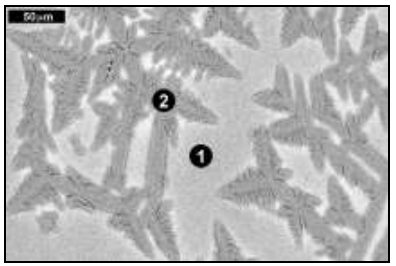

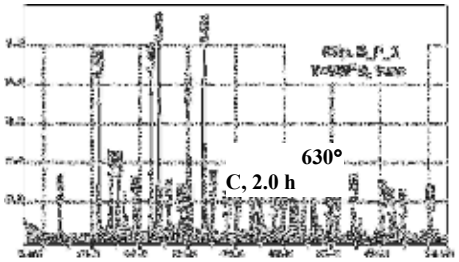

630°
C, 2.0 h

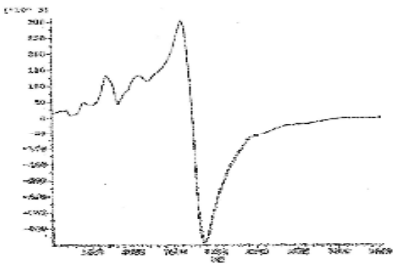

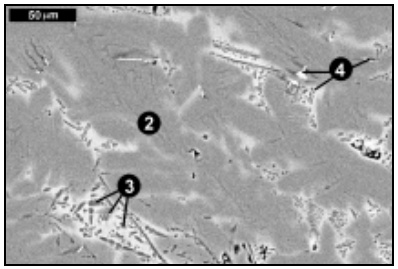

630°
C, 3.0 h

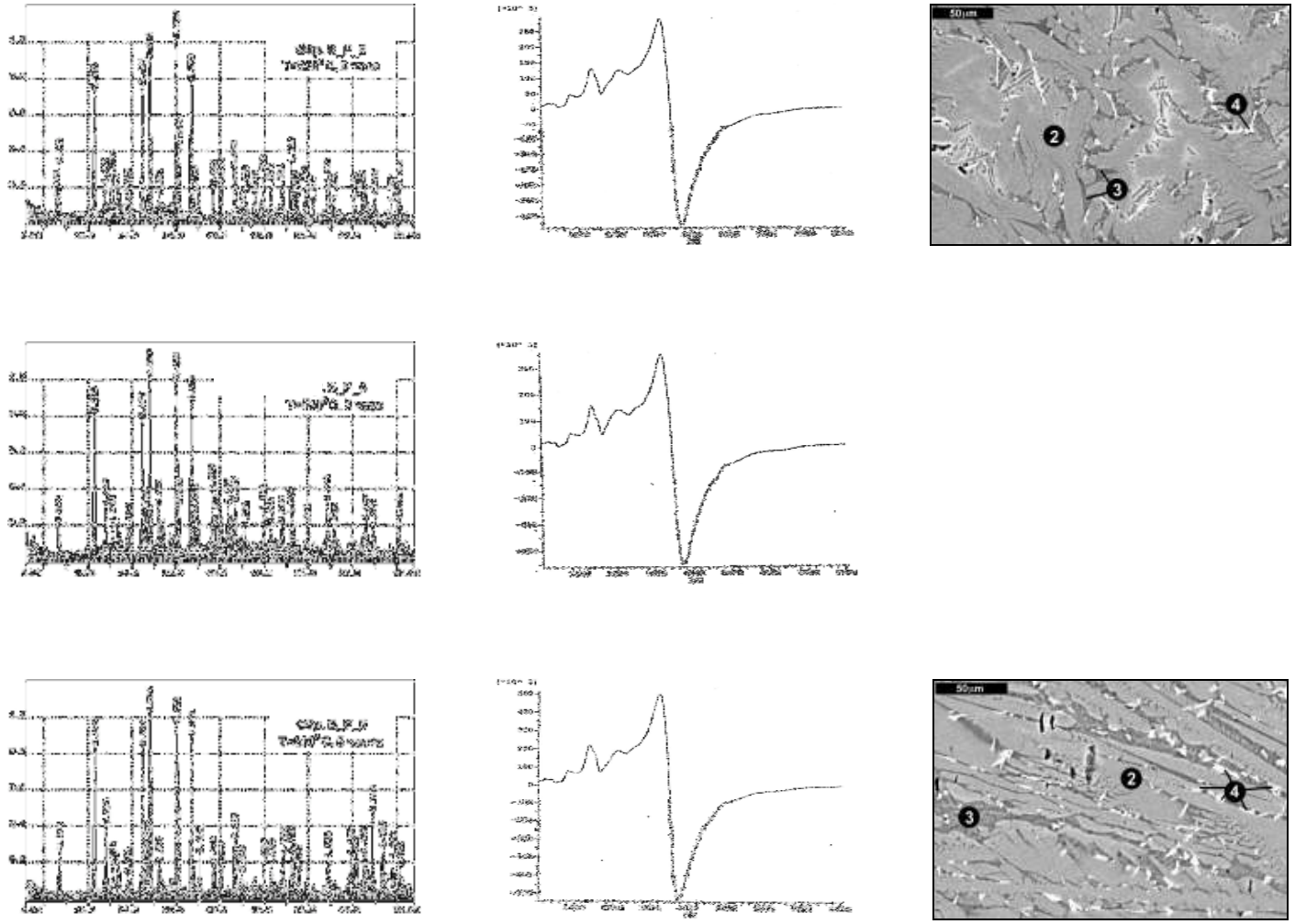

FIG. 5. X-ray powder diffraction patterns, EPR spectra, and SEM micrographs of borophosphate glass samples

The external appearance of a number of borophosphate glass samples and the graphs indicating their heat treatment conditions are represented in Fig. 6.

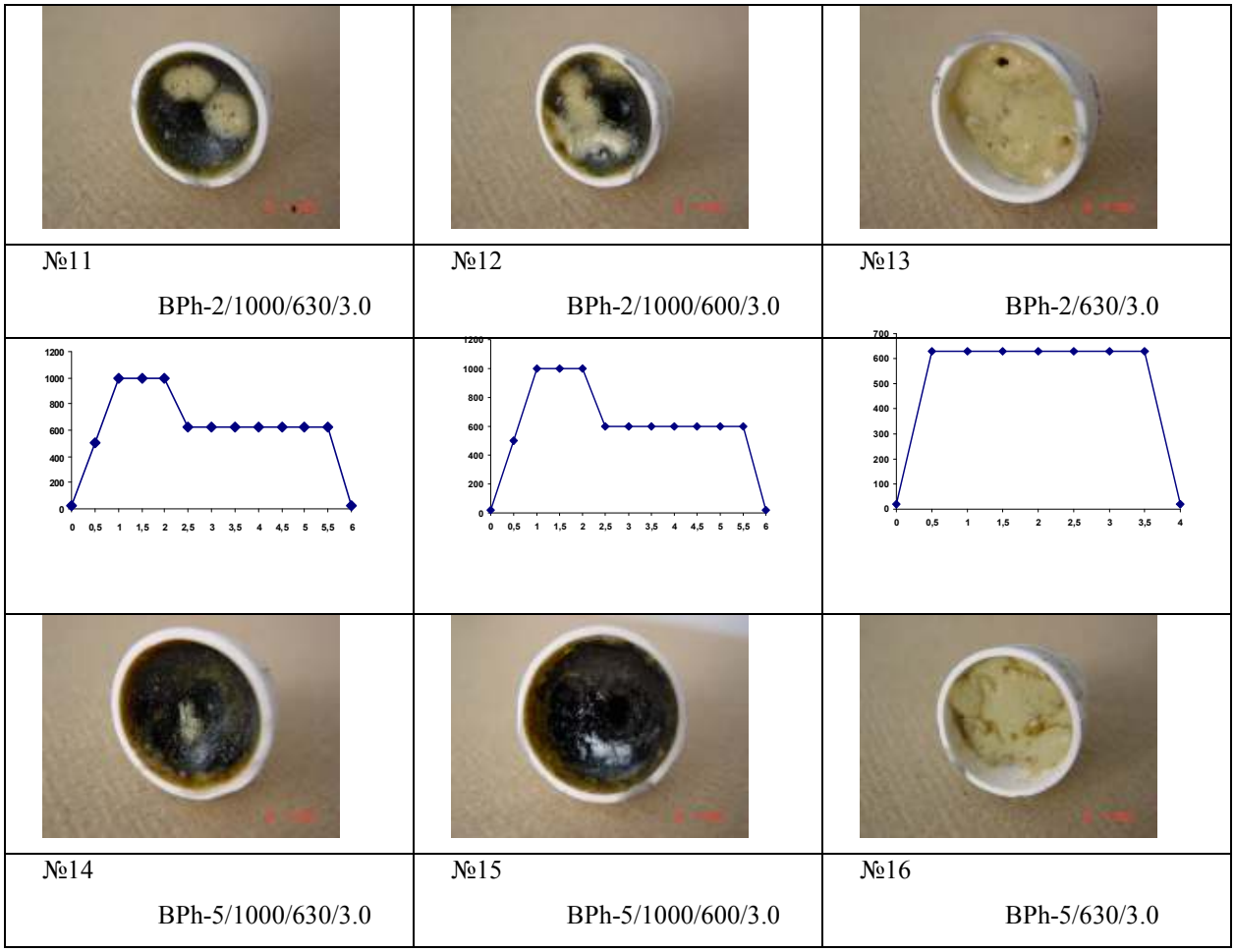

Fig. 6. External appearance of the surface layers of samples of blocks nos. 11-16 and graphs indicating their heat treatment conditions.

This figure clearly shows the influence of heat treatment conditions on the structure and quality of glass blocks. Actually, the cooling of the glass melt (T = 1000°C to 600 - 630°C and holding at this temperature for 3 h) leads to the formation of glass-ceramic blocks containing an insignificant amount of a crystalline phase only in surface layers of glass blocks (the simulation of cooling of melt after pouring). The heating of borophosphate glass samples from room temperature to 600 - 630°C and holding at this temperature for 3 h results in the formation of almost completely crystallized materials (the simulation of possible self-heating of blocks due to the decay of radioactive components in wastes).

Undeniably, the proposed approach and methodology of investigating solidified forms of radioactive wastes will require a further refinement with allowance made for progress in scientific and technological approaches to the solution of the problems associated with the radioactive-waste management. The proposed method of accumulating the data on the methods and technologies for preparing (synthesizing)

solidified radioactive wastes and their physicochemical properties will enable to create the required database. The analysis of the accumulated experimental data will make possible to compare correctly the proposed methods for immobilizing radioactive wastes with due regard for the degree of their development (equipment and technology) and the properties of final products for safe management with a particular type of radioactive wastes and their subsequent burial.

REFERENCES

[1] Polyakov, A.S., Borisov, G.B., Moiseenko, N.I., et al., Experience in Applying an EP-500/1R Ceramic Melter to Vitrification of High-Level Liquid Wastes, At. Energ., 1994, Vol. 76, no. 3, pp. 183-188.

[2] Glagolenko, Yu.V., Dzekun, E.G., Medvedev, G.M., et al., Reprocessing of Spent Nuclear Fuel of Nuclear Power Plants and Liquid Radioactive Wastes at the PA "Mayak", At. Energ., 1997, Vol. 83, no. 6, pp. 446-452.

[3] Glagolenko, Yu.V., Dzekun, E.G., Rovnyi, S.I., et al., Reprocessing of Spent Nuclear Fuel on an RT-1 Plant: History, Problems, and Prospects, Vopr. Radiat. Bezopasnosti, 1997, no. 2, pp. 3-12.

[4] Glagolenko, Yu.V., Rovnyi, S.I., Medvedev, G.M., and Poluektov, P.P., Development of the Technological Scheme for the Management of Liquid Radioactive Wastes of the PO "Mayak", Vopr. Radiat. Bezopasnosti, 2003, no. 1, pp. 5-13.

[5] Spent Nuclear-Fuel Regeneration Plant (RT-1), www.minatom.ru (17.02.2003).

[6] Demine, A.V., Poluektov, P.P., Smelova, T.V., Gorn, V.F. et al. The use of induction melting in cold crucible for the solidification of HLW. Proceedings of the international conference MRS-2000, Australia, 2000.

[7] S. I. Rovny, V. I. Guzhavin, «The Technology of Alpha-active Materials Incorporation in Glassy and Mineral Matrixes» In Proceedings of the 3rd Annual Meeting for Coordination and Review of LLNL Contract Work, UCRL-ID-149341, State Regional Education Center, St. Petersburg, Russia, January 14-18, 2002, p. 111-117.

[8] Demin A.V., Matyunin Yu.I., Fedorova M.I., "Noble Metal (NM) Behavior During Simulated HLLW Vitrification in Induction Melter with Cold Crucible", Fifth International Conference on Radioactive Waste Management and Environmental Remediation, ICEM'95, Berlin, Germany, September 3-7, Proceeding Vol. 1, p. 443-445.

[9] T.V. Smelova, I.N. Shestoperov, N.V. Krylova, “Synthetic mineral-like matrices for the HLW solidification: preparation by CCIM method”, Proceedings of the Embedded Topical Meeting on DOE Spent Nuclear Fuel & Fissile Material Management, Reno, Nevada, USA, 1996, p.197-200.

[10] Yu.I. Matyunin, “Cold Crucible Induction Melter Study of Glasses and Ceramic Composition for Immobilization of Pu-containing Materials (UTA 96-330-MOD-1)”, in “Excess Weapons Plutonium Immobilization in Russia: A Review of LLNL Contract Work”, UCRL-ID-138361, LLNL, 2000, Proceedings of the Meeting for Coordination and Review of Work Held in St. Petersburg, Russia, November 1-4, 1999, p. 83-102.

[11] Matyunin, Yu.I. and Yudintsev, S.V. Investigation of Uranium-Containing Borosilicate Glasses Synthesized in an Induction Melter with a Cold Crucible (CCIM), Vopr. Radiat. Bezopasnosti, 2000, no. 1, pp. 15-23.

[12] I.A. Sobolev, F.A. Lifanov, S A. Dmitriev, S.V. Stefanovsky, A.P. Kobelev, «Vitrification of Radioactive wastes by Coreless Induction Melting in Cold Crucible», Proceedings Nuclear and Hazardous Waste Management International Topic Meeting SPECTRUM'94, Atlanta, Georgia, USA, 1994, p.2250-2255.

[13] I.A. Sobolev, S.A. Dmitriev, F.A. Lifanov et al, "Waste Vitrification: Using Induction Melting and Glass Composite Materials", International Conference of Evaluation of Emerging Nuclear Fuel Cycle Systems - CLOBAL 1995, Versalles, France, 1995, September 11-14, Procceding Vol.1, p. 734-740.

[14] I.A. Sobolev, S.V. Stefanovsky, B.I. Omelianenko, S.V. Yudintsev et al, "Comparative Study of Synroc-C Ceramics Produced by Hot-Pressing and Inductive Melting", Materials Research Society Symposium Proceedings "Scientific Basis for Nuclear Waste Management XX", vol. 465, Boston, Massachusetts, USA, 2-6 December, 1996, p. 371-378.

[15] «Waste control and management in Moscow», Nuclear Engineering International, December 2002, p. 39-41.

[16] K.G. Kudinov, A.A. Tretyakov, Y.P. Sorokin, «CPL Experience in Improving Design of Lab-Scale Microwave Facility Placed in Hot Cell: Analysis and Results», In Proceedings of the Meeting for Coordination and Review of Work Held in St. Petersburg, Russia November 13-16, 2000, UCRL-ID-143846, p. 33-38.

[17] G.B. Borisov, A.V. Balashov, O.A. Mansourov, A.V. Nasarov, Y.Y. Volchok, «Glass Matrices for Vitrification of Pu-containing Sludge of MCC UsingMicrowave Heating», In Proceedings of the Meeting for Coordination and Review of Work Held in St. Petersburg, Russia November 13-16, 2000, UCRL-ID-143846, p. 57-60.

[18] A.S. Aloy, P.E. Burkhanov, F.H. Gofman, E.Yu. Ivanov, B.S. Kuznetsov, «A System of Control and Monitoring for Process SolidificationPu-Containing Sludges of MCC by Microwave Heating», In Proceedings of the Meeting for Coordination and Review of Work Held in St. Petersburg, Russia November 13-16, 2000, UCRL-ID-143846, p. 65-69.

[19] K. G. Kudinov, A. A. Tretyakov, Yu. P. Sorokin, V. V. Bondin, L.F. Manakova, «Technological Aspects of MChC Pu-containing Sludges Vitrification, Using MW Melter» In Proceedings of the 3rd Annual Meeting for Coordination and Review of LLNL Contract Work, UCRL-ID-149341, State Regional Education Center, St. Petersburg, Russia, January 14-18, 2002, 51-54.

[20] Yu.I. Matyunin, T.V. Smelova, S.V. Yudintsev, "Immobilization of Uranium and Plutonium into borobasalt, piroxen and andradite mineral-like compositions", Int. Conf. "ATALANTE 2000", 23 - 26 October 2000, Avignon, France.

[21] A. N. Lukinykh, S. V. Tomilin, A. A. Lizin, A. V. Bychkov, «Investigation of Radiation and Chemical Stability of Titanate Ceramics Intended for Actinides Disposal», In Proceedings of the 3rd Annual Meeting for Coordination and Review of LLNL Contract Work, UCRL-ID-149341, State Regional Education Center, St. Petersburg, Russia, January 14-18, 2002, p. 273-283.

[22] I. A. Kulikov, A. A. Vashman, V. M. Filine, T. N. Ananina, V. E. Samsonov, O. Y. Panov, «Investigation of Accelerated Radiation Damages of the US-specified Pyrochlore-like Ceramics Containing ^{238}Pu», In Proceedings of the 3rd Annual Meeting for Coordination and Review of LLNL Contract Work, UCRL-ID-

149341, State Regional Education Center, St. Petersburg, Russia, January 14-18, 2002, p. 285-294.

[23] B. E. Burakov, E. B. Anderson, «KRI Radiation Damage Studies of the US Pu Ceramics», In Proceedings of the 3rd Annual Meeting for Coordination and Review of LLNL Contract Work, UCRL-ID-149341, State Regional Education Center, St. Petersburg, Russia, January 14-18, 2002, p. 295-300.

INFLUENCE OF RADIATION, ENVIRONMENT AND TEMPERATURE ON THE INTERACTION OF THE SPENT FUEL RBMK–1000 AND BOROSILICATE GLASSES UNDER SIMULATED REPOSITORY CONDITIONS

A.S.ALOY**,** TN.V.SAPOZHNIKOVA

RPA «V.G. Khlopin Radium Institute», St. Petersburg, Russian Federation

Authors and Contributors: .I. KOLTSOVA, A.B. KOLYADIN, YU.M. ROGOZIN,

Abstract

The study of UO_2 oxidation in the RBMK-1000 spent nuclear fuel (SNF) specimens was undertaken depending on oxygen content in the gas medium and on the temperature. The second part of the study was concentrated on the barrier properties of the mountain rocks potentially acceptable for disposal of a deep repository. It is a necessary stage for the safe isolation of radionuclides from environment. The results of sorption barriers properties of typical granitoids from Nizhnekanskiy rock massif are presented in this paper.

1. EXPERIMENT

1.1. Behavior of UO_2 in the RBMK-1000 Spent Fuel at Oxidizing Conditions

RBMK is light-water cooled, graphite moderated power reactor of channel type. Currently, nuclear power plants (NPPs) with RBMK–1000 have accumulated large amounts of SNF (more than 70 000 spent fuel assembles). The residual power density RBMK of irradiated SNF is ~ 0.1kW/SNF at 2 % fuel enrichment and 10-year storage in water (with an average burn-up rate of 20.5 MW·day/kgU).

Table I shows the specific amount of actinides in the SNF after 20 years of storage. The total amount of plutonium radionuclides in the SF may reach 4 kg/t, americium – 0.43 kg/t [1].

TABLE I. FISSION PRODUCTS CONTENT IN THE SNF RBMK–1000 AT 2% FUEL ENRICHMENT AFTER 20 YEARS STORAGE

Radionuclide	$T_{1/2}$	Specific content, Bq/t	Mass, g/t
Cs-134	30.2 years	$2{,}3\cdot10^{15}$	713
Cs-135	2.06 years	$1{,}4\cdot10^{14}$	2.8
Cs-137	$2.3\cdot10^{6}$ years	$9{,}3\cdot10^{9}$	218
Sr-90	28.5 years	$1{,}5\cdot10^{15}$	300
I-129	$1.6\cdot10^{6}$ years	$9{,}25\cdot10^{8}$	140
Cd-113m	13.6 years	$3{,}7\cdot10^{1}$	$4{,}3\cdot10^{-2}$
Ce-144	284.3 days	$3{,}4\cdot10^{12}$	$2{,}8\cdot10^{-2}$
I-1116	$5.0\cdot10^{15}$ years	$2{,}8\cdot10^{2}$	1.2

The general approach to RBMK-1000 SNF management is based in Russia on a once-through cycle without reprocessing. After discharge from the reactor, SNF is stored in cooling water ponds at NPPs. According to world-wide experience, subsequent storage is preferred as "dry" storage facilities which, due to the lower costs than those of cooling ponds. It is then important to know the changes in UO_2 structure and properties before transfering it to repository conditions.

To study and predict the behaviour of the RBMK spent fuel in dry storage, through samples of the fuel exposed to air, moisture saturated at room temperature, and to nitrogen mixed with 0.08, 0.48, and 1.3 vol.% oxygen. The experiments were conducted at temperatures of 100, 160, and 200°C for humid air and at 300 °C for nitrogen.

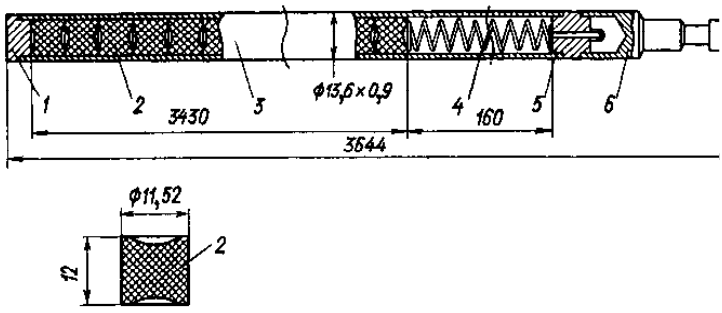

FIG.1 Cutaway of typical RBMK-1000 fuel element and UO_2 pellet: 1 – fuel element, 2 – UO_2 pellet

The samples used in the experiments were pieces of the Leningrad nuclear power station fuel rods with a burn-up of 10.07 and 19.7 MW·day/kg U. After 5-year cooling in the local cooling pond, the rods were taken out and kept in air in a stainless steel container as 150÷200 mm segments. To prepare the test samples, the segments were cut into 30÷35 mm pieces and put in special casings. The cutaway of typical RBMK-1000 fuel assembles (FA) and UO_2 pellet is presented in Fig.1.

A portion of these casings was sealed, the other had bores 0.23, 1.0 or 3.0 mm in diameter to simulate leakage. Certain of the samples were fragments of bare fuel pellets. The samples were tested for 3500 to 4000 hours. The preliminary gravimetric and XRD tests proved that all uranium in the samples was in the form of $UO_{2.01}$ (Fig.2).

Being subjected to humid air at 100°C, the RBMK-1000 fuel is not oxidized. Oxidation rate becomes perceptible at temperatures above 160°C, and at 200°C. UO_2 transforms almost completely into the high temperature hexagonal U_3O_8. Stabilization of this form at room temperature is, evidently, caused by fission products (La, Sr, Ce).

The influence of humid nitrogen with minor mixture of oxygen on the RBMK-1000 fuel oxidation kinetics was studied at 300°C, i.e. as the maximum fuel storage temperature in a dry storage. When fed into the reactor, nitrogen was humidified by bubbling through the distilled water at room temperature at a rate of 1,7±0,2 l/h, to keep the composition of gas environment in sample cans constant. The Fig. 3 shows the sample's mass change with time at isothermal heating in nitrogen environment.

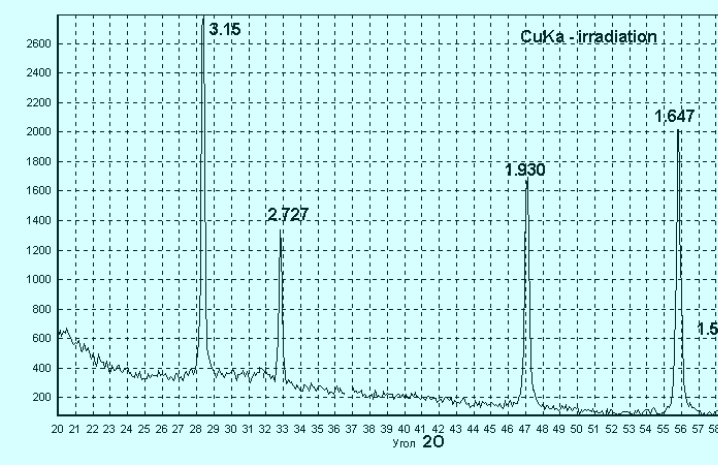

FIG.2. XRD data for the sample of RBMK–1000 fuel.
Phase composition is $UO_{2.01}$

The kinetics of fuel oxidation in nitrogen-oxygen mixtures at 0.08 and 0,48 vol.% oxygen is similar to that described above for cans with 1.0 and 3.0 mm bores (See curves 1 and 2 in A and B, correspondingly). The 1.0 and 3.0 mm bores, most likely, do not limit any gas intake and so do not virtually affect the oxidation rate of the fuel.

The test conducted at 0.48 vol.% oxygen during roughly the same time interval did not result in the complete oxidation of UO_2. (final O/U ratio was 2.56). Oxidation of a fuel section opened at ends (curve 3 in C) results in the 4.86% mass increase at O/U ratio of 2.82 after 640 hours of the gas-thermal test. Seemingly, UO_2 in the sealed fuel element (curve 4 in C) is oxidized solely by the free oxygen contained inside the fuel can.

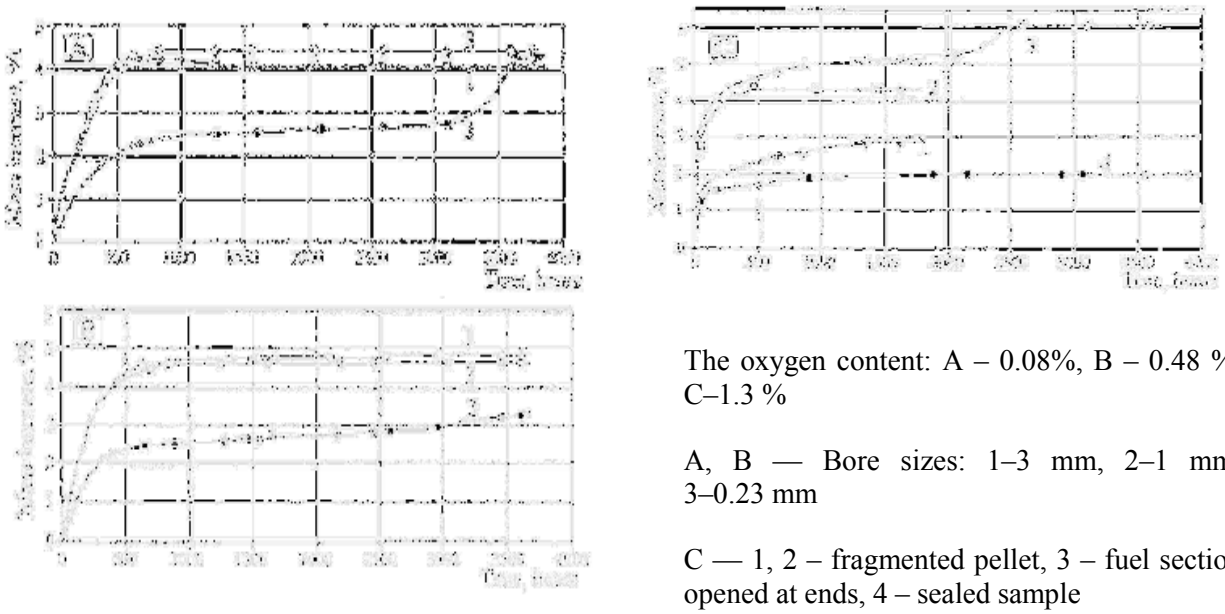

The oxygen content: A – 0.08%, B – 0.48 %, C–1.3 %

A, B — Bore sizes: 1–3 mm, 2–1 mm, 3–0.23 mm

C — 1, 2 – fragmented pellet, 3 – fuel section opened at ends, 4 – sealed sample

FIG. 3. Oxidation of the RBMK-1000 fuel at 300°C in the flow of humid nitrogen with the admixture of oxygen.

Oxidation of two samples of irradiated fragmented pellets was conducted in open containers in a different way (curves 1 and 2 in C). Oxidation rate of the sample #2 was very high and after ~500 hours its mass stabilized at O/U value corresponding to uranium mixed oxide U_3O_{8+x}.

With the sample #1 the oxidation rate in the initial stage was slower ($K_{0\text{-}250h}$=6,70 * 10^{-5} g/$m_{0(g)}$ $\Delta\tau_h$). Then, after a short plateau on the isotherm between 650 and 850 h, a new mass increase was observed ending in mass stabilization at Δm=2,81% and O/U=2,49. XRD showed that the final product of oxidation consisted of two phases with a ratio of $U_3O_8/UO_{2,15}$=1:1 (Fig. 4).

Oxidation mechanism of UO_2 is believed to depend on the size of the oxide particles [2]. Thus, the first stages of the process in UO_2 with specific surface exceeding 1 m^2/g are determined by diffusion, whereas in UO_2 with specific surface of 0,05 m^2/g oxidation is limited by nucleation and development of grains of a new phase. In studies of the stabilization process account should be taken of high-yield fission products – lanthanides neodymium and cerium. These elements are able to form solid solutions of fluorite structure with lattice parameters close of mass and to those of U_4O_9, and may, therefore work as stabilizing agents in oxidation process.

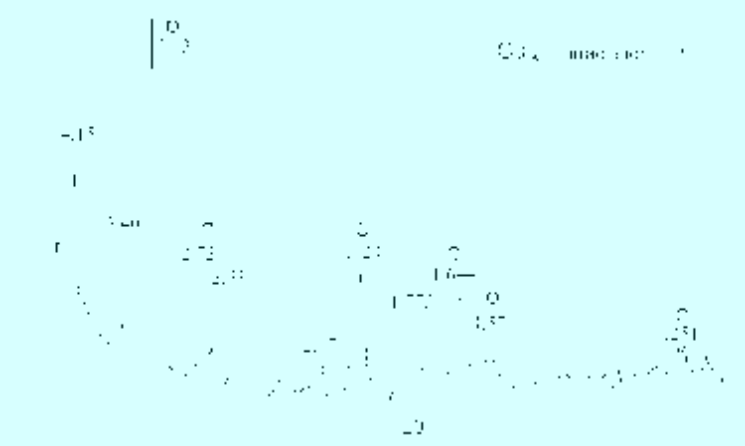

FIG. 4 The fuel sample after oxidation at 300 °C in the flow of humid nitrogen with the 1,3% vol. admixture of oxygen. Quantitative phase ratio U_3O_8/ $UO_{2.15}$ = 1:1

Taking into account that after long-term storage SNF will be transferred to the repository in the geological formation, the investigation of UO_2 solubility in the solutions, simulated underground water, in contact with atmospheric air was studied.

Table II represents the results on the solubility of uranium dioxide $UO_{2.1}$ with the specific surface 1.3 m^2/g, uranium dioxide in form of pellets from non-irradiated fuel of the RBMK-1000 reactor and separate particles of the spent fuel with the grain size 0.3 – 0.45 mm and the burn-up 11 MW·day/kg.

TABLE II. URANIUM SOLUBILITY FOR UO_2 POWDER, PELLETS IN NON-IRRADIATED FUEL AND SPENT FUEL PARTICLES

Time, hours	**U concentration in solutions, mg/l**		
	$UO_{2,1}$	**Fuel pellet**	**SF particles**
1	12 – 20	0,2 – 0,5	
2	15 – 25	0,5 – 0,7	$(4 – 6) \cdot 10^{-3}$
3 – 4	15 – 25	0,5 – 0,7	$(6 – 9) \cdot 10^{-3}$

Uranium saturation in solutions with the phases ratio Liquid:Solid = $100 cm^3/g$ was being completed for several hours. The solubility of uranium in water phase differs considerably for all investigated samples and was up 15–25 mg/l for UO_2 powder, 0.5-0.7 mg/l for UO_2 pellets from non-irradiated fuel and $(4–9)\cdot10^{-3}$ mg/l for spent fuel particles. The solubility of UO_2 from the spent fuel is considerably lower than the solubility of fresh reactive uranium oxide. Basically, such large differences indicate that pre-history of tested material has very strong influence on the dissolution behaviour of UO_2.

1.2. The barrier properties of the mountain rocks

Designing the underground repository for RBMK-1000 SNF one should take into account the possibility of long-term influence of radiation and temperature upon the rock massif. The process of radionuclides migration within the underground waters is defined by hydrodynamical conditions in a mountain massif and by the properties radionuclides. The determining factors of keeping properties of the rocks thickness are their permeability regarding ectoplasm and sorption property concerning radionuclides.

Nizhnekanskiy massif is one of the greatest granitoid massifs of Intermediate Siberia. The massif is presented by complex granitoids of several phases with different age, mainly of biotite granites and granodiorites. His northwest part is situated in the immediate vicinity of a mining chemical complex (MCC) and the nuclear fuel-reprocessing plant RT-2 [3].

The studies of the samples of the granitoids from Nizhnekanskiy massif, taken away from the surface, showed, that the porosity of the monolithic samples averages about 1-2 vol.%. The filtration coefficients for granite (granodiorite) compose $(0.5–5)\cdot10^{-4}$ m/day. For more compact samples of quartzous diorite, the filtration coefficients compose $(2.6\text{-}60)\cdot10^{-7}$ m/day. At the hydraulic pressure of the underground water ~ 0.01mm and the porosity of the rock is ~ 1%, the true speed of the water migration at such values of the filtration coefficient is subject from $1\cdot10^{-4}$m/year for dense rock to $0.02\div0.2$ m/year for weak zones. Thus, the zones of monolithic rock are practically impenetrable to migrating waters and to radionuclides.

Geological formation is the main barrier on the way of the dissipation of particularly long-lived and actinide elements. Consequently the sorption ability of typical rock samples of Nizhnekansk granitoid massif in reference to some actinide elements from the solutions was investigated, simulating underground waters with pH=8,4 and Eh = –280 mV and containing containing sodium bicarbonate with $3.6\cdot10^{-3}$ mol/l concentration. The tests were performed under static conditions with the bits of fractured rocks, sampled at the places where granitoids come out to the surface and from a drill at various depths (500-700m). Rock samples were of 0.1-0.25 mm and 0.25-0.5 mm. The time of phase contact was 7-30 days. The formal interphase distribution coefficient in reference to the mass of the rock sample K_d (cm^3/g) was used as characteristics of the sorption process. The results of the test, presented in Table III, show that the distribution coefficient values are quite high for americium and plutonium sorption in granitoids, and they do not exceed 2 cm^3/g for neptunium (V).

TABLE III. DISTRIBUTION COEFFICIENTS (K_D) OF AM, PU AND NP DURING THE SORPTION BY FRACTURED ROCKS

Rock sample, depth (m)	**K_d, cm^3/g**		
	Americium	**Plutonium**	**Neptunium**
Leucocratic granite, 513	650	100	0,9
Middle–grain tonalite, 542	680	750	1,5
Large–grain granodiorite, 700	4200	670	<0,2
Granite (surface)	1200	900	1,8
Granodiorite (surface)	800		1,4

Samples taken at 700m depth had the highest values of the distribution coefficient for americium, for the sorption in granodiorite,. The distribution coefficient for plutonium is of the same magnitude in practically all the samples. It could be expected that under reducing conditions in a granitoid rock at large depths, neptunium may exist in an oxidizing state (IV) and its sorption in the rock would take place in correspondence with the plutonium distribution coefficients.

The other investigations of the sorption ability of the granitoid massif rocks were conduced under the same conditions. The plutonium (IV) concentration was not more than $n \cdot 10^{-8}$ mol/l in the laboratory experiments. It is lower than the solubility of plutonium hydrate at the given pH value and carbonate ions content.

TABLE IV. PLUTONIUM SORPTION DEGREE ON THE CRUSHED ROCK

Contact time of the phases, day	**Plutonium sorption degree, %**		
	Leucogranite	**Tonalite**	**Granodiorite**
10	38	45	55
28	60	68	80
42	66	78	88
77	76	82	93
100	80	85	95
199	88	89	97

The plutonium exists in a form of complex compounds with the hydroxyl and carbonate ions in the neutral and alkalescent solutions. The plutonium sorption is extended during the time on the crushed rock samples. As an example, the changes of a plutonium sorption degree on the crushed samples of leucogranite, tonalite, granodiorite having sizes of 0,1-0,12 mm are given in Table IV. The ratio of a liquid phase volume to rock weight was equal to 220 cm^3/g.

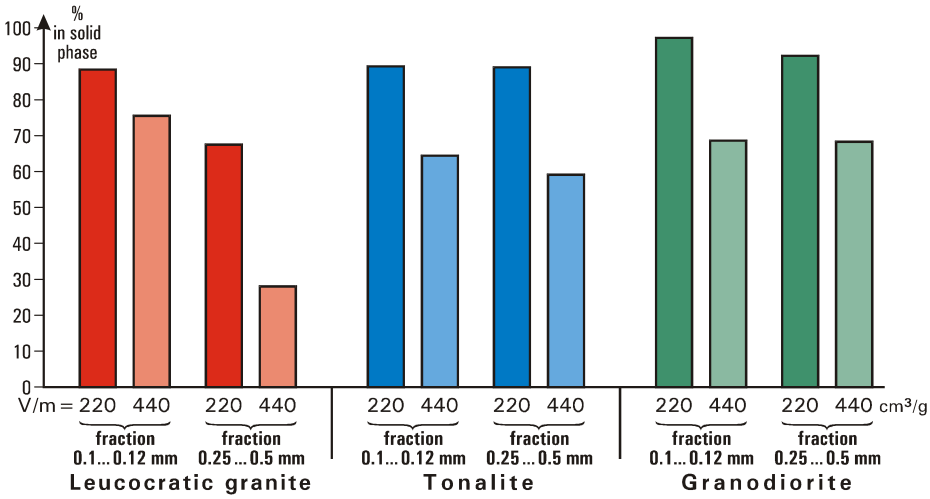

FIG. 5. Extent of ^{238}Pu extraction by crushed samples of different granitoids from simulated groundwater depending on the proportions of phases and sizes of the samples

The slow increase of a plutonium sorption degree with time is obviously connected to slow diffusion of radionuclides penetration into the volume of rock grains.

In Fig. 5, the plutonium sorption degree on the crushed samples having various sample sizes and volume to mass. It results that the sorption degree depends on dispersion (sizes) of the samples in some cases. Those results confirm the difficulty of the plutonium penetration in the volume of the rock grains. On the basis of the received results on plutonium sorption on samples of crushed rocks the value of the distribution coefficients Kd (cm^3/g) and retention factors R were appreciated. The estimated results are given in Table V.

TABLE V. THE DISTRIBUTION COEFFICIENTS KD AND THE RETENTION FACTORS R OF PLUTONIUM SORPTION

Rock	K_d, cm^3/g	R
Leucogranite	430÷560	$(2÷3) \cdot 10^5$
Tonalite	380÷790	$(1÷3) \cdot 10^5$
Granodiorite	430÷1500	$(0,8÷3) \cdot 10^6$
Biotite granite	900	$\sim 2 \cdot 10^5$
Quarts diorite	800	$\sim 2 \cdot 10^5$

From those data we can deduct that the plutonium retention factor, as a result of its sorption on the rock, cannot be less than $n \cdot 10^5$, i.e. the rate of plutonium migration in the weak zones of a mountain massif with the underground waters will be about five orders lower than the rate of water migration. If the rate of the underground waters migration in the weak zones of a mountain rock will be ~ 0,04 m/years, the

rate of the plutonium migration will be no more ~ $4 \cdot 10^{-7}$ m/years. The obtained high distribution coefficient and retention factor provide the good basis to follow the study of the protective properties of the Nizhnekanskiy massif as a future repository site.

2. CONCLUSION

- UO_2 oxidation in the samples of the RBMK-1000 spent fuel was detected in humid air even at 150 ^oC, whereas at 200^oC virtually all UO_2 is transformed into U_3O_8 after 3500÷4000 hours.
- Defects in spent fuel cladding ($S \geq 0{,}8$ mm^2) give rise to oxidation of fuel composition during storage in nitrogen environment with oxygen content of over 0.05 vol.%.
- With damages <0.04 mm^2 the oxidation process goes on slower, and after ~3000 hours of exposure uranium-to-oxygen ratio reaches 2.56.
- Stabilization of the UO_2 oxidation process in the RBMK-1000 fuel samples studied is not observed up to U/O ratio of 2.4, which, in our opinion, may be attributed to the small burn-up of the fuel tested.
- High values of diffusion coefficients and retention factors (Kd and R) for actinide elements are some of the potentially significant protective properties of Nizhnekansk granitoid massif.

REFERENCES

[1] V.G. Aden, “Operating experience of RBMK Fuel under normal conditions and analysisi of its damage causes”., IAEA–TECDOC–709, 1992, p.106.

[2] Woodley R.E. J. Nucl. Technol., 1989, v. 85, N1, pp. 74-88.

[3] “Study of Granitoids from Nizhnekanskiy Massif as a Potential Disposal RW Site”. CRP for design RT–2 near MCC, Zheleznogorsk, 16–20 March 1998, Published in St. Petersburg, 1999.

EXPERIMENTAL STUDIES RELATED TO CHEMICAL DURABILITY OF SPENT FUEL ANDER REPOSITORY CONDITIONS

A. MARTÍNEZ-ESPARZA,

ENRESA. Madrid, Spain

Authors and Contributors: J.A. GAGO (ENRESA, Madrid, Spain), J. QUIÑONES, J. SERRANO, J. COBOS, P. DÍAZ AROCAS, A. GLEZ HUEBRA (CIEMAT, Madrid, Spain), I. CASAS, J. DE PABLO (UPC, Spain), J. MERINO, E. CERA (ENVIROS, Madrid, Spain)

Abstract

Chemical durability of spent fuel under repository conditions is one of the main topics of interest in national and international projects from the last two decades. During the last decade Enresa's activities in related to the deep disposal concept have been growing with the aim of developing a spent fuel alteration model for the understanding of the behaviour of this nuclear waste under repository conditions. In this context, the development and utilisation of models and sub-models based on experimental work have been of great importance.

Experimental studies with spent fuel and spent fuel analogues in several environmental conditions have been carried out in most of international research centres in order to reach a better knowledge of the relevant processes and to quantify the spent fuel behaviour under repository conditions.

In this work, it is showed the utility of data provided from experiments with spent fuel analogues to test the mechanisms and the influence of relevant parameters in the spent fuel alteration under repository conditions.

The occurrence of natural uraninites with several alteration degrees as a function of their location has supplied complementary information about the behaviour in natural systems of uranium dioxides, and some radionuclides included in it. In addition, dissolution experiments by using these minerals as solid samples have also given some new evidences on the processes taking place in such systems.

The evolution of irradiated fuel under interim storage conditions and in deep geologic disposal and its oxygen to metal ratio (O/M) before the water access to the fuel is another factor of great influence on enhanced spent fuel leaching. This effect has also been studied by means of spent fuel analogues and by using artificially aged fuel.

Based on the experimental work presented in this project but also on all the experimental work carried out during the last decade by the different groups involved in the R+D of Enresa (de Pablo et al., 1999, de Pablo et al., 2001, de Pablo et al., 2003, Giménez et al., 2001, Quiñones et al. 2001, Quiñones et al., 2002, Serrano et al., 1998, Serrano 2000, Serrano et al., 2001, Torrero, 1995), we have developed a conceptual and mathematical model with the aim of studying the stability of spent fuel under repository conditions, for both the alteration of the fuel matrix and the radionuclide release.

Finally, we present a comparison of the different approaches used in performance assessment exercises to describe spent fuel alteration under repository conditions. The results are also presented for comparison.

1. EXPERIMENTAL STUDIES

1.1. Surface and dissolution studies of uraninite

First we proceeded to study the surface oxidation of some uraninites from Palmottu (Finland). The reactive surface area of the samples was determined by using the BET methodology. The mean value obtained was 0.36 ± 0.01 m^2 g^{-1}. Uraninites were examined by X-ray Photoelectron Spectroscopy (PHI Perkin Elmer ESCA Multianalyzer 5500 using an Al-K X-ray source: 1486.6 eV). The contribution of U(IV) and U(VI) on the solid surface was based on the deconvolution of the U(4f) peak.

Results of the deconvolution treatment are shown in Table I. As it can be observed, surface oxidation of the uraninites can be easily related to the depth.

TABLE I. U(IV) AND U(VI) RATIO ON THE URANINITE SURFACE

Bore hole(depth)	Area U(IV)	Area U(VI)	U(IV)/U(VI)
R304 (71.70 m)	18349	4816	3.81
R304 (15.10 m)	6753	4385	1.54

Dissolution studies were performed with uraninites from Borehole 304 (depth 71.1 m) for having a lower oxidised surface being similar to the oxidation degree determined in UO_2 samples. Two dissolution experiments were performed in batch conditions and at room temperature, sodium perchlorate 0.01 mole·dm^{-3} was used as constant ionic medium. The first one was carried out in contact with air, and the second one in a nitrogen atmosphere.

Uraninite dissolution under oxidising conditions

The general trend of the uranium concentration in solution with time was an initial release of uranium until reaching a steady-state. This steady state was in accordance with the calculated solubility of schoepite. Therefore, in order to model by means of a kinetic approach dissolution data, the following processes were considered

— Uraninite dissolution to form the predominant $(UO_2)_2CO_3(OH)_3^-$ aqueous complex, which is the predominant aqueous complex under the experimental conditions, approximately 90%., and

— Schoepite precipitation from the dissolved U(VI) species.

By solving the corresponding rate equations, we obtained the following expression for the uranium concentration as a function of time:

$$[U] = \frac{C}{D} \times (1 - \exp(-D \times t)) + \frac{A}{B} \times (1 - \exp(-B \times t)) \times \exp(-D \times t) \quad (1)$$

where:

$$A = k_1 \times [HCO_3^-]$$
$$B = k_{-1} \times [H^+]^4 \times [e^-]^4$$
$$C = k_{-2} \times [HCO_3^-]$$
$$D = k_2$$

The fitting of the model to the dissolution data is shown in Figure 1.

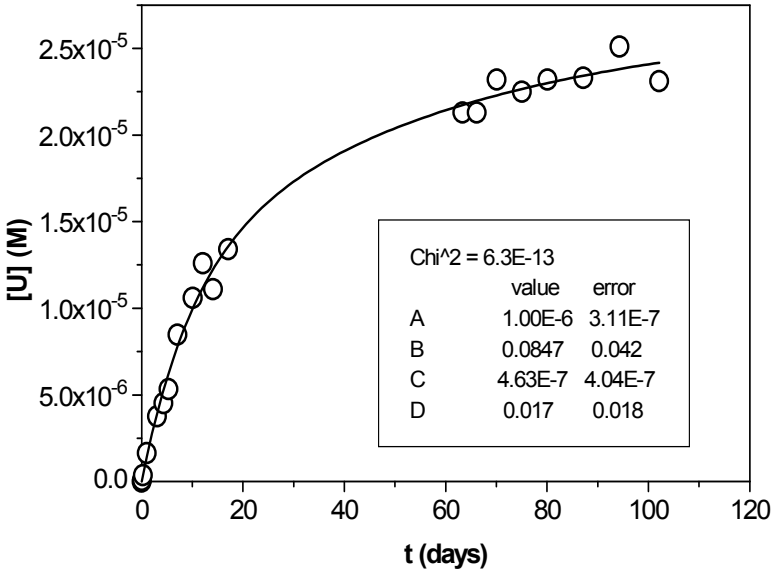

FIG. 1. Uranium concentration as a function of time, solid line gives the fitting of the experimental data by the analytical equation

By using the fitted parameters we obtained an initial dissolution rate of $4.22 \cdot 10^{-12}$ mol·dm^{-2}·s^{-1}, a value in good agreement with the one obtained by using dissolution data from saturation conditions.

Uraninite dissolution under anoxic conditions

A dissolution experiment was also carried out in a nitrogen atmosphere; the general trend of the evolution with time of the uranium concentration in the solution was, as in the previous case, an initial release of uranium until it reaches a steady-state level. The measured U concentrations in solution at the steady state would correspond to the uraninite solubility under anoxic conditions ($5 \cdot 10^{-8}$ mole·dm^{-3}). However, the test continued with two sequential U(VI) inputs into the system. As depicted in Figure 2, the data show a rapid decrease of the induced U concentrations to reach the same levels as the ones previously attained in equilibrium with uraninite. They indicate a

very efficient and reproducible scavenging effect of the U(VI) by the UO_2 surface. Two potential mechanisms could be responsible of this phenomenon:

— sorption of U(VI) at the UO_2 surface.

— sorption of U(VI) at the UO_2 surface followed by the reduction of the attached U(VI) to U(IV).

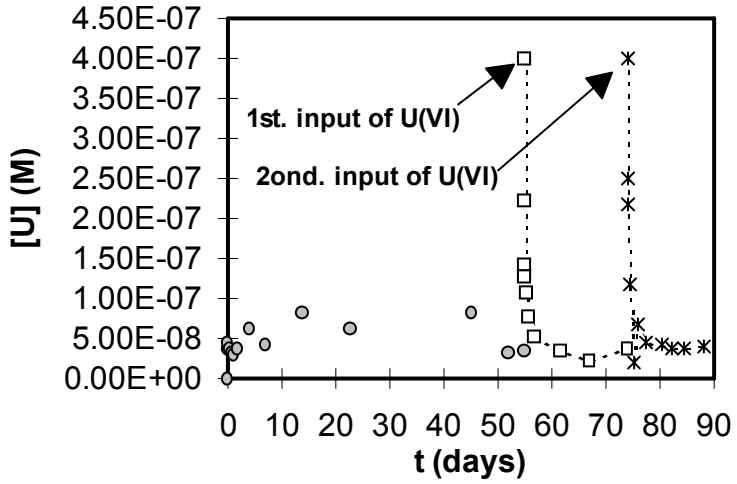

FIG. 2. Uranium concentration as a function of time. The arrows indicate the inputs of U(VI) added in the test solution.

1.2. Influence of the O/M ratio on the dissolution behaviour of spent fuel, UO_2 and MOX

Specimen fragments about 0.3 g in weight were taken from the central part of LWR UO_2 and MOX spent fuel pellets irradiated to burn-ups of 53 and 39 GWd/t respectively. The O/M ratios calculated assuming that all the weight change is due to the oxygen reaction with uranium are shown in Table II.

TABLE II. O/M RATIO OF THE SPECIMENS USED IN LEACHING TESTS.

Spent Fuel	**Oxidation time (days)**			
	0	**10**	**30**	**120**
UO_2	2.0	2.35	2.40	2.44
MOX	2.0	2.34		2.53

Dissolution tests with the oxidised fuel fragments were performed in batch, at room temperature and in deionised water. Assuming an ideal spherical form, the geometric area of the sample gave a calculated surface/volume ratio of approximately 2 m^{-1}. Solid samples were taken sequentially, by using new leaching solutions in each sampling interval. Chemical analyses were performed by ICP-MS (ELAN 5000, Perkin Elmer Sciex).

The cumulative fractional release of U from UO_2 and MOX specimens at different O/M ratios is represented in Figure 3.

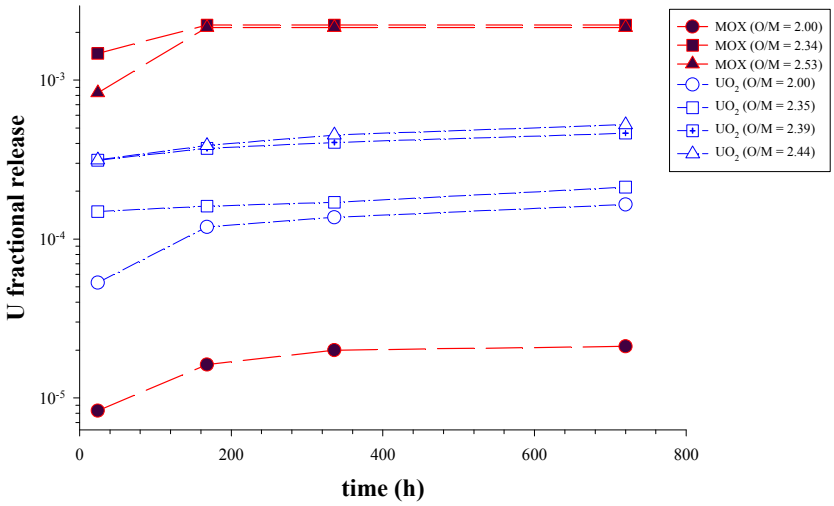

FIG. 3. Cumulative fractional release for U as a function of contact time from UO_2 and MOX fuel specimens.

As expected, for both types of fuel the initial fractional release is higher when the O/M ratio increases, due to the presence of increasing amounts of soluble U(VI) at the surface of the fuel particle. An additional contribution probably comes from less dense U phases formed during the oxidation treatment, leading to a higher surface area exposed to the water attack. However, this effect is strictly limited to the first instantaneous release represented by the first measurement after 24 h. Subsequent leaching steps were not affected by the oxidation degree of the fuel and showed very low leaching rates ($3 \cdot 10^{-7}$ g.cm^{-2}.d^{-1} for UO_2 and 2 10^{-7} g.cm^{-2} d^{-1} for MOX fuel) independently from the oxidation degree of the fuel.

Comparing the non-oxidised samples, the U fractional release of UO_2 fuel is about one order of magnitude higher than for the MOX fuel. This strong difference is related to the different microstructure mentioned above. In fact, in MOX fuel, fission events are of course mainly concentrated at the Pu-agglomerates and leave the main matrix, i.e. most of the surface exposed to the leachant is practically unchanged. For UO_2, on the contrary, the fission events and the related surface changes are homogeneously distributed on the total surface of the fuel particle.

The situation changes for the oxidised fuel samples. For UO_2, the U release rate increases by about half an order of magnitude and for MOX fuel by more than two orders of magnitude. This result can be explained by the fact, that MOX fuel presents a higher bias to oxidation at low temperature than irradiated UO_2 fuel. This higher U(VI) content and also the physical degradation due to the formation of a less dense phase leads to a higher fractional release explaining the values obtained.

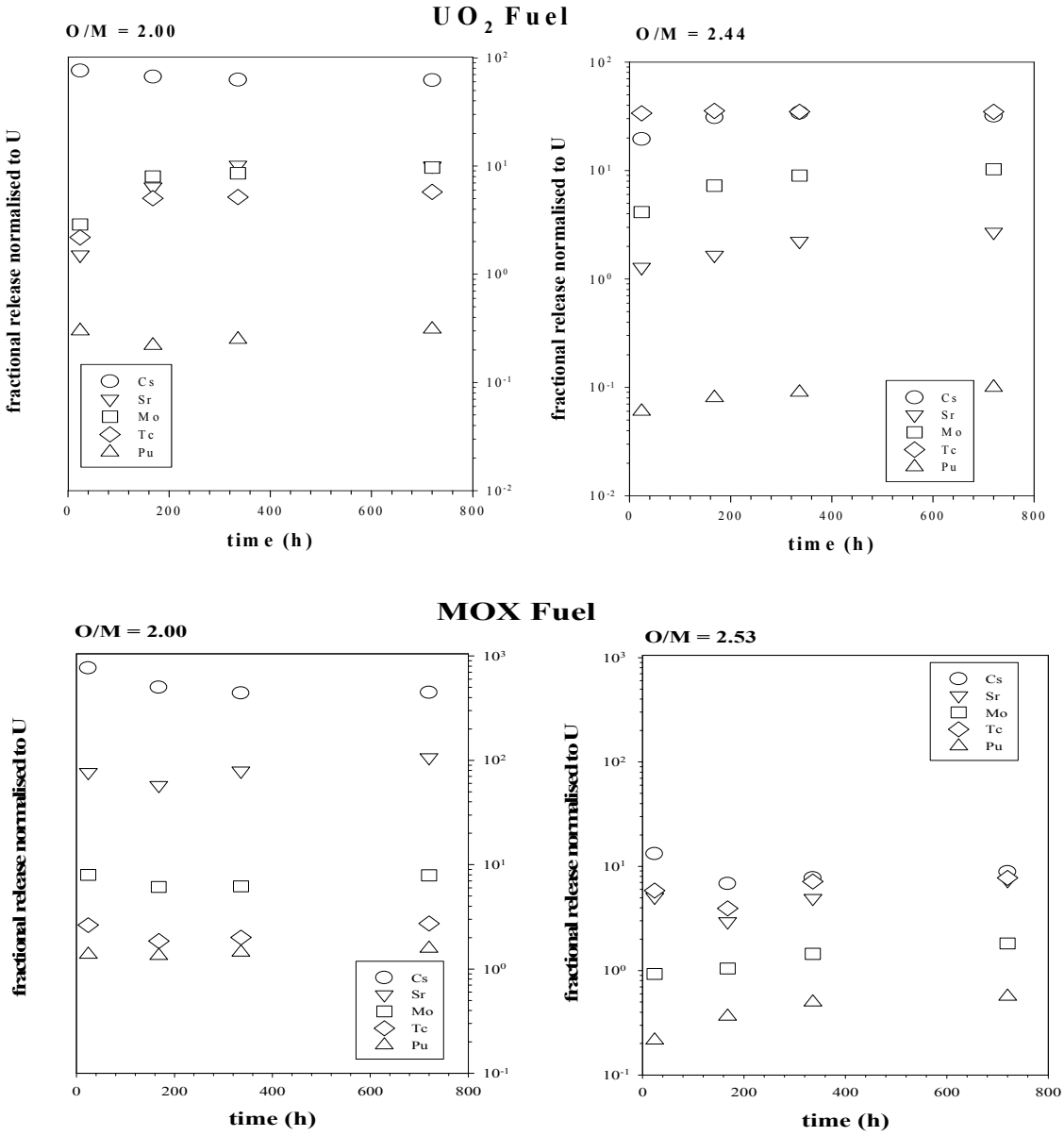

FIG. 4. Influence of the O/M ratio on fractional release normalised to U for several fission products and Pu.

The fractional release normalised to U for the main fission products and for Pu is shown in Figure 4. A comparison is made between the non-oxidised specimen and the one with the highest oxidation degree. Fission products show in all cases a higher fractional release than U. This has been attributed in some cases to the migration of the fission products to the grain boundaries upon irradiation which becomes weaker after the oxidation treatment or to the inherent higher solubility of some elements.

The difference between the fission products and U fractional release is reduced for the oxidised sample, especially in the case of MOX. The exception is Tc due to its known intrinsic redox sensitivity. The oxidation has led to an extensive oxidation of Tc, present at the grain boundaries, to the highly soluble TcO_4^-.

For Pu the normalised fractional release is lower than that of U with the exception of the non-oxidised MOX sample, where, as shown above, the U release rate is very low.

The special structure of MOX fuel with Pu agglomerates incorporated in a matrix of natural UO_2 leads to an increased sensitivity towards oxidation and as a consequence to a higher fractional release of U compared to UO_2. MOX can be considered as a two-phase material with Pu and fission products mainly contained in agglomerates. The Pu amount released from the UO_2-fuel is low and not affected by the oxidation level of the fuel.

2. SPENT FUEL ALTERATION MODEL

The kinetic model of oxidation-dissolution of the spent fuel we have developed is based on a mass balance approach including thermodynamic and kinetic information in order to study the evolution of the fuel/water subsystem with time. The main points on which the model is based are:

— The fuel/water interface is a dynamic redox system. This is because there is a time-dependent generation of oxidants and reductants at the fuel/water interface due to α radiolysis. Only alpha radiation is considered as it is assumed a long delay before the engineered barriers fail (a thousand years).

— Experimental studies of dissolution of irradiated fuel and generation of oxidants have showed a deficit in the production of oxidants related to hydrogen. This deficit has been interpreted as an uptake of the oxidants by the UO_2 surface (Eriksen et al., 1995, Bruno et al., 1999).

— The uranium dioxide allows additional oxygen in its cubic structure without destabilising it up to a threshold oxidation state corresponding to the solid phase $UO_{2.33}$ (Allen and Tyler, 1986; Shoesmith and Sunder, 1992). From this oxidation state, the oxidative dissolution of the fuel matrix evolves to the formation of $UO_3 \cdot xH_2O$ and the consequent formation of oxi-hydroxides of uranium(VI) (becquerelite) and silicates and phosphates of uranium(VI) (soddyte, uranophane, etc) (Forsyth and Werme, 1992; Wronkiewicz et al., 1992; Finch and Ewing, 1991).

— The rate of matrix dissolution increases in the presence of oxidants and complexing agents in the system, particularly bicarbonates (Forsyth and Werme, 1992; Torrero, 1995).

The chemical stability of the used fuel will depend on a few parameters, basically pH, Eh and contents of bicarbonates in the water. It is clear that the redox potential is the most critical of all of them. The oxidant species generated by the radiolysis of water will, consequently, be a factor in the destabilisation of the fuel/water interface.

Based on the previous statements, the alteration processes we may expect under repository conditions for the spent fuel matrix are described below.

The radiolysis of water generates oxidant species able to oxidise the surface of the spent fuel matrix according to the general reaction scheme:

$$UO_2(s) + \text{oxidants } (O_2, H_2O_2, \ldots) \rightarrow UO_{2+x}(s) \quad (2)$$

Once the surface is oxidised, its dissolution proceeds favoured by the interaction of the carbonate ligands with the uranium in its oxidised form, given the strong complexation of this metal with these aqueous ligands. This process can be depicted with the following reaction:

$$UO_{2+x}(s) + 2CO_3^{2-} \rightarrow x\ UO_2(CO_3)_2^{2-} + UO_2(s) \quad (3)$$

The concentration of the dissolved uranium will increase with time until reaching concentrations high enough to trigger the precipitation of secondary solid phases. The first phases to precipitate, which correspond to the kinetically favoured phases, are oxides and hydroxides like schoepite. This process can be written:

$$UO_2(CO_3)_2^{2-} + 2H_2O \rightarrow UO_3 \bullet H_2O(s) + 2H^+ \quad (4)$$

The next steps in the alteration processes of the spent fuel matrix will be quite dependent on the chemical composition of the waters contacting the surface of the fuel. The sequence of alteration commonly seen in natural systems (Finch and Ewing, 1992) and laboratory studies (Wronkiewicz et al., 1992) is the alteration of uranium oxides and hydroxides to silicates and phosphates depending on the water composition.

The alteration and dissolution of the spent fuel matrix leads to the release of the radionuclides contained in it. The more soluble radionuclides located in the gaps will be washed out as soon as the water gets in contact with the spent fuel. The radionuclides embedded in the matrix will be released as the dissolution of the matrix proceeds. The radionuclides forming metallic inclusions will be also dissolved although its dissolution pattern is not well known.

Conceptual model

The main factors affecting the release of the radionuclides associated to the fuel matrix are:

— The generation of oxidants due to the alpha radiolysis of water and subsequent matrix alteration due to the contact of groundwater.

— Release by dissolution of the radionuclides embedded in the matrix.

— Possible precipitation of secondary phases and eventual equilibrium conditions by means of their saturation.

A schematic representation of the system is depicted in Figure 5.

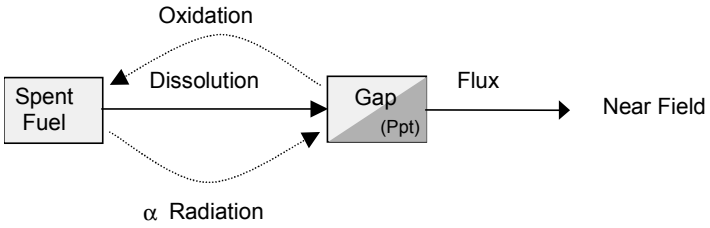

FIG. 5. Conceptual model of the system.

The release of the radionuclides and stable isotopes from the fuel will depend on their location (matrix, gap/grain boundary) or their physico-chemical association in the matrix. In order to simplify the system, we consider an instantaneous release of the elements located in the gap/grain boundary and a congruent dissolution of the elements located in the matrix with the main component, uranium.

The data concerning the matrix alteration as a result of the radiolytic processes is taken from a previous work (Merino et al., 2001). The radiolytic model developed for quantifying the spent fuel matrix alteration rate is included in the next section as a direct application to the PA exercises carried out by Enresa both in granite and in clay environments. The unit rate of matrix dissolution that varies with time as a function of the dose rate is included in the present model for calculating the dissolution rates of the radionuclides embedded in the spent fuel according to congruency.

From the initial dissolution, the elements accumulate in the gap. Pure or mixed secondary phases will precipitate if solubility limits are reached. The stability of these phases depends on the geochemical conditions and residence time of the water in the gap.

Mathematical model

As aforementioned, the mathematical model has been developed based on kinetic mass balance equations in order to study the evolution of the spent fuel – water interface as a function of time. Several processes have been kinetically modelled: instant release fraction, congruent dissolution, radioactive decay and ingrowth (in the pellet, the water and the precipitate) and water turnover in the gap. A description of the equations used can be found in a previous work (Cera et al., 2001). The precipitation/redissolution of secondary solid phases has been taken into account from a thermodynamic point of view. The solubility limits have been given as a function of time as the chemical conditions in the contact water evolve due to the interaction with the bentonite. The thermodynamic calculations have been performed with the code EQ3NR (Wolery, 1992) using a previously compiled database (Cera et al., 2000). Both kinetic and thermodynamic approaches have been coupled using a compartmental modelling software called AMBER (1999) which solves non-linear features such as those given by the use of the solubility limit concept.

Results

The modelling results are shown in the following figures where quite different behaviours can be observed.

In the case of Sr (Figure 6) there is an existing secondary phase but without determining its concentration in the gap water, as the release of this element is not high enough to reach the solubility limit. As a consequence, the concentration of Sr is kinetically controlled. Similar behaviours are observed for Cl and Cs although they are not reported in this work.

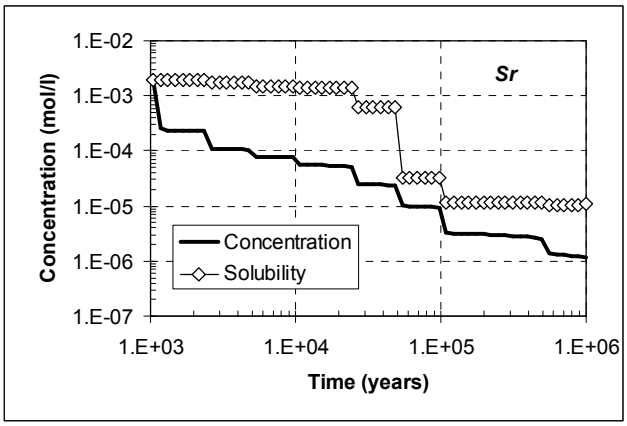

FIG. 6. Evolution of the concentration of Sr in the gap water.

The concentration of Np is expected to be always limited by the precipitation of $Np(OH)_4(s)$ in the repository conditions studied (Figure 7). The solubility increase with time is given by the evolution of the intruding waters. ^{237}Np is the main isotope (~100%) at 1.000 years with a half-life of $2.14 \cdot 10^6$ years, consequently the evolution with time of this isotope will be the same.

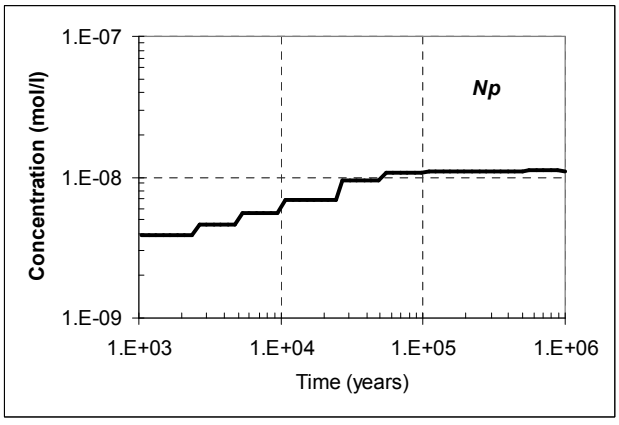

FIG. 7. Evolution of the concentration of Np in the gap water

The concentration of Pu will be thermodynamically controlled by the solubility of $Pu(OH)_4(s)$ (Figure 8). The different solubility limits are also a result of the

geochemical evolution of the water. The evolution of its main isotopes is the result of their different half-lives coupled with their common share of the solubility of the element. The concentration of ^{242}Pu (t1/2 = $3.76 \cdot 10^5$ years) increases with time because the shorter lived and initially predominant isotopes; ^{239}Pu and ^{240}Pu (t1/2 = $2.41 \cdot 10^4$ and $6.54 \cdot 10^3$ years respectively) decay away in the pellet, water and precipitate. At the end of the simulation, only ^{242}Pu remains in the precipitate and dissolves to keep the concentration in the gap at the solubility level.

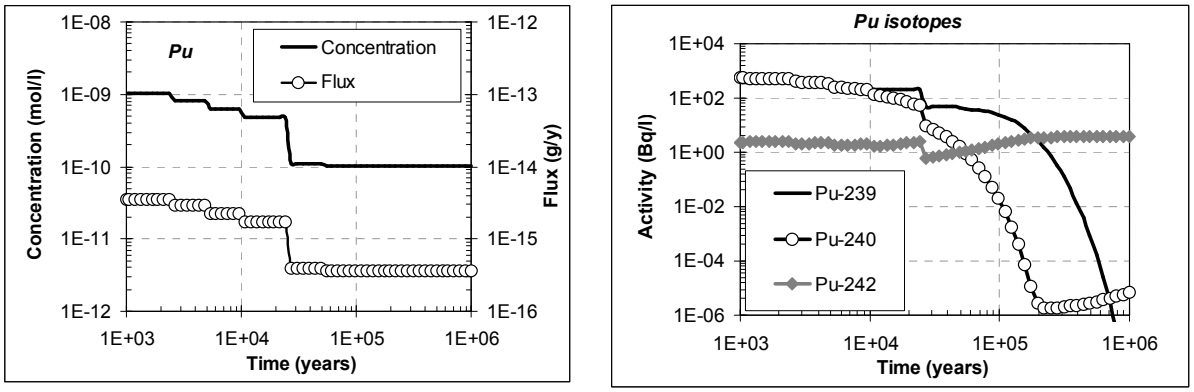

FIG. 8. Evolution of the concentration of Pu in the gap water, and flux out of the system (left). Evolution of the activity of several Pu isotopes in the gap water (right)

Finally, for Am, a solubility control limited by the precipitation of $AmOHCO_3(s)$ is obtained in the early stages of the simulation following a kinetic control until the end (Figure 9). This mixed behaviour is explained by the half-lives of the main radionuclides, Am-241 with t1/2 = 432 years and Am-243 with t1/2 = 7.380 years, that lead to their radioactive decay in relatively short time periods.

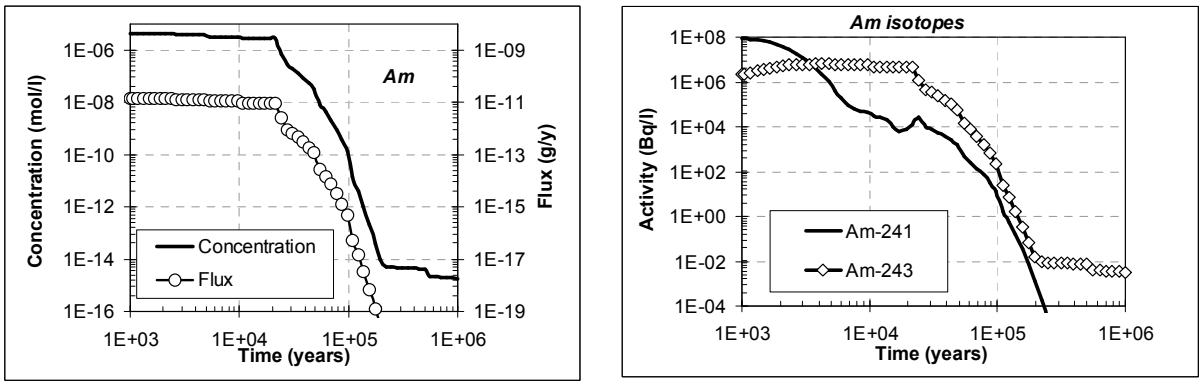

FIG. 9. Evolution of the concentration of Am in the gap water, and flux out of the system (left). Evolution of the activity of the main Am isotopes in the gap water (right).

The results of the model show that three groups of elements can be distinguished. A first group, with highly insoluble secondary phases, is characterised by a thermodynamic control of their concentrations in the gap: Zr, Pd, Ag, Sn, Sm,

Np, Pu and Am. Secondly, there are elements, like C, Cl, Rb, Sr, Nb, I, Cs, Bi and Pa, with no identified secondary phase under the assumed chemical conditions or the initial inventory of the elements in the pellet is not high enough to reach the solubility limit. Therefore, the concentration of these elements in the gap is kinetically controlled. A third group comprises the rest of the elements, where a mixture of kinetic and thermodynamic control is given depending on solubility, initial inventory and half-life of their radioactive isotopes. These elements are Ni, Se, Mo, Tc, Ra, Th, Am and Cm.

The conceptual and numerical findings of this work are relevant to establish source term models for spent fuel repository performance assessment calculations.

3. MODELS USED IN PA TO DESCRIBE WASTE FORMS DURABILITY UNDER REPOSITORY CONDITIONS

In this section we performed a comparative analysis of the different spent fuel alteration models used in PA exercises by reviewing six works: ENRESA 2003 (Clay), ENRESA 2000 (Granite) (Enresa, 2001), Opalinus Clay (Nagra 2002), Yucca Mountain Project (DOE 2000), SAFIR (ONDRAF/NIRAS 2001, ONDRAF, 2001), H-12 (JNC 2000). Here after, we present a brief summary of the critical review, as well as the spent fuel matrix alteration model used by ENRESA in both PA exercises, clay and granite.

3.1. ENRESA 2000 and ENRESA 2003

The matrix alteration model developed by ENRESA is based on several sets of chemical reactions involving radicals and species produced by the radiolysis of water that is a radiolytic model. In order to quantify the amount of species generated radiolytically as well as the alteration degree of the spent fuel matrix the model integrates the processes described above, that is:

— Generation and recombination of radiolysis products, i.e. generation of oxidant and reductant compounds and radical species and recombination reactions.

— Spent fuel surface alteration processes. Spent fuel oxidation processes are included in the reactions scheme for taking into account the effect on the oxidants consumption by the spent fuel surface in the overall balance of the species generated radiolytically. Different assumptions lead to different reactions schemes taking part in the evolution of the system.

The model assumes that when the groundwater achieves the surface of the fuel α radiolysis is done. Because of the generation of oxidants and reductants, the surface of the fuel will oxidise as well as other sensitive radionuclides. Dissolution of the oxidised surface will occur due to attachment of aqueous ligands. Finally, the precipitation of pure phases will be taken into account when solubility limits are reached.

The radiolytic model used in Enresa 2000 and Enresa 2003 consisted on an irradiated UO_2 pellet from a typical PWR fuel in contact with water, the geometry of the system (Figure 10) as well as the parameters of interest are reported in Quiñones et al. (2000).

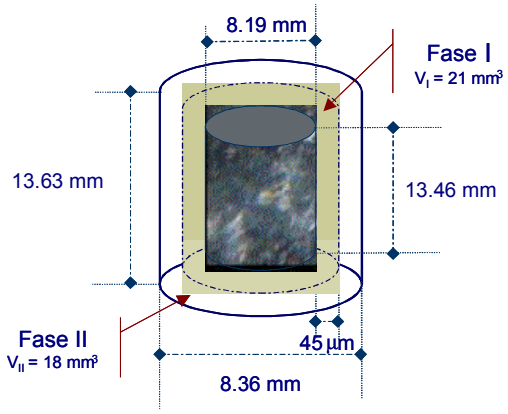

FIG. 10. Scheme of the geometry considered in ENRESA–2000 and ENRESA–2003 PA studies

Recombination reactions of radicals and species were taken from (Christensen and Sunder, 1998). In Enresa 2000 two approaches were used to characterise the alteration of the matrix by the oxidants present in the water. The first approach was a set of reactions between all the radicals and molecular species and the UO_2 surface, assuming that these heterogeneous reactions can be described as reactions in monophase with appropriate kinetic constants. This is the "conservative" case named GTI02. The other approach was to include the reactions of O_2 and H_2O_2, the main oxidants in the system, with the UO_2. In such case kinetic constants were derived form experimental works. This represents the "realistic" case named GTI04. A more detailed description can be found in Quiñones et al. (2000). In Enresa 2003 only the realistic approach was used, in such case, an UO_2 alteration scheme was derived from semi-empirical models developed by de Pablo and co-workers (de Pablo et al., 1999, de Pablo et al. 2001, de Pablo et al., 2003). A more detailed description can be found in Cera et al. (2003).

Computer codes, i.e. CHEMSIMUL (Kirkegaard and Bjergbakke, 1999) and Maksima (Carver et al., 1979) are used to solve the system of differential equations representing the chemical reactions of the system.

Figure 11 shows the evolution of the matrix alteration calculated in both exercises.

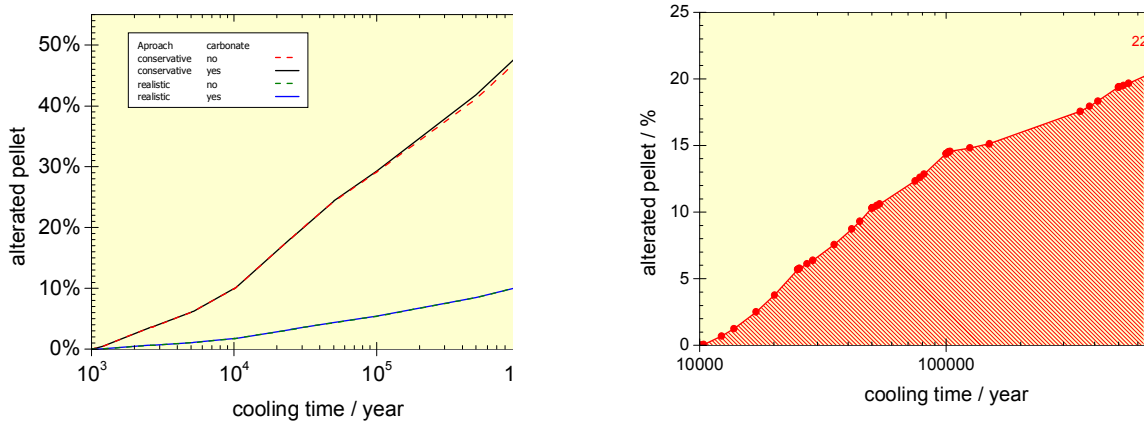

FIG. 11. Evolution of the spent fuel pellet in Enresa 2000 (left) and Enresa 2003 (right)

Figure 11 on the left shows the final results obtained in Enresa 2000 considering both approaches; conservative and realistic. As can be observed the conservative one produces a higher alteration of the matrix than in case of the realistic one. In both cases there is not any difference when considering or not the presence of carbonate. This is because in the reaction scheme considered in Enresa 2000 exercise, only the interaction of carbonate with water species was considered and there was not any reaction involving carbonates and the spent fuel matrix. Figure 11 on the left shows the results obtained in Enresa 2003. This new matrix alteration mechanism considers the oxidation of the pellet surface by O_2 and H_2O_2 (radiolytically generated) and the dissolution of the oxidised surface by interaction with water and carbonate species (Cera et al., 2003).

Differences are also attributed to different boundary conditions i.e., the presence of a constant hydrogen overpressure in the system, the different canister failure times and the slightly different groundwater evolutions.

The comparison of the results presented from both PA exercises could mislead that the repository in clay host rock is worse than in granite since the percentage of spent fuel pellet altered is higher. However, this is a direct consequence of the different mechanisms used. It is important to highlight that both developments are a consequence of an iterative study, which improves day to day and will continue in the future.

3.2. OPALINUS CLAY

The assumptions made and parameter values used in the Reference Case in the Opalinus clay were generally based on the expected evolution of the system components (NAGRA, 2002). Specifically, for spent fuel and vitrified high level waste the assumptions concerning alteration of the matrix and radionuclides release were:

For spent fuel:

— IRF is released from SF immediately upon canister breaching.

— Other RNs in the SF are released congruently with fuel matrix dissolution, at a rate dependent to the alpha activity of the fuel.

— All C-14 originating from the SF, including the IRF, is assumed to be in inorganic form. All C-14 from the zircaloy cladding s assumed to be in organic form (the overall IRF contains a mixture of organic and inorganic.

— A 20% of IRF C-14 is assumed is IRF. Other radionuclides in cladding are released congruently with cladding corrosion, assumed at a constant rate.

And for high level wastes:

— Vitrified HLW is solidified in thin stainless steel fabrication flasks, which are then placed in massive carbon steel canisters. The flasks do not have any assigned barrier function.

— Radionuclides in vitrified HLW are released congruently with glass dissolution at a constant rate per unit the waste surface area.

— Glass fragments are conceptualised as a number of equal sized spheres, with a total volume equal to the total volume of glass, and a total surface area that accounts for the cracking of the glass. The surface area of the spheres decreases with time as they dissolve.

— All canisters are assumed to breach simultaneously at a reference time of 10.000 years. No defective canisters are present. Conservatively assumption of there is not physical barrier to water ingress or radionuclide release.

— No credit is taken for the integrity of the SF zircaloy cladding and HLW fabrication flasks.

Four different compartments were considered: waste, bentonite, host rock and biosphere governed by a set of equations that were solved using the computer codes STMAN for the near-field and PICNIC for the host rock, together with biosphere dose conversion factors for the surface environment calculated with the code TAME (NAGRA, 2002).

The reference model chain of STMAN-PICNIC was used to model the radionuclide release and migration of a range of radionuclides that were judged to be safety relevant. Calculations were evaluated up to 100 million years. The results are described in (NAGRA, 2002) some results for illustrating are also depicted in Figure 12.

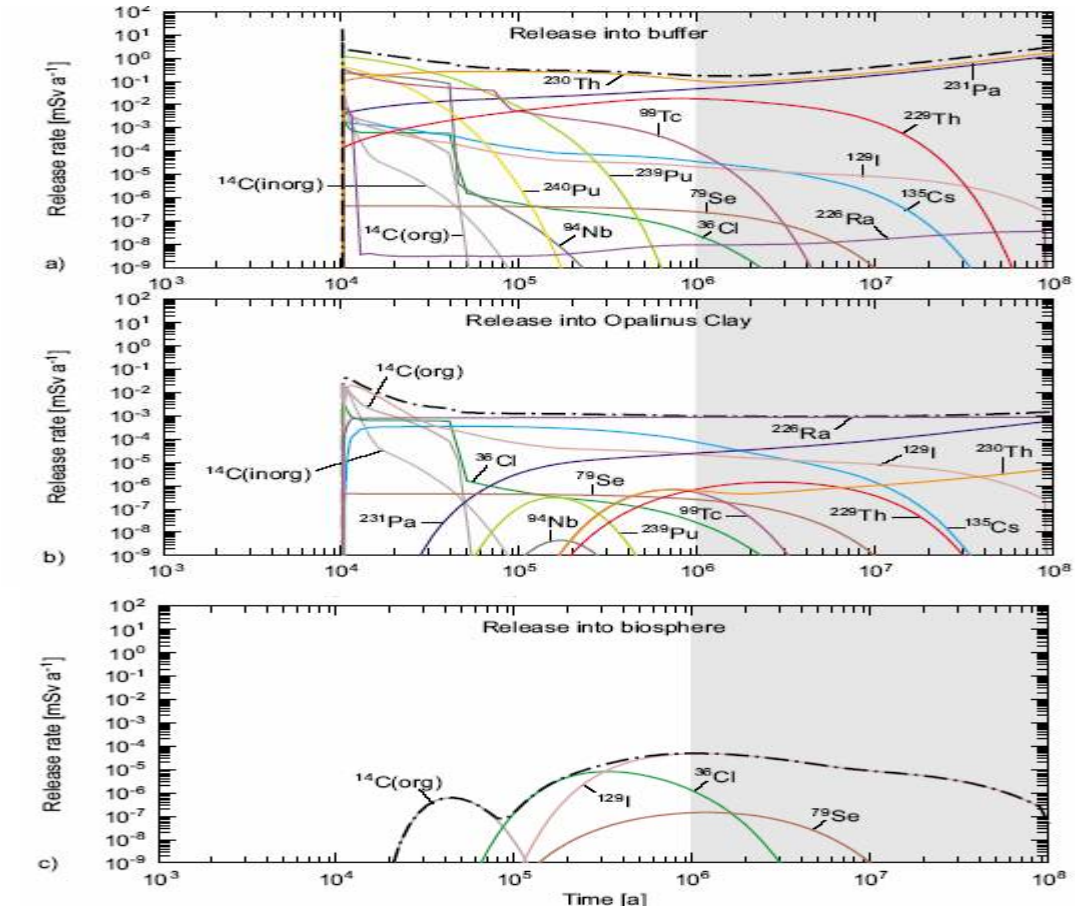

FIG. 12. Radionuclides release from SF to, a) the bentonite, b) the Opalinus Clay, c) the biosphere (taken from Nagra, 2000).

3.3. YUCCA MOUNTAIN PROJECT

Some of the assumptions made in the waste degradation model are listened below. More information on the assumptions made and the model conceptualisation may be found in the Waste form Degradation Model Report (2000).

- Type of wastes: SF and Vitrified wastes.
- Semi-empirical electrochemical model based on a large set of qualified experiments.
- Types of tests: Drip test, (in service conditions); dynamic tests (upper limit with no secondary phases formation), and batch tests (available in the literature for comparisons).
- Oxidant conditions; pH from 3 to 10.
- P_{O2} 0,002-0,2 atm.
- Cladding degradation model based on literature on cladding fuel. Dry unzipping and wet unzipping.
- Assumptions on instantaneous release for C-14, Cs-135, Cs-137, I-129, Tc-99, Se-79.
- 0,2% of total inventory (0-0,4%) all radionuclides.

— I-129, 4% of total inventory.
— Cs-137, 1,4% of total inventory.
— Tuft volcanic site (Yucca Montain).
— Containers SS+Alloy 22.

Two differentiated models were developed, for spent fuel and for glass matrices. A short description of both models is described below.

Spent fuel model

Electrochemical studies have shown fast reduction in dissolution currents when thin layers of corrosion products form, but an increase of UO_2 reactivity as the applied potential is increased.

The likely electrochemical reaction sequence is:

Surface oxidation	Bulk Oxidation	Dissolution

$UO_2 \Rightarrow UO_{2+x} \Rightarrow UO_{2.33}$ $\{UO_2^{+2}\}_{surface}$ $\Rightarrow [UO_2^{+2}]_{bulk}$ $\Rightarrow$ $[UO_2^{+2}]_{soln}$ $\Rightarrow$ Secondary Phases

From the tests and results obtained by a series of studies the dissolution model for alkaline conditions is:

$$\text{Log Rate} = 4.69 + [- 1085/T] - 0.12.\ p[CO_3]T - 0.32\ pO_2\ (mg/m^2/day)$$

where T is temperature (Kelvin); p denotes the negative logarithm of either the carbonate concentration (mol/l) or the oxygen partial pressure (atm).

To construct the abstracted acid dissolution model, the temperature and oxygen rate dependencies derived under alkaline conditions were assumed to hold for acid conditions. The pH 7 alkaline rate was then assumed to be common to the alkaline and acid pH rate laws (within the uncertainty of both rate laws) A qualified data point (pH = 3) was used to define the low pH end of the acid pH rate law. The latter, which describes rates at pH ≤ 7, is given:

$$\text{Log rate} = 7.13 + [- 1085/T] -.\ 0.32\ pO_2 - 0.41.\ pH$$

Model gives upper limits of matrix dissolution rate, Figure 13 shows the results of this semi-empirical model for all the pH range. Congruent dissolution of RNs included in the matrix was assumed. Concentrations in dissolution were controlled by solubility's limits in such conditions.

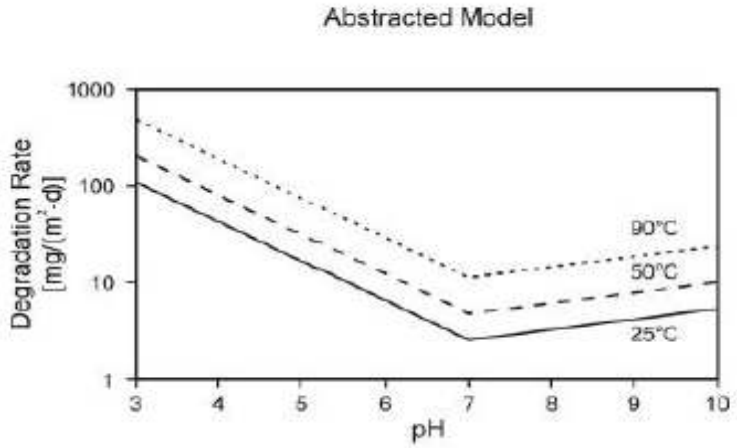

FIG. 13. Spent fuel matrix alteration rates (taken from Yucca Mountain Project, 2000).

Glass matrix model

Glass dissolution models are based on rate expressions for aqueous dissolution of borosilicate glasses.

Dissolution rates provide an upper bound to the release rates of radionuclides. Tests with a wide range of waste glass compositions have shown that radionuclides are released to solution more slowly than boron and other soluble glass matrix components. The dependence of pH and temperature is assumed to be the same for all waste compositions.

— The temperature dependence for glass degradation in humid air and dripping water follows Arrhenius behaviour like in water immersion.

— The glass corrosion is nil when glass is exposed to humid air at less 80% relative humidity.

— The rate expression used to calculate the dissolution of waste glass immersed in water is reported in the TSPA-VA (CRWMS M&O) and is expressed as follows:

$$\text{Rate} = S \{k . [1-(Q/K)] + klong\}$$

where

R = the dissolution rate of the glass, in units of mass/time

S = the surface area of glass immersed in water, in units of area

k = the glass dissolution rate, which is a function of the glass composition, temperature, and solution pH, in units of mass//(area. time)

Q = the concentration of dissolved silica in the solution, in units of mass/volume

K = a quasi-thermodynamic fitting parameter equal to the apparent silica saturation concentration for the glass, in units of mass/volume

klong = minimum long-term dissolution rate, in units of mass/(area time)

Figure 14 shows the results of the matrix degradation model for glasses.

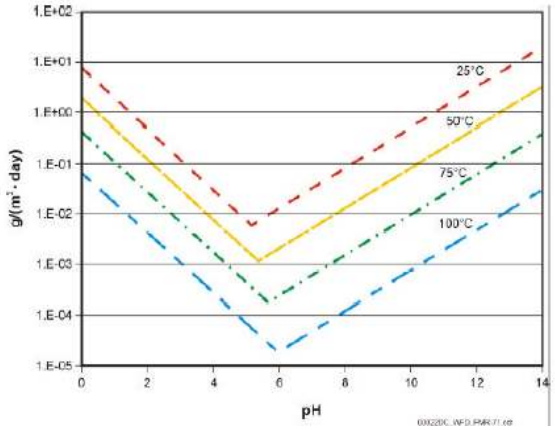

FIG. 14. Glass matrix dissolution rates (taken from Yucca Mountain Project, 2000).

3.4. SAFIR2

Two differentiated models are described, for spent fuel and for glass matrices. A short description of both models is described below.

Vitrified waste, (source term model)

Conceptually, dissolution takes place in three main steps:

— Interdiffusion, resulting in the formation of a hydrated zone that is impoverished in alkaline elements (ionic exchange with the alkaline in the glass).
— Hydrolysis of the glass network.
— Condensation and/or precipitation of the hydrolysed species resulting in the formation of an amorphous altered layer.

Modelling work is based on experimental data, experimental results show that the dissolution rate falls by several orders of magnitude over time, reaching very low levels under so-called saturation conditions, which are function of the system considered.

The retention of radionuclides in the altered layer on the glass surface depends on the nature of the element considered, the pH, and the presence or not of solid phases such as the boom clay or the FoCa clay. Safety assessments assume that radionuclide leaching is determined by the glass dissolution rate (retention factor of 1).

Modelling exercises on glass dissolution consider:

— Geochemical modelling aims to identify the secondary phases that are likely to form and to control the concentration of key elements like silica and critical, or

potentially critical, radionuclides released in the medium when the glass dissolves.

— Modelling of glass dissolution (kinetic model) aims to develop an analytical model linking the law of glass dissolution with the diffusion and sorption of silicates in the surrounding medium. This modelling has made some significant progress and has been helped by a very promising and original technique recently developed by SCK.CEN for studying dissolution mechanisms (including the formation of the altered layer) at microscopic level, and hence for verifying some of the hypotheses used to elaborate an analytical model.

The results of geochemical modelling of the system glass-water-clay suggest the Boom Clay could act as a silica pump. Within the limits of the thermodynamically selected data, the models predict no formation of secondary phases. The dynamics of the process of glass dissolution could, however, impose steady- state conditions different from those corresponding to thermodynamic equilibrium.

Long-term safety assessments conservatively assume that the glass-water-Clay system does not evolve towards saturation conditions. Despite this assumption, the durability of glass under repository conditions is several tens of thousands of years, the minimum durability calculated from the theoretical possible maximum dissolution rate.

Spent fuel, (source term model)

Conceptually, dissolution can take place as follows:

— Immediate dissolution of part of the radionuclides, then dissolution at a constant rate of the matrix for 1 million years and of the hulls and end pieces for 1000 years.

— Model of alpha auto-dissolution as in the previous case, but matrix dissolution is influenced by the oxidation, due to alpha radiolysis, of uranium oxide when placed in contact with water in a reducing medium.

An initial study of the solubility of UO_2 in the Boom clay as a function of key parameters such as the concentrations of dissolved carbonate and organic carbon indicates that organic matter has no significant effect on the solubility of uranium, which is very low in a reducing medium such as the Boom clay (approximately 10^{-8} $mol \cdot l^{-1}$). The influence of the carbonates is only observed in less severe redox conditions (complexation of the hexavalent uranium present in solution). According to the data reported in the literature, the UO_2 matrix also have significant durability over the time scales considered in the safety assessments.

Despite the importance of the spent fuel, the literature provides few data about its behaviour in the argillaceous environment. The first (recent) safety assessments of the disposal of spent fuel into the Boom clay therefore defined the source term by extrapolating to Clay the data available for disposal in granite. Studying the behaviour of spent fuel is further complicated by the need to consider different components, each characterised by a specific release rate and isotope inventory, and requires

simplifications for safety assessments. Studies give priority to the UO_2 matrix, which of course contains most of the activity.

For illustrating Figure 15 presents a picture of the activity fluxes at the interface between the Boom Clay and the Neogene Aquifer for the vitrified waste, the spent fuel, and the hulls and end pieces, assuming congruent dissolution and no formation of secondary phases (R=1).

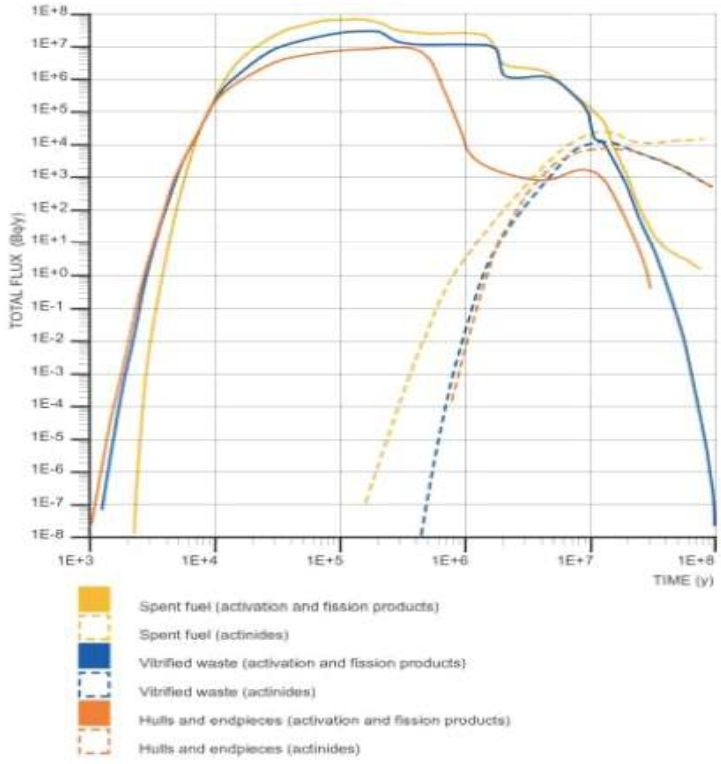

FIG. 15. Total Activity fluxes to aquifers for vitrified HLW, SF and hulls and end pieces (taken from ONDRAF/NIRAS 2001).

3.5. H-12

The H-12 safety assessment considers a source term model based on the following premises:

— RN dissolution from the vitrified waste.

— Diffusion and sorption in the buffer material.

— Radioactive decay and ingrowth.

— Release into the surrounding rock.

— The overpack is designed to have a minimum lifetime of 1,000 years. Subsequent to the first 1,000 year, it will fail mechanically due to decreased strength caused by corrosion.

— At the time of overpack failure, the heat generated by the vitrified waste (VW) will have decayed to a negligible level and the temperature in the repository will approach that of surrounding host rock. The buffer material will be completely

water-saturated, providing a homogeneous low-permeability barrier around the overpack.

— The surface area of the VW after disposal will exceed its original geometric surface area due to cracking during cooling in the vitrification process and fragmentation due to corrosion expansion of the overpack (A factor of 5 is used).

The glass dissolution is expressed in terms of a long-term glass dissolution rate. The concentrations in the vicinity of the VW are described by the mass balance equation (1), which includes the effects of congruent release with glass dissolution, solubility limits with precipitation/dissolution, diffusion into the buffer and radioactive decay/ingrowth.

$$V^R(\delta A_{ij}^R/\delta t) = 2\pi r_{in} L \varepsilon^B D_{pi} (\delta C_{ij}^B/\delta r)\Big|_{r=r_{in}} + M_{ij}^{Glass} g_{Si} - V^R \lambda_{ij} A_{ij}^R + V^R \lambda_{IJ} A_{IJ}^R \qquad (1)$$

where

V^R : Volume of the hypothetical water-filled region [m^3]

M_{ij}^{Glass} : Inventory of isotope *j* of element *i* in the VW [mol]

g_{Si}: Fractional rate of decrease of the glass volume [y^{-1}]

L: Buffer length [m]

D_{pi}: Diffusion coefficient in porewater [$m^2 y^{-1}$]

ε^B: Porosity of the buffer material [-]

r : Distance from the center of VW [m]

r_{in}: Inner radius of the buffer material [m]

t : Time after overpack failure [y]

λ_{ij} : Decay constant [y^{-1}]

RN sorption in the hypothetical water-filled region is not considered.

The VW form is surrounded by buffer material, and thus the dissipation of dissolved silica released from the glass is limited by molecular diffusion. As the glass dissolution reaction progresses, the concentration of dissolved silica in the vicinity of the glass increases and approaches the saturation level. For the Reference Case, the glass dissolution rate at 60ºC is defined to be 1mg m^2 d^{-1}. Based on the glass hydration model, the glass dissolution rate should decrease further on a longer time scale. However, this possibility in the safety assessment is conservatively ignored.

RN migration in the EBS is calculated for a single WP. Because the modelling of diffusion is one-dimensional it does not account for transport through the buffer in the axial directions. The initial volume between the waste and the overpack is 0.15 m^3. A hypothetical length water filled surrounding the vitrified waste of 10^{-3} m^3 is assumed. The transport through the host rock and from here to the biosphere is solved

using a compartmental model, in which the concentrations of nuclides within compartments are uniform.

Calculated doses in the reference case are depicted in the following figure and compared to the results obtained in other safety assessments.

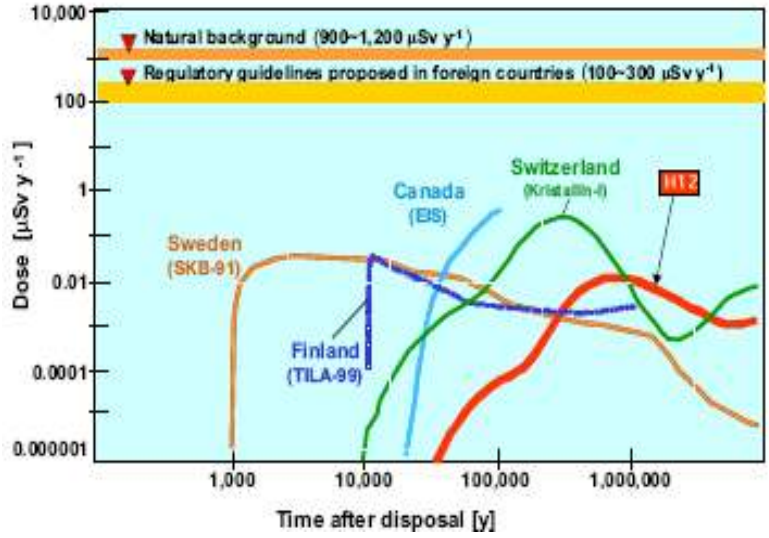

FIG. 16. Calculated doses in several safety assessment exercises (taken from JNC, 2000).

REFERENCES

[1] Allen G.C. and Tyler J.W., 1986. Surface Characterisation of α-U3O7 using X-ray photoelectron spectroscopy. J. Chem. Soc., Faraday Trans. 1, 82, 1367-1379.

[2] AMBER, 4.0 (1999) Reference Guide. QSL-5046a-1 Version 1.0 Oct 1998 Enviros Software Solutions, AMBER 4.2 Release Note QSL-5046A-4 Version 1.0 Nov 1999 QuantiSci Limited, Henley-on-Thames UK.

[3] Bruno J., Cera E., Eklund U.-B., Eriksen T.E. and Grivé M., 1999. Experimental determination and chemical modelling of radiolytic processes at the spent fuel/water interface. SKB Technical Report. TR-99-26.

[4] Carver, M. B., Hanley, D. V. y Chaplin, K. R., 1979. Maksima Chemist. A program for mass action kinetics simulation by automatic chemical equation manipulation and integration by using Stiff techniques, Vol. AECL-6413. AECL.

[5] Cera E., Merino J. and Bruno J. (2000), Liberación de los radionucleidos e isótopos estables contenidos en la matriz del combustible. Modelo conceptual y modelo matemático del comportamiento del residuo, Enresa Publicación Técnica 3.

[6] Cera E., Merino J. and Bruno J. (2001) Release of radionuclides from spent fuel under repository conditions: mathematical modelling and preliminary results. *Mater. Res. Soc. Symp. Proc* Vol. 663, 459-468.

[7] Cera E., Merino J., Bruno J., Quiñones J., Martínez-Esparza A. (2003) ENRESA2003. AGP Arcilla. Modelo de alteración del combustible nuclear gastado. Enviros, Informe Final v.3. Noviembre, 2003.

[8] Christensen H. and Sunder S. (1998) Current state and knowledge in radiolysis effects on spent fuel corrosion. Studsvik Technical Report M-98/71.

[9] de Pablo J., Casas I., Giménez J., Molera M., Rovira M., Duro L. y Bruno J., 1999. The oxidative dissolution mechanism of uranium dioxide. I. The effect of temperatura in hydrogen carbonate medium. Geochim. et Cosmochim. Acta, 63 (19/20), 3097-3103.

[10] de Pablo J., Casas I., Clarens F., El Aamrani F. y Rovira M., 2001. The effect of hydrogen peroxide on the oxidative dissolution of unirradiated uranium dioxide. Mater. Res. Soc. Symp. Proc. 663, pp 409-416.

[11] de Pablo J., Casas I., Giménez J., Clarens F., Duro L. y Bruno J., 2003. The oxidative dissolution mechanism of uranium dioxide. The effect of pH and oxygen. Aceptado para presentar en el Materials Research Society Symposium de Kalmar, Suecia, junio 2003.

ENRESA (2001), ENRESA-2000. Evaluación del comportamiento y de la seguridad de un almacenamiento de combustible gastado en una formación granítica. 49-1 PP-M-15-01.

[12] Eriksen T.E., Eklund U.-B., Werme L.O. and Bruno J., 1995. Dissolution of irradiated fuel: a radiolytic mass balance study. J. Nucl. Mater. 227, 76-82.

[13] Finch R. and Ewing R., 1991. Uraninite alteration in an oxidizing environment and its relevance to the disposal of spent nuclear fuel. SKB Technical Report TR 91-15.

[14] Finch R. and Ewing R., 1992. Journal of Nuclear Materials 190**,** 133.

[15] Forsyth R.S. and Werme L.O., 1992. Spent fuel corrosion and dissolution. J. Nucl. Mater. 190, 3-19.

[16] Giménez J., Clarens F., Casas I., Rovira M., de Pablo J. y Bruno J., 2001. Oxygen consumption in uranium dioxide dissolution experiments inbicarbonate medium. Presentado en el Migration'01. Bregenz, Austria.

[17] JNC (2000). H-12 project to establish technical basis for HLW disposal in Japan. Project overview report and three supporting reports, JNC TN 1410.

[18] Kirkegaard, P. and Bjergbakke, E.., 1999. CHEMSIMUL: A Simulator for Chemical Kinetics. Riso National Laboratory.

[19] Merino J., Cera E., Bruno J., Eriksen TE., Quiñones J., Martínez-Esparza A., (2001) Long term modelling of spent fuel oxidation/dissolution under repository conditions, at: 8th International Conference on Radioactive Waste Management and Environmental Remediation, Bruges, Belgium.

[20] NAGRA, (2002). Project Opalinus Clay. Safety Report. Demonstration of Disposal Feasibility for Spent Fuel, vitrified high level waste and long-lived intermediate waste.

[21] ONDRAF/NIRAS (2001). SAFIR. Safety assessment and feasibility Report 2. Technical overview. December 2001.

[22] ONDRAF (2001). Aperçu technique du rapport SAFIR 2. ONDRAF, NIROND 2001-05F. Document pdf format from www.ondraf.be.

[23] Quiñones, J., Serrano, J., Díaz Arocas, P., Rodríguez Almazán, J.L., Bruno, J., Cera, E., Merino, J., Esteban, J.A., Martínez-Esparza, A., (2000). Cálculo de la generación de productos radiolíticos en agua por radiación □. Determinación de la velocidad de alteración de la matriz del combustible nuclear gastado. Publicación Técnica ENRESA 2/2000.

[24] Quiñones, J., Serrano, J. A. y Díaz Arocas, P. P., 2001. The effect of coprecipitation in solution and in the surface layer. J. Nucl. Mater. 298(63-68).

[25] Quiñones, J. y Serrano, J. A., 2002. Influencia del material del contenedor en la retención de radionucleidos. En: Participación del Ciemat en la reunión anual de la Sociedad Nuclear Española. Madrid: Ciemat, 2002. ISBN: 84-7834-415-2.
[26] Serrano J.A., Glatz J.P.,. Toscano E.H, Papaioannou D., Barrero J., Coquerelle M. (1998) Journal of alloys and Compunds 271-273 573-576.
[27] Serrano, J. A. (2000) Caracterización y lixiviación de combustibles nucleares irradiados y de sus análogos químicos, Complutense de Madrid.
[28] Serrano, J. A., Quiñones, J., Cobos, J., Díaz Arocas, P. P., Rondinella, V. V., Glatz, J. P., Matzke, H. j., Martínez Esparza, A. y Esteban, J. A. (2001) Leaching study of the behaviour of spent fuel and SIMFUEL under simulated granitic repository conditions. VIII Int. Conf. On Environmental Management.
[29] Shoesmith D.W. and Sunder S., 1992. The prediction of nuclear fuel (UO2) dissolution rates under waste disposal conditions. J. Nucl. Mater. 190, 20-35.
[30] Torrero M.E., 1995. Estudio de la disolución del UO2 como análogo químico de la matriz del combustible nuclear gastado. Influencia de los principales parámetros fisicoquímicos que definen los repositorios en medios salino y granítico. Ph. D. Thesis, Univ. de Barcelona.
[31] Wolery T.J. (1992) A Computer Program for Geochemical Aqueous Speciations-Solubility Calculations: Theoretical Manual, User's Guide, and Related Documentation, UCRL-MA-110662 PT III.
[32] Wronkiewicz D.J., Bates J.K., Gerding T.J., Veleckis E. and Tani B.S., 1992. Uranium release and secondary phase formation during unsaturated testing of UO2 at 90 oC. J. Nucl. Mater 190, 101-106.
[33] Yucca Mountain project. Waste form Degradation Model Report (2000). TDR-WIS-MD-0000001. July 2000

CHEMICAL DURABILITY AND PERFORMANCE ASSESSMENT OF SPENT FUEL AND HIGH LEVEL WASTE UNDER SIMULATED REPOSITORY CONDITIONS

S. KING
United Kingdom Nirex Limited, UK

Abstract

Nirex has developed a generic post-closure performance assessment (GPA) for intermediate-level waste (ILW) that is based on a range of geological characteristics consistent with conditions that could be found in the UK. The GPA is used to test the generic repository design, and to test the compatibility and safety of waste producers' packaging proposals with the repository concept and compliance with the Generic Waste Package Specifications. This approach has been expanded by Nirex to cover UK high-level waste (HLW) and spent nuclear fuel (SF) and other radioactive materials that may require long-term management.

Work started with performing a range of scoping studies and literature reviews to investigate the feasibility of co-location of UK intermediate-level waste, high-level waste (HLW) and spent nuclear fuel (SF) in a shared repository. The extent and impact of chemical interactions on HLW/SF repository performance were investigated by performing a range of sensitivity and scoping studies. Scoping studies were also performed to investigate the implications of including separated stocks of plutonium (if declared as waste or used as fuel) in a geological repository. These scoping studies suggest that the co-location and the geological disposal of plutonium is feasible.

More recently, working with SKB, Nirex has developed a Reference Repository Concept for UK HLW/SF, associated Waste Package Specifications (WPS) and supporting generic safety assessments (including generic a post-closure safety assessment). This work has identified the key parameters and data required for the generic post-closure safety assessment.

Nirex is using the repository concepts for ILW and HLW/SF, associated WPS, as a basis for assessing the disposability of other UK radioactive wastes and materials (if declared as wastes).

This work has been used to support Nirex inputs to the UK Government Managing Radioactive Waste Safely Programme that is reviewing the options for the long-term management of radioactive wastes, including whether some radioactive materials such as UK separated stocks of plutonium should be declared as wastes.

1. INTRODUCTION

United Kingdom Nirex Limited is an independent body responsible, in support of Government policy, for developing and advising on safe, environmentally sound and publicly acceptable options for the long-term management of radioactive materials in the UK. Nirex has therefore carried out extensive development work on

geological disposal of radioactive waste and more recently on its Phased Geological Repository Concept (PGRC) for ILW and a reference repository concept for the UK's high-level waste (HLW) and spent nuclear fuel (SF).

UK Government policy for long-term waste management is currently under review. The UK Government Department for Environment, Food and Rural Affairs (Defra) and the Devolved Administrations for Scotland, Wales and Northern Ireland are currently undertaking a programme of work and consultation on "Managing Radioactive Waste Safely" (MRWS) to develop a strategy for the long-term management of solid radioactive wastes [1].

A diverse range of radioactive waste types have been generated in the UK through various activities. As part of this UK Government MRWS programme, a review of waste management options is being undertaken and it is being considered whether UK radioactive materials such as spent fuel, plutonium and depleted and reprocessed uranium should be declared as waste.

To provide an open and transparent set of data of radioactive materials Nirex commissioned and published a study [2] to establish the quantities of other wastes and materials that would need to be considered in developing a long-term waste management policy for the UK.

Historically, Nirex's remit has been focused on the long-term management of solid intermediate-level waste (ILW) and that low-level waste (LLW) which is unsuitable for disposal in near-surface facilities. The majority of Nirex's work has therefore been devoted to the long-term management of these wastes. Nirex's remit is now to look at options for all types of radioactive materials and not to simply focus on ILW as it did in the past. Nirex has therefore applied the approaches developed for assessing the compatibility and safety of waste packages with all management phases, including pos-closure, to its recent work on developing options for HLW and SF.

At present, there is no site selected for the development of a repository in the UK. Nirex has, therefore, developed a Generic Post-closure Performance Assessment (GPA) [3]. This is based on a range of geological characteristics consistent with conditions that could be found in the UK.

The GPA forms part of a suite of documents that captures Nirex's understanding of geological disposal as one possible option for the long-term management of such wastes. These documents have been produced to show the viability of the repository concept and to define a reference concept against which waste producers' packaging proposals can be assessed [4]. The GPA is used to test the generic repository design, and to test the compatibility and safety of waste producers' packaging proposals with the Nirex Phased Geological Repository Concept [5] and compliance with the Nirex Generic Waste Package Specification [6].

The suite of documents includes a generic disposal system specification, transport and repository design, and assessments of transport, operational and post-closure safety. Demonstration of the viability of the concept is an on-going process and an important output, from the generic documents, is the identification of issues that need to be addressed in the future programme of work.

The assessment of post-closure safety (GPA) is based upon a reference case which includes assumptions regarding a number of key parameters related to the hydrogeological properties of a generic site:

— the groundwater flux through the repository (Q);

— the nominal groundwater travel time (T);

— the mixing flux in overlying rocks (F).

Values for these parameters for the reference case have been chosen to be realistic and achievable in the UK and consistent with the safety standard set by the regulators for the land-based disposal of ILW/LLW. This is a target that the resulting radiological risk to an individual should be less than one in a million per year (10^{-6} risk target) [7].

This report describes the research performed by Nirex on the geological disposal of UK HLW and spent nuclear fuel during the period 1/5/2000 to 31/12/2004 that has contributed to the IAEA Co-ordinated Research Project on "Chemical durability and performance assessment of spent fuel and high level waste under simulated repository conditions" and covers the work undertaken to investigate:

— feasibility of co-locating a repository for ILW/LLW and a repository for HLW/SF in a shared facility in the UK;

— implications of including separated stocks of plutonium as waste if declared as waste or used as fuel in a new nuclear programme;

— the development of a reference HLW/SF repository concept and derivation of waste package standards and specifications for HLW/SF.

2. FEASIBILITY OF CO-LOCATION

In September 1997, following the failure to gain planning permission for a Rock Characterisation Facility, Nirex was given new objectives by the nuclear industry and Government shareholders. These objectives specifically included:

"Contribute to Government review of policy and make the case for the proposed strategy, repository milestone timings or sequence of steps which need to be achieved. Also explore HLW co-disposal options".

Co-disposal (here on in referred to as co-location) offers potential cost savings over the development of separate facilities for different types of waste, and would involve the development and consequential disturbance of a single site; an integrated process for consultation and planning applications; and a single programme of transport, site selection and characterisation.

Nirex has performed preliminary scoping studies to investigate the feasibility of co-locating ILW/LLW (based on the Nirex Phased Geological Repository Concept)

and HLW/SF[1] (based on a bentonite-lined repository concept) in different excavations within the same rock mass using a common access [8]. For the purpose of these studies, co-location was taken to mean the disposal of HLW/SF and ILW/LLW in different excavations within the same or adjacent rock mass using common access.

These initial studies started in 1998 and were based on an example HLW/SF repository design that was used for the purposes of a desk based European Commission study titled "*Building the Safety Case for a Hypothetical Underground Repository in Crystalline Rock"* [9]. This design was used by Nirex for the purposes of initial scoping studies as it was well described, readily available and the description included the co-location with an ILW/LLW repository. As noted in these studies this was not necessarily a design concept that Nirex would propose. A nominal separation distance between the two repositories of 500m was adopted in the illustrative design concept. This distance would be optimised as part of the programme of research and development and siting.

The potential risks arising from the groundwater, gas and human intrusion pathways were studied. The work was based on the data and models which have been developed in support of GPA for the geological disposal of ILW/LLW and an extension of these models to a generic concept for the disposal of HLW/SF [8].

The post-closure radiological risk from the groundwater pathway for the HLW/SF repository combined the model for the geosphere used in the modelling of the ILLW/LLW part of the repository (in the generic assessment) with a simple representation of the near-field for an HLW/SF repository [8]. The ILW/LLW and HLW/SF source terms were modelled separately and assumed not to interact in the base case.

The radionuclides from the HLW/SF repository that contribute 10% or more to the total calculated risk were found to be: technetium-99, tin-126, iodine-129, radium-226, uranium-233 and uranium-234.

A key issue to be considered when assessing the feasibility of co-location is the compatibility of the two wasteforms and engineered barrier systems. The following interactions of the modified groundwater plume from the ILW/LLW repository with the bentonite and wasteforms in the HLW/SF repository were identified as potentially the most significant adverse effects:

A. water with high pH and high calcium and potassium content derived from the cementitious ILW/LLW vaults adversely affecting the containment properties of the bentonite buffer in the HLW/SF deposition tunnels;

B. high pH waters from the ILW/LLW vaults increasing the rate of dissolution of borosilicate glasses in the HLW/SF deposition tunnels;

[1] The conditioned volume of vitrified HLW from reprocessing of all Magnox spent fuel and some AGR spent fuel is estimated to be 1250m^3. In addition eventual unreprocessed spent fuel (of the order 2900tHM from the AGR stations and 1200tHM from the Pressurised Water Reactor (PWR) Sizewell B) may be declared as waste and require long-term management.

C. organic material and their degradation products from the ILW/LLW affecting the solubility and speciation of radionuclides arising from the HLW/SF deposition tunnels.

The potential importance of effects (B) and (C) both depend upon the containment properties of the bentonite clay buffer. Degradation of the bentonite performance is, therefore, considered the most important of the three issues. However, it is recognised that cement/clay (i.e. bentonite) interactions are an issue for a HLW/SF repository in itself (i.e. interactions between construction cement and bentonite backfill) [10].

The extent and impact of chemical interactions on HLW/SF repository performance have been investigated by performing a range of sensitivity and scoping studies. Overall, the calculated risk was insensitive to the rate of glass dissolution, and controlled mainly by diffusion through bentonite and the travel time through the geosphere [8].

3. IMPLICATIONS OF INCLUDING PLUTONIUM

In the UK the eventual stocks of separated plutonium oxide are estimated to be 118 tonnes [2]. This material is not considered at the present time to be a waste material, as it represents a major potential energy source. The UK Government MRWS programme is currently considering whether some or all of this stockpile should be declared as waste or used as fuel.

Nirex has performed a range of studies on the long-term management of plutonium, including:

— Literature reviews to identify some of the options suggested for the long-term management of plutonium (including conditioning and packaging) [11, 12].

— Scoping studies to identify the issues for the geological disposal of plutonium drawing on Nirex's expertise on geological disposal and, where possible, the safety assessments developed for the Nirex Phased Geological Repository Concept [13].

3.1. A review of international literature on immobilisation matrices for separated stocks of plutonium

The objective of this review was to provide an overview of the immobilisation options for separated plutonium and their relationship to long-term management policy for the material, if specified, and summarise the status of the understanding for the immobilisation options [11].

The review describes options for disposition of plutonium involving immobilisation in a solid matrix suitable for eventual final disposal.

The matrices that have been identified from the literature search are as follows:

— Ceramics – Synroc, zirconolite, pyrochlore, zircon, zirconia, monazite and apatite;

— Glasses - borosilicate and phosphate glasses (including more specialised glasses designed specifically for disposition of plutonium);

— Glass-ceramics;

— Other options - mixed oxide fuel (MOX), inert matrix fuel and cements.

The literature review findings suggest ceramic wasteforms perform better than glasses in terms of chemical durability. In general, it is very difficult to make absolute comparison of leaching rates of plutonium from the wasteforms, because of the variability of target wasteform compositions, experimental conditions and reporting. Many papers considered in the literature review [11] present apparently conflicting results for leach rates, with small differences being masked by "noise" due to differences in experimental conditions, in particular:

— unreported (or unknown) differences in wasteform composition;

— the presence of more than one phase (such as consistent occurrence of zirconolite in pyrochlore and vice-versa);

— attempts to compare leach test results on samples aged using different methods of irradiation (natural samples aged by U/Th, artificial samples irradiated by Pu-239 or Cm-244, heavy ion bombardment, neutron irradiation etc.);

— different leach test methods (single pass flow through and static tests);

— in some papers, lack of clarity as to whether leach tests have been carried out on samples actually containing plutonium or on those containing a Pu-simulant (such as thorium or cerium).

Overall, this review suggested that more systematic studies would be required to determine the impact of different conditions on long-term behaviour and leach rates from different plutonium wasteforms.

3.2. Scoping Calculations

Many of the issues surrounding long-term waste management, including associated engineering and assessment requirements, are common across all waste categories, particularly if a common overall policy of geological disposal for higher-activity and long-lived wastes were to be adopted in the UK. For example, the projected quantities of plutonium and uranium associated with the UK Inventory of ILW are 7 tonnes and 3,000 tonnes, respectively. Consequently, the long-term management of ILW needs to take account of the issues that arise in relation to both spent fuel and to stocks of separated plutonium and uranium. Although this report focuses on the development and implementation of strategies for the geological disposal of HLW and SF, it is envisaged that the general approach would be similar for any long-lived waste and for any disposal option. HLW, SF and ILW are therefore regarded as a good basis for the development of geological repository concepts.

In 2001 scoping studies were performed [13] to determine the implications in the event that the UK's stocks of separated plutonium were to be disposed of either in an adaptation of:

i) the Nirex Phased Geological Repository Concept (plutonium conditioned in cement and packaged in stainless steel drums) or

ii) in a bentonite lined HLW/SF repository concept[2] (plutonium immobilised in borosilicate glass[3] or as MOX spent fuel).

Based on the assumptions made for this study the disposal of separated stocks of plutonium in a geological repository appears to be feasible. These studies included post-closure radiological risk calculations for the groundwater pathway based on data and models that have been developed for use in the GPA.

For cement and glass plutonium wasteforms the key contributing radionuclides to the calculated risk from the groundwater pathway were found to be the daughter produces such as uranium isotopes U-233, U-234 and U-236, and protoactinium-231.

For the MOX spent nuclear fuel post-closure safety assessment, the long-term release of radionuclides from spent fuel is typically considered to be controlled by the dissolution rate of the oxide matrix. The majority of the radionuclides are contained within the fuel matrix. Certain radionuclides, however, are enriched at grain boundaries, at pellet cracks and in the fuel/sheath gap as a result of thermally driven segregation during operation of the fuel in the reactor [14]. There is a strong correlation between the segregation of fission products and their rapid release (usually termed the instant release fraction) [14, 15]. It is therefore important to gain a good understanding of these radionuclides for the development of the assessment of long-term repository performance [16, 17, 18]. Based on the work by Guerin *et al* [19] for MOX fuel the release of long-lived fission products from MOX fuel (instant release fraction) is expected to increase by a factor of 2 to 3 compared to PWR UO_2 fuel. If significant quantities of MOX fuel were to require disposal, the release of these radionuclides could be important.

When disposing of MOX fuel elements, special attention is required for the enhanced inventory of plutonium-242 and plutonium-239 and their decay products [20]. However, the impact of a much larger inventory of many long-lived actinides in MOX fuel relative to UO_2 fuel is expected to have limited consequences in the assessment of long-term doses from MOX spent fuel. This is because of low solubilities and strong retention on bentonite and geological materials.

Studies of the disposal of UO_2 fuel allow the deduction to be made that safe disposal of MOX fuel elements would feasible [20]. However, inclusion of MOX fuel in a geological repository for HLW and spent fuel raises several important issues that should be considered in developing engineered barrier and repository designs, evaluating costs and assessing operational phase and long-term safety.

More recently Nirex has extended these studies to consider plutonium immobilised as a ceramic. Although, there has been extensive experience and research into glass as an immobilisation matrix (especially for HLW), evidence based mostly

---

[2] Based on an adaptation of design used for preliminary scoping studies of co-location in the UK.

[3] Probabilistic modelling approach based on dissolution rate constants for HLW: best estimate glass dissolution rate of 10^{-4} per year, with a lower and upper boundary of 10^{-6} and 10^{-2} per year respectively.

on the study of natural analogues would suggest that various ceramic wasteforms could possess a better potential for the long-term containment of plutonium under repository conditions. Small-scale research has been conducted on various ceramic wasteforms which have shown initial leach rates for ceramics to be roughly 3-4 orders of magnitude less than those of the glass form [11]. In addition, ceramics can potentially incorporate substantial quantities of U-238, which is not as feasible in glass due to the lower solubility of uranium in glass.

4. DEVELOPMENT OF A REFERENCE REPOSITORY CONCEPT AND WASTE PACKAGE STANDARDS AND SPECIFICATIONS FOR UK HLW/SF

With encouragement from Government, Nirex is working with sister organisations (SKB, Nagra and NUMO) to examine the extent to which the vast amount of work undertaken internationally on the long-term management of HLW and spent nuclear fuel can be applied in the UK. Through a series of workshops Nirex has developed a strategy, a reference concept for a geological repository for UK HLW/SF and a programme for developing the concept through an iterative process of design, assessment and research.

Internationally, a range of geological disposal concepts have been discussed and investigated for HLW and SF over a number of years. The concepts vary according to the nature and quantity of the waste and the different geological and social settings. Nirex has reviewed this range of concepts and has selected a concept to demonstrate the viability of HLW and SF disposal in the UK. Concepts were screened in order to select a concept that was at an advanced stage of development, based on well-established properties of the engineered and natural containment barrier systems, allowed for ease of retrieval and was supported by extensive R&D.

The Reference Repository Concept for UK HLW/SF selected by Nirex for this ‘viability demonstration’ (here on in referred to as the Reference HLW/SF Concept) is based on the KBS-3 concept developed by SKB for spent fuel in Sweden. This concept has been extensively studied by the Swedish and Finnish national programmes for more than 20 years [21]. This selection also reflects the maturity of the Swedish and Finnish programmes, their involvement of stakeholders and their level of regulatory scrutiny and, in the case of Sweden, international peer review.

The KBS-3 repository concept is based on encapsulating spent fuel in copper canisters with a cast iron insert. (Under suitable geochemical conditions, the corrosion of copper is extremely slow, and the copper canister is expected to maintain its integrity for an extremely long time). The copper canisters are surrounded by bentonite clay mixed with sand and deposited in vertical holes drilled along a series of access tunnels excavated at a depth of approximately 500m in saturated granitic rock. The tunnels and rock caverns would be backfilled with a mixture of bentonite and crushed rock.

A preliminary assessment of long-term safety of the Reference HLW/SF Concept was performed recently in collaboration with SKB [22]. In assessing the long-term safety, advantage has been taken of the large amount of assessment work on the safety of the KBS-3 concept already undertaken by SKB, as well as relevant Nirex work on the UK geosphere and biosphere conditions. To do this, SKB and

Nirex have developed a model for the assessment of the Reference HLW/SF Repository Concept. The model is underpinned by both Nirex and SKB R&D programmes.

The input data for the near-field, with uncertainty estimates, used for the post-closure assessment of the Reference HLW/SF Concept is described in Reference [23]. The data required for the modelling included:

— radionuclide inventory;

— instant release fractions from spent fuel;

— wasteform dissolution rate;

— radionuclide solubility under repository conditions;

— rate and form of carbon -14 released in the gas phase.

A probabilistic calculation of risk has been carried out using the model developed with SKB[4] [22]. The peak value of the mean annual individual radiological risk was found to be 10^{-11}, which is substantially below the radiological risk that defines the target applicable in the UK to ILW and LLW of 10^{-6} per year [7]. This means a risk to a person of 1 in 100,000 million per year of developing either a fatal cancer or a serious hereditary defect. The very low calculated risk is due to the combination of a long groundwater travel time for the UK geological characteristics used in the GPA and a robust engineered physical containment barrier (the copper canister). As part of the development of a safety assessment for the Reference HLW/SF Concept, Nirex is performing further calculations to address the sensitivity of the system to key processes or components.

This work has been used to identify the key R&D priorities for development of the Reference HLW/SF Concept. For the wasteform, further work was identified to increase confidence in the robustness of the source data for the assessments [24].

Apart from this demonstration of fundamental concept viability, a further objective of developing a reference concept for a repository for UK HLW and SF was to provide guidance to waste producers on waste characterisation and packaging.

Guidelines for the packaging of radioactive waste destined for disposal routes (not then available or developed) were issued in 1982 by the UK Department of the Environment [25]. These guidelines were deemed appropriate for all radioactive wastes. It was stated that more detailed specifications could not be developed until a site or sites had been selected for the disposal of these radioactive wastes.

However, a significant amount of research and development on short and long-term management of radioactive wastes has been, and continues to be, performed around the world. On the basis of past experience and international practice and the IAEA guidelines Nirex has set out its initial view of waste packaging standards and specifications for the following material types in [26]:

---

[4] On the basis of research and development performed by SKB on the evolution of copper canisters it was assumed that one canister each of UK HLW and PWR and AGR spent fuel has a defect that ultimately fails.

— vitrified HLW,

— spent civil reactor fuel,

— plutonium,

— uranium.

The Waste Package Specification (WPS) is the key document defining standards and performance requirements, which ensures that all waste packages are compatible with the repository concept, and underlying safety and performance assessments. Nirex has therefore defined a WPS that is explicitly and clearly based on a Reference HLW/SF Concept in a similar manner to that adopted for the production of WPS for ILW and LLW.

5. CONCLUDING REMARKS

Initial scoping studies performed by Nirex suggest that the co-location of a HLW/SF repository and ILW/LLW repository in the UK is feasible. The extent and impact of chemical interactions on HLW/SF repository performance have been investigated by performing a range of sensitivity and scoping studies. Overall, the calculated risk was insensitive to the rate of glass dissolution, and controlled mainly by diffusion through bentonite and the travel time through the geosphere.

Literature reviews and Nirex scoping studies indicate that geological disposal of the UK's stock of separated plutonium is feasible. Overall, this work suggests that more systematic studies are required to determine the impact of different conditions on long-term behaviour and leach rates from different plutonium waste forms.

Nirex has selected a Reference HLW/SF Concept to demonstrate the viability of the deep geological disposal option for UK HLW/SF, prioritise R&D and to support the development of waste packaging standards and specifications. The PGRC and Reference HLW/SF Concept, and associated WPS, are being used as a transparent basis for the assessment the disposability of the other UK radioactive wastes and materials (if declared as wastes).

REFERENCES

[1] Department for Environment Food and Rural Affairs and Devolved Administrations, Managing Radioactive Waste Safely – Proposals for Developing a Policy for Managing Solid Radioactive Waste in the UK, September 2001.

[2] United Kingdom Nirex Limited, Identification and Description of UK Radioactive Wastes and Materials Potentially Requiring Long-term Management, Nirex Report N/085, 2003.

[3] United Kingdom Nirex Limited, Generic Repository Studies, Generic Post-closure Performance Assessment, Nirex Report N/080, July 2003.

[4] United Kingdom Nirex Limited, Generic Phased Disposal System Documentation, Nirex Reports N/074, N/075, N/076, N/077, N/078, N/079, N/080, 2003.

[5] United Kingdom Nirex Limited, Generic Repository Studies, The Nirex Phased Disposal Concept, Nirex Report N/074, July 2003.

[6] United Kingdom Nirex Limited, Generic Repository Studies, Generic Waste Package Specification, Nirex Report N/104, June 2005.
[7] Environment Agency, Scottish Environment Protection Agency and Department of the Environment for Northern Ireland, Disposal Facilities on Land for Low and Intermediate Level Radioactive Wastes: Guidance on Requirements for Authorisation (Radioactive Substances Act 1993), HMSO, London, 1997.
[8] United Kingdom Nirex Limited, Nirex Technical Note: Feasibility of Co-disposal, January 2003.
[9] Deutsche Gesellschaft zum Bau und Betrieb von Endlagern für Abfallstoffe mbh (DBE), Building the Safety Case for a Hypothetical Underground Repository in Crystalline Rock, Final Report, Contract ETNU-CT-93-0103, Volume 1, Preparation and Discussion of the Safety Case, May 1996.
[10] Hooper A, Alexander Wr, Mathieson J And Shiotsuki, M, Review Of International Progress In Transuranic And Long-Lived Intermediate Level Waste Disposal, 10th International Conference On Radioactive Waste Management And Environmental Remediation, Glasgow, September 4-8 2005.
[11] United Kingdom Nirex Limited, A Review of International Literature on Immobilisation Matrices for Separated Stocks of Plutonium, Nirex Report N/107, 2005.
[12] D.G. Bennett, J.J.W. Higgo and S.M. Wickham. Review of Waste Immobilisation Matrices. Contractor Report to Nirex by Galson Sciences Limited, December 2001.
[13] United Kingdom Nirex Limited. Nirex Technical Note: Implications of Declaring UK Stockpiles of Plutonium as Waste, March 2002.
[14] Johnson, L.H. & Tait, J.C. Release of Segregated Radionuclides from Spent Fuel, SKB Technical Report 97-18, 1997.
[15] Garisto, N.C., Vance, E., Stroes-Gascoyne, S. and Johnson, L.H. Instant Release Fractions for the Assessment of used Nuclear Fuel Disposal. Atomic Energy of Canada Report AECL-9584. Atomic Energy of Canada Ltd., Pinawa, Manitoba, Canada, 1989.
[16] SKB, Deep Repository for Spent Nuclear Fuel. SR-97 - Post-closure Safety, SKB Technical Report TR-99-06, 1999.
[17] Vieno, T. & Nordmann, H. Safety Assessment of Spent Fuel Disposal in Hastholmen, Kivety, OlkIuoto and Romuvaara: TILA-99. Posiva Report 99-07, 1999.
[18] AECL, Environmental Impact Statement on the Concept for Disposal of Canada's Nuclear Fuel waste. Atomic Energy of Canada Limited Report AECL-10711, COG-93-1, 1994.
[19] Guerin, Y., Lespiaux, C., Struzik, C. & Caillot, L. Behaviour of MOX fuel as compared to UO_2 fuel. In Physics and Fuel Performance of Reactor-Based Plutonium Disposition. Workshop Proceedings, Paris, 28-30 September 1998. NEA Paris, 1999.
[20] Baltes, B. Long-term Safety Aspects of Geological Disposal of Large Quantities of Plutonium. E. R. Merz and C.E. Walter (eds), Disposal of Weapon Plutonium, pp 269-273, 1996.
[21] SKB, Interim Main Report of the Safety Assessment SR-Can, SKB Technical Report TR-04-11, 2004.
[22] United Kingdom Nirex Limited, Nirex Technical Note: Preliminary Post-closure Assessment of a Reference Repository Concept for UK High-level Waste/ Spent Fuel, 2005.

[23] United Kingdom Nirex Limited, Nirex Technical Note: Compilation of Data for Radionuclide Transport Calculations for a Reference Repository Concept for UK High-level waste and Spent nuclear fuel, 2005.
[24] United Kingdom Nirex Limited, Nirex Technical Note: Review and Appraisal of R&D to Support the Development of a Reference Repository Concept for UK High-level Waste/ Spent Fuel, 2005.
[25] Department of Environment, Radioactive Waste Management: Information Note 1 Packaging Radioactive Wastes, 1982.
[26] United Kingdom Nirex Limited, Initial Consideration of Waste Acceptance Criteria for the Long-term Management of Certain UK Radioactive Wastes and Potential Wastes, Nirex Report N/118, 2004.